Utilizing IgG1 Fc As An Immunomodulator

By

© 2019

Derek R. White
M.S., Pharmaceutical Chemistry, 2013, The University of Kansas, Lawrence, KS
B.S., Biochemistry, 2010, The University of Wisconsin – La Crosse, La Crosse, WI

Submitted to the graduate degree program in Pharmaceutical Chemistry and the Graduate Faculty of the University of Kansas in partial fulfillment of the requirements for the degree of Doctor of Philosophy.

_____

Chair: Thomas J. Tolbert, PhD

_____

Teruna J. Siahaan, PhD

_____

David B. Volkin, PhD

_____

John F. Stobaugh, PhD

_____

David D. Weis, PhD

Date Defended: 28 March 2019

The dissertation committee for Derek R. White certifies that this is the approved version of the following dissertation:

Utilizing IgG1 Fc As An Immunomodulator

_____

Chair: Thomas J. Tolbert, PhD

Date Approved: 28 March 2019

Abstract

Antibody-based therapeutics are a rapidly expanding class of biopharmaceuticals. The number of approved antibody-based therapeutics by the FDA and EMA has more than doubled in the last five years, and they are expanding into areas such as antibody-drug conjugates, Fc fusions, bispecific antibodies, and biosimilars. Most antibody-based therapeutics use the Immunoglobulin isotype G subclass 1 (IgG1) antibody. Some IgG1-based therapeutics obtain their therapeutic efficacy by modulating the immune system for the treatment of several disease-types including cancer, autoimmune disease, and organ transplant rejection. This work further explores our understanding of IgG1-mediated immunomodulation by utilizing the fragment crystallizable (Fc) region of IgG1 in three research projects.

In the first project, an IgG1 Fc fusion was prepared as a potential treatment for multiple sclerosis, an autoimmune disease that affects > 2.3 million people worldwide. This disease involves immune system attack and destruction of the myelin protein surrounding the neurons in the central nervous system. One promising class of compounds that selectively prevent the activation of immune cells involved in the destruction of myelin are Bifunctional Peptide Inhibitors (BPIs). In an effort to further improve the bioactivity of BPIs, the BPI peptides were conjugated to the termini of IgG1 Fc to prepare a BPI-Fc fusion. This fusion was tested in a mouse model of multiple sclerosis. Compared to the PBS-treated control, mice treated with the BPI-Fc fusion showed significantly reduced disease symptoms, did not experience weight loss, and showed reduced demyelination. These results demonstrated that the BPI peptides were highly active at suppressing the disease when prepared as an Fc fusion.

In the second project, the N-glycosylation of IgG1 Fc was modified. The N-glycosylation of IgG1 can markedly affect its function, stability, pharmacokinetics, solubility, and

immunogenicity. However, recombinant expression of IgG1 results in a mixture of N-glycoforms. This heterogeneity makes it difficult to understand how N-glycosylation affects IgG1 because different N-glycoforms can affect the antibody differently. To solve this problem, this work utilized IgG1 Fc as a model system to prepare homogenous IgG1 Fc N-glycoforms, and their effects on IgG1 Fc were studied individually. *In-vitro* enzymatic synthesis was used to prepare homogenous oligomannose, hybrid, and complex N-glycoforms. The effect of each non-fucosylated N-glycoform on IgG1 Fc stability was compared using differential scanning calorimetry. The results showed that the complex N-glycoform was more stable than the hybrid and oligomannose N-glycoforms. Additionally, the effect of each N-glycoform on IgG1 Fc function was compared in an *in-vitro* receptor-binding assay using FcγRIIIa, the receptor involved in activating Antibody-dependent Cellular Cytotoxicity (ADCC). Results showed that the binding affinity increased with increased N-glycan processing. Lastly, the hybrid and complex IgG1 Fc N-glycoforms were compared for their abilities to accept core-linked fucose. Results showed that the complex N-glycoform accepted fucose much more slowly compared to the hybrid N-glycoforms.

In the third project, IgG1 Fc was assembled as a protein-polymer conjugate in order to increase its valency. Multivalent display of IgG1 is necessary in order to obtain an avidity effect strong enough to activate immune system effector functions, such as ADCC. IgG1 Fc-polymer conjugate was prepared using controlled polymerization to first synthesize a water soluble, linear poly(acrylamide-peptide) co-polymer. This co-polymer was then used as a scaffold onto which multiple IgG1 Fc proteins were site-specifically ligated. The IgG1 Fc-polymer conjugate was compared against IgG1 Fc in a receptor binding assay with FcγRIIIa. The results showed that the IgG1 Fc-polymer conjugate bound FcγRIIIa 800 times stronger compared to free IgG1 Fc. This

large increase in binding strength was caused by the multimer having a much slower dissociation rate.

The research presented in this dissertation improves our fundamental understanding IgG1-mediated immunomodulation and may also help in the development of improved antibody-based therapeutics.

Dedicated to

My mother

For her unwavering support.

Acknowledgements

First and foremost, I would like to express my extreme gratitude to my PhD advisor, Dr. Thomas Tolbert. I thank him for his patience, his breadth of scientific expertise, his time, his research ideas, his insistence on high quality research, and for allowing me to work on interesting projects. I am also thankful to him for teaching me molecular biology and protein expression/purification techniques in lab during my first year.

Thank you to my dissertation committee members: Thomas Tolbert, Teruna Siahaan, David Volkin, John Stobaugh, and David Weis. I am thankful for their comments about my work, for reviewing this dissertation, and for their help in progressing it to completion.

Thank you to my research collaborators. In Chapter 2, thank you to Teruna Siahaan and Paul Kiptoo for performing the *in-vivo* mouse study. Also, thank you to Zahra Khedri for synthesizing the triglycine-containing antigenic peptides. In Chapter 3, thank you to David Volkin and Vishal Toprani for performing the DSC, OD350, and analytical SEC experiments. Additionally, thank you to Khalid Al-Kinani, Ishan Shah, and Dr. Tolbert's former students from IU for preparing some of the glycosidases and glycotransferases. In Chapter 4, thank you again to Zahra Khedri for synthesizing the poly(acrylamide-peptide) co-polymers. Without the contributions from these collaborations, this work would not have been possible.

Thank you to my former laboratory co-workers in the Tolbert lab: Ishan Shah, Kevin Hutchison, Khalid Al-Kinani, Shaofeng Duan, Solomon Okbazghi, and Zahra Khedri. I am thankful for their friendships and for being helpful co-workers. A special thanks to Ishan Shah and Khalid Al-Kinani for teaching me how to use laboratory equipment, how to perform various laboratory techniques, and for their troubleshooting advice. Also, thank you to Ishan Shah for our research conversions during our afternoon coffee trips. Thank you again to Khalid Al-Kinani

for reviewing this dissertation and for being a role model to me, in both personal and professional aspects. And a special thanks to Zahra Khedri with whom I collaborated most closely. The high quality of her work made my work easier.

Thank you to the people and organizations that supported this research behind the scenes. Thank you to André Faucher for always being helpful, friendly, and an amazing Research Support Services Manager. Also, thank you to the KU Department of Pharmaceutical Chemistry administrative staff: Nancy Helm, Nicole Brooks, Ann Heptig, Karen Hall, and Michelle Huslig. Their effort made my research go smoother. Furthermore, thank you to the National Institute of Health (NIH R01 GM090080) for funding the research.

Thank you to my family and friends. Thank you to my family for always being a source of support. Thank you to my mother: Diane; stepdad: Randy; brothers: Blake and Dustin; cousin: Lauralye and her family; dad: Steve; nephews: Matthew, Michael, Marcus, and Elijah; and the rest of my family. I especially thank my mother for always being there for me. Also, I am extremely grateful for my friends that I made during my time in Lawrence. I am lucky to be a part of "the gang": Cavan Kalonia, Jayant Arora, Joe St. Amand, Justine Kalonia, Laura Northrup, and Yamini Mutreja. I am also thankful to my fellow graduate students and postdocs for their friendship and for helping me with various laboratory aspects: Ryan Moulder, Huan Khang, Mario Moral, Björn Peters, Peter Kleindl, Chad Pickens, and Matt Behymer.

Thank you to the KU Department of Pharmaceutical Chemistry. Thank you for challenging me, for demanding high standards, for rewarding me, for providing a platform on which to grow both as a scientist and as a person, and for being an example of what I can aspire to. I hope to contribute to the high-quality reputation that the faculty and graduates have set.

And lastly, thank you to my dog, Linus "Paw"ling.

Table of Contents

List of Figures

List of Tables

Chapter 1

Introduction

1.1 Overview of the immune system

The immune system protects the body from invading pathogens.[1] It is roughly divided into two categories: innate and adaptive. Innate immunity is the initial response to an invading pathogen. Its response is very rapid (hours) because most of the active components are ready even before an infection. The mechanisms to clear a pathogen by innate immunity include phagocytosis and initiating an inflammatory response. The innate immune system recognizes broad classes of molecules such as non-human nucleic acid, glycan, and polypeptide sequences.[2] However, these features are not pathogen-specific, so not all pathogens are detected. On the other hand, the adaptive immune system is activated in response to a pathogen, so the response is slow (days). However, the response is extremely specific to the pathogens through the production of antigen-specific molecules called antibodies (i.e. Immunoglobulins (Ig)). Based on the possible genetic combinations that exist, there are theoretically $>10^{11}$ different antibody specificities.[3] With that breadth of diversity, antibodies can be tailored to almost any pathogen. Although there are differences between the innate and adaptive immune systems, they often function cooperativity to rid a pathogen from the body.

1.2 Structure and function of the IgG1 antibody

There are five isotypes of antibodies: IgA, IgD, IgE, IgG and IgM. Of all isotypes found in human serum, IgG accounts for about 80%.[1] IgG is divided into 4 subclasses: IgG1, IgG2, IgG3, and IgG4. Their DNA sequences are 90-95% homologous but vary in several properties including half-life, ability to activate immune system effector functions, and ability cross the placenta and mucosal membranes.[1] IgG1 accounts for 60% of all IgGs found in serum.[4]

IgG1 is a Y-shaped structure that is ~150 kDa in size (**Figure 1.1A**). It is a hetero-tetramer consisting of two conserved light chains and two conserved heavy chains.[5] Each heavy-light chain pairing are connected by a disulfide bond. The two heavy chains are held together by two inter-chain disulfide bonds in the hinge as well as though non-covalent interactions in the CH3 domain. In total, IgG1 contains 12 Ig domains that consist of two β-sheet 2º structures that are connected by a disulfide bond.[6] Furthermore, there are two main regions of the antibody that are divided by the hinge. These regions are the fragment antigen binding (Fab) and the fragment crystallizable (Fc). They have different functions (**Figure 1.1B**): The Fab region contains complementarity-determining regions (CDR) that recognizes a particular antigen. There are billions of possible CDR sequences, which gives IgG1 its extreme specificity.[1] The Fc region gives IgG1 its biological activity by binding to Fcγ receptors (FcγRs). Additionally, IgG1 is a glycoprotein. Each heavy chain contains a conserved N-glycosylation site at Asn297. The type of biological activity that is elicited depends on the particular FcγR that is engaged as well as the particular N-glycosylation.

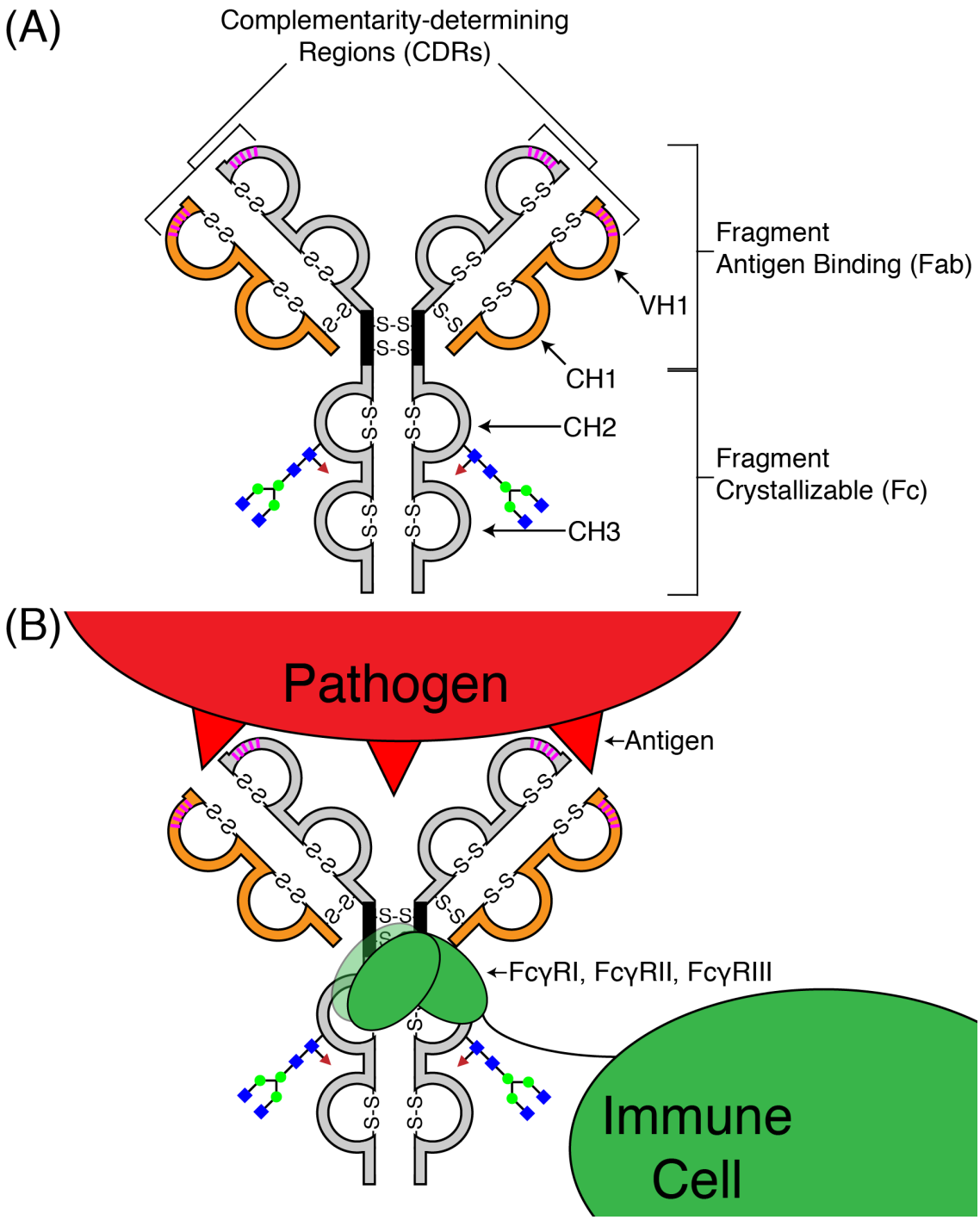

Figure 1.1: Representation of the structure and function of an IgG1 antibody. (A) Structure of IgG1. Polypeptide colors: grey = heavy chain, orange = light chain, black bars = hinge, magenta = CDRs. Glycosylation symbols: blue square = N-acetylglucosamine, green circle = mannose, red triangle = fucose. (B) Function of IgG1. Antibodies are responsible for both recognizing the antigen as well as recruiting immune cells to evoke an appropriate immune response against the pathogen.

1.3 Antibody-mediated effector functions

IgG1 is capable of eliciting antibody-mediated effector functions that utilize both the adaptive and innate branches of the immune system to selectively locate and destroy harmful cells. First, the Fab region from an antibody of the IgG subclass recognizes a foreign antigen on a target cell and binds to it. Next, the Fc region binds to an activating FcγR (**Table 1.1**) on an effector cell. A single binding event is not enough. Multiple binding events are required in order to create an immune complex that activates the effector cell.

The well-studied effector functions are Complement-dependent Cytotoxicity (CDC), Antibody-dependent Cellular Phagocytosis (ADCP), and Antibody-dependent Cellular Cytotoxicity (ADCC) (**Figure 1.2**).[4] The CDC pathway involves initial binding of C1q to the Fc. C1q contains 6 heads, and each head can bind to an Fc. The binding affinity between a C1q head and Fc is very low, but multiple binding events can increase the avidity of binding 100,000-fold.[7] The strong binding upon avidity starts an activation cascade of serum proteins leading to the destruction of the target cell's cell membrane. The ADCP pathway involves recognition of a target cell by a phagocyte, such as a macrophage, by binding to the Fc of the bound antibody by a FcγR such as FcγRIIa.[8] Activation leads to the macrophage engulfing the target cell and destroying it by phagocytosis. ADCC works by activating an effector cell to release cytotoxic molecules, such as perforin and granzyme, which kill the target cell. The most well-studied activating receptor and effector cell type combination for ADCC is FcγRIIIa on natural killer (NK) cells. Although, other activating receptors and effector cells have also been shown to elicit ADCC.[9] There are several ways to influence ADCC activity. For instance, it has been shown that ADCC activity can be increased by increasing the affinity of the antibody to the foreign antigen.[10, 11] Additionally, ADCC activity increases with increasing density of the antigen on the

target cell.[11] Third, ADCC activity can be increased by increasing the affinity of the Fc region of the antibody to FcγRIIIa.[12] There have been several methods developed to increase affinity of the antibody Fc to FcγRIIIa. One such way involved modifying the N-linked glycosylation on the Fc. For example, antibodies without core-linked fucose have been shown to increase binding to FcγRIIIa and thereby increase ADCC activity.[13] In fact, knocking out the gene responsible for adding core-linked fucose resulted in antibodies with 100-fold increased ADCC activity.[14] Furthermore, mutating certain residues within the Fc has also been shown to increase binding to FcγRIIIa and also increase ADCC activity.[15-17]

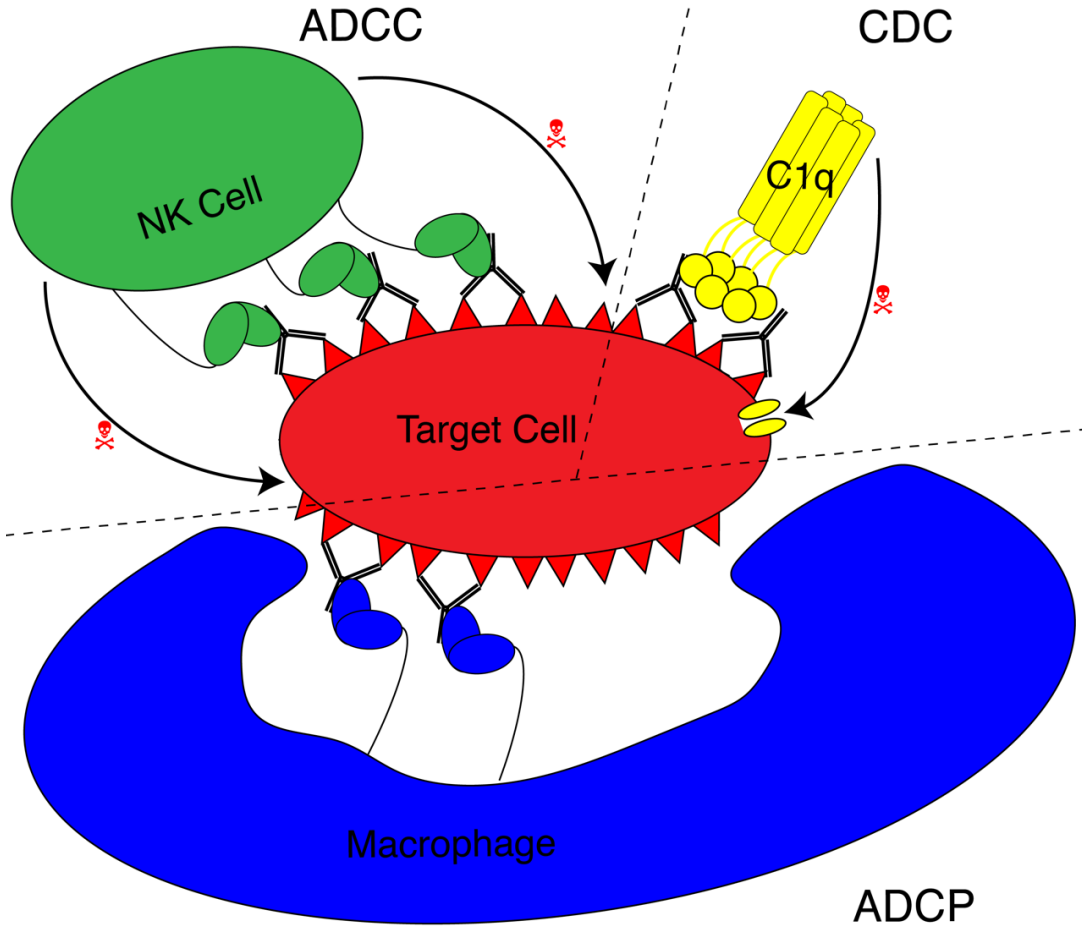

Figure 1.2: Antibody-mediated effector mechanisms that lead to death of a target cell. ADCC = Antibody-dependent Cellular Cytotoxicity, CDC = Complement-dependent Cytotoxicity, and ADCP = Antibody-dependent Cellular Phagocytosis.

1.4 FcγRs

FcγRs are part of the Immunoglobulin superfamily.[18] They are found on the surfaces of immune cells. An immune cell can be either activated or suppressed depending on which FcγR is acted upon. An FcγR is acted upon when it binds to the Fc region of an IgG antibody. There are three classes of FcγRs (FcγRI, FcγRII, and FcγRIII), some of which are be further divided (FcγRIIa/b and FcγRIIIa/b).[19] These receptors differ in several ways, such as in their binding affinity to antibody Fcs, their activating or inhibitory action, the subclass(es) of IgG that they interact with, and the immune cell type(s) they are found on. These differences are summarized in **Table 1.1**. All FcγRs bind to IgG with low affinity except FcγRIa. The low affinity binders require multiple binding events in order to activate the immune cell.[18] Multiple binding events is a regulatory mechanism developed by the immune system in order prevent unnecessary immune stimulation, which would cause harm to the body. Another regulatory mechanism used by the immune system is the balance between activating and inhibitory FcγRs. All FcγRs are activating receptors except FcγRIIb. Activating FcγRs are able to activate proinflammatory responses and antibody-mediated effector functions. For example, FcγRIIIa-mediated signaling can activate ADCC, and FcγRIIa-mediated signaling can activate ADCP.[8, 9] All FcγRs, except FcγRIIIb which is attached to the cell membrane by glycosylphosphatidylinositol, are transmembrane receptors. The activating FcγRs, except FcγRIIIb, contain an immunoreceptor tyrosine-based activation motif (ITAM) in their cytoplasmic regions that leads to intracellular signalizing to activate the effector cell. IgG1 and IgG3 are the two IgG subclasses that best bind the activating receptors.[18] The only inhibitory receptor is FcγRIIb, however, it is found on almost all immune cell types.[19] FcγRIIb contains an immunoreceptor tyrosine-based inhibitory motif (ITIM) instead of an ITAM on its cytoplasmic region. FcγRIIb functions to inhibit the activation in both

adaptive an innate immunity as FcγRIIb can induce apoptosis on B cells and down regulate dendritic cell activation.[20] Furthermore, mice deficient in FcγRIIb saw increased inflammation and phagocytosis.[20] Both activating and inhibitory FcγRs can be found on the same immune cells which helps to regulate the immune response. The binding between FcγRs and IgGs serve as the link between innate and adaptive immunity, and that link is influenced by IgG N-glycosylation.

Table 1.1: Properties of Human FcγRs[19]

FcγR	Poly-morph	Affinity	Activating or Inhibitory	Binds IgG Subclass	Present On Cell Types
FcγRIa		High	Activating	IgG1 IgG2[a] IgG3 IgG4	Dendritic Cells Inflammatory Monocytes Resident Monocytes Macrophages
FcγRIIb		Low/Med	Inhibitory	IgG1 IgG3 IgG4[a]	Neutrophils Dendritic Cells Inflammatory Monocytes Resident Monocytes Macrophages B cells
FcγRIIa	H131	Low/Med	Activating	IgG1 IgG3 IgG4[a]	Neutrophils[b] Dendritic Cells Inflammatory Monocytes[b] Resident Monocytes Macrophages
	R131	Low/Med		IgG1 IgG2 IgG3 IgG4[a]	
FcγRIIc		Low/Med	Activating	IgG1 IgG3	NK Cells[c]
FcγRIIIa	V158	Low/Med	Activating	IgG1 IgG2 IgG3 IgG4[a]	NK Cells Dendritic Cells Resident Monocytes Macrophages
	F158	Low/Med		IgG1 IgG3	
FcγRIIIb		Low/Med	Activating[d]	IgG1 IgG3	Neutrophils

[a]Binding may only occur during immune complex formation.
[b]Found on cell types in spleen and lymph nodes but mostly absent on cell types in blood.
[c]May be present on NK cells in about 20% of the population.
[d]Role in neutrophil activation is mainly through facilitating FcγRIIa signaling.[21]

1.5 Effect of IgG N-glycosylation on FcγR binding

IgG1 contains, in the Fc region on both heavy chains, a conserved N-linked glycosylation site, which is critical for FcγR binding. In fact, complete removal of the glycan structure has been shown to inhibit binding of IgG1 to any FcγR.[16, 22] Modifications to the glycan structure affect the strength of binding to Fc receptors, altering the effector response. For instance, removal of the fucose residue strengthens binding to FcγRIIIa and has been reported to increase binding affinity up to 50-fold and ADCC activity up to 100-fold.[13, 14] Furthermore, the addition of α-2,6-linked sialic acid to the terminal glycan structure reduces the immunogenicity of the antibody by both reducing IgG binding to FcγRIIIa and upregulating presentation of FcγRIIb, the FcγR that inhibits effector activity.[23, 24] Additionally, the N-glycosylation profile of antibodies has been shown to change during disease progression, as shown in HIV and Rheumatoid Arthritis.[4] The number of ways a glycan structure can be configured is immense (**Figure 1.3**), so further study into the effect of IgG glycan composition on FcγR binding is needed.

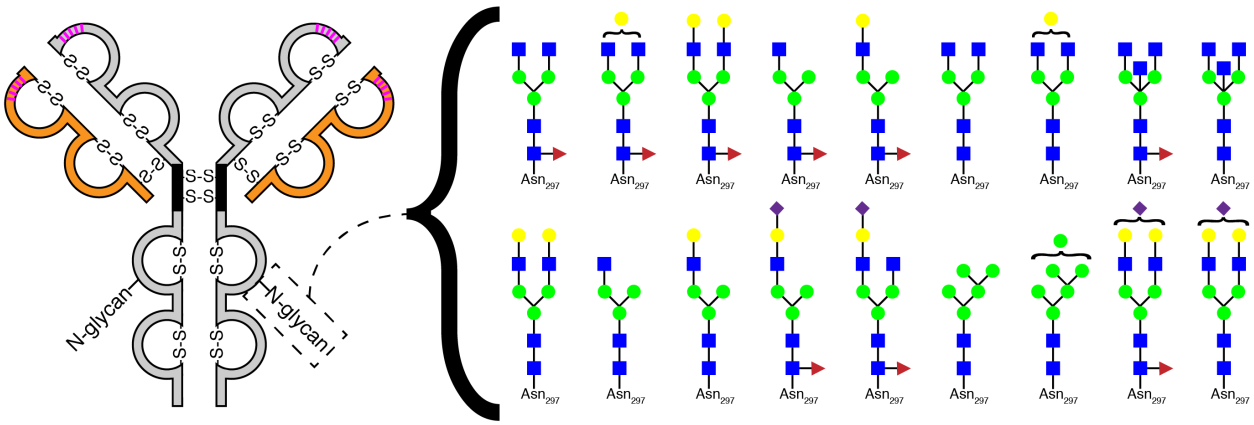

Figure 1.3: Representation of N-glycan heterogeneity on IgG1. The N-glycoforms presented are only the most common from mammalian cell expression of IgG1 and are not a complete representation of all possibilities. Glycosylation symbols: blue square, N-acetylglucosamine; green circle, mannose; red triangle, fucose; yellow circle, galactose; and purple diamond, sialic acid.

1.6 N-glycan biosynthesis and heterogeneity

N-glycosylation is a non-template driven process (unlike polypeptide synthesis which is blueprinted by the preceding DNA sequence). N-glycosylation occurs on Asn residues that are part of the consensus sequence (-Asn-Xxx-Ser/Thr-, where Xxx ≠ Pro).[25] The synthesis of N-glycans occurs in the Endoplasmic Reticulum (ER) and Golgi organelles of a cell (**Figure 1.4**).[26] First, a Dolichol compound that is membrane-bound on the outside of the ER contains, through a pyrophosphate linkage, two N-acetylglucosamine (GlcNAc) and five mannose (Man) residues (Dolichol-P-P-$GlcNAc_2Man_5$). Then, a flippase enzyme orients this glycan inside the ER. Once inside, it is modified by Asn-linked Glycosylation enzymes that add 4 more Man resides to the α-1,6 arm and three glucose (Glu) residues to the α-1,3 arm (termed Dolichol-P-P-$GlcNAc_2Man_9Glu_3$). This entire 14 sugar structure then transferred by two oligosaccharyltransferase enzymes onto the Asn residue of the nascent polypeptide. The glycan is β-linked to Asn by an N-glycosidic bond. The protein is then folded with the help of chaperones such as Calnexin and Calreticulin. The three Glu residues are important during this folding process, and they are sequentially trimmed off during the folding process by α-glucosidases. Then, an ER α1,2-mannosidase removes a Man residue to create a $Man_8GlcNAc_2$-Asn glycoprotein.

The glycoprotein is then directed into the Golgi for further N-glycan processing by a sequential series of glycosidases and glycotransferases.[25] First, $Man_8GlcNAc_2$-Asn is trimmed to $Man_5GlcNAc_2$-Asn by the removal of three α-1,2-linked Man residues by Mannosidase-I. Then, $Man_5GlcNAc_2$-Asn is converted to $GlcNAcMan_5GlcNAc_2$-Asn by the addition of one GlcNAc to the α-1,3-arm by N-acetylglucosaminyltransferase-I. Next, $GlcNAcMan_5GlcNAc_2$-Asn is trimmed to $GlcNAcMan_3GlcNAc_2$-Asn by the sequential removal of two Man residues on the α-

1,6 arm by Mannosidase-II. Then $GlcNAcMan_3GlcNAc_2$-Asn is converted to $GlcNAc_2Man_3GlcNAc_2$-Asn by the addition of one GlcNAc to the α-1,6-arm by N-acetylglucosaminyltransferase-II. Furthermore, core-linked fucose (Fuc) can be added to the innermost GlcNAc by α-1,6-fucosyltransferase to create $GlcNAc_2Man_3GlcNAc_2Fuc$-Asn. This N-glycoform is the most common N-glycoform found on IgG1 in both serum and in monoclonal antibody therapeutics.[27, 28] The N-glycan can be further decorated by additional glycotransferases such as galactosyltransferase which adds galactose, sialyltransferase which adds sialic acid, and N-acetylglucosaminyltransferase-III which adds bisecting GlcNAc.

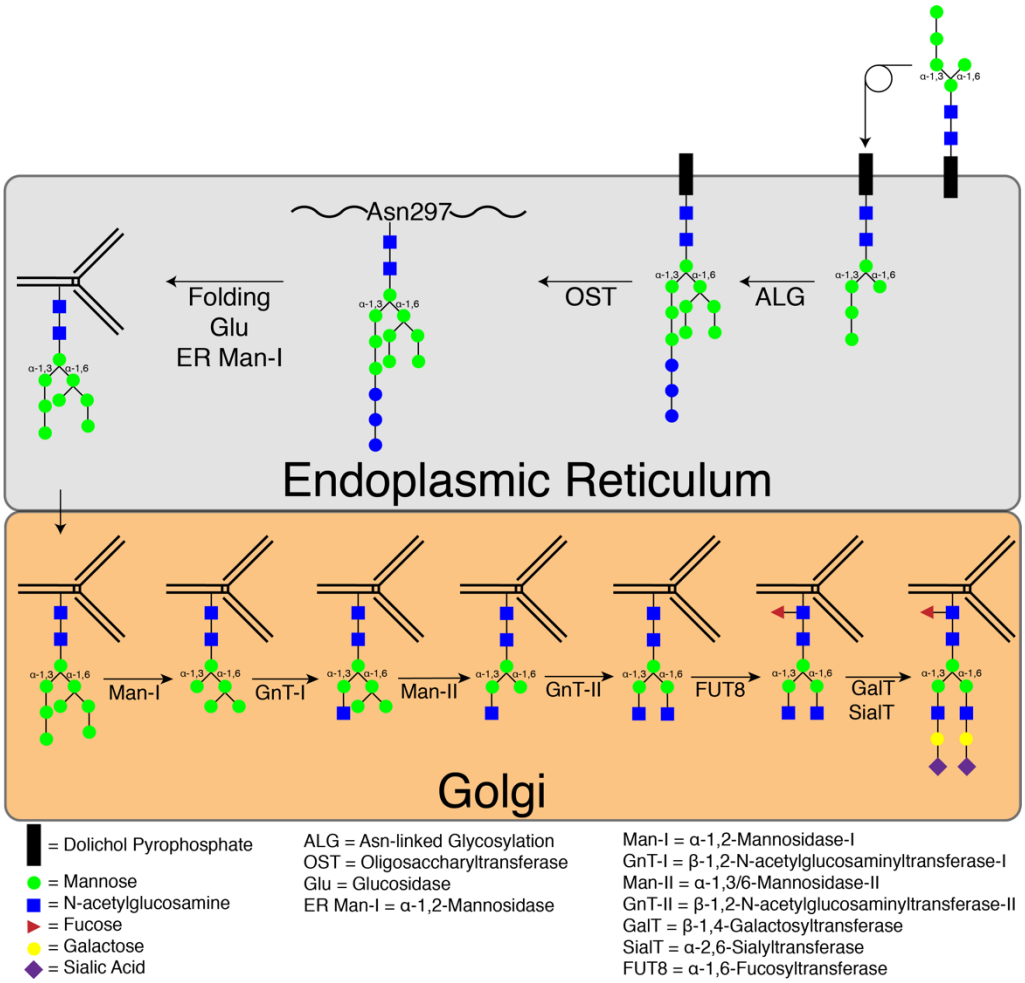

Figure 1.4: Pathway for N-glycan biosynthesis in mammalian cells. The glycoprotein depicted is IgG1 for the relevance to this dissertation, but this pathway applies to other proteins. This figure is a simplified description of N-glycan biosynthesis. For a more complete description, please see Moremen, Tiemeyer, and Nairn (2012) or Stanley, Taniguchi, and Aebi (2017).[25, 26]

N-glycan biosynthesis is an assembly line process, and the substrate specificities of these enzymes are very dependent on the processing by earlier enzymes in the assembly line. Incomplete processing at a particular step will truncate the process, which, given the numerous steps, gives rise to the heterogeneity of N-glycoforms that are observed during expression. There are two categories of heterogeneity: Macro and micro. Macroheterogeneity refers to the presence or absence of the entire N-glycan at the -Asn-Xxx-Ser/Thr- site. The addition of the STT3D gene from *Leishmania major* has been shown to increase glycan site occupancy of IgG1 expressed in the yeast *Pichia pastoris*.[29] Microheterogeneity refers to differences within a glycan, which is represented in **Figure 1.3**. Biantennary N-glycans are divided into three classifications: oligomannose, hybrid, and complex (**Figure 1.5**). All classifications share a penta-saccharide core, but the classifications are differentiated by the sugar residue that extends the two antennae from the penta-saccharide core. Oligomannose N-glycans are extended on both antennae by Man residues. Hybrid N-glycans are extended on one antenna by Man and the other by GlcNAc. Complex N-glycans are extend on both antennae by GlcNAc. In the biosynthetic pathway, oligomannose N-glycans are processed into hybrid, which are further processed into complex. Although complex is the predominant type, IgG1-based therapeutics show the presence of oligomannose, hybrid, and complex N-glycoforms.[27]

N-glycosylation is a highly variable process that depends on the organism, cell type, protein, site within the protein, and even the extracellular conditions.[26] In pharmaceuticals, glycosylation can have a big effect on product quality, influencing properties such as stability, solubility, susceptibility to proteases, susceptibility to aggregation, pharmacokinetics, and bioactivity.[28, 30] Therefore, it is important to have consistent expression conditions during

manufacturing in order to obtain a reproducible N-glycosylation profile from batch to batch. It is also a big concern for the production of biosimilars, which is currently an expanding market.[31, 32]

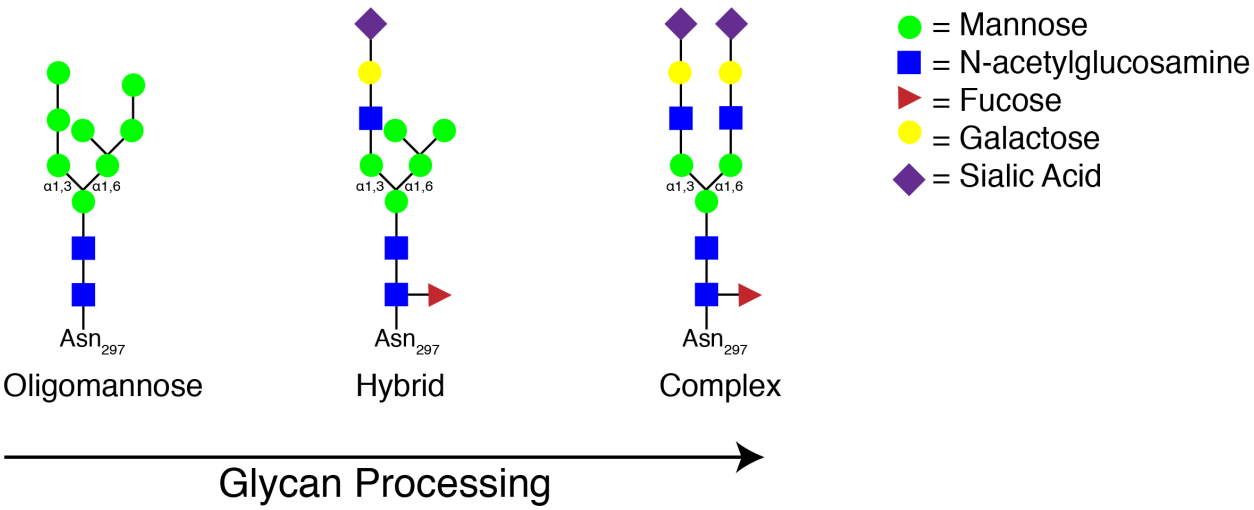

Figure 1.5: Representative examples of oligomannose, hybrid, and complex N-glycoforms.

1.7 Production of homogenous N-glycoforms

N-glycan heterogeneity makes it difficult to understand how N-glycosylation affects IgG1 because different N-glycoforms can affect the antibody differently.[28] For instance, the addition of terminal sialic acid to the N-glycan reduces ADCC activity,[33] whereas the addition of terminal galactose increases ADCC.[34, 35] Therefore, there is a lot of interest to develop antibodies with more homogenous glycosylation and then study each N-glycoform individually. To accomplish this, several methods have been employed. First, genetically modifying the expression cell lines by deleting a particular gene that encodes a particular glyco-processing enzyme can truncate the N-glycoform at a particular step. For example, near-homogenous Man_5-$GlcNAc_2$-Asn IgG1 Fc N-glycoforms have been obtained by expressing the protein in HEK293S cells, which are deficient in N-acetylglucosaminyltransferase-I.[36, 37] In another example,

afucosylated antibodies have been produced by expressing the antibodies in cells that are deficient in α1,6-fucosyltransferase.[14] Second, using *in-vitro* enzymatic synthesis can be used to produce homogenous N-glycoforms post-expression. This method first requires the expression of a near-homogenous N-glycoform, which is obtained during in the earlier stages of the biosynthetic pathway. Then, enzymatic synthesis is performed *in vitro*. For example, homogenous IgG Fc N-glycoforms have been produced using this method for obtaining a crystal structure and for biosimilarity analysis.[38, 39] Third, enzyme inhibitors can be added to the culture medium during expression to inhibit activity of a particular glyco-processing enzyme, which truncates the N-glycoform at a particular step.[40] This method has been used to produce somewhat homogenous IgG1 Fc N-glycoforms for structural analysis. All three of these methods have been used to prepare homogenous IgG1 Fc N-glycoforms in order to better understand the impact of N-glycosylation on IgG1.

1.8 IgGs have extended half-lives

Most peptides and small proteins have short half-lives because their small size makes them susceptible to rapid removal from the body by renal clearance. In contrast, most IgG subclasses have relatively long half-lives. IgG1 has a reported half-life in humans of 21 days.[41] The long half-life of IgGs is due in part to their large size (150 kDa) but also because of their salvation from lysosomal degradation by neonatal Fc receptors (FcRn) (**Figure 1.6**). This receptor is named neonatal because it was initially discovered on neonatal epithelial cells as a way to transport IgG antibodies from mother to fetus during gestation.[42] However, FcRn has since been found on a variety other cell types in adults to prevent degradation of internalized IgG.[43-46] When circulating proteins are endocytosed, they are typically shuttled to the lysosome

for degradation. However, endocytosed IgG are bound by FcRn in the early endosome and recycled back into circulation. The acidic pH of the endosome promotes Fc binding to FcRn, whereas the neutral pH of the plasma reduces the binding affinity by two orders of magnitude[47]. Mice deficient in FcRn showed approximately a 10-fold increase in IgG elimination over wild-type mice.[48] Conversely, an IgG1 antibody was mutated to increase affinity for FcRn at acidic pH but not affect the affinity at neutral pH, and it exhibited an 11-fold increase in half-life.[49] An increased half-life due to binding FcRn has been correlated to an increased therapeutic efficacy.[50]

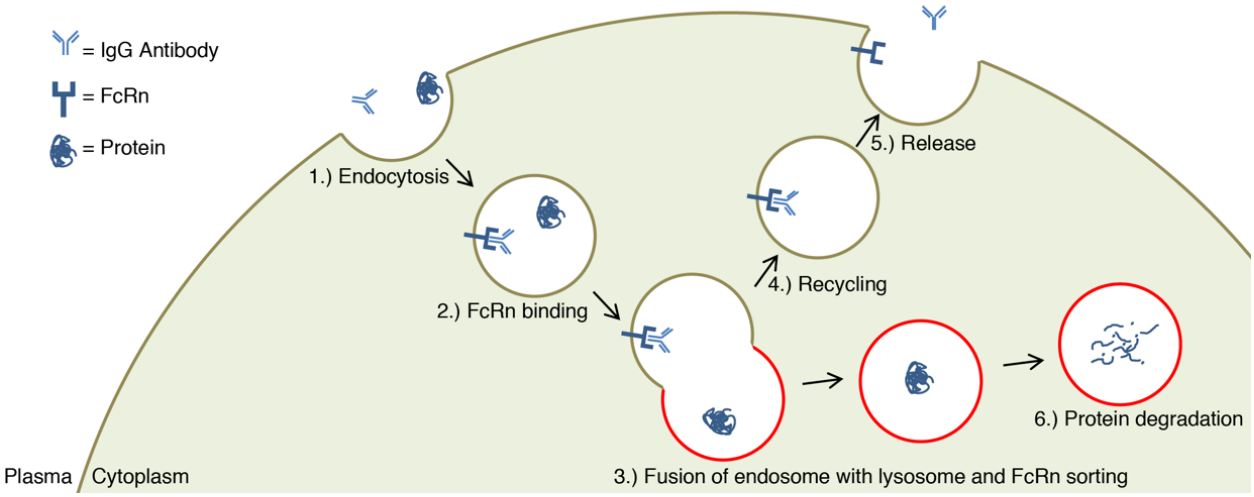

Figure 1.6: Neonatal Fc receptor (FcRn) prolongs half-life of circulating of IgGs. 1.) Proteins in plasma are endocytosed. 2.) As the endosome matures, the pH in the endosome lowers, which causes FcRn bind IgG. 3.) The endosome fuses with lysosome. 4.) IgG bound to FcRn is trafficked out of the lysosome. 5.) Endosome buds with plasma membrane and the pH increases, which weakens binding of IgG to FcRn, and IgG is released back into circulation. 6.) Proteins that did not bind to FcRn are degraded in the lysosome.

1.9 Importance of Antibody-based Therapeutics

Antibody-based therapeutics are a rapidly expanding class of biopharmaceuticals. The number of approved antibody-based therapeutics by the FDA and EMA has more than doubled

in the last five years, and they are expanding into areas such as antibody-drug conjugates, bispecific antibodies, and biosimilars.[51] Antibodies serve as attractive drug platforms because their specificity can be designed, their long half-life, their ability to elicit antibody effector functions, and their divalent binding to target. Some antibody-based therapeutics function by modifying the immune system. These drugs have been used to treat a variety of disease-types including cancer,[52] autoimmune diseases,[53] and organ transplant rejection.[54, 55] Some therapeutics are immunostimulants, such as trastuzumab (Herceptin®) and cetuximab (Erbitux®), which have been shown activate ADCC.[56, 57] On the other hand, some work by suppressing the immune system by blocking immune cell activation or upregulating the inhibitory mechanisms.[23, 24, 55] The stimulating or inhibitory activity of antibody-based therapeutics can depend on the particular FcγRs that are activated, which can be tailored by modifying the antibody's subclass and N-glycosylation.

1.10 IgG1 Fc Fusion Proteins

IgG1 Fc fusion proteins are a prominent class of biopharmaceutics, exemplified by the blockbuster drug etanercept (Enbrel®).[58, 59] In 2010, etanercept grossed $7.3 billion in global sales, which was more than any monoclonal antibody that year. Seven IgG1 Fc fusions have been approved by the FDA for the treatment of several immune disorders including rheumatoid arthritis and organ transplant rejection. IgG1 Fc fusions are composed of both a bioactive fusion partner, typically a peptide or small protein, and the Fc region of the human IgG1 antibody (**Figure 1.7**). The conjugation of these two species provide the bioactive fusion partner with several potential benefits: 1.) Increased half-life. IgG1 has a long half-life, which is mainly due to salvation from intracellular degradation by FcRn (**Figure 1.6**). 2.) Increased solubility. Fusion

proteins have been used to increase the solubility of poorly soluble peptides and proteins.[60] IgG1 is capable of being formulated at very high concentrations (>150 mg/mL).[61] 3.) The ability to elicit antibody-mediated effector functions. The Fc region can bind with FcγRs, which can activate antibody-mediated effector functions. 4.) Increased valency. IgG1 Fc fusions are most commonly prepared using recombinant DNA technology. The Fc is a homodimer, so recombinant fusion to the N- or C-terminus results in 2 bioactive fusion partners per Fc. Fusion to both termini results in 4 bioactive fusion partners per Fc. Furthermore, one fusion partner can be fused to one terminus and a different fusion partner to the other terminus, resulting in an Fc fusion with bi-specificity. A good example of utilizing an IgG1 Fc fusion for increased valency is etanercept. Etanercept is an IgG1 Fc fusion protein with two Tumor Necrosis Factor (TNF) receptors on its N-termini. Etanercept functions to compete with TNF receptors on immune cells for the proinflammatory-inducing cytokine TNF-α. TNF-α is trivalent, so having two TNF receptors on etanercept binds TNF-α with 50-1000X stronger avidity than monomeric TNF receptor.[62]

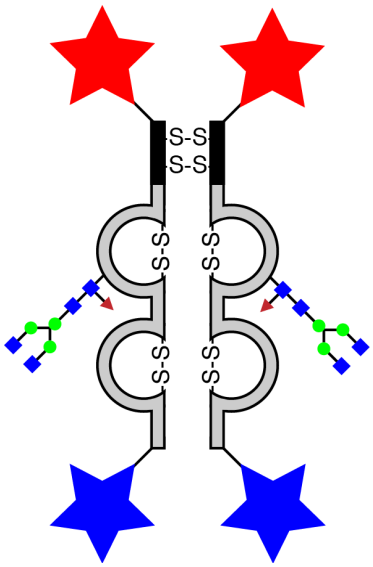

Figure 1.7: Representation of an Fc Fusion. The stars represent the bioactive fusion partners. The colors of the stars on the Fc termini are different to represent that two different bioactive fusion partners could be added

1.11 References

(1) Kindt, T. J., Goldsby, R. A., Osborne, B. A., and Kuby, J. (2007) *Kuby Immunology*, W. H. Freeman, New York.

(2) Takeuchi, O., and Akira, S. (2010) Pattern recognition receptors and inflammation. *Cell 140*, 805-820.

(3) Janeway, C. J., Travers, P., and Walport, M. (2001) The generation of diversity in immunoglobulins, in *Immunobiology: The Immune System in Health and Disease*, Garland Science, New York.

(4) Jennewein, M. F., and Alter, G. (2017) The immunoregulatory roles of antibody glycosylation. *Trends in immunology 38*, 358-372.

(5) Rajpal, A., Strop, P., Yeung, Y. A., Chaparro-Riggers, J., and Pons, J. (2013) Introduction: Antibody Structure and Function, in *Therapeutic Fc-Fusion Proteins*, Wiley.

(6) Berg, J. M., Tymoczko, J. L., and Stryer, L. (2002) The Immunoglobulin Fold Consists of a Beta-Sandwich Framework with Hypervariable Loops, in *Biochemistry*, W H Freeman, New York.

(7) Duncan, A. R., and Winter, G. (1988) The binding site for C1q on IgG. *Nature 332*, 738.

(8) Bredius, R., Fijen, C., De Haas, M., Kuijper, E., Weening, R., Van de Winkel, J., and Out, T. (1994) Role of neutrophil Fc gamma RIIa (CD32) and Fc gamma RIIIb (CD16) polymorphic forms in phagocytosis of human IgG1-and IgG3-opsonized bacteria and erythrocytes. *Immunology 83*, 624.

(9) Román, V. R. G., Murray, J. C., and Weiner, L. M. (2014) Antibody-Dependent Cellular Cytotoxicity (ADCC), in *Antibody Fc* pp 1-27, Elsevier.

(10) Tang, Y., Lou, J., Alpaugh, R. K., Robinson, M. K., Marks, J. D., and Weiner, L. M. (2007) Regulation of antibody-dependent cellular cytotoxicity by IgG intrinsic and apparent affinity for target antigen. *The Journal of Immunology 179*, 2815-2823.

(11) Velders, M., Van Rhijn, C., Oskam, E., Fleuren, G., Warnaar, S., and Litvinov, S. (1998) The impact of antigen density and antibody affinity on antibody-dependent cellular cytotoxicity: relevance for immunotherapy of carcinomas. *British journal of cancer 78*, 478-483.

(12) Lazar, G. A., Dang, W., Karki, S., Vafa, O., Peng, J. S., Hyun, L., Chan, C., Chung, H. S., Eivazi, A., and Yoder, S. C. (2006) Engineered antibody Fc variants with enhanced effector function. *Proceedings of the National Academy of Sciences of the United States of America 103*, 4005-4010.

(13) Shields, R. L., Lai, J., Keck, R., O'Connell, L. Y., Hong, K., Meng, Y. G., Weikert, S. H., and Presta, L. G. (2002) Lack of fucose on human IgG1 N-linked oligosaccharide improves binding to human FcγRIII and antibody-dependent cellular toxicity. *Journal of Biological Chemistry 277*, 26733-26740.

(14) Yamane-Ohnuki, N., Kinoshita, S., Inoue-Urakubo, M., Kusunoki, M., Iida, S., Nakano, R., Wakitani, M., Niwa, R., Sakurada, M., and Uchida, K. (2004) Establishment of FUT8 knockout Chinese hamster ovary cells: An ideal host cell line for producing completely defucosylated antibodies with enhanced antibody-dependent cellular cytotoxicity. *Biotechnology and bioengineering 87*, 614-622.

(15) Oganesyan, V., Damschroder, M. M., Leach, W., Wu, H., and Dall'Acqua, W. F. (2008) Structural characterization of a mutated, ADCC-enhanced human Fc fragment. *Molecular immunology 45*, 1872-1882.

(16) Strohl, W. R. (2009) Optimization of Fc-mediated effector functions of monoclonal antibodies. *Current opinion in biotechnology 20*, 685-691.

(17) Stavenhagen, J. B., Gorlatov, S., Tuaillon, N., Rankin, C. T., Li, H., Burke, S., Huang, L., Johnson, S., Bonvini, E., and Koenig, S. (2007) Fc optimization of therapeutic antibodies enhances their ability to kill tumor cells in vitro and controls tumor expansion in vivo via low-affinity activating Fcγ receptors. *Cancer research 67*, 8882-8890.

(18) Nimmerjahn, F., and Ravetch, J. V. (2008) Fcγ receptors as regulators of immune responses. *Nature Reviews Immunology 8*, 34-47.

(19) Nimmerjahn, F., Gordan, S., and Lux, A. (2015) FcγR dependent mechanisms of cytotoxic, agonistic, and neutralizing antibody activities. *Trends in immunology 36*, 325-336.

(20) Nimmerjahn, F., and Ravetch, J. V. (2006) Fcγ receptors: old friends and new family members. *Immunity 24*, 19-28.

(21) Nagarajan, S., Venkiteswaran, K., Anderson, M., Sayed, U., Zhu, C., and Selvaraj, P. (2000) Cell-specific, activation-dependent regulation of neutrophil CD32A ligand-binding function. *Blood 95*, 1069-1077.

(22) Hogarth, P. M., and Pietersz, G. A. (2012) Fc receptor-targeted therapies for the treatment of inflammation, cancer and beyond. *Nature reviews. Drug discovery 11*, 311-31.

(23) Kaneko, Y., Nimmerjahn, F., and Ravetch, J. V. (2006) Anti-inflammatory activity of immunoglobulin G resulting from Fc sialylation. *Science's STKE 313*, 670-673.

(24) Anthony, R. M., Kobayashi, T., Wermeling, F., and Ravetch, J. V. (2011) Intravenous gammaglobulin suppresses inflammation through a novel TH2 pathway. *Nature 475*, 110-113.

(25) Moremen, K. W., Tiemeyer, M., and Nairn, A. V. (2012) Vertebrate protein glycosylation: diversity, synthesis and function. *Nature reviews Molecular cell biology 13*, 448-462.

(26) Stanley P, Taniguchi N, and M, A. (2017) N-Glycans, in *Essentials of Glycobiology*, Cold Springs Harbor, New York.

(27) Giorgetti, J., D'Atri, V., Canonge, J., Lechner, A., Guillarme, D., Colas, O., Wagner-Rousset, E., Beck, A., Leize-Wagner, E., and François, Y.-N. (2018) Monoclonal antibody N-glycosylation profiling using capillary electrophoresis–Mass spectrometry: Assessment and method validation. *Talanta 178*, 530-537.

(28) Higel, F., Seidl, A., Sörgel, F., and Friess, W. (2016) N-glycosylation heterogeneity and the influence on structure, function and pharmacokinetics of monoclonal antibodies and Fc fusion proteins. *European Journal of Pharmaceutics and Biopharmaceutics 100*, 94-100.

(29) Choi, B.-K., Warburton, S., Lin, H., Patel, R., Boldogh, I., Meehl, M., d'Anjou, M., Pon, L., Stadheim, T. A., and Sethuraman, N. (2012) Improvement of N-glycan site occupancy of therapeutic glycoproteins produced in Pichia pastoris. *Applied microbiology and biotechnology 95*, 671-682.

(30) Solá, R. J., and Griebenow, K. (2009) Effects of glycosylation on the stability of protein pharmaceuticals. *Journal of pharmaceutical sciences 98*, 1223-1245.

(31) Pisupati, K., Tian, Y., Okbazghi, S., Benet, A., Ackermann, R., Ford, M., Saveliev, S., Hosfield, C. M., Urh, M., and Carlson, E. (2017) A multidimensional analytical comparison of Remicade and the biosimilar Remsima. *Analytical chemistry 89*, 4838-4846.

(32) Pisupati, K., Benet, A., Tian, Y., Okbazghi, S., Kang, J., Ford, M., Saveliev, S., Sen, K. I., Carlson, E., Tolbert, T. J., Ruotolo, B. T., Schwendeman, S. P., and Schwendeman, A. (2017) Biosimilarity under stress: a forced degradation study of Remicade® and Remsima™. *MAbs 9*, 1197-1209.

(33) Scallon, B. J., Tam, S. H., McCarthy, S. G., Cai, A. N., and Raju, T. S. (2007) Higher levels of sialylated Fc glycans in immunoglobulin G molecules can adversely impact functionality. *Molecular immunology 44*, 1524-1534.

(34) Thomann, M., Reckermann, K., Reusch, D., Prasser, J., and Tejada, M. L. (2016) Fc-galactosylation modulates antibody-dependent cellular cytotoxicity of therapeutic antibodies. *Molecular immunology 73*, 69-75.

(35) Wada, R., Matsui, M., and Kawasaki, N. (2019) Influence of N-glycosylation on effector functions and thermal stability of glycoengineered IgG1 monoclonal antibody with homogeneous glycoforms. *mAbs 11*, 350-372.

(36) Yu, X., Baruah, K., Harvey, D. J., Vasiljevic, S., Alonzi, D. S., Song, B.-D., Higgins, M. K., Bowden, T. A., Scanlan, C. N., and Crispin, M. (2013) Engineering hydrophobic protein–carbohydrate interactions to fine-tune monoclonal antibodies. *Journal of the American Chemical Society 135*, 9723-9732.

(37) Barb, A. W. (2014) Intramolecular N-Glycan/Polypeptide Interactions Observed at Multiple N-Glycan Remodeling Steps through [13C, 15N]-N-Acetylglucosamine Labeling of Immunoglobulin G1. *Biochemistry 54*, 313-322.

(38) Okbazghi, S. Z., More, A. S., White, D. R., Duan, S., Shah, I. S., Joshi, S. B., Middaugh, C. R., Volkin, D. B., and Tolbert, T. J. (2016) Production, characterization, and biological evaluation of well-defined IgG1 Fc glycoforms as a model system for biosimilarity analysis. *Journal of pharmaceutical sciences 105*, 559-574.

(39) Shah, I. S., Lovell, S., Mehzabeen, N., Battaile, K. P., and Tolbert, T. J. (2017) Structural characterization of the Man5 glycoform of human IgG3 Fc. *Molecular immunology 92*, 28-37.

(40) Chang, V. T., Crispin, M., Aricescu, A. R., Harvey, D. J., Nettleship, J. E., Fennelly, J. A., Yu, C., Boles, K. S., Evans, E. J., and Stuart, D. I. (2007) Glycoprotein structural genomics: solving the glycosylation problem. *Structure 15*, 267-273.

(41) Morell, A., Terry, W. D., and Waldmann, T. A. (1970) Metabolic properties of IgG subclasses in man. *Journal of Clinical Investigation 49*, 673-680.

(42) Jones, E. A., and Waldmann, T. A. (1972) The mechanism of intestinal uptake and transcellular transport of IgG in the neonatal rat. *Journal of Clinical Investigation 51*, 2916-2927.

(43) Roopenian, D. C., and Akilesh, S. (2007) FcRn: the neonatal Fc receptor comes of age. *Nature reviews immunology 7*, 715-725.

(44) Lobo, E. D., Hansen, R. J., and Balthasar, J. P. (2004) Antibody pharmacokinetics and pharmacodynamics. *Journal of pharmaceutical sciences 93*, 2645-2668.

(45) Suzuki, T., Ishii-Watabe, A., Tada, M., Kobayashi, T., Kanayasu-Toyoda, T., Kawanishi, T., and Yamaguchi, T. (2010) Importance of neonatal FcR in regulating the serum half-life of therapeutic proteins containing the Fc domain of human IgG1: a comparative study of the affinity of monoclonal antibodies and Fc-fusion proteins to human neonatal FcR. *The Journal of immunology 184*, 1968-1976.

(46) Ober, R. J., Martinez, C., Lai, X., Zhou, J., and Ward, E. S. (2004) Exocytosis of IgG as mediated by the receptor, FcRn: an analysis at the single-molecule level. *Proceedings of the National Academy of Sciences of the United States of America 101*, 11076-11081.

(47) Raghavan, M., Bonagura, V. R., Morrison, S. L., and Bjorkman, P. J. (1995) Analysis of the pH dependence of the neonatal Fc receptor/immunoglobulin G interaction using antibody and receptor variants. *Biochemistry 34*, 14649-14657.

(48) Junghans, R., and Anderson, C. (1996) The protection receptor for IgG catabolism is the beta2-microglobulin-containing neonatal intestinal transport receptor. *Proceedings of the National Academy of Sciences 93*, 5512-5516.

(49) Petkova, S. B., Akilesh, S., Sproule, T. J., Christianson, G. J., Al Khabbaz, H., Brown, A. C., Presta, L. G., Meng, Y. G., and Roopenian, D. C. (2006) Enhanced half-life of genetically engineered human IgG1 antibodies in a humanized FcRn mouse model: potential application in humorally mediated autoimmune disease. *International immunology 18*, 1759-1769.

(50) Zalevsky, J., Chamberlain, A. K., Horton, H. M., Karki, S., Leung, I. W., Sproule, T. J., Lazar, G. A., Roopenian, D. C., and Desjarlais, J. R. (2010) Enhanced antibody half-life improves in vivo activity. *Nature Biotechnology 28*, 157-159.

(51) Grilo, A. L., and Mantalaris, A. (2019) The increasingly human and profitable monoclonal antibody market. *Trends in biotechnology 37*, 9-16.

(52) Weiner, G. J. (2015) Building better monoclonal antibody-based therapeutics. *Nature Reviews Cancer 15*, 361-370.

(53) Graf, J., Aktas, O., Rejdak, K., and Hartung, H.-P. (2019) Monoclonal Antibodies for Multiple Sclerosis: An Update. *BioDrugs*, 1-18.

(54) Pescovitz, M. (2006) Rituximab, an anti-cd20 monoclonal antibody: history and mechanism of action. *American Journal of Transplantation 6*, 859-866.

(55) Powelson, J. A., Cosimi, A. B., and Wee, S. (1993) Monoclonal antibodies in organ transplantation. *Biotechnology advances 11*, 725-740.

(56) Kurai, J., Chikumi, H., Hashimoto, K., Yamaguchi, K., Yamasaki, A., Sako, T., Touge, H., Makino, H., Takata, M., and Miyata, M. (2007) Antibody-dependent cellular cytotoxicity mediated by cetuximab against lung cancer cell lines. *Clinical Cancer Research 13*, 1552-1561.

(57) Arnould, L., Gelly, M., Penault-Llorca, F., Benoit, L., Bonnetain, F., Migeon, C., Cabaret, V., Fermeaux, V., Bertheau, P., and Garnier, J. (2006) Trastuzumab-based treatment of HER2-positive breast cancer: an antibody-dependent cellular cytotoxicity mechanism? *British journal of cancer 94*, 259-267.

(58) Beck, A., and Reichert, J. M. (2011) in *MAbs* pp 415-416, Landes Bioscience.

(59) Czajkowsky, D. M., Hu, J., Shao, Z., and Pleass, R. J. (2012) Fc-fusion proteins: new developments and future perspectives. *EMBO Mol Med 4*, 1015-1028.

(60) Marblestone, J. G., Edavettal, S. C., Lim, Y., Lim, P., Zuo, X., and Butt, T. R. (2006) Comparison of SUMO fusion technology with traditional gene fusion systems: enhanced expression and solubility with SUMO. *Protein Science 15*, 182-189.

(61) Neergaard, M. S., Kalonia, D. S., Parshad, H., Nielsen, A. D., Møller, E. H., and van de Weert, M. (2013) Viscosity of high concentration protein formulations of monoclonal antibodies of the IgG1 and IgG4 subclass–Prediction of viscosity through protein–protein interaction measurements. *European Journal of Pharmaceutical Sciences 49*, 400-410.

(62) Goffe, B., and Cather, J. C. (2003) Etanercept: an overview. *Journal of the American Academy of Dermatology 49*, 105-111.

Chapter 2

Synthesis of a Bifunctional Peptide Inhibitor–IgG1 Fc Fusion that Suppresses Experimental Autoimmune Encephalomyelitis

2.1 Introduction

Multiple sclerosis (MS) is an autoimmune disease of the central nervous system.[1] The disease affects approximately 2.3 million people worldwide.[2] Those affected experience a wide variety of neurological disabilities including impairments in mobility[3], cognition[4], and psychological health[5]. These neurological disabilities result from the loss of myelin, which is the lipoprotein sheath coating the axons of the central nervous system. Demyelination can be observed in the brain scans of MS patients as brain lesions.[6] The etiology of MS is still unknown but suspected reasons include genetic, environmental, geographical, viral, and lifestyle factors.[7-10] The disease is extremely complex and heterogeneous, with involvement by both the humoral and cellular immune responses.[11-13] The disease involves the activation of autoreactive T-cells against myelin proteins that infiltrate the brain to damage the myelin sheath of the neuronal axons. [14-16] The myelin proteins that are recognized by the autoreactive T-cells include proteolipid protein (PLP), myelin oligodendrocyte protein (MOG), and myelin basic protein (MBP). Currently, there is no cure for MS, and the currently available treatments such as beta interferons, glatiramer acetate, fingolimod, teriflunomide, dimethyl fumarate, and monoclonal antibodies are geared toward reducing symptom severity and frequency of attack.[17-19] Some of the current treatments suppress general immune responses, which can increase pathogenic infections in treated patients. Therefore, there is a need to develop MS treatments that selectively suppress autoreactive T-cells against myelin proteins.

Bifunctional Peptide Inhibitors (BPIs) are a promising new class of peptide conjugates that are designed to selectively inhibit the maturation of T-cells specific for myelin protein.[20] BPIs are composed of a myelin-specific antigenic peptide tethered to a signal-2-blocking peptide

derived from lymphocyte function-associated antigen-1 (LFA-1), a protein found on T-cells that binds to intercellular adhesion molecule-1 (ICAM-1) (**Table 2.1**).

Table 2.1: BPI-Fc Fusion Peptides

Peptide Name	Representation	Sequence[a]
ICAM-1 Binding Peptide $CD11a_{237–246}$ (LABL)[b]	LABL	G**ITDGEATDSG**GG
Proteolipid $Protein_{139-151}$ (PLP)[c]	PLP	GGG**HSLGKWLGHPDKF**G
Myelin Oligodendrocyte $Glycoprotein_{38-50}$ (MOG)[c]	MOG	GG**GWYRSPFSRVVHL**GRR
Sortase A Substrate Tag (ST)[d]	ST	AAALPETGGG

[a]The active regions of the sequences are shown in bold.
[b]Signal-2-blocking peptide derived from LFA-1 that binds ICAM-1.
[c]Myelin-derived antigenic peptides.
[d]Peptide tag for enzymatic C-terminal protein ligations.

For example, a myelin antigenic peptide (e.g., $PLP_{139-151}$[21-26] or MOG_{38-50}[25]) linked to a LABL ($CD11a_{237-246}$) peptide,[21-23, 25] derived from the I-domain of LFA-1, through a short linker is a BPI. It is hypothesized that BPIs suppress autoreactive T-cells by blocking the formation of the immunological synapse (IS) at the interface of a T-cell and antigen presenting cell (APC) because the mechanism of activating T-cells is initiated by the formation of the IS (**Figure 2.1**).[20, 27, 28] The IS is formed by at least two signals in which the first signal (signal-1) is generated via the interactions between the complex of antigen-major histocompatibility complex class II (Ag-MHC-II) and a T-cell receptor (TCR). The second signal (signal-2) can be generated by ICAM-1/LFA-1 interactions. Initially, signal-2 is formed in the center of the interface between an APC and a T-cell while signal-1 is formed at the periphery of the interface to form a bullseye-like arrangement. Then, the signal-1 molecules translocate to cluster at the center while the signal-2 molecules migrate to peripheral region of the bullseye to form an IS. The IS

formation initiates the activation of a naïve T-cell into a proinflammatory T-cell (**Figure 2.1**). This proinflammatory T-cell promotes antigen-specific immune system attack on myelin, causing its inflammation and breakdown.[15] BPI molecules are hypothesized to bind simultaneously to MHC-II and ICAM-1 on the surface of an APC and inhibit the formation of the IS.[29] As a result, BPIs alter the commitment of naïve T-cells from an inflammatory phenotype to regulatory or suppressor phenotypes, and this suppresses autoimmune diseases in an antigen-specific manner. While antigenic peptides and signal-2 blocker peptides have been shown to have some ability to reduce T-cell activation on their own, Kobayashi *et al.* have demonstrated that linking the two types of peptides to form BPIs results in significantly lower clinical scores in an EAE model.[21] However, one potential problem with BPIs is the short *in vivo* half-lives of a few hours (2-3 hours) as measured in rat plasma; therefore, there is a need to investigate methods to lengthen the *in-vivo* half-lives of these types of molecules.[22]

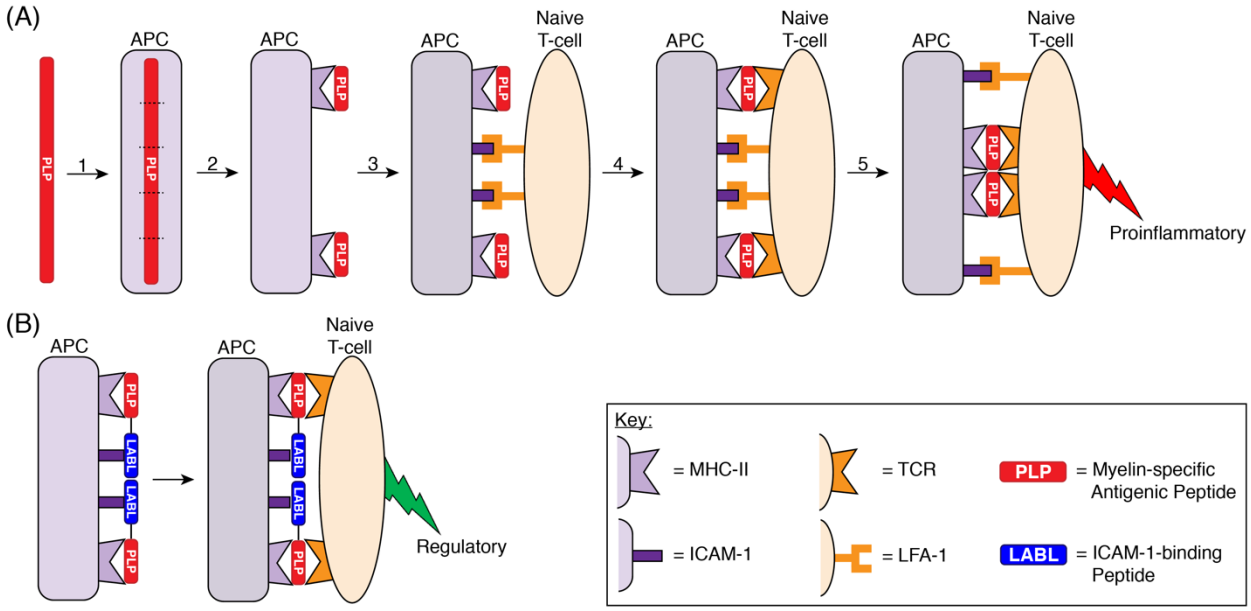

Figure 2.1: Two-signal model of T-cell activation highlighting the role of the ICAM-1–LFA-1 receptor pairing for both adhesion and costimulation are highlighted as well as the alteration of T-cell activation by a BPI. (A) Mechanism of proinflammatory T-cell activation against myelin protein. (1) Myelin-specific antigen is internalized by an APC and broken into fragments. (2) The antigen fragments are presented on the APC cell surface by MHC-II. (3) A naïve $CD4^+$ T-cell binds to the APC through the adhesion receptor pairings of ICAM-1 on the APC and LFA-1 on the T-cell. (4) If the naïve T-cell contains TCRs capable of recognizing the particular antigen presented by MHC-II, then the TCR binds the Ag-MHC-II complex to initiate signal-1 on the periphery. The ICAM-1–LFA-1 receptor pairings also function as costimulatory molecules to constitute signal-2 in a central cluster. (5) The two signals reorganize so that signal-1 pairings localize in the central cluster and the signal-2 pairings localize to the periphery of the signal-1 cluster to form the immunological synapse, which directs the maturation of a naïve T-cell into a proinflammatory T-cell against the myelin antigen. (B) Intervention of myelin-specific T-cell activation by a BPI. A BPI molecule consists of two peptides, a myelin-specific antigenic peptide (PLP) and a signal-2 blocking peptide (LABL), conjugated together. The antigenic peptide of the BPI allows formation of Ag–MHC-II pairing with the TCR to form signal-1 but inhibits the ICAM-1–LFA-1 receptor pairing to prevent formation of signal-2. Because the BPI peptides are conjugated together, the BPI is hypothesized to inhibit formation of the IS and alter the maturation of the naïve T-cell into a regulatory T-cell.

In this work, a BPI-Fc fusion was prepared in which the two BPI peptides, a myelin-specific antigenic peptide and a signal-2-blocking peptide, were conjugated to the N- and C-termini of the fragment crystallizable (Fc) region of a human IgG1 antibody. This BPI-Fc fusion protein was designed with the goal of suppressing experimental autoimmune encephalomyelitis

(EAE) in mice. Using the Fc as a platform may increase the half-life of the BPI-Fc due to recycling by the FcRn receptor as well as reduced renal clearance because of increased molecular weight (4 kDa of traditional BPI compared to 57 kDa of BPI-Fc).[30] Additionally, the Fc is a homodimer which allows the attachment of two of each of the BPI peptides to the Fc scaffold, potentially increasing avidity in binding interactions of the BPI peptides to their respective receptors. Furthermore, fusing to the Fc allows for increased solubility of insoluble peptides. This work was a proof-of-concept project to determine whether a BPI-Fc fusion could be prepared and whether the BPI peptides could still function to protect against EAE when they are separated by a 223 amino acid Fc protein.[31]

2.2 Materials and Methods

2.2.1 Materials

DNA primers were ordered from Eurofins (Huntsville, AL). IgG1 cDNA (MGC: 12853) was previously purchased from the American Tissue Culture Collection (Manassas, VA).[32] pGAPzαA and pPICzαA vectors were purchased from Invitrogen (USA). All restriction enzymes, T4 Polynucleotide Kinase (PNK), T4 DNA Ligase, and protein markers were purchased from New England BioLabs (Ipswich, MA). All final DNA constructs were confirmed by DNA sequencing. Zeocin was purchased from InvivoGen (San Diego, CA). Tryptone and yeast extract were both purchased from Becton, Dickinson and Company (Sparks, MD). Yeast nitrogen base was purchased from Sunrise Science Products (San Diego, CA). Fmoc-PAL-PEG-PS resin and 1-[Bis(dimethylamino)methylene]-1H-1,2,3-triazolo[4,5-b]pyridinium 3-oxid hexafluorophosphate (HATU) were obtained from Applied Biosystems (Foster City, CA) and Chem-Impex International, Inc. (Wood Dale, IL), respectively. Protected amino acids were

purchased from Peptides International (Louisville, KY), Bachem (Torrance, CA), and Sigma-Aldrich (St. Louis, MO). Triisopropylsilane (TIPS) and N,N-diisopropylethylamine (DIEA) were also purchased from Sigma-Aldrich. Detoxi-Gel Endotoxin Removing Gel was purchased from Thermo Scientific (Waltham, MA). All other chemicals were obtained from commercial sources without further purification. Protein G resin was prepared in house as previously described.[33, 34] All materials and reagents, except for the protein markers, used for SDS-PAGE were purchased from Bio-Rad Laboratories (Hercules, CA), and the experimental method used for SDS-PAGE is described in **Appendix 1: A.1.1.3.1**. All protein mass spectra, except those pertaining to PLP-Fc-LABL (spinner flask with media change), MOG-Fc, and LABL-Fc-ST (spinner flask) proteins were acquired using an Agilent 6520 electrospray ionization time-of-flight liquid chromatography mass spectrometer (LC-MS) using a method previously described.[34] Mass spectra for PLP-Fc-LABL (spinner flask with media change), MOG-Fc, and LABL-Fc-ST (spinner flask) proteins were acquired by the KU Mass Spectrometry & Analytical Proteomics Laboratory using a Waters Synapt G2 quadrupole time-of-flight LC-MS using a method previously described.[35] Peptide:N-Glycosidase F (PNGase F) was prepared in house using a method previously described.[36] Cloning procedures for pPICzαA-PLP-Fc-LABL and pPICzαA-MOG-Fc and expression procedures for PLP-Fc- LABL (spinner flask, fermentor, and spinner flask with media change) are described in **Appendix 2: A.1.1**.

2.2.2 Cloning of pPICzαA-LABL-Fc-ST

A construct consisting of a human IgG1 Fc cDNA ($T_{225}\rightarrow K_{447}$) subcloned into pGAPzαA with a silent mutation to introduce a SacI restriction site near the 5' end of the Fc coding region (termed pGAPzαA-Fc) was produced previously in our laboratory and used as a starting point for producing the peptide-Fc fusion proteins described herein. The sortase A recognition tag (ST), a

peptide, was attached C-terminal to the Fc polypeptide sequence. This was accomplished by inserting DNA between the NotI site, which occurs after the last human IgG1 Fc encoded amino acid, and the XbaI site. Primers containing the ST DNA sequence (5'-ggccgccttgccagaaactggaggtggataat-3' and 5'-ctagattatccacctccagtttctggcaaggc-3') were designed so that when they anneal, they create the proper NotI and XbaI sticky ends. The 5'-termini of the primers were phosphorylated by PNK. pGAPzαA-Fc was digested with NotI-HF and XbaI, gel purified, and the ST DNA sequence was ligated to the 3' side of the Fc DNA using T4 DNA Ligase to create pGAPzαA-Fc-ST. The LABL DNA sequence was cloned on the 5' side of the Fc DNA in pGAPzαA-Fc-ST. Primers containing the LABL DNA sequence (5'-tcgagaaaagaggaattactgatggagaagctactgattctggaggtggaacatgcccaccgtgcccagcacctgagct-3' and 5'-caggtgctgggcacggtgggcatgttccacctccagaatcagtagcttctccatcagtaattcctcttttc-3') were designed so that when they anneal, they create the proper XhoI and SacI sticky ends. The 5'-termini of the primers were phosphorylated by PNK. pGAPzαA-Fc-ST was digested with XhoI and SacI, gel purified, and the digested LABL DNA sequence was ligated into pGAPzαA-Fc-ST on the 5' side of the Fc DNA using T4 DNA Ligase to create pGAPzαA-LABL-Fc-ST. To allow for inducible expression under the strong AOX promoter, the LABL-Fc-ST was cut out of pGAPzαA and ligated into pPICzαA. To perform this transfer, both pGAPzαA-LABL-Fc-ST DNA and pPICzαA were digested with XhoI and XbaI and gel purified. LABL-Fc-ST and pPICzαA digested products were ligated together using T4 DNA Ligase to create pPICzαA-LABL-Fc-ST. The plasmid was linearized using PmeI and transformed into a strain of *P. pastoris* with the OCH1 gene deleted as previously described.[32]

2.2.3 Expression and purification of LABL-Fc-ST (Fermentor)

A colony of *P. pastoris* OCH1 KO transformed with pPICzαA-LABL-Fc-ST was inoculated in a culture tube containing 2 mL of YPD media and 100 µg/mL Zeocin. The culture was grown in a shaker/incubator at 25°C. After 3 days, the 2 mL culture was transferred to a baffled shake flask containing 250 mL of YPD media, 100 µg/mL Zeocin, and 1 drop of antifoam. The culture was grown in a shaker/incubator at 25°C. After 3 days, the 250 mL culture was transferred to a New Brunswick BioFlo 415 fermentor (Hauppauge, NY) containing 5 L of sterilized Buffered Glycerol Complex Medium and PTM_1 salts at pH 6.0. The pH was maintained by the fermentor-controlled addition of concentrated NH_4OH, which also served as the nitrogen source. Agitation and gas flow were set under cascade control, which maintained an agitation range of 200-1000 rpm and a gas flow range of 1-20 L/min. The cells were grown on a carbon source feed of 50% glycerol in water for two days. After which, the carbon source was changed to 100% methanol to allow for induction of target protein. After 3 days of induction, the culture was harvested by centrifugation at 6,693 x g for 20 min using a Beckman JLA 10.5 rotor in a Beckman Avanti J-series centrifuge (USA). The supernatant was collected and filtered using a Buon Vino Mini Jet Wine Filter with 0.5 µm filter pads (Cambridge, Ontario). The filtered supernatant was then concentrated to 1 L using a Sartorius 30,000 MWCO tangential flow concentrator (USA). The LABL-Fc-ST protein was purified from the supernatant using Protein G affinity chromatography. First, 10 mL of Protein G resin was packed in a 1.5x20 cm diameter Bio-Rad Econo-column (Hercules, CA) and equilibrated with 250 mL of 20 mM Sodium Phosphate buffer pH 6.0. Then the concentrated supernatant was loaded onto the column and washed with 500 mL of 20 mM Sodium Phosphate buffer and 0.5 M NaCl at pH 6.0. The captured protein was eluted using 0.1 M Glycine-Cl buffer, pH 2.7. The column was re-equilibrated with 250 mL Sodium Phosphate buffer pH 6.0. This process was repeated until no

more protein eluted from the column. The collected protein was dialyzed against 4 L of TBS, pH 7.5 using Spectra/Por 3500 MWCO dialysis tubing (USA) at 4°C with two buffer changes. 105 mg of purified protein was obtained as determined by measuring the optical density of the solution at 280 nm (MW = 54006.8 Da, ε_{280} = 71570 $M^{-1}cm^{-1}$).[37]

2.2.4 Preparation of the PLP peptide (GGGHSLGKWLGHPDKFG)

The PLP peptide used in this work was purchased as 60% pure from Shanghai Mocell Biotech Co. (Shanghai, China) and RP-HPLC purified. The peptide was purified on a Thermo Separation Products HPLC (preparative run) using a C18 Vydac column 218TP1022 with a linear gradient of water/acetonitrile (6 mL/min, detection 220 nm, eluent A is 5% acetonitrile and 0.1% TFA in water and eluent B is acetonitrile, 14-90% B in 40 min). The fractions were analyzed by HPLC on a 5 μm C18 Econosphere column (4.6 x 250 mm) and lyophilized. The purity was determined by HPLC analysis using a Shimadzu UFLC and UV detector at 220 nm. The mass was determined using a Matrix-assisted laser desorption/ionization (MALDI) mass spectrometer (**Appendix 1: Figure A.1.1**). $[M+H]^+$ mass (Da): Expected = 1749.9 and Observed = 1750.0.

2.2.5 Solid-phase peptide synthesis of the MOG peptide (GGGWYRSPFSRVVHLGRR)

The MOG peptide was synthesized manually using Fmoc-PAL-PEG-PS resin (0.18 meq/g) and employing standard Fmoc solid-phase peptide synthesis strategy. Couplings were performed using 4-fold molar excess of each Fmoc L-amino acid, 4-fold molar excess of HATU and 8-fold molar excess of DIEA. The peptide was then removed from the resin by treatment with TFA/TIPS/H_2O (95/2.5/2.5 by volume) for 2 hours under nitrogen at room temperature. The resin beads were filtered; the filtrate was precipitated in cold diethyl ether, centrifuged, washed twice by diethyl ether, and dissolved in water. The crude peptide was purified by RP-HPLC

using the same conditions that were used for purification of the PLP peptide. The mass was determined by MALDI mass spectrometry (**Appendix 1: Figure A.1.2**). $[M+H]^+$ mass (Da): Expected = 2087.1 and Observed = 2087.2.

2.2.6 Expression and purification of Sortase A

A construct of sortase A ($SrtA_{\Delta 1\text{-}59}$) cloned with a C-terminal His_6 tag into pET23 (a gift from Richard DiMarchi, Indiana University) was transformed into *Escherichia coli* Rosetta 2 strain. $SrtA_{\Delta 1\text{-}59}$ was expressed and purified according to a similar procedure previously described.[38] The enzyme was characterized using intact mass spectrometry and SDS-PAGE (**Appendix 1: Figure A.1.3**). 242 mg/L of purified enzyme was obtained as determined by measuring the optical density of the solution at 280 nm (MW = 17719.0 Da, ε_{280} = 14440 $M^{-1}cm^{-1}$).[37]

2.2.7 Small-scale sortase-mediated ligations of LABL-Fc-ST + PLP and MOG peptides

The PLP and MOG peptides were separately ligated to the C-terminus of LABL-Fc-ST using sortase-mediated ligations on a sub-milligram scale. In each ligation, 10 μM LABL-Fc-ST protein was combined with 6 mM $CaCl_2$, 1 mM GGG-peptide (either PLP or MOG), and 5 μM sortase in TBS, pH 7.5 in a 150 μL reaction.[39] The ligations were incubated at 35°C for 24 hours. After which, they were quenched by the addition of 25 mM EDTA. The ligations were then observed by mass spectrometry and SDS-PAGE, which showed a 90% ligation yield for both peptides.

2.2.8 Large-scale sortase-mediated ligation of LABL-Fc-ST + PLP peptide

On a 60 mg protein scale (the total of 6 pooled reactions), the PLP peptide was ligated to the C-terminus of LABL-Fc-ST protein using a sortase-mediated ligation. In total, the ligation contained: 37 μM LABL-Fc-ST protein (60 mg), 6 mM $CaCl_2$, 1 mM PLP peptide (52 mg), and

7 μM $SrtA_{\Delta 1\text{-}59}$ (3.7 mg). The pH was adjusted to pH 7.5 using 1 M Tris base. The ligation was allowed to proceed 24 hours at 35°C and then stored at -20°C until purification.

2.2.9 Purification of large-scale LABL-Fc-ST-PLP

The reaction mixture was adjusted to pH 7.0 using 1 N HCl. The Fc-containing protein was separated from $SrtA_{\Delta 1\text{-}59}$ and unreacted PLP peptide using protein G affinity chromatography. The column was first equilibrated using TBS, pH 7.0. Then the reaction mixture was loaded onto the Protein G column, and the captured Fc protein was washed with 500 mL of 50 mM Tris and 500 mM NaCl, pH 7.0. Then the Fc-containing protein (unreacted LABL-Fc-ST and product LABL-Fc-ST-PLP) was eluted using 0.1 M glycine-HCl buffer pH 2.7 and immediately dialyzed against TBS, pH 7.5. The protein was then passed through a Detoxi-Gel endotoxin removal column (Thermo Scientific) to remove endotoxin contaminants that may have been introduced during the expression and/or purification steps.[40] The flow through from the endotoxin removal column was concentrated using an EMD Millipore 10 kDa MWCO centrifugal concentrator (USA). Concentration was stopped when the volume of the protein solution was 2 mL because precipitation was observed. The concentrated protein was dialyzed against 4 L of 1x PBS pH 7.4 with one buffer change at 4°C overnight and then filtered through an EMD Millipore 0.2 μm syringe filter. The concentration of the end product was determined to be 168 μM (9.6 mg/mL, 19 mg total) by optical density of the solution at 280 nm (MW = 57128.3 Da, $\varepsilon_{280} = 82570\ M^{-1}cm^{-1}$).[37]

2.2.10 Evaluation of BPI-Fc (LABL-Fc-ST-PLP) in EAE mice

The LABL-Fc-ST-PLP fusion protein was tested in mice induced with EAE using a similar protocol that was used by Manikwar *et al.* to test the I-domain protein, a 197 amino acid region of the αL subunit of LFA-1, conjugated to $PLP_{139\text{-}151}$ peptide.[41,42] Mice were housed and

maintained in the University of Kansas Animal Care Unit and the protocol for this animal work had been approved by the Institutional Animal Care and Use Committee (IACUC). Ten 5-7 week old Female SJL/J mice (Charles River Labs) were immunized with $PLP_{139-151}$ peptide in CFA on day 0. The PLP/CFA emulsion was injected above the shoulders and flanks of the mice (4 doses at 50 µL/dose) by subcutaneous injection. Additionally, on both days 0 and 2, the mice were administered 200 ng of pertussis toxin by intraperitoneal injection. On both days 4 and 7, five mice were administered 150 µL of 168 µM LABL-Fc-ST-PLP protein (2 doses at 25 nmol/dose) and five mice were administered 150 µL of PBS by intravenous injection. During the 25-day study, the mice were scored based on the severity of the physical symptoms associated with EAE. Scores ranged from 0 to 5 as follows: 0 = no symptoms, 1 = tail weakness, 2 = incomplete paralysis of one or two hind limbs, 3 = complete paralysis of one or two hind limbs, 4 = complete paralysis of one or two hind limbs plus paralysis one or two fore limbs, and 5 = moribund or dead. Additionally, the mice were weighed throughout the study to observe their change in weight relative to their weight on day 0. On day 14, one mouse from each group was sacrificed and 5 µm slices of each mouse's brain tissue were prepared as previously described.[24] The brain sections were sent to IHC World (Woodstock, MD) for staining with LFB and cresyl violet as previously described.[43] The stained tissues were imaged by IHC World using a EPI Fluorescence Trinocular Microscope (Model# FM320-9M). IHC World also quantified the amount of LFB staining in each brain tissue using ImageJ software. Statistical significance between the stained tissue samples was determined using a one-way ANOVA (α=0.05) followed by a Tukey multiple comparisons test.

2.3 Results and Discussion

2.3.1 Construction of a BPI-Fc fusion

The fusion of small, rapidly cleared peptides and proteins to the Fc region of IgG antibodies is an effective way to improve their half-lives, and because of this Fc fusion proteins have become a prominent class of biopharmaceutics.[44, 45] The initial attempt to prepare a BPI-Fc fusion used recombinant DNA technology to fuse both the antigenic and signal-2 blocking peptides to the human IgG1 Fc. A DNA construct was prepared consisting of the PLP and LABL peptides fused to the N- and C-termini of the Fc, respectively ($^{+}H_3N$-HSLGKWLGHPDKFGGG-Fc-AAAGGGITDGEATDSG); however, recombinant expression of this construct in glycosylation-deficient yeast resulted in severe proteolysis of the PLP region as detected by intact protein mass spectrometry. Three attempts were performed to express this dual fusion construct. The first attempt was performed using a 1 L spinner flask and the conventional 3-day induction time (**Appendix 1: Figure A.1.4**). Mass spectrometry showed that unproteolyzed PLP-Fc-LABL dual fusion protein was present; however, it was not the major peak. Several other peaks of smaller molecular weight were present, all of which corresponded to proteolysis within the PLP region. Based on the ratio of peak heights in the mass spectrum, only 33% of the PLP-Fc-LABL protein was unproteolyzed.

In a second attempt, the PLP-Fc-LABL dual fusion construct was expressed in a fermentor. Expression in a fermentor allows for more precise control over air flow, agitation rate, pH, dissolved oxygen concentration, and carbon source feed rate. Having more precise control over these expression conditions may help to reduce proteolysis. Expression in a fermentor did result in unproteolyzed PLP-Fc-LABL being the major peak in the mass spectrum (**Appendix 1: Figure A.1.5**). However, proteolysis was still severe. In fact, there were additional proteolyzed

species in the fermentor expression compared to the spinner flask expression. Similar to the spinner flask expression trial, all of the observed proteolysis occurred within the PLP region. Based on the mass spectrometry peak heights, expression of the PLP-Fc-LABL protein in a fermentor resulted in only 31% of the protein being unproteolyzed.

The PLP-Fc-LABL DNA construct was cloned in frame of the *Saccharomyces cerevisiae* alpha factor prepro sequence to allow for secretion of the target protein into the media. During protein expression, proteases may also be secreted and can cleave the secreted PLP-Fc-LABL protein. In order to reduce the level of proteases present in the media, a third expression was attempted. In this attempt, the cells were grown to density in a 1 L spinner flask, pelleted by centrifugation under sterile conditions, and transferred to 1 L of fresh media immediately before methanol-induced protein expression. Transferring the cells to fresh media before induction resulted in fewer proteolysis products. Based on the peak heights in the mass spectrum, 46% of unproteolyzed protein was obtained (**Appendix 1: Figure A.1.6**). Although the third attempt produced the most uncut protein (46%), proteolysis was unfortunately still severe. Since IgG1 Fc is a dimer linked by inter-chain disulfide bonds, the presence of only 46% uncut monomer in the reduced protein detected by mass spectrometry translates to only approximately 21% of the disulfide-bonded dimer having two full PLP peptides. It was decided that even with the reduced proteolysis, having only 21% full-length dimer would potentially compromise future experiments.

Since changing the expression conditions did not improve the proteolysis observed within the PLP region sufficiently, expression of a different antigenic peptide fused to IgG1 Fc was attempted to determine if the proteolysis problem was specific to the PLP peptide sequence. The MOG peptide was fused to the N-terminus of the Fc ($^{+}H_3N$-GWYRSPFSRVVHLGGG-Fc) and

expressed as a single Fc fusion. However, expression of this fusion showed that proteolysis was even more severe within the MOG region than observed in the PLP fusion (**Appendix 1: Figure A.1.7**). Based on the mass spectrometry peak heights, only 5% of unproteolyzed MOG-Fc was obtained. For both the PLP-Fc-LABL and MOG-Fc fusions, proteolysis was observed within the antigenic peptide sequence. Fortunately, the LABL peptide sequence showed no proteolysis in all three expression attempts of PLP-Fc-LABL. Given these results, an alternative method to prepare the BPI-Fc fusion was pursued.

IgG1 Fc fusions are most commonly prepared by recombinant protein expression.[46, 47] However, the applicability of recombinant expression for the production of peptides and proteins is limited by proteolysis and low expression yields. To circumvent these limitations, the fusion partners can be prepared separately and conjugated *in-vitro* using a variety of bioconjugation techniques.[48, 49] Such bioconjugation techniques can target natural conjugation sites on proteins such as the thiol of cysteine residues, the primary amine of lysine residues, and particular sugar residues of attached glycans. Additionally, non-native sites can be added to the protein such as unnatural amino acid residues, sugar residues, and peptide tags. Peptide tags are attractive, because the fusion partners can be conjugated site-specifically, and the conjugation occurs on the peptide tag instead of the native protein. A popular method for protein conjugation that requires a peptide tag substrate is sortase-mediated ligation.[50] Over the past decade, sortase A from *Staphylococcus aureus* has served as an important conjugation tool to attach a variety of materials to proteins in a site-specific manner.[38, 50-54] In addition to site-specificity, this enzymatic conjugation method is very attractive for proteins as it is performed under mild conditions and requires only that one species contain the LPXTG recognition motif, where X is any amino acid, while the other species contains at least a single N-terminal glycine (**Table**

2.1).[39] The mechanism of this reaction is as follows: sortase A recognizes the LPXTG motif, cleaving between the threonine and glycine residues using an active site cysteine. The glycine is released, and a thioester intermediate is formed between the C-terminal threonine of the sortase-tagged substrate protein and the active site cysteine of sortase A. Next, a ligand containing an N-terminal glycine acts as a nucleophile, attacking the thioester to displace sortase A and form an amide bond between the protein and ligand (**Figure 2.2**).[50, 53]

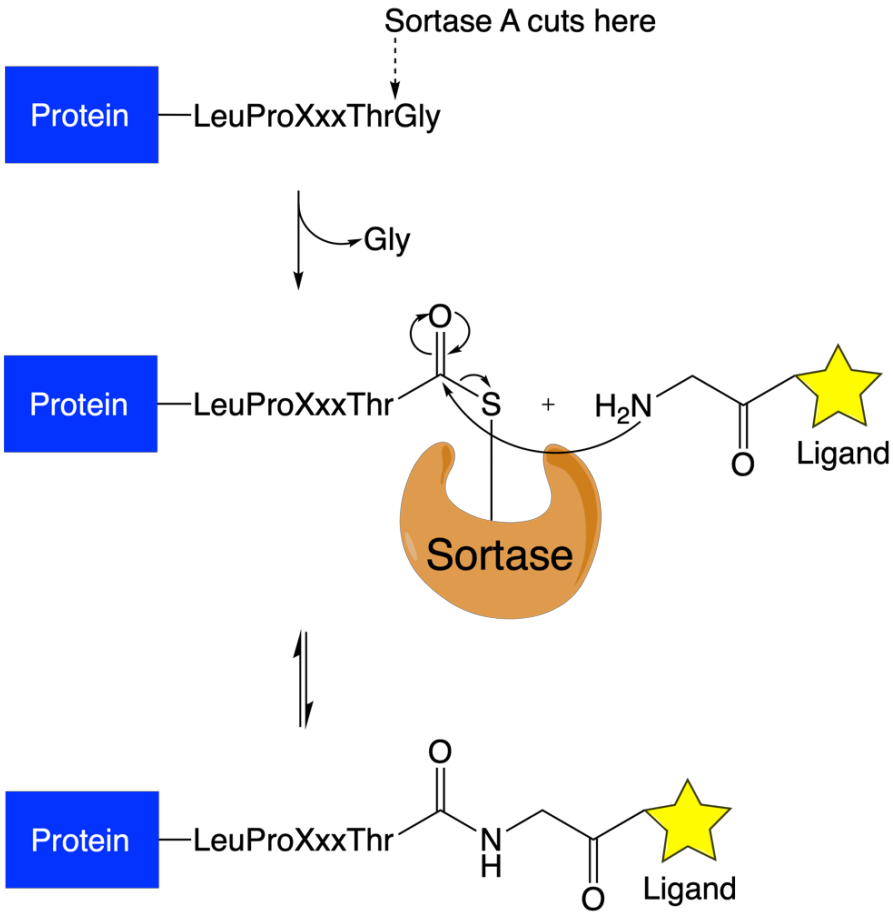

Figure 2.2: Mechanism of sortase-mediated ligations. The ligation requires a substrate to bear a LPXTG peptide tag. This peptide tag is recognized by sortase A. The enzyme cleaves between threonine and glycine residues to form an acyl-enzyme intermediate. The acyl-enzyme intermediate is then susceptible to nucleophilic attack by a ligand bearing an N-terminal glycine residue, leading to the formation of an amide bond between the substrate and the ligand.

A new Fc fusion protein was prepared that consisted of the LABL sequence fused to the N-terminus of the Fc, and a sortase A recognition tag (AAALPETGGG = ST) fused to the C-terminus. This construct was named LABL-Fc-ST ($^{+}H_3N$-GITDGEATDSGGG-Fc-AAALPETGGG). The LABL sequence was capped with an N-terminal glycine so that the positively charged N-terminus was not directly part of the LABL sequence. Also, a two glycine spacer was added in between the LABL and Fc to reduce the likelihood of the Fc sterically hindering the binding activity of the LABL peptide. Similarly, a three alanine spacer was added in between the Fc and ST recognition tag to reduce the likelihood of the Fc sterically hindering the sortase-mediated ligation. LABL-Fc-ST was expressed in yeast and showed no proteolysis (**Appendix 1: Figure A.1.8**). Furthermore, the 1 L spinner flask expression yield of LABL-Fc-ST was 5x higher than PLP-Fc-LABL (15 mg vs. 3 mg, respectively). This approach avoids expression of the problematic antigenic peptides and instead allows conjugation of antigenic peptides after expression using a C-terminal sortase-mediated ligation (**Figure 2.3**).

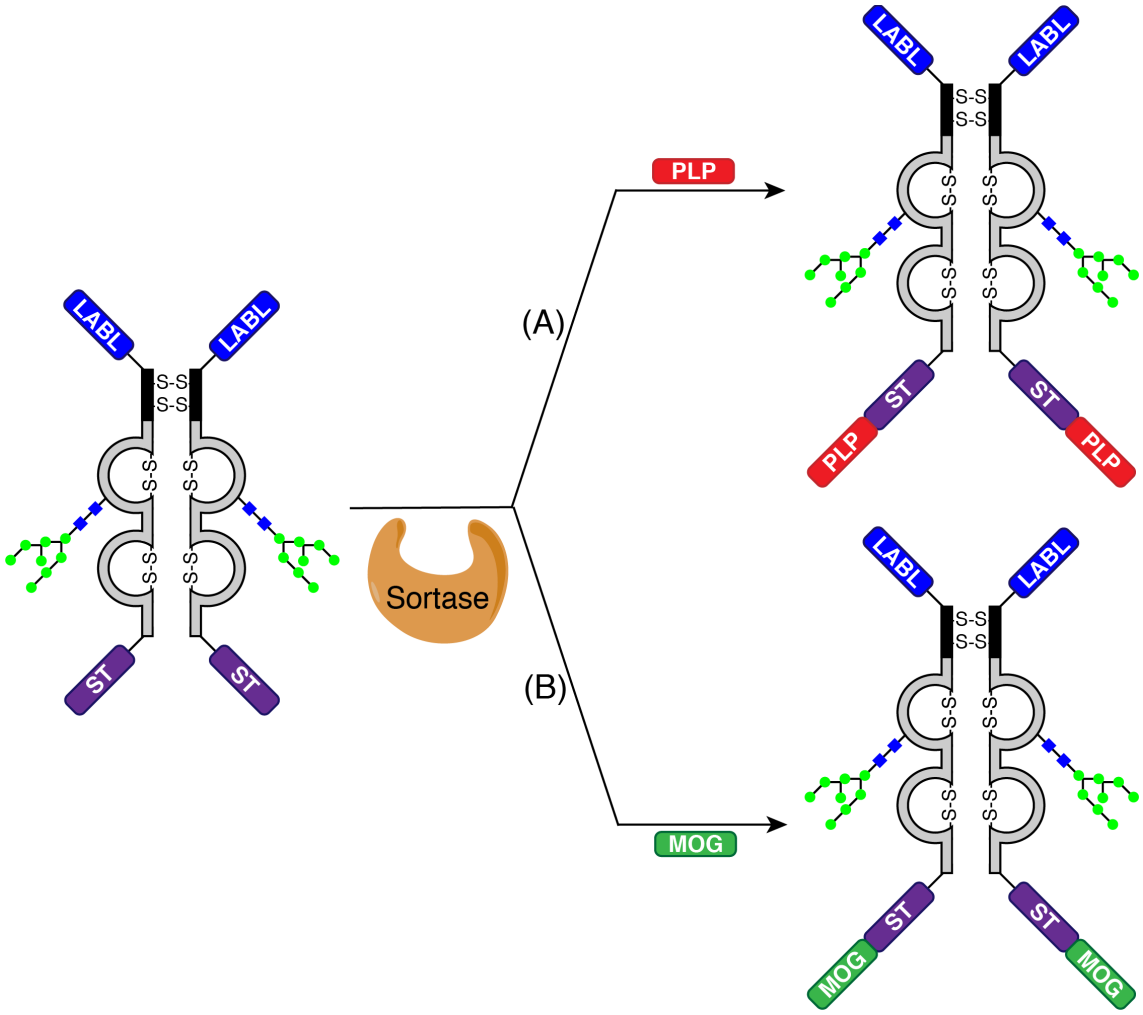

Figure 2.3: Sortase-mediated addition of two different antigenic peptides to the C-terminus of LABL-Fc-ST. An IgG1 Fc fusion containing an N-terminal LABL peptide and a C-terminal sortase A recognition tag was reacted in a sortase-dependent manner with the (A) PLP and (B) MOG peptides to produce LABL-Fc-ST-PLP and LABL-Fc-ST-MOG, respectively.

2.3.2 Preparation of antigenic peptides

The PLP peptide was purchased at ~60% purity and then RP-HPLC purified in our laboratory. The peptide was constructed with three glycine residues N-terminal to PLP since at least one N-terminal glycine residue was required for this peptide to be a nucleophile in a sortase-mediated ligation. The PLP peptide was designed with three sequential N-terminal glycine residues because a previous study comparing the number of sequential glycine residues

on ligation yield showed that three N-terminal glycine residues gave a higher yield than two or one but more than three didn't result in a much higher yield.[55] An additional C-terminal glycine was also added to the PLP peptide so that the negative charge of the carboxy terminus of the polypeptide backbone was spaced away from the PLP peptide.

The MOG peptide was chemically synthesized with two N-terminal glycine residues instead of three because the native MOG_{38-50} sequence begins with glycine. However, the MOG peptide is very hydrophobic and doesn't dissolve well in the aqueous buffer required for the sortase-mediated ligation. Previously, active BPIs have been produced with linkers and peptides attached to the C-terminus of MOG, and therefore we explored increasing the solubility of MOG by C-terminal modification.[25] In order to increase solubility under aqueous conditions, two arginine residues were added to the C-terminus. Additionally, a one glycine spacer was added in between MOG and the two arginine residues to reduce the likelihood the positive charges of the arginine side changes interfering with binding of MOG_{38-50} to the MHC-II and TCR.

2.3.3 Sortase-mediated ligations

On sub-milligram scales, the two antigenic peptides, PLP and MOG, were enzymatically ligated to the C-terminus of LABL-Fc-ST in a sortase-mediated manner to produce the ligation products LABL-Fc-ST-PLP and LABL-Fc-ST-MOG, respectively. These reactions were performed on small scale to optimize the ligation yields, and because there was no downstream application, they were not purified prior to characterization. Based on the peak heights in the mass spectra, the ligation yields were both 90% (**Figure 2.4B-C**). The addition of the antigenic peptides to LABL-Fc-ST was also observed by SDS-PAGE, which showed an upward gel shift for LABL-Fc-ST-PLP and LABL-Fc-ST-MOG compared to LABL-Fc-ST (**Figure 2.4D**). The method to prepare LABL-Fc-ST-PLP using a sortase-mediated ligation was scaled up to produce

enough material to conduct a mouse study to determine whether the BPI-Fc was active in mice induced with EAE. A drawback of the sortase-mediated ligation is that the product still contains the LPXTG recognition tag, so the product is also a sortase substrate. In order to drive the sortase-mediated ligation to near completion, a large excess of peptide was required (≥1 mM). In order to prepare enough LABL-Fc-ST-PLP for a mouse study, 52 mg of PLP peptide was prepared. Also, the expression of LABL-Fc-ST protein was scaled up from a 1 L spinner flask to a 5 L fermentor to produce enough protein for the mouse study. Fermentor expression of LABL-Fc-ST provided 105 mg of protein and scaling up production of LABL-Fc-ST did not result in any proteolysis (**Appendix 1: Figure A.1.8** vs. **Figure 2.4A**).

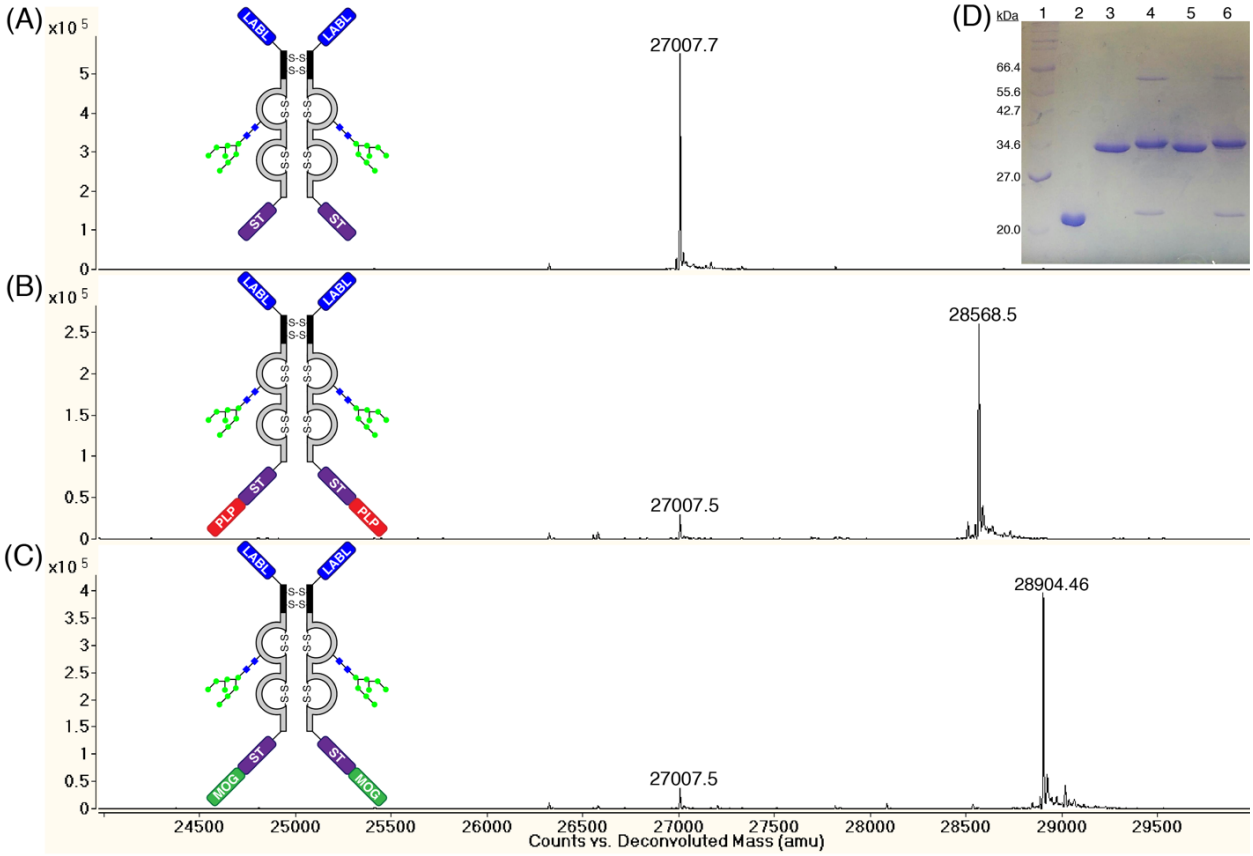

Figure 2.4: Characterization of LABL-Fc-ST and small-scale sortase-mediated ligations of LABL-Fc-ST with the PLP and MOG peptides. Prior to characterization, the proteins were de-glycosylated with PNGase F and reduced to their monomeric states using dithiothreitol (DTT). (A) Mass spectrum of recombinant expression of LABL-Fc-ST. LABL-Fc-ST MW (Da): Expected = 27010.41and Observed = 27007.71. (B) Mass spectrum of small-scale sortase-

mediated ligation of LABL-Fc-ST + PLP peptide. LABL-Fc-ST-PLP MW (Da): Expected = 28571.19 and Observed = 28568.53. (C) Mass spectrum of small-scale sortase-mediated ligation reactions of LABL-Fc-ST + MOG peptide. LABL-Fc-ST-MOG MW (Da): Expected = 28908.62 and Observed = 28904.46. (D) SDS-PAGE of LABL-Fc-ST and sortase-mediated ligations of LABL-Fc-ST + PLP and MOG peptides. Lanes: 1, 2-212 kDa MW marker; 2, $SrtA_{\Delta 1\text{-}59}$; 3&5, LABL-Fc-ST; 4, sortase-mediated ligation of LABL-Fc-ST + PLP peptide; and 6, sortase-mediated ligation of LABL-Fc-ST + MOG peptide**.**

In order to conserve peptide, almost a four-fold higher concentration of LABL-Fc-ST was used (10 μM for small scale vs. 37 μM for large scale). Based on the mass spectrometry peak height ratio of LABL-Fc-ST-PLP/(LABL-Fc-ST + LABL-Fc-ST-PLP), the large scale ligation yield was 87% (**Figure 2.5A**). This ligation yield was slightly lower than what was observed for the small-scale reaction, but it was still nearly complete. The near-completeness of the ligation can also be observed by SDS-PAGE (**Figure 2.5B**) where the LABL-Fc-ST-PLP migrated slower (higher) than LABL-Fc-ST. However, SDS-PAGE also showed side products of higher molecular weight than the expected product. These products could have been caused by the N-terminal glycine that was added to LABL-Fc-ST, which may have caused the N-terminus of LABL-Fc-ST to act as a nucleophile in the sortase-mediated ligation to form LABL-Fc-ST–LABL-Fc-ST dimers. Also, another possibility is that lysine residues have been shown to act as nucleophiles in the sortase-mediated ligation because their primary amine side chains can compete with the GGG-peptide for thioester attack.[56] The LABL-Fc-ST sequence contains 19 lysine residues in each chain, and $SrtA_{\Delta 1\text{-}59}$ also contains 19 lysine residues. Additionally, the mass spectrum from the large-scale ligation showed that approximately 14% of the product had a loss of a terminal glycine. Because the terminal glycines are not part of the active PLP and MOG peptides, the loss of this glycine was not seen as a problem that would interfere with the testing of this fusion protein. If this loss of glycine variant is included as an active product, then the overall ligation yield is 89% instead of 87%. After the reaction, the ligation product was purified

by Protein G affinity chromatography. The TIC overlay of LABL-Fc-ST-PLP before and after purification showed that the $SrtA_{\Delta 1\text{-}59}$ and unreacted PLP peptide were no longer present in the purified sample (**Appendix 1: Figure A.1.9**).

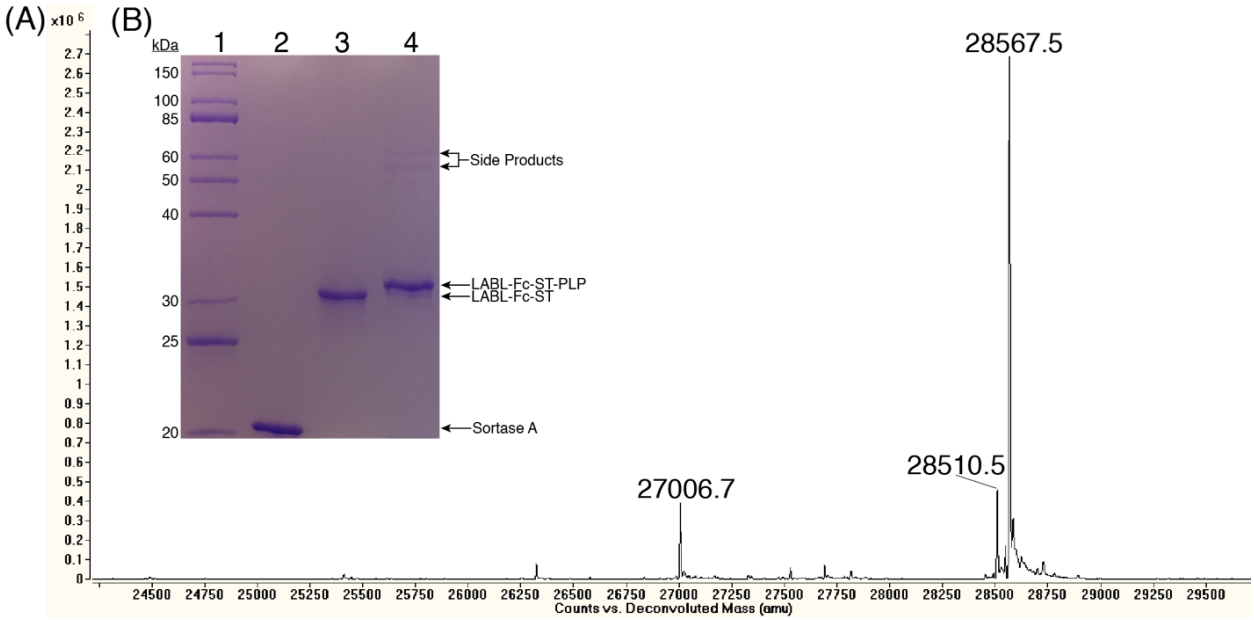

Figure 2.5: Characterization of the large-scale sortase-mediated ligation of LABL-Fc-ST + PLP peptide. Prior to characterization, the protein was de-glycosylated with PNGase F and reduced to its monomeric state using DTT. (A) Mass spectrum of LABL-Fc-ST + PLP peptide ligation reaction. LABL-Fc-ST MW (Da): Expected = 27010.4 and Observed = 27006.7, LABL-Fc-ST-PLP MW (Da): Expected = 28571.2 and Observed = 28567.5, and LABL-Fc-ST-PLP (-Glycine) MW (Da): Expected = 28514.1 and Observed = 28510.5 (B) SDS-PAGE of large-scale LABL-Fc-ST + PLP peptide ligation. Lanes: 1, 10-200 broad range protein marker; 2, $SrtA_{\Delta 1\text{-}59}$; 3, LABL-Fc-ST; and 4, LABL-Fc-ST-PLP.

2.3.4 Evaluation of the BPI-Fc in EAE mice

Ten 5-7 week old SJL/J mice were induced with EAE by immunizing them with an emulsion of $PLP_{139\text{-}151}$ peptide in CFA as well as pertussis toxin. To test whether the LABL-Fc-ST-PLP fusion conjugate called BPI-Fc was able to suppress the effects of EAE, on days 4 and 7 post-immunization, five mice were intravenously injected with 25 nmol of the BPI-Fc and five with a PBS control. The study required approximately 15 mg of BPI-Fc. In order to inject two doses of 25 nmol/dose into five mice, the protein had to be concentrated to 168 µM (9.6 mg/mL)

to allow for injection volumes of 150 µL per dose. During the course of the study, the mice were weighed and their physical symptoms associated with the disease were scored (**Figure 2.6**). The BPI-Fc treated mice showed significantly milder symptoms compared to the PBS control (**Figure 2.6A**). At the height of symptoms, the PBS control mice experienced complete paralysis of one or two hind limbs (average score = 3), whereas the BPI-Fc treated mice experienced, at most, tail weakness (average score = 0.4). Furthermore, at no point during the study did the BPI-Fc treated mice weigh less than their respective weights at day 0 (**Figure 2.6B**). In fact, the overall trend in the % change in body weight showed that the BPI-Fc treated mice were gaining weight throughout the study. On the other hand, the PBS control mice lost an average of 16% of body weight at the height of symptoms (day 12). These results show that the BPI-Fc protected the mice against the physical disablements and weight loss caused by EAE.

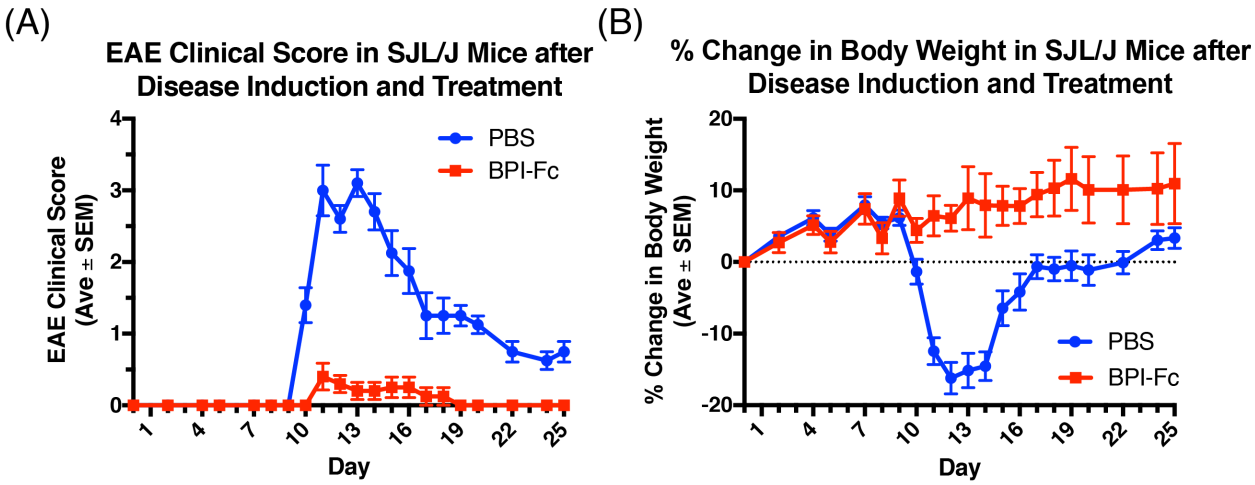

Figure 2.6: Comparison of EAE mice treated with BPI-Fc (LABL-Fc-ST-PLP) vs. PBS control (n = 5). (A) EAE clinical score in SJL/J mice after disease induction and treatment. Mice were scored during the course of the study from 0-5 based on the physical symptoms observed. (B) % change in body weight in SJL/J mice after disease induction and treatment. Each mouse was weighed during the course of the study and the weight at each of the measured days compared against the mouse's weight at day 0.

On day 14, one mouse from the BPI-Fc treated and one mouse from the PBS control group was sacrificed along with a normal mouse that was neither induced with EAE nor treated. A brain slice from each mouse was sent to IHC World for Luxol Fast Blue (LFB) staining (**Figure 2.7**). The amount of staining is representative of the amount of myelin present in the brain slice, which is representative of the severity of the disease. A one-way ANOVA showed that there was a statistical difference between the three tissue groups ($p = 0.0004$). A Tukey multiple comparisons test showed no statistical difference in the amount of myelin staining between the normal control mouse that was neither induced with the EAE disease nor treated and the BPI-Fc-treated mouse ($p = 0.2288$). On the other hand, there was a statistical difference in the amount of myelin staining between the normal control mouse and the PBS control mouse ($p = 0.0004$). These results show that the BPI-Fc protected the mice against the demyelination caused by EAE.

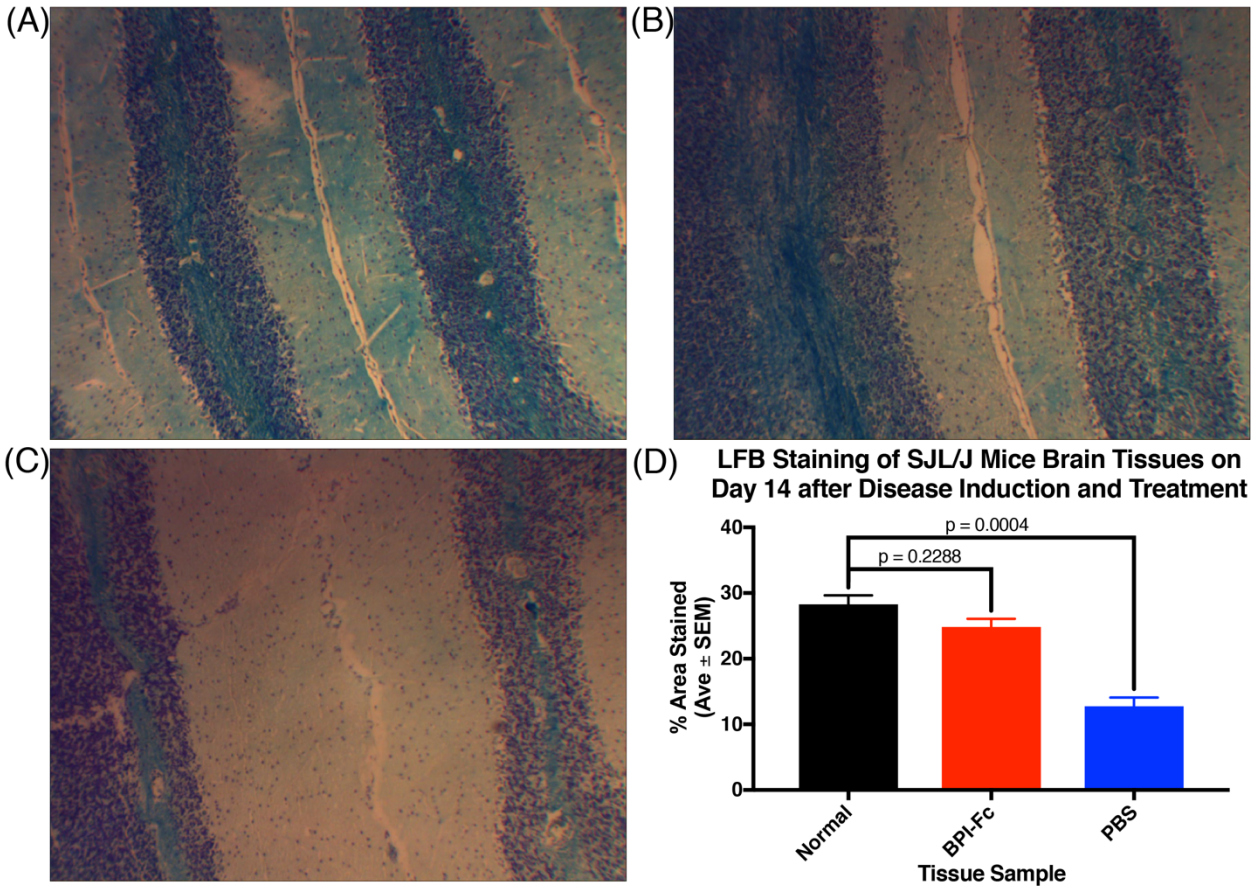

Figure 2.7: Luxol fast blue staining of mice brain slices on day 14 after EAE induction. (A) Normal: mouse neither induced with EAE nor treated. (B) BPI-Fc: mouse induced with EAE and treated with BPI-Fc. (C) PBS: mouse induced with EAE and treated with PBS. (D) Quantification of the area stained by LFB in each tissue. The % Area Stained by LFB for each tissue was measured in triplicate, and the results between the three tissue samples were compared for statistical significance using a one-way ANOVA and Tukey multiple comparisons test.

2.4 Conclusions

MS is an autoimmune disease that causes demyelination of the neurons in the central nervous system. There is currently no cure for MS, and current therapies globally suppress the immune system. BPIs are a promising novel approach to treating autoimmune diseases like MS and can potentially be designed to specifically prevent the activation of immune cells against a particular antigen. They are composed of an antigenic peptide fused to a signal-2 blocking peptide. In this work, we set out to test if the BPI peptides could be prepared as Fc fusions and if

the BPI peptides could still work when fused to an IgG1 Fc scaffold. The initial strategy was to fuse both peptides (antigenic peptide $PLP_{139-151}$ and signal-2 blocking peptide LABL) to the Fc using recombinant DNA technology. However, this strategy didn't work because expression in yeast resulted in proteolysis of the PLP peptide. Three different expression conditions were tested, but severe proteolysis of the PLP peptide was observed in all three expressions. Furthermore, a different antigenic peptide (MOG_{38-50}) was tested instead of PLP. However, proteolysis of the MOG region was even more severe than PLP.

Alternatively, a sortase-ligation strategy was developed to conjugate the antigenic peptides to a human IgG1 Fc fused to LABL. When IgG1 Fc fused to LABL and a sortase tag was expressed in glycosylation-deficient yeast, there was no proteolysis and good yield of the protein. The sortase ligation worked well to attach both the PLP and MOG antigenic peptides to the LABL-Fc-ST fusion protein in high yields (90% for both ligations). The advantage of this approach is that it avoids the proteolysis and expression problems that seem to be associated with the antigenic peptides that we have experienced. It also allows a single fusion protein (LABL-Fc-ST) to be expressed in quantity and then ligated to multiple antigenic peptides, which may be helpful to combat antigen spreading.[57] Additionally, this method may be used to screen peptides for improved BPI-Fcs. The ligation strategy to produce LABL-Fc-ST-PLP was scaled up to produce enough material (19 mg) to conduct a mouse study. Scaling up reduced the ligation yield some, but not much (90% small scale vs. 87-89% large scale). The mouse study was conducted in EAE-induced mice, and it was found that the BPI-Fc worked very well and significantly suppressed EAE in a mouse model. BPI-Fc fusions are a promising line of research and will be explored further in the future.

2.5 Permissions

Reprinted (adapted) with permission from (White, D. R., Khedri, Z., Kiptoo, P., Siahaan, T. J., and Tolbert, T. J. (2017) Synthesis of a Bifunctional Peptide Inhibitor–IgG1 Fc Fusion That Suppresses Experimental Autoimmune Encephalomyelitis. *Bioconjugate Chemistry 28*, 1867-1877.). Copyright (2017) American Chemical Society.

2.6 References

(1) Compston, A., and Coles, A. (2008) Multiple sclerosis. *The Lancet 372*, 1502-1517.

(2) Browne, P., Chandraratna, D., Angood, C., Tremlett, H., Baker, C., Taylor, B. V., and Thompson, A. J. (2014) Atlas of Multiple Sclerosis 2013: A growing global problem with widespread inequity. *Neurology 83*, 1022-1024.

(3) Sosnoff, J. J., Socie, M. J., Boes, M. K., Sandroff, B. M., Pula, J. H., Suh, Y., Weikert, M., Balantrapu, S., Morrison, S., and Motl, R. W. (2011) Mobility, balance and falls in persons with multiple sclerosis. *PLoS One 6*, 1-5.

(4) Chiaravalloti, N. D., and DeLuca, J. (2008) Cognitive impairment in multiple sclerosis. *The Lancet Neurology 7*, 1139-1151.

(5) Bakshi, R., Shaikh, Z., Miletich, R., Czarnecki, D., Dmochowski, J., Henschel, K., Janardhan, V., Dubey, N., and Kinkel, P. (2000) Fatigue in multiple sclerosis and its relationship to depression and neurologic disability. *Multiple Sclerosis 6*, 181-185.

(6) Lucchinetti, C., Bruck, W., Parisi, J., Scheithauer, B., Rodriguez, M., and Lassman, H. (2000) Heterogeneity of multiple sclerosis lesions: implications for the pathogenesis of demyelination. *Annals of neurology 47*, 707-717.

(7) Sawcer, S., Franklin, R. J., and Ban, M. (2014) Multiple sclerosis genetics. *The Lancet Neurology 13*, 700-709.

(8) Ascherio, A., and Munger, K. L. (2016) in *Seminars in neurology* pp 103-114, Thieme Medical Publishers.

(9) Ramagopalan, S. V., Dobson, R., Meier, U. C., and Giovannoni, G. (2010) Multiple sclerosis: risk factors, prodromes, and potential causal pathways. *The Lancet Neurology 9*, 727-739.

(10) Milo, R., and Kahana, E. (2010) Multiple sclerosis: geoepidemiology, genetics and the environment. *Autoimmunity reviews 9*, A387-A394.

(11) McFarland, H. F., and Martin, R. (2007) Multiple sclerosis: a complicated picture of autoimmunity. *Nature immunology 8*, 913-919.

(12) Disanto, G., Morahan, J., Barnett, M., Giovannoni, G., and Ramagopalan, S. (2012) The evidence for a role of B cells in multiple sclerosis. *Neurology 78*, 823-832.

(13) Krumbholz, M., and Meinl, E. (2014) B cells in MS and NMO: pathogenesis and therapy. *Semin. Immunopathol. 36*, 339-350.

(14) Minagar, A., and Alexander, J. S. (2003) Blood-brain barrier disruption in multiple sclerosis. *Multiple sclerosis 9*, 540-549.

(15) Goverman, J. (2009) Autoimmune T cell responses in the central nervous system. *Nature Reviews Immunology 9*, 393-407.

(16) Ciccarelli, O., Barkhof, F., Bodini, B., De Stefano, N., Golay, X., Nicolay, K., Pelletier, D., Pouwels, P. J., Smith, S. A., and Wheeler-Kingshott, C. A. (2014) Pathogenesis of multiple sclerosis: insights from molecular and metabolic imaging. *The Lancet Neurology 13*, 807-822.

(17) Goldenberg, M. M. (2012) Multiple sclerosis review. *Pharmacy and Therapeutics 37*, 175-184.

(18) Wingerchuk, D. M., and Carter, J. L. (2014) in *Mayo Clinic Proceedings* pp 225-240, Elsevier.

(19) Northrup, L., Christopher, M. A., Sullivan, B. P., and Berkland, C. (2016) Combining antigen and immunomodulators: Emerging trends in antigen-specific immunotherapy for autoimmunity. *Advanced drug delivery reviews 98*, 86-98.

(20) Manikwar, P., Kiptoo, P., Badawi, A. H., Büyüktimkin, B., and Siahaan, T. J. (2012) Antigen-specific blocking of CD4-specific immunological synapse formation using BPI and current therapies for autoimmune diseases. *Medicinal Research Reviews 32*, 727-764.

(21) Kobayashi, N., Kobayashi, H., Gu, L., Malefyt, T., and Siahaan, T. J. (2007) Antigen-specific suppression of experimental autoimmune encephalomyelitis by a novel bifunctional peptide inhibitor. *Journal of Pharmacology and Experimental Therapeutics 322*, 879-886.

(22) Ridwan, R., Kiptoo, P., Kobayashi, N., Weir, S., Hughes, M., Williams, T., Soegianto, R., and Siahaan, T. J. (2010) Antigen-specific suppression of experimental autoimmune encephalomyelitis by a novel bifunctional peptide inhibitor: structure optimization and pharmacokinetics. *Journal of Pharmacology and Experimental Therapeutics 332*, 1136-1145.

(23) Badawi, A. H., Kiptoo, P., Wang, W.-T., Choi, I.-Y., Lee, P., Vines, C. M., and Siahaan, T. J. (2012) Suppression of EAE and prevention of blood–brain barrier breakdown after

vaccination with novel bifunctional peptide inhibitor. *Neuropharmacology 62*, 1874-1881.

(24) Kiptoo, P., Büyüktimkin, B., Badawi, A., Stewart, J., Ridwan, R., and Siahaan, T. (2013) Controlling immune response and demyelination using highly potent bifunctional peptide inhibitors in the suppression of experimental autoimmune encephalomyelitis. *Clinical & Experimental Immunology 172*, 23-36.

(25) Badawi, A. H., and Siahaan, T. J. (2013) Suppression of MOG-and PLP-induced experimental autoimmune encephalomyelitis using a novel multivalent bifunctional peptide inhibitor. *Journal of neuroimmunology 263*, 20-27.

(26) Badawi, A. H., Kiptoo, P., and Siahaan, T. J. (2015) Immune Tolerance Induction against Experimental Autoimmune Encephalomyelitis (EAE) Using A New PLP-B7AP Conjugate that Simultaneously Targets B7/CD28 Costimulatory Signal and TCR/MHC-II Signal. *Journal of multiple sclerosis 2*, 1-10.

(27) Smith-Garvin, J. E., Koretzky, G. A., and Jordan, M. S. (2009) T cell activation. *Annual review of immunology 27*, 591.

(28) Grakoui, A., Bromley, S. K., Sumen, C., Davis, M. M., Shaw, A. S., Allen, P. M., and Dustin, M. L. (1999) The immunological synapse: a molecular machine controlling T cell activation. *Science 285*, 221-227.

(29) Murray, J. S., Oney, S., Page, J. E., Kratochvil-Stava, A., Hu, Y., Makagiansar, I. T., Brown, J. C., Kobayashi, N., and Siahaan, T. J. (2007) Suppression of type 1 diabetes in NOD mice by bifunctional peptide inhibitor: modulation of the immunological synapse formation. *Chemical biology & drug design 70*, 227-236.

(30) Wu, B., and Sun, Y. N. (2014) Pharmacokinetics of Peptide–Fc Fusion Proteins. *Journal of Pharmaceutical Sciences 103*, 53-64.

(31) White, D. R., Khedri, Z., Kiptoo, P., Siahaan, T. J., and Tolbert, T. J. (2017) Synthesis of a Bifunctional Peptide Inhibitor–IgG1 Fc Fusion That Suppresses Experimental Autoimmune Encephalomyelitis. *Bioconjugate Chemistry 28*, 1867-1877.

(32) Xiao, J., Chen, R., Pawlicki, M. A., and Tolbert, T. J. (2009) Targeting a homogeneously glycosylated antibody Fc to bind cancer cells using a synthetic receptor ligand. *Journal of the American Chemical Society 131*, 13616-13618.

(33) Xiao, J., and Tolbert, T. J. (2009) Synthesis of polymerizable protein monomers for protein-acrylamide hydrogel formation. *Biomacromolecules 10*, 1939-1946.

(34) Okbazghi, S. Z., More, A. S., White, D. R., Duan, S., Shah, I. S., Joshi, S. B., Middaugh, C. R., Volkin, D. B., and Tolbert, T. J. (2016) Production, characterization, and biological evaluation of well-defined IgG1 Fc glycoforms as a model system for biosimilarity analysis. *Journal of pharmaceutical sciences 105*, 559-574.

(35) Alsenaidy, M. A., Okbazghi, S. Z., Kim, J. H., Joshi, S. B., Middaugh, C. R., Tolbert, T. J., and Volkin, D. B. (2014) Physical Stability Comparisons of IgG1-Fc Variants: Effects of N-Glycosylation Site Occupancy and Asp/Gln Residues at Site Asn 297. *Journal of pharmaceutical sciences 103*, 1613-1627.

(36) Loo, T., Patchett, M. L., Norris, G. E., and Lott, J. S. (2002) Using secretion to solve a solubility problem: high-yield expression in Escherichia coli and purification of the bacterial glycoamidase PNGase F. *Protein expression and purification 24*, 90-98.

(37) Pace, C. N., Vajdos, F., Fee, L., Grimsley, G., and Gray, T. (1995) How to measure and predict the molar absorption coefficient of a protein. *Protein science 4*, 2411-2423.

(38) Mao, H., Hart, S. A., Schink, A., and Pollok, B. A. (2004) Sortase-mediated protein ligation: a new method for protein engineering. *Journal of the American Chemical Society 126*, 2670-2671.

(39) Guimaraes, C. P., Witte, M. D., Theile, C. S., Bozkurt, G., Kundrat, L., Blom, A. E., and Ploegh, H. L. (2013) Site-specific C-terminal and internal loop labeling of proteins using sortase-mediated reactions. *Nature protocols 8*, 1787-1799.

(40) Kluger, M. J., Singer, R., and Eiger, S. M. (1985) Polymyxin B use does not ensure endotoxin-free solution. *Journal of immunological methods 83*, 201-207.

(41) Manikwar, P., Büyüktimkin, B., Kiptoo, P., Badawi, A. H., Galeva, N. A., Williams, T. D., and Siahaan, T. J. (2012) I-domain-antigen conjugate (IDAC) for delivering antigenic peptides to APC: synthesis, characterization, and in vivo EAE suppression. *Bioconjugate chemistry 23*, 509-517.

(42) Shimaoka, M., Xiao, T., Liu, J.-H., Yang, Y., Dong, Y., Jun, C.-D., McCormack, A., Zhang, R., Joachimiak, A., and Takagi, J. (2003) Structures of the αL I domain and its complex with ICAM-1 reveal a shape-shifting pathway for integrin regulation. *Cell 112*, 99-111.

(43) Klüver, H., and Barrera, E. (1953) A method for the combined staining of cells and fibers in the nervous system. *Journal of Neuropathology & Experimental Neurology 12*, 400-403.

(44) Beck, A., and Reichert, J. M. (2011) Therapeutic Fc-fusion proteins and peptides as successful alternatives to antibodies. *MAbs 3*, 415-416.

(45) Czajkowsky, D. M., Hu, J., Shao, Z., and Pleass, R. J. (2012) Fc-fusion proteins: new developments and future perspectives. *EMBO Mol Med 4*, 1015-1028.

(46) Strohl, W. R. (2015) Fusion proteins for half-life extension of biologics as a strategy to make biobetters. *BioDrugs 29*, 215-239.

(47) Kumar, M., Hunag, Y., Glinka, Y., Prud'Homme, G., and Wang, Q. (2006) Gene therapy of diabetes using a novel GLP-1/IgG1-Fc fusion construct normalizes glucose levels in db/db mice. *Gene therapy 14*, 162-172.

(48) Patterson, D. M., Nazarova, L. A., and Prescher, J. A. (2014) Finding the right (bioorthogonal) chemistry. *ACS chemical biology 9*, 592-605.

(49) Agarwal, P., and Bertozzi, C. R. (2015) Site-specific antibody–drug conjugates: the nexus of bioorthogonal chemistry, protein engineering, and drug development. *Bioconjugate chemistry 26*, 176-192.

(50) Tsukiji, S., and Nagamune, T. (2009) Sortase-Mediated Ligation: A Gift from Gram-Positive Bacteria to Protein Engineering. *ChemBioChem 10*, 787-798.

(51) Clow, F., Fraser, J. D., and Proft, T. (2008) Immobilization of proteins to biacore sensor chips using Staphylococcus aureus sortase A. *Biotechnology letters 30*, 1603-1607.

(52) Levary, D. A., Parthasarathy, R., Boder, E. T., and Ackerman, M. E. (2011) Protein-Protein Fusion Catalyzed by Sortase A. *PloS one 6*, 1-6.

(53) Popp, M. W. L., Antos, J. M., and Ploegh, H. L. (2009) Site-Specific Protein Labeling via Sortase-Mediated Transpeptidation. *Current Protocols in Protein Science 15*, 15.3.1-15.3.9.

(54) Swee, L. K., Guimaraes, C. P., Sehrawat, S., Spooner, E., Barrasa, M. I., and Ploegh, H. L. (2013) Sortase-mediated modification of αDEC205 affords optimization of antigen presentation and immunization against a set of viral epitopes. *Proceedings of the National Academy of Sciences 110*, 1428-1433.

(55) Ling, J. J., Policarpo, R. L., Rabideau, A. E., Liao, X., and Pentelute, B. L. (2012) Protein thioester synthesis enabled by sortase. *Journal of the American Chemical Society 134*, 10749-10752.

(56) Möhlmann, S., Mahlert, C., Greven, S., Scholz, P., and Harrenga, A. (2011) In vitro sortagging of an antibody Fab fragment: overcoming unproductive reactions of sortase with water and lysine side chains. *Chembiochem 12*, 1774-1780.

(57) McMahon, E. J., Bailey, S. L., Castenada, C. V., Waldner, H., and Miller, S. D. (2005) Epitope spreading initiates in the CNS in two mouse models of multiple sclerosis. *Nature medicine 11*, 335-339.

Chapter 3

β1,2-N-acetylglucosamine On The α1,6-Arm Of The N-glycan Of IgG1 Fc Increases Stability And FcγRIIIa Binding Affinity But Decreases Core-linked Fucosylation Kinetics

3.1 Introduction

Antibody-based therapeutics are a rapidly expanding class of biopharmaceuticals. The number of approved antibody-based therapeutics by the FDA and EMA has more than doubled in the last five years, and they are expanding into areas such as antibody-drug conjugates, bispecific antibodies, and biosimilars.[1] Most antibody-based therapeutics use the Immunoglobulin isotype G subclass 1 (IgG1) antibody. IgG1 consists of two light chains and two heavy chains. Both heavy chains have a conserved N-glycosylation site in the fragment crystallizable (Fc) region at Asn297 (**Figure 1.1A**). The glycosylation at this site can markedly affect the antibody's stability, solubility, susceptibility to proteolysis, pharmacokinetics, and immune system function through engagement of C1q and FcγRs.[2-5] Therefore, it is important to study IgG1 N-glycosylation. However, expression of IgG1, in both natural and recombinant systems, results in a mixture of N-glycoforms.[6, 7] This heterogeneity makes it difficult to understand how N-glycosylation affects IgG1 stability and function because different N-glycoforms can affect the antibody differently.[3] For instance, the addition of terminal sialic acid to the N-glycan reduces antibody-dependent cellular cytotoxicity (ADCC),[8] a vital effector function that contributes to the cell-killing activity of some cancer immunotherapeutics,[9, 10] whereas the addition of terminal galactose increases ADCC.[11, 12]

The composition of the N-glycan determines the intramolecular glycan-protein contacts. There are contacts between specific sugar residues of the N-glycan and specific amino acid residues of the polypeptide. One important contact is a hydrogen bond between the innermost N-acetylglucosamine (GlcNAc) of the N-glycan and Asp265 of the Fc polypeptide.[13] This contact helps to stabilize the C'E loop of the Fc. Another important interaction is a hydrophobic interaction between second GlcNAc and Phe241 of the Fc polypeptide. A third contact is another

hydrophobic interaction between GlcNAc on the α1,6-arm of the N-glycan and Phe243 of the Fc polypeptide. Abolishing any of these three interactions by mutating the amino acid residues at these sites weakens the affinity of the Fc for binding the FcγRIIIa, the primary FcγR on natural killer (NK) cells that activates ADCC.[13-15] For example, the complete removal of the N-glycan prevented binding to FcγRIIIa (highest Fc concentration tested = 20 μM), but the addition of just a single GlcNAc allowed for binding at low μM affinity.[16] Abolishing these contacts also increases the mobility of the N-glycan as observed from solution NMR spectroscopy.[15] A more mobile N-glycan resulted in a weaker affinity to FcγRIIIa.[15] These contacts orient the Fc interface to allow for optimal binding to FcγRIIIa.[13-15] In general, the longer the glycan, the higher the binding affinity because more intramolecular protein-glycan contacts exist.[2] Additionally, removal of these contacts through amino acid mutations causes increased N-glycan processing, leading the increased levels of galactose, sialic acid, and bisecting GlcNAc.[13, 14] The increased dynamics may be allowing the N-glycan to be more accessible to the processing enzymes during N-glycan biosynthesis.

IgG1 is expressed, in both native and recombinant systems, mostly with core-linked fucose present on the N-glycan.[6, 7] An analysis of 10 FDA-approved monoclonal antibody therapeutics showed that the antibodies ranged from 90-98% fucosylated.[6] The presence of fucosylation on the Fc N-glycan has been shown to dramatically reduce binding affinity for FcγRIIIa and decrease ADCC activity.[17] However, reported K_D values that compare fucosylated vs. afucosylated Fc binding to FcγRIIIa vary significantly, with between 2 to 50-fold differences being reported.[12, 17-21] The reported differences are likely due to several factors such as differences in Fc N-glycosylation, differences in FcγRIIIa N-glycosylation, FcγRIIIa valency, and experimental methodology. Therefore, it would be advantageous to perform a consistent

receptor-binding assay that compares a variety of oligomannose, hybrid, and complex homogenous N-glycoforms. Because of the increased ADCC observed by removing core-linked fucose, there is interest in the pharmaceutical industry to reduce fucosylation levels in order to develop more effective monoclonal antibody-based therapies.[22] Furthermore, previous studies that observed relative rates of fucosylation between different N-glycoforms did so using the free glycan. However, the aforementioned intramolecular contacts between the Fc N-glycan and polypeptide may be influencing the affinity of the α1,6-fucosyltranferase (FUT8) for the glycan. Therefore, it would be advantageous to observe the rates of fucosylation on N297-bound glycan substrates in order to better understand where fucosylation is occurring in the biosynthetic pathway.

This work further investigates the effect of N-glycosylation on IgG1 stability and function. IgG1 Fc was used as a model system to prepare several homogenous IgG1 Fc N-glycoforms, and their effects on IgG1 Fc stability, function, and core-linked fucosylation kinetics were studied individually. This was performed by first expressing IgG1 Fc in glycosylation-deficient yeast to obtain a high mannose N-glycoform. The high mannose N-glycoform was then converted, using a stepwise series of glycosidases and glycotransferases, into seven oligomannose, hybrid, and biantennary complex N-glycoforms with and without fucose using *in-vitro* enzymatic synthesis. The stability of each non-fucosylated N-glycoform was compared using differential scanning calorimetry. Next, the function of all seven homogenous IgG1 Fc N-glycoforms was compared in an *in-vitro* receptor-binding assay using FcγRIIIa. The receptor binding affinity of two previously unreported N-glycoforms is reported. Lastly, the hybrid and complex N-glycoforms were compared for their relative abilities to accept core-linked fucose in both their free and IgG1 Fc Asn297-bound states.

3.2 Materials and Methods

3.2.1 Materials

The pPICzαA and pET28a expression vectors were purchased from Invitrogen (USA) and Novagen (Madison, WI), respectively. The QIAprep Spin Miniprep Kit, QIAquick Gel Extraction Kit, and Ni-NTA agarose resin were purchased from Qiagen (Germantown, MD). Yeast extract, tryptone, and agar were purchased from Becton, Dickinson, and Co. (Franklin Lakes, NJ). Zeocin was purchased from Invivogen (San Diego, CA). Yeast nitrogen base was purchased from Sunrise Science (San Diego, CA). All molecular biology enzymes and protein markers were purchased from New England BioLabs (Ipswich, MA). The protein A-sepharose and phenyl-sepharose resins were purchased from GE Healthcare (Waukesha, WI). All dialysis tubing was purchased from Spectrum Labs (Rancho Dominguez, CA). Dithiothreitol (DTT) and the materials used to prepare the polyacrylamide gels for SDS-PAGE were purchased from Bio-Rad (Hercules, CA). Protease-free bovine serum albumin was purchased from VWR (USA). Streptavidin biosensor tips were purchased from FortéBio (Menlo Park, CA). Pyruvate kinase and lactate dehydrogenase were purchased from Millipore-Sigma (St. Louis, MO). An expression plasmid for peptide: N-glycosidase F (PNGase F) was gifted by the Lott laboratory at Massey University, from which PNGase F was prepared as previously described.[23] Additionally, an expression plasmid for *Staphylococcus aureus* sortase A was gifted by the DiMarchi laboratory at Indiana University, from which sortase A was prepared as previously described.[24] Standard chemicals were purchased from commercial sources.

3.2.2 Expression and purification of IgG1 Fc

Our laboratory previously cloned the fragment crystallizable region of the heavy chain of human IgG1 (MGC-12853) into the Pichia expression vector pPICzαA to create pPICzαA-IgG1

Fc.[16, 25] This plasmid was linearized with the restriction endonuclease SacI-HF and transformed using electroporation into a glycosylation-deficient strain of the yeast *Pichia pastoris* (deleted och1, pno1, and bmt 1&2 genes and inserted STT3D gene from *Leishmania major* in order to improve N-glycosylation site occupancy).[25-27] The transformed cells were plated on YPD agar (1% yeast extract, 2% tryptone, 2% glucose, 1.5% agar) containing 100 µg/mL zeocin and grown for 6 days at 30ºC.

A colony was selected and transferred to a shake tube containing 2 mL of YPD media (1% yeast extract, 2% tryptone, 2% glucose) and 100 µg/mL zeocin, which was grown at 30ºC for 3 days and 250 rpm. After 3 days, the 2 mL culture was transferred to a baffled Erlenmeyer flask containing 50 mL YPD media and 100 µg/mL zeocin, which was grown at 30ºC and 250 rpm. After 2 days, the 50 mL culture was transferred to a 1 L spinner flasks containing 1% yeast extract, 2% tryptone, 2% glycerol, 100 mM sodium phosphate buffer pH 6.2, 1.34% yeast nitrogen base, 0.00004% biotin, and 1 drop antifoam. The culture was stirred on a stir plate at r.t., and air flow was maintained at 3 L/min through an in-line sterile filter. The culture was grown for 3 days. After which, the pH of the culture was adjusted back to 6.2 using concentrated NH_4OH. Then, induction was started by adding 0.5% methanol, which was maintained by adding 0.5% methanol approximately every 12 hours for 3 days. After induction, the culture was harvested by centrifugation at 6693 x g for 20 min using a Beckman JLA 10.5 rotor and Beckman Avanti J-series centrifuge (USA). The pellet was discarded, and the pH of the supernatant was adjusted to 6.5 using KOH. This expression procedure was repeated eight times to produce a total of nine liters.

The supernatant was filtered through Whatman #1 filter disks using vacuum filtration. The IgG1 Fc protein was purified from the supernatant using protein A affinity chromatography. 20 mL of protein A-sepharose resin was packed into a 2.5 cm x 20 cm column. A flow rate of 15

mL/min was maintained throughout the purification using a peristaltic pump. A UV detector was set up in-line after the column outlet. The column was equilibrated with 10 CV of 20 mM sodium phosphate buffer pH 6.5. Then, 2 L of filtered supernatant was passed through the column. Next, the column was washed with 25 CV of 20 mM sodium phosphate buffer pH 6.5. Lastly, 3 CV of 100 mM glycine-HCl buffer pH 3.0 was passed through the column to elute the IgG1 Fc protein. The eluted protein was immediately dialyzed in 2 L of 20 mM sodium phosphate buffer pH 7.5 using 3500 MWCO dialysis tubing. The protein was dialyzed at 4ºC overnight with one buffer change the following day. This purification procedure was repeated for the remaining 6 liters of supernatant in 2 L batches. The IgG1 Fc was characterized by intact mass spectrometry and SDS-PAGE (**Figure 3.1A&C**). The amount of IgG1 Fc obtained after protein A affinity chromatography was 243 mg. Observed vs. expected MW (**Table 3.1**).

Table 3.1: IgG1 Fc Expression Products After Protein A affinity Chromatography

Species	**Observed MW (Da)**	**Expected MW (Da)**
Non-glycosylated	25066.4	25066.5
M8	26770.3	26770.7
M9	26932.4	26932.1
M10	27094.7	27094.2

The IgG1 Fc was further purified using hydrophobic interaction chromatography (HIC). Solid $(NH_4)_2SO_4$ was dissolved in the IgG1 Fc solution to a final concentration of 1 M, and the solution was filtered through a 0.2 µm syringe filter. The purification was performed using 125 mL of phenyl-sepharose resin and a GE Healthcare ÄKTAmicro FPLC (Waukesha, WI) controlled by the UNICORN software (version 5.20). Throughout the purification, the flow rate was maintained at 2 mL/min. Elution from the column was monitored using an in-line UV/VIS spectrophotometer at 220 nm. All buffers were prepared using Milli-Q water and filtered through

a 0.2 μm filter using vacuum filtration prior to use. The column was first washed with 5 CV of Milli-Q water. Then the column was equilibrated with 5 CV of buffer A (20 mM sodium phosphate pH 7.5 containing 1 M $(NH_4)_2SO_4$). Next, 40-50 mg of IgG1 Fc protein containing 1 M $(NH_4)_2SO_4$ was loaded onto the column using a peristaltic pump. Next, the following sequential method was used: 0% buffer B (20 mM sodium phosphate pH 7.5) for 1 CV, a linear gradient of 0-27% buffer B for 1 CV, a linear gradient of 27-31% buffer B for 9.5 CV, a linear gradient of 31-100% buffer B for 1 CV, and 100% buffer B for 1 CV. During the linear gradient of 27-31% buffer B, 10 mL fractions were collected using a fraction collector. The fractions that showed a signal at 220 nm were analyzed using intact mass spectrometry in order to determine their N-glycan site occupancy. Fractions that contained ≥99% di-glycosylated IgG1 Fc were pooled and concentrated using a 10 kDa MWCO centrifugal concentrator and dialyzed using 3500 MWCO dialysis tubing in 2 L of 20 mM MES buffer pH 6.5 containing 150 NaCl at 4ºC with 1 buffer change. This purification method was repeated in 40-50 mg batches. The IgG1 Fc was characterized by intact mass spectrometry and SDS-PAGE (**Figure 3.1D&F**). The amount of di-glycosylated IgG1 Fc obtained after HIC was 99 mg (41% yield). Observed vs. expected MW (**Table 3.2**).

Table 3.2: IgG1 Fc Expression Products After HIC

Species	Observed MW (Da)	Expected MW (Da)
Non-glycosylated	Not observed	25066.5
M8	26770.2	26770.7
M9	26932.3	26932.1
M10	27094.3	27094.2

3.2.3 *In-vitro* enzymatic synthesis of homogenous IgG1 Fc N-glycoforms

3.2.3.1 Synthesis of M5-IgG1 Fc

Preparation of the α-1,2-mannosidase (Mannosidase-I) and endomannosidase enzymes can be found in Appendix 2 (**A.2.1.1.1**). For the conversion of HM-IgG1 Fc to M5-IgG1 Fc, the total reaction consisted of the following: 93 mg HM-IgG1 Fc at 0.5 mg/mL, 6 mg of α1,2-mannosidase[26, 28], and 0.4 mg of endomannosidase[26] in 20 mM MES buffer pH 6.5. The reaction was mixed and pipetted into dialysis tubing and allowed to react during dialysis at r.t. in 2 L of 20 mM MES buffer pH 6.5 containing 150 mM NaCl and 5 mM $CaCl_2$. The reaction was allowed to proceed for 4 days at r.t. The resulting M5-IgG1 Fc was analyzed by ESI-qTOF MS and SDS-PAGE (**Figure 3.3A** and **Figure 3.4 lane 2**). ESI-qTOF MS: observed 26285.2 Da, expected 26283.5 Da. Total protein yield: 83 mg (89%).

3.2.3.2 Synthesis of M5H-IgG1 Fc

Preparation of the β1,2-N-acetylglucosaminyltransferase-I (GnT-I) enzyme can be found in Appendix 2 (**A.2.1.1.2**). For the conversion of M5-IgG1 Fc to M5H-IgG1 Fc, the total reaction consisted of the following: 78 mg of M5-IgG1 Fc at 3 mg/mL, 1 mM UDP-GlcNAc, 10 mM $MnCl_2$, and 0.9 mg of GnT-I[29] in 20 mM HEPES buffer pH 7.5. The reaction was incubated at 25ºC for one day. The resulting M5H-IgG1 Fc was analyzed by ESI-qTOF MS and SDS-PAGE (**Figure 3.3B** and **Figure 3.4 lane 3**). ESI-qTOF MS: observed 26488.6 Da, expected 26486.7 Da. Yield: 74 mg (95%).

3.2.3.3 Synthesis of M3H-IgG1 Fc

Preparation of the α-1,3/6-mannosidase (Mannosidase-II) enzyme can be found in Appendix 2 (**A.2.1.1.3**). For the conversion of M5H-IgG1 Fc to M3H-IgG1 Fc, the total reaction consisted of the following: 45 mg of M5H-IgG1 Fc at 0.5 mg/mL and 3 mg of mannosidase-II in 20 mM MES buffer, pH 6.0. The reaction was incubated at 25ºC for one day. The resulting

M3H-IgG1 Fc was analyzed by ESI-qTOF MS and SDS-PAGE (**Figure 3.3C** and **Figure 3.4 lane 4**). ESI-qTOF MS: observed 26163.0 Da, expected 26162.5 Da. Yield: 42 mg (93%).

3.2.3.4 Synthesis of G0-IgG1 Fc

Preparation of the N-acetylglucosaminyltransferase-II (GnT-II) enzyme can be found in Appendix 2 (**A.2.1.1.4**). For conversion of M3H-IgG1 Fc to G0-IgG1 Fc, the total reaction consisted of the following: 30 mg of M3H-IgG1 Fc at 3 mg/mL, 1 mM UDP-GlcNAc, 10 mM $MnCl_2$, 0.09 mg of GnT-II in 20 mM MES buffer pH 6.5. The reaction was incubated at 25ºC. After 2 days, another 0.04 mg of GnT-II was added and the reaction was incubated for another day. The resulting G0-IgG1 Fc was analyzed by ESI-qTOF MS and SDS-PAGE (**Figure 3.3D** and **Figure 3.4 lane 5**). ESI-qTOF MS: observed 26364.0 Da, expected 26365.6 Da. Yield: 26 mg (87%).

3.2.3.5 Chemoenzymatic synthesis of GDP-Fucose

L-fucokinase/guanosine 5'-diphosphate-L-fucose pyrophosphorylase (FKP) was expressed by Dr. Khalid Al-Kinani in *E. coli* Rosetta 2 using a similar procedure as previously described.[30] FKP concentration was determined using a Pierce BCA Protein Assay Kit (Thermo Scientific, Waltham, MA) according to manufacturer's instructions. On 25 mL scale, the following reaction was prepared: 5 mM ATP, 10 mM L-fucose, 10 mM $MgCl_2$ and 104 µg/mL FKP in 100 mM HEPES buffer pH 7.5. The reaction was incubated at 28ºC for 18 hrs. After which, 70 mg of solid GTP (yielding a final concentration of 5 mM GTP) was added along with 1 U of yeast inorganic pyrophosphatase (New England BioLabs, Ipswich, MA). The reaction was incubated at 28ºC for 22 hrs. After which, 100 U of calf intestinal alkaline phosphatase was added. The reaction was allowed to proceed at 28ºC for 71 hrs.

The progress of the reaction was monitored using ion pair chromatography (IPC) using a method developed by Dr. Al-Kinani, which was similar to a method previously described.[31] A

Thermo Scientific Hypersil C18 column (5 μm, 4.6 mm x 250 mm) was attached to a Shimadzu UPLC. The column was equilibrated with 100 mL of buffer A (100 mM potassium phosphate pH 6.4, 8 mM tetrabutylammonium hydrogen sulfate) A linear gradient consisted of the following: 0% buffer B (70 mM potassium phosphate pH 6.4, 30% acetonitrile, 8 mM tetrabutylammonium hydrogen sulfate) for 8 min, a linear gradient of 0-77% buffer B for 8 min, a linear gradient of 77-100% buffer B for 4 min, 100% buffer B for 3 min, and finally 100% buffer A for 8 min. The flow rate was 1.3 mL/min, and the column oven temperature was 40ºC. Throughout the method, UV absorbance at 254 nm was monitored (**Appendix 2: Figures A.2.3** and **A.2.4**)

GDP-fucose was purified from the reaction using size exclusion chromatography. A flow rate of 0.3 mL/min was maintained using an ÄTKAmicro. A 2.5 cm x 30 cm column was packed with 100 mL of Bio-Gel P2 resin (Bio-Rad, Hercules, CA). A peristaltic pump was used to load the GDP-fucose reaction mixture. 5 mL of the reaction mixture ($1/5^{th}$ of the total reaction) was loaded on to the column. Then, 1.2 CV of Milli-Q water was pumped through during which 1 mL fractions were obtained. This purification procedure was repeated 4 times for the remaining 20 mL of reaction mixture. The fractions that corresponded to GDP-fucose were pooled and reanalyzed using IPC. After determining that those fractions contained GDP-fucose but no ADP, the fractions were lyophilized. In order to remove residual alkaline phosphatase, the lyophilized GDP-fucose was dissolved in 50 mM HEPES buffer pH 7.5 and then passed through a Strata C18-E solid phase extraction sorbent (Phenomenex, Torrance, CA). The flow through was collected. The concentration of purified GDP-fucose was determined using UV spectrophotometry at 254 nm using the extinction coefficient for GDP (ε_{254} = 13,800 $M^{-1}cm^{-1}$).[32] Based on the starting amount of GTP, the GDP-fucose yield was 42%.

3.2.3.6 Synthesis of M5HF-IgG1 Fc

Preparation of the α1,6-fucosyltransferase (FUT8) enzyme can be found in Appendix 2 (**A.2.1.1.5**). For conversion of M5H-IgG1 Fc to M5HF-IgG1 Fc, the following reaction was performed: 16 mg of M5H-IgG1 Fc at 1 mg/mL, 1 mM of impure GDP-fucose, 0.1 mg FUT8 in 20 mM MES buffer pH 7.0. The reaction was incubated at 25ºC for 2 days. The resulting M5HF-IgG1 Fc was analyzed by ESI-qTOF MS and SDS-PAGE (**Figure 3.3E** and **Figure 3.4 lane 6**). ESI-qTOF MS: observed 26629.0 Da, expected 26632.8 Da. Yield: 14 mg (87%).

3.2.3.7 Synthesis of M3HF-IgG1 Fc

Preparation of the Mannosidase-II enzyme can be found in Appendix 2 (**A.2.1.1.3**). For conversion of M5HF-IgG1 Fc to M3HF-IgG1 Fc, the following reaction was performed: 12 mg of M5HF-IgG1 Fc at 0.5 mg/mL and 0.7 mg mannosidase-II in 20 mM MES buffer pH 6.0. The reaction was incubated at 25ºC for 1 day. The resulting M3HF-IgG1 Fc was analyzed by ESI-qTOF MS and SDS-PAGE (**Figure 3.3F** and **Figure 3.4 lane 7**). ESI-qTOF MS: observed 26304.0 Da, expected 26306.5 Da. Yield: 10 mg (83%).

3.2.3.8 Synthesis of G0F-IgG1 Fc

Preparation of the GnT-II enzyme can be found in Appendix 2 (**A.2.1.1.4**). For conversion of M3HF to G0F, the following reaction was performed: 8 mg of M3HF at 3 mg/mL, 1 mM of UDP-GlcNAc, 10 mM of $MnCl_2$, 0.02 mg of GnT-II in 20 mM MES buffer pH 6.5. The reaction was incubated at 25ºC. After 2 days, another 0.01 mg of GnT-II was added and the reaction was incubated for another day. The resulting G0F-IgG1 Fc was analyzed by ESI-qTOF MS and SDS-PAGE (**Figure 3.3G** and **Figure 3.4 lane 8**). ESI-qTOF MS: observed 26508.0 Da, expected 26511.7 Da. Yield: 6 mg (75%).

3.2.3.9 General procedures for reaction analysis and purification

The progress of each reaction was monitored using intact mass spectrometry under reducing conditions. At the end of each enzymatic step, the IgG1 Fc N-glycoform product was

purified from the reaction using protein A affinity chromatography. First, the reaction was diluted 5X with 20 mM MES buffer pH 6.5. A column containing 20 mL of Protein A resin was equilibrated with 25 CV of 20 mM MES buffer pH 6.5. Then, the diluted reaction mixture was loaded. Next, the column was washed with 25 CV of 20 mM MES buffer pH 6.5 containing 500 mM NaCl. Lastly, the IgG1 Fc glycoprotein was eluted using 2-3 CV of 100 mM Gly-Cl buffer pH 3.0. The eluted protein was immediately pipetted in 3500 Da MWCO dialysis tubing and dialyzed into 2 L of buffer needed for the next enzymatic step. All dialyses occurred at 4ºC with 1 buffer change. The purified IgG1 Fc N-glycoforms were analyzed using intact mass spectrometry by injecting 6 µg of each non-fucosylated N-glycoform under reducing conditions, 11 µg for each fucosylated N-glycoform under reducing conditions, and 11 µg for all N-glycoforms under non-reducing conditions. The N-glycoforms were also analyzed using SDS-PAGE according to a method previously described.[24]

3.2.4 Intact protein mass spectrometry

An Agilent 6520 Quadrupole Time-Of-Flight LC/MS with an electrospray ionization source was used (Santa Clara, CA). All samples were prepared with a pH between 6-8. For samples analyzed under reducing conditions, 10 mM DTT was added. For samples analyzed under reducing conditions, no DTT was added. The samples were centrifuged for 5 min at 16,100 x g using an Eppendorf 5415D centrifuge (Hauppauge, NY). The supernatant was pipetted into an autosampler vial containing a glass insert. 6-11 µg of each IgG1 Fc N-glycoform was injected onto the LC column (Vydac 214 MS C4, 50 mm length x 2.4 mm ID, 300 Å particle size, 5 µm pore size). The two LC mobile phases were composed of the following: A = Milli-Q water and B = 99.9% acetonitrile, 0.02% LC/MS-grade trifluoroacetic acid, 0.08% LC/MS-grade formic acid. The following sequential LC method was employed: 5% mobile phase B at 1.0 mL/min for 6.0 min, a linear gradient of 5-90% mobile phase B at 0.5 mL/min for 7 min, 90%

mobile phase B for 3.0 min at 0.5 mL/min, a linear gradient of 90-5% mobile phase B for 0.5 min at 1.0 mL/min, and 5% mobile phase B for 1.5 min at 1 mL/min. Data was collected using the Agilent MassHunter Acquisition software (version B.02.00) and processed using the Agilent MassHunter Qualitative Analysis software (version B.03.01).

3.2.5 Analytical size exclusion chromatography

The non-fucosylated N-glycoforms were characterized using SEC according to a method previously described.[16] Briefly, 30 µg of each non-fucosylated N-glycoform (40 µL at 0.75 mg/mL) were injected on a TSKgel G3000SW$_{XL}$ column (5 µm, 7.8 mm ID x 30 cm) (TOSOH Bioscience, King of Prussia, PA). An isocratic gradient of 0.2 M sodium phosphate buffer pH 6.8 was used at a flow rate of 0.7 mL/min for 30 minutes per run. Each IgG1 Fc N-glycoform was performed in triplicate. Monomer and soluble aggregate values were quantified using the Shimadzu LC Solutions Software (Kyoto, Japan).

3.2.6 Thermal stability assessed by turbidity measurements at 350 nm

The non-fucosylated N-glycoforms were characterized using OD350 nm measurements at various temperatures using a method previously described.[2] Briefly, 250 µL of 0.2 mg/mL in 20 mM MES buffer pH 7.0 of each non-fucosylated N-glycoform was analyzed using a Cary 100 Bio UV-Visible Spectrophotometer (Agilent, Santa Clara, CA). The temperature parameters were as follows: temperature range of 10-100ºC, ramp of 1ºC/min, and a measurement was taken every 1.25ºC with a 2 min hold before each measurement. The sample was monitored using UV/VIS spectrophotometry at 350 nm. Each IgG1 Fc N-glycoform was measured in triplicate.

3.2.7 Differential Scanning Calorimetry (DSC)

Approximately 1 mg of each non-fucosylated IgG1 Fc N-glycoform was dialyzed in 2 L of 20 mM MES buffer pH 7.0 overnight at 4ºC with 1 buffer change the following day. Each N-glycoform was concentrated using 30 kDa MWCO centrifugal concentrators. After

concentration, the N-glycoforms were filtered using 0.2 μm syringe filters. Then, the concentration of each N-glycoform was adjusted to 0.5 mg/mL by measuring the absorbance at 280 nm using UV/VIS spectrophotometry (ε_{280} = 71570 $M^{-1}cm^{-1}$)[33] and diluting as necessary. Each IgG1 Fc N-glycoform was analyzed using DSC. A MicroCal VP-Auto DSC (Northampton, MA) was used. 200 μL of 0.5 mg/mL of each sample was injected. The samples were analyzed from 10-100ºC with a temperature ramp of 1ºC/min. Each sample was measured in triplicate. Also, a reference sample containing 20 mM MES buffer pH 7.0 was analyzed in triplicate. A water blank was injected between each sample. Samples were stored in an autosampler at 4ºC until injection. Data was processed using Origin 7 software containing a MicroCal LLC DSC plug in. The data for each sample was subtracted against the reference sample. The data were also normalized for concentration and adjusted to a consistent baseline. The data were fitted to a three-transition model to calculate T_{m1}, T_{m2}, and T_{m3}, which corresponded to the temperature that correlated with the maximum heat capacity. T_{onset} was determined as the earliest temperature to cause the heat capacity to reach 0.5 kcal/mol/ºC.

3.2.8 Production of FcγRIIIa

3.2.8.1 Molecular cloning

The extracellular region of human FcγRIIIa (accession# BC017865) V158 polymorph was cloned with a C-terminal ST tag followed by a hexahistidine (His6) tag. This modification was performed using PCR with primers (forward 5'- ggcgccgctagctatgcggactgaagatctcccaaaggc and reverse 5'-gccgcgcgcgcggccgcttaatgatgatggtggtggtgtccacctccagtttctggcaatccaccaccttg agtgatggtgatgttcac), and pPICzαA-FcγRIIIa, produced previously in our laboratory,[25] was used as a template to amplify the FcγRIIIa-ST-His6 PCR product. This PCR product was purified using a QIAquick Gel Extraction Kit and then digested with the restriction endonucleases NheI

and NotI-HF. A pPICzA plasmid containing the α-factor secretion peptide (but not the α-factor protein) followed by an NheI restriction site was designed by Dr. Tolbert. This plasmid was digested with the same restriction endonucleases. Both were gel purified and then ligated together using T4 DNA Ligase. The construct was then transformed into electrocompetent *E. coli* Top10f' cells, which were plated on low salt LB agar (0.5% yeast extract, 1% tryptone, 0.5% NaCl, 1.5% agar) containing 25 μg/mL zeocin and grown overnight at 37ºC. To confirm the correct sequence, the plasmid DNA was extracted using a QIAprep Spin Miniprep Kit (Germantown, MD) and sequenced by the UC-Berkeley DNA Sequencing Facility (Berkeley, CA). The plasmid DNA with a confirmed sequence was then linearized using the restriction endonuclease SacI and transformed into electrocompetent, glycosylation-deficient *P. pastoris* (deleted och1, pno1, and bmt 1&2 genes and inserted STT3D gene from *L. major* in order to improve N-glycosylation site occupancy)[25-27] cells using electroporation. The cells were then plated on YPD agar containing 100 μg/mL zeocin and grown at 30ºC for 6 days.

3.2.8.2 Expression and purification

A colony was transferred to a shake tube containing 2 mL YPD media and 100 μg/mL zeocin and grown at 30ºC and 250 rpm. After 3 days, the culture was transferred to a 250 mL baffled Erlenmeyer flask containing 50 mL YPD media and 100 μg/mL zeocin and grown at 30ºC and 250 rpm. After 2 days, the culture was transferred to a 1 L spinner flask containing 1% yeast extract, 2% tryptone, 100 mM sodium phosphate buffer pH 6.2, 2% glycerol, 1.34% yeast nitrogen base, 0.00004% biotin, and 1 drop of Antifoam 204. Each culture was stirred on a stir plate at r.t. The air flow was maintained at 3 L/min and contained an in-line sterile filter. After 3 days of growth, the pH of the culture was adjusted back to 6.2 using concentrated NH_4OH. The FcγRIIIa-ST-His6 expression was induced by adding 0.5% methanol, which was added every 12

hours for 3.5 days. After induction, the cultures were centrifuged at 6,693 x g for 20 min using a Beckman Avanti J-series centrifuge (USA). The supernatant was collected, and the pH of the supernatant was raised to 7.5 using KOH. The precipitate was allowed to settle at 4ºC for 4 hrs. This procedure was repeated three times for a total of four liters.

The supernatant was filtered through Whatman #1 filter disks using vacuum filtration. The FcγRIIIa-ST-His6 protein was purified from the supernatant using Ni-NTA affinity chromatography. A 2.5 x 20 cm column was packed with 10 mL of Ni-NTA-Agarose resin. The flow rate was maintained at 15 mL/min using a peristaltic pump. A UV detector was installed in-line post-column. The column was first equilibrated with 30 CV of 50 mM sodium phosphate buffer pH 7.5. Then, 1 L of supernatant was passed through. Then the column was washed with 50 CV of wash buffer (50 mM sodium phosphate buffer pH 7.5, 500 mM NaCl, 5% glycerol, 20 mM imidazole). Finally, the FcγRIIIa-ST-His6 was eluted using 2 CV 50 mM sodium phosphate buffer pH 7.5 containing 250 mM imidazole. The eluted protein was pipetted into 3500 Da MWCO dialysis tubing and dialyzed in 2 L of 20 mM sodium phosphate buffer pH 7.5 at 4ºC with 1 buffer change. It was observed that passing the supernatant through the column stripped much of the Ni^{2+} off the column. The Ni^{2+} was re-loaded by passing 2 CV of 100 mM $NiSO_4$ through the column, with 5 CV dH_2O passed through before and after. This purification method was repeated for the remaining 3 L of supernatant in 1 L batches. The amount of FcγRIIIa-ST-His6 protein obtained was determined by measuring the absorbance at 280 nm using UV spectrophotometry (MW = 21683.2 Da, ε_{280} = 39670 $M^{-1}cm^{-1}$).[33] The final yield was 40 mg (10 mg/L).

Solid $(NH_4)_2SO_4$ was dissolved in the solution of 40 mg of FcγRIIIa-ST-His6 to a final concentration of 2 M, and the solution was filtered through a 0.22 μm syringe filter. All solutions

used in the purification were pre-filtered through a 0.22 μm filter using vacuum filtration. The flow rate was maintained at 2 mL/min. An GE Healthcare ÄKTAmicro was used throughout this purification. A UV/VIS detector was installed in-line post-column, and absorbance at 220 nm was observed. A GE Healthcare column was packed with 125 mL phenyl-sepharose resin. The column was first washed with 5 CV of Milli-Q water. Then, the column was equilibrated with 5 CV of buffer A (20 mM sodium phosphate pH 7.5 containing 2 M $(NH_4)_2SO_4$). Next, 40 mg of FcγRIIIa-ST-His6 was loaded onto the column using a peristaltic pump. Finally, the following sequential method was employed: a linear gradient of 33-40% buffer B (20 mM sodium phosphate pH 7.5) for 1 CV, a linear gradient of 40-70% buffer B for 9.5 CV, a linear gradient of 70-100% buffer B for 1 CV, 100% buffer B for 2 CV. During the linear gradient of 40-70% buffer B, 10 mL fractions were collected using a fraction collector. Fractions were analyzed for N-glycan site occupancy using intact mass spectrometry. Fractions that showed receptor with all 5 N-linked glycosylation sites occupied were pooled, concentrated using a 10.5 kDa MWCO centrifugal concentrator, and dialyzed in 2 L of tris-buffered saline (TBS, 50 mM tris buffer containing 150 mM NaCl) pH 7.5 at 4ºC with 2 buffer changes. The amount of FcγRIIIa-ST-His6 protein obtained was determined by measuring the absorbance at 280 nm using UV spectrophotometry (MW = 21683.2 g/mol, ε_{280} = 39670 $M^{-1}cm^{-1}$).[33] The final yield was 10 mg (25% yield).

3.2.8.3 Sortase-mediated biotinylation

A sortase-mediated ligation was performed to C-terminally biotinylate the FcγRIIIa. For this reaction, Dr. Shaofeng Duan synthesized a compound containing triglycine with a free amino terminus conjugated to biotin via an ethylenediamine linker (Gly3-EDA-Biotin), similar to the compound previously prepared in our laboratory.[16] The sortase-mediated ligation was

performed on a 10 mL scale as follows: 8 μM FcγRIIIa-ST-His6 (1.8 mg), 2 mM $CaCl_2$, 1 mM Gly3-EDA-Biotin, and 8 μM sortase A[24] in TBS pH 7.5. The reaction was allowed to proceed at 37ºC for 40 hrs. After which, FcγRIIIa-Biotin was purified from the reaction using Ni-NTA affinity chromatography to remove unreacted FcγRIIIa-ST-His6. This purification was performed with gravity flow. First, 2 mL of Ni-NTA agarose resin was equilibrated with 15 CV of TBS pH 7.5. Then the sortase-mediated biotinylation reaction was loaded onto the column. Then the column was washed with 15 CV of TBS pH 7.5 containing 500 mL NaCl, 5% glycerol, and 20 mM imidazole. Finally, the elution buffer was passed through the column (TBS pH 7.5 containing 250 mM Imidazole). The purification steps were analyzed by SDS-PAGE, which showed that the majority of the FcγRIIIa-biotin eluted during the wash step. The collected wash step was pipetted into 3500 MWCO dialysis tubing and dialyzed in 2 L of PBS pH 7.4 at 4ºC with 2 buffer changes. The amount of FcγRIIIa-biotin obtained was determined by measuring the absorbance at 280 nm using UV spectrophotometry (MW = 21128.7 g/mol, ε_{280} = 39670 $M^{-1}cm^{-1}$).[33] The final yield was 1.4 mg (78% yield from biotinylation).

3.2.9 Bio-Layer Interferometry for FcγRIIIa binding assay

The concentration of each IgG1 Fc N-glycoform was measured in triplicate (ε_{280} = 71570 $M^{-1}cm^{-1}$). First, a biosensor tip coated with streptavidin was hydrated in PBS pH 7.4 for 10 minutes. The tip was further hydrated in kinetic buffer (PBS pH 7.4 containing 1 mg/mL BSA) overnight. Then, the tip was inserted in to a FortéBio BLItz instrument (Menlo Park, CA). The tip was placed in kinetic buffer and shaken for 30 sec, which was repeated 3 times to obtain a steady baseline. Next, 0.01 μM FcγRIIIa-biotin in kinetic buffer was loaded onto the tip to a response level of 0.3 nm. The tip was then placed in kinetic buffer for 6 minutes. After loading the receptor, a reference was performed wherein the tip was placed in kinetic buffer for 570 sec

(the total time to complete an experiment). Next, each IgG1 Fc N-glycoform was tested in a series of concentrations from low to high. For each concentration, the following steps were performed: 1.) a baseline was established by placing the tip in kinetic buffer for 30 sec, 2.) an association phase was performed by placing the tip in IgG1 Fc N-glycoform solution for 180 sec for non-fucosylated N-glycoforms (360 sec for fucosylated N-glycoforms), and 3.) a dissociation phase was performed by placing the tip in kinetic buffer for 360 sec. The tip was regenerated after each dissociation step by placing the tip in 1 mM NaOH for 30 sec followed by kinetic buffer for 60 sec and repeating once. The following IgG1 Fc concentrations were analyzed (nM): M5, M5H, and M3H = 4, 8, 16, 31, 63, 125, 250, 500; G0 = 2, 4, 8, 16, 31, 63, 125, 250; M5HF = 35, 70, 141, 281, 563, 1125, 2250, 4500; M3HF and G0F = 18, 35, 70, 141, 281, 563, 1125, 2250. This method was performed for all IgG1 Fc N-glycoforms in triplicate. The data for each set of IgG1 Fc measurements were fitted using a 1:1 binding model with reference correction (no Fc loading) using the BLItzPro Software. The kinetic rate constants (k_a and k_d) and the dissociation constant (K_D) were determined and their averages ± standard deviations were reported. Additionally, an equilibrium KD for each N-glycoform was measured by plotting the binding response at the end of the association phase (206.0-208.0 sec for the non-fucosylated N-glycoforms and 386.0-388.8 sec for the fucosylated N-glycoforms) against the respective IgG1 Fc concentration, which was fitted to a non-linear regression using the “one site-specific binding” model in Prism 7 software. The equilibrium K_D for each N-glycoform was reported as the average ± standard deviation. Statistical significance ($p < 0.05$) of the k_a, k_d, and kinetic K_D values were determined by performing a one-way ANOVA followed by a Tukey’s Multiple Comparisons test using the Prism 7 software.

3.2.10 Fucosylation kinetics

3.2.10.1 FUT8 activity assay

The coupled enzyme assay was performed using a Thermo Scientific Evolution 260 Bio UV/VIS Spectrophotometer with a Peltier Control and Cooling Unit (Waltham, MA). The assay was monitored at 340 nm. Each assay was performed in a Starna 100 µL quartz, low head space, µ-cuvette (Atascadero, CA) at 37°C in HBS pH 7.5. The assay was performed in 125 µL total reaction volume according to the following steps: 1.) the N-glycoform or glycan was mixed with 0.75 mM phosphoenolpyruvate, 2.5 mM $MgCl_2$, 50 mM KCl, 1.25 U pyruvate kinase, 1.75 U lactate dehydrogenase, and 175 µU FUT8, 2.) the spectrophotometer was blanked and 0.15 mM NADH was added, 3.) a baseline was established for 10 min, and 4.) the fucosylation reaction was started by adding 0.36 mM of GDP-fucose. The slope from the initial 4% of the reaction was measured, which was reference-corrected from the average slope of triplicate runs containing no N-glycoform/glycan.

3.2.10.2 Determination of FUT8 activity

The activity of FUT8 was determined using free M3H glycan, which was performed according to the FUT8 activity assay (**3.2.10.1**) procedure with 80 µM free M3H glycan substrate. The slope from the initial 4% of the reaction was measured, which was converted to µmol fucosylation/min.

3.2.10.3 K_M and V_{max} determination of free glycans

The concentration of each glycan tested (M5H, M3H, and G0) was determined by measuring the concentration of IgG1 Fc dimer at 280 nm (ε_{280} = 71570 $M^{-1}cm^{-1}$)[33] and multiplying that concentration by 2 (2 N-linked glycans per Fc dimer). After measuring the concentration, the free glycans were obtained by treating the IgG1 Fc N-glycoforms with PNGase F. Complete de-glycosylation was confirmed using intact mass spectrometry. The free glycans were tested in a FUT8 coupled enzyme assay according to the FUT8 activity assay (**3.2.10.1**) procedure. The free glycan concentrations tested were 2.5, 5, 10, 20, 40 and 80 µM.

The slopes from the initial 4% of each concentration was measured in triplicate. The slopes were plotted against their respective free glycan concentrations and fitted to the Michaelis-Menton model using the Prism 7 software to obtain K_M and V_{max} values.

3.2.10.4 K_M and V_{max} determination of IgG1 Fc N-glycoforms

The concentration of each IgG1 Fc N-glycoform tested (M5H, M3H, and G0) was determined by measuring the concentration of IgG1 Fc dimer at 280 nm (ε_{280} = 71570 $M^{-1}cm^{-1}$)[33] and multiplying that concentration by 2 (2 N-linked glycans per Fc dimer). The IgG1 Fc N-glycoforms were tested in a FUT8 coupled enzyme assay according to the FUT8 activity assay (**3.2.10.1**) procedure. The IgG1 Fc N-glycoform concentrations tested for M5H and M3H were 9, 18, 36, 75, 150, and 300 µM and for G0 were 25, 50, 100, 200, 400, and 800 µM. The slope from the initial 4% of each concentration was measured in triplicate. The slopes were plotted against their respective free glycan concentrations and fitted to the Michaelis-Menton model using the Prism 7 software to obtain K_M and V_{max} values.

3.2.10.5 Analysis of IgG1 Fc N-glycoform fucosylation kinetics by LC/MS

The IgG1 Fc N-glycoforms were also compared for their relative abilities to accept fucose using intact mass spectrometry. For each IgG1 Fc N-glycoform (M5H, M3H, and G0), the following reaction was prepared: 0.15 mg/mL IgG1 Fc, 19 µg/mL of FUT8, and 1 mM of impure GDP-fucose in 20 mM MES buffer, pH 7.0. The total volume of each reaction was 400 µL, and the reactions were incubated at 25ºC. The time point was determined by the time of injection onto the LC/MS. At each time point, 7.5 µg of IgG1 Fc N-glycoform was injected. The % fucosylation at each time point was determined by observing the ratio in peak heights: % Fucosylated = Fucosylated/(Fucosylated + Non-fucosylated) x 100.

3.3 Results and Discussion

3.3.1 Expression and purification of HM-IgG1 Fc

The Fc region of IgG1 was used as a model system for studying the effect of N-glycosylation on IgG1 stability, function, and core-linked fucosylation. Using IgG1 Fc as a model system eliminated the variability within the Fab region. IgG1 Fc was expressed in a glycosylation-deficient yeast strain of *P. pastoris*.[16, 26] Preparing a genetically modified strain was necessary in order to create an active glycan substrate for the *in-vitro* glycosidases and glycotransferases. The deletion of the PNO1 gene helped to eliminate phosphomannose residues observed in yeast.[34] Additionally, deletion of the BMT 1 & 2 genes helped to eliminate beta-linked mannose.[35, 36] β-1,2 mannose linkages have been shown to not be substrates for the α-1,2-mannosidases.[37] Lastly, the deletion of the OCH1 gene prevents initiation of an α-1,6-mannose linked branch point that produces non-human like N-glycans, allowing for IgG1 Fc to be expressed as high mannose N-glycoforms with 8 to 10 mannose residues (**Figure 3.1**).[38, 39] This N-glycoform set was labeled high mannose (abbreviated "HM") and used as a starting substrate for the *in-vitro* enzymatic synthesis of the homogenous oligomannose, hybrid, and complex N-glycoforms (**Figure 3.2**).

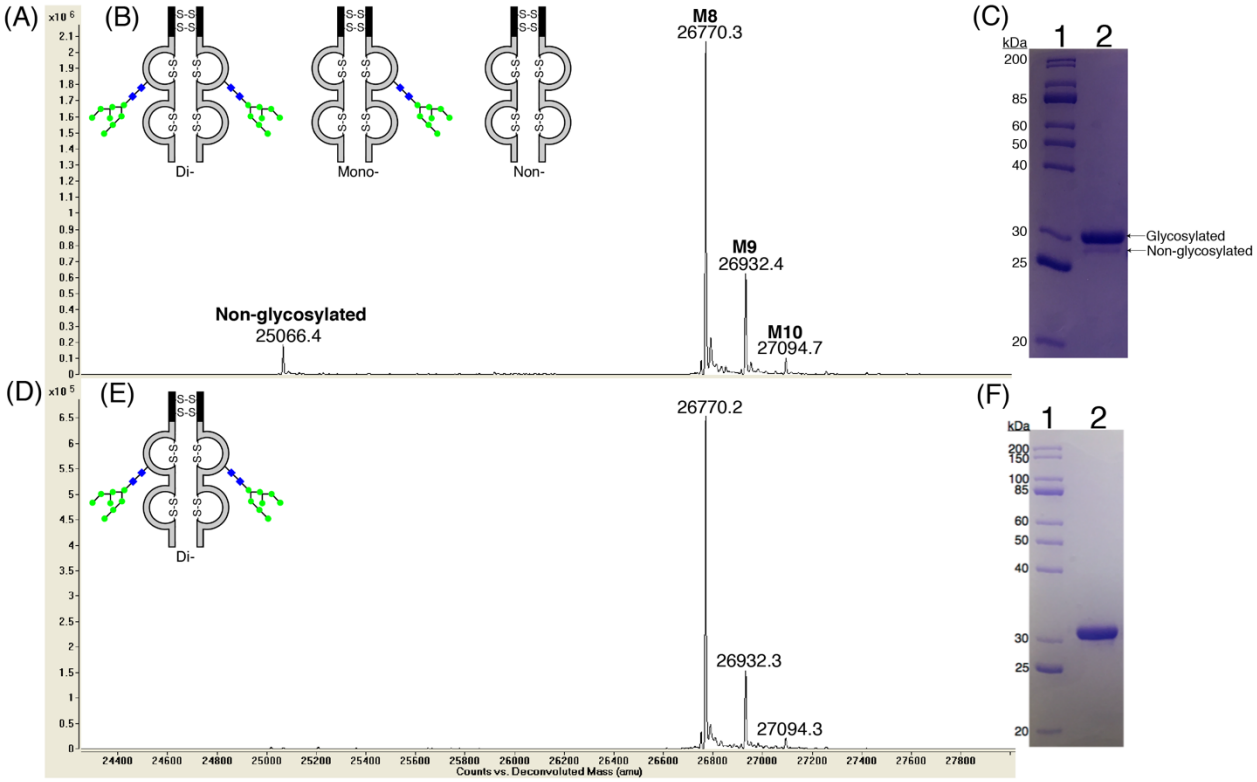

(G)

IgG1 Fc Expression Products	
Species	**Expected MW (Da)**
Non-glycosylated	25066.5
M8	26770.7
M9	26932.1
M10	27094.2

Figure 3.1: Characterization of di-glycosylated IgG1 Fc. (A) Intact mass spectrum of IgG1 Fc after purification by protein A affinity chromatography. (B) Representation of the observed incomplete N-glycan site occupancy. (C) SDS-PAGE of IgG1 Fc after purification by protein A affinity chromatography. Lanes: 1, 10-200 kDa MW protein marker and 2, IgG1 Fc. (D) Intact mass spectrum of IgG1 Fc after purification by HIC. (E) Representation of complete N-glycan site occupancy. (F) SDS-PAGE of IgG1 Fc after purification by HIC. Lanes: 1, 10-200 kDa MW protein marker and 2, IgG1 Fc. (G) Table showing expected MWs of observed IgG1 Fc N-glycoforms. All samples were reduced with DTT prior to analysis.

The STT3D gene from *L. major* was added to improve the N-glycosylation site occupancy of proteins produced in *P. pastoris*.[27] However, it did not completely eliminate site-occupancy heterogeneity during expression of IgG1 Fc. This observation was shown in the intact mass spectrometry where there was the presence of a non-glycosylated peak under reducing conditions (**Figure 3.1A**). The non-glycosylated peak height was 7% of the total peak heights,

which translated to 86% di-glycosylated, 13% mono-glycosylated, and <1 % non-glycosylated. The presence of incomplete N-linked site occupancy was also observed on SDS-PAGE (**Figure 3.1C**), which showed two bands that corresponded to glycosylated and non-glycosylated IgG1 Fc under reducing conditions. It has been shown that mono-glycosylated IgG1 reduces thermal stability and binding affinity to FcγRs.[40] Because this work focused on modifying the N-linked glycosylation, it was desirable to obtain fully di-glycosylated protein. This was accomplished using HIC as a purification step as previously performed.[16] After purification by HIC, purely di-glycosylated HM-IgG1 Fc was obtained as shown by intact mass spectrometry by the absence of the non-glycosylated peak (**Figure 3.1D**) under reducing conditions as well as by the SDS-PAGE showing only one band (**Figure 3.1F**). The yield after HIC was 40%. A higher yield could have been obtained if more mono-glycosylated IgG1 was allowed.

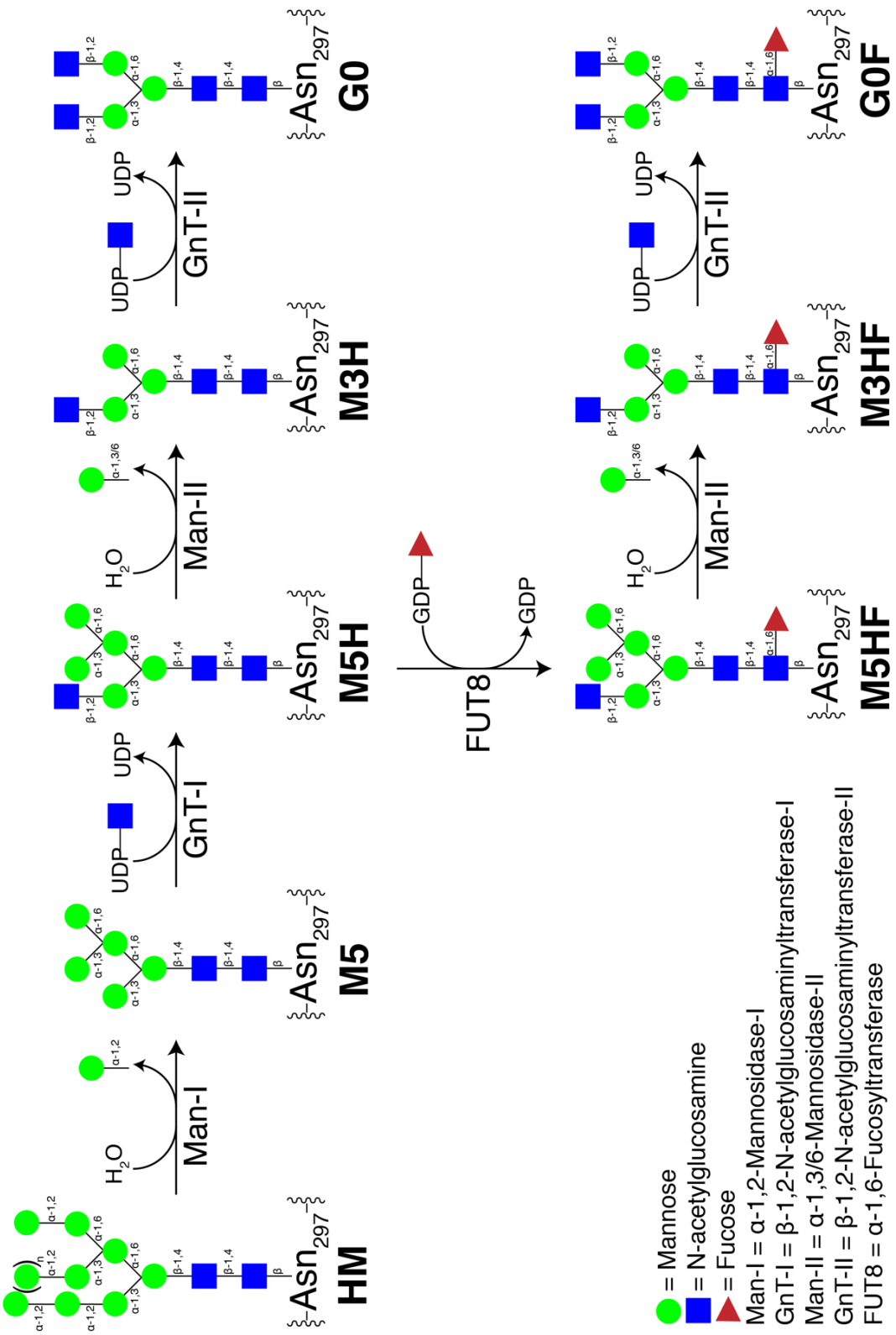

Figure 3.2: Representation of *in-vitro* enzymatic synthesis of homogenous oligomannose (M5), hybrid (M5H, M3H, M5HF, and M3HF), and complex (G0 and G0F) IgG1 Fc N-glycoforms from HM-IgG1 Fc. The IgG1 Fc protein structure was not depicted in order to emphasize changes in the N-glycosylation at each enzymatic step.

3.3.2 *In-vitro* enzymatic synthesis of homogenous IgG1 Fc N-glycoforms

In order to study the effect of N-glycosylation on IgG1 Fc function and stability, a series of homogenous IgG1 Fc N-glycoforms were produced. *In-vivo*, the N-glycosylation is assembled as the protein passes through the endoplasmic reticulum and Golgi organelles.[41] In these organelles, there is an assembly-line series of glycosidases and glycotransferases that modify the glycan. These enzymes require specific processing by the enzymes earlier in the pathway to be a substrate. Incomplete conversion at a particular step truncates the N-glycoform, which, given the multitude of steps in this process, results in the mixture of N-glycoforms that is observed during recombinant expression.[6]

In this work, a series of homogenous N-glycoforms were produced by reproducing the glyco-processing that occurs in mammalian cells *in vitro*. This required the production of the mammalian glyco-processing enzymes. These enzymes were not commercially available, so they were cloned, expressed, and purified in house. Mannosidase-I from *Bacteroides thetaiotaomicron* was cloned in a pET28a vector and expressed in *Escherichia coli* Rosetta 2 cells (Novagen) by Dr. Ishan Shah (**Appendix 2, A.2.1.1.1**).[26, 28] GnT-I from *Homo sapiens* was cloned into *E. coli* Rosetta gami2(DE3) (Novagen) by Dr. Mark Pawlicki and expressed and purified by Dr. Khalid Al-Kinani (**Appendix 2, A.2.1.1.2**).[29] Mannosidase-II from mouse was cloned in pPICzαA by Dr. Brian Hamilton, expressed in *P. pastoris* KM71H (Invitrogen) and purified (**Appendix 2, A.2.1.1.3**). GnT-II mammalian gene sequence was codon optimized for expression in yeast then cloned into the pPICzαA vector by Dr. Tolbert and expressed and purified by Dr. Khalid Al-Kinani (**Appendix 2, A.2.1.1.4**). FUT8 from *mus musculus* was cloned, expressed, and purified by Dr. Khalid Al-Kinani (**Appendix 2, A.2.1.1.5**).

In-vitro enzymatic synthesis allowed us to perform one step at a time, obtain complete conversion, and then move on to the next step. This stepwise scheme was performed in the following order (**Figure 3.2**): HM → M5 → M5H → M3H → G0. Additionally, the M5H N-glycoform was fucosylated to produce M5HF, which was then converted to other fucosylated N-glycoforms: M5H → M5HF → M3HF → G0F. Each enzymatic step was monitored using intact mass spectrometry. Based on the peak heights, the yield at each enzymatic step was >98% under both reducing conditions (**Figure 3.3**) and non-reducing conditions (**Appendix 2: Figure A.2.1**).

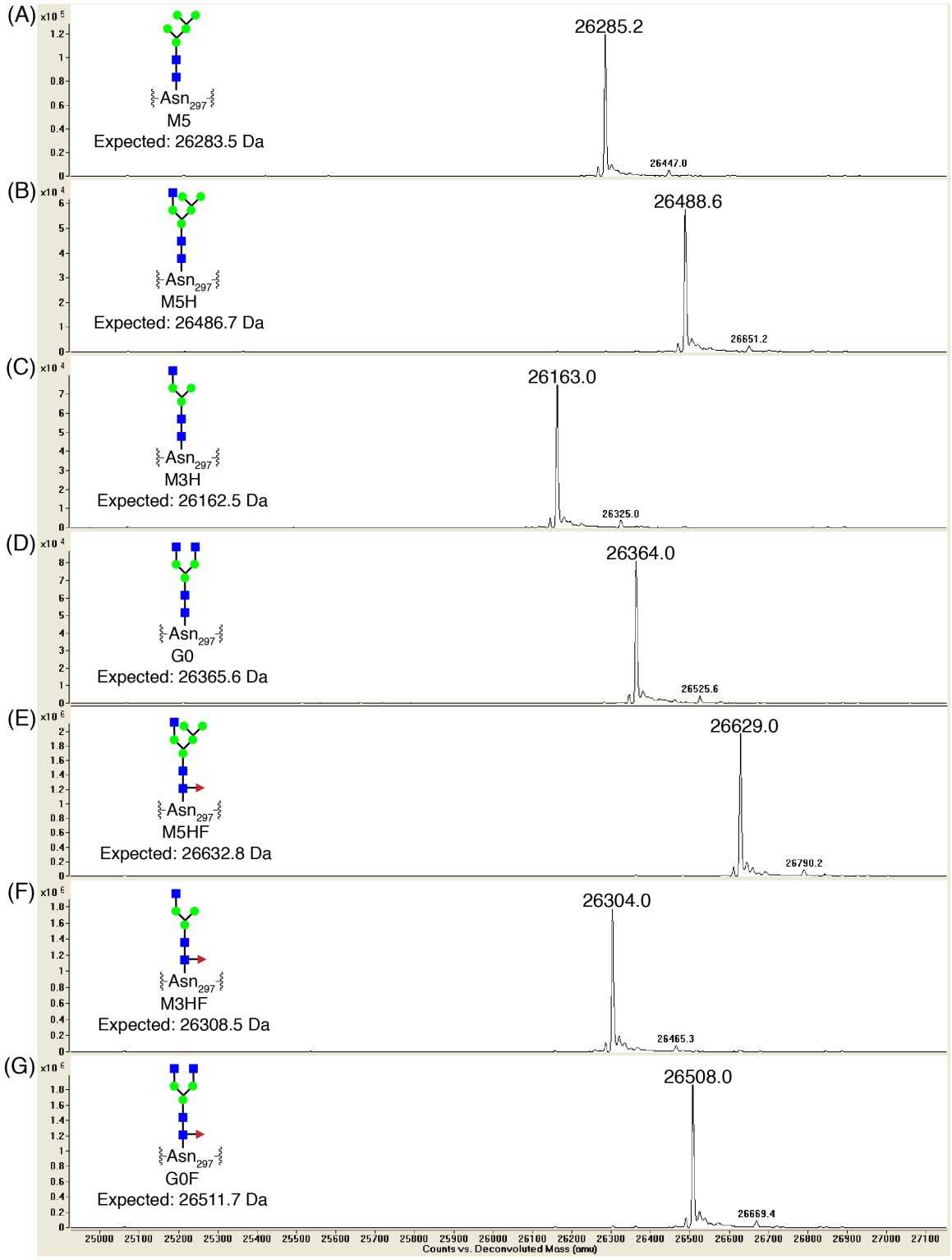

Figure 3.3: Intact mass spectra of homogenous IgG1 Fc N-glycoforms prepared by *in-vitro* enzymatic synthesis. Also shown are the glycan representations and expected MWs of each IgG1 Fc N-glycoform. N-glycoforms: (A) M5, (B), M5H, (C) M3H, (D) G0, (E) M5HF, (F) M3HF, (G) G0F. All samples were reduced with DTT prior to analysis. Glycosylation symbols: blue square GlcNAc; green circle, mannose; and red triangle, fucose.

In order to produce the non-fucosylated N-glycoforms, four *in-vitro* enzymatic steps were performed. The first step was to convert HM to M5. For this step, two enzymes were used: mannosidase-I to cleave terminal α1,2-mannose residues[28] and an endomannosidase in case some of the higher-order +162 peaks were glucose.[42] After removal of the α1,2-mannose residues, there was still a small peak of +162 from the expected M5 molecular weight. This was determined to not be part of the N-linked glycan because treating the protein with PNGase F, which removes N-linked glycans, did not remove the small +162 peak from the de-glycosylated IgG1 Fc mass spectra (**Appendix 2: Figure A.2.2**). Based on literature, this peak is likely O-linked mannose.[43, 44] The next step was to convert M5 to M3H. For this step, M5 was treated with GnT-I, which adds the β1,2-GlcNAc to the α1,3-arm of the N-glycan.[45] The next step was to convert M5H to M3H. For this step, M5H was treated with mannosidase-II, which sequentially cleaves the α1,6-linked followed by the α1,3-linked mannose residues from the α1,6-arm of the N-glycan.[46] The last step was to convert M3H to G0. This was performed by treating M3H with GnT-II, which adds the β1,2-GlcNAc to the α1,6-arm of the N-glycan.[47, 48] Furthermore, three fucosylated N-glycoforms were produced. This required the use of GDP-fucose. It is expensive to purchase commercially, so it was produced in-house from less expensive materials using chemoenzymatic synthesis. FKP is a bifunctional enzyme that was used to convert fucose and ATP into fucose-1-phosphate, which was then converted, in the presence of GTP, into GDP-fucose.[49] The reaction was monitored using ion pair chromatography (**Appendix 2: Figures A.2.3 and A.2.4**). After synthesis, alkaline phosphatase was added to convert the ADP byproduct into adenosine to make it smaller so that it could be removed using SEC. GDP-fucose was then purified from the reaction mixture using SEC and lyophilized. GDP-fucose was used as a fucose donor to produce the three fucosylated N-glycoforms. M5H was

converted to M5HF. For this step, M5H was treated with FUT8, which adds an α1,6-fucose residue onto the GlcNAc that is closest to Asn297.[50-53] The next steps were to convert MH5F to M3HF and M3HF to G0. These steps were performed using the same enzymes that were used for the synthesis of their non-fucosylated counterparts.

After completion of each enzymatic step, the IgG1 Fc N-glycoform was purified from the enzymes using protein A affinity chromatography. The protein yield after each enzymatic step and subsequent purification using protein A affinity chromatography was 75-97%. After which, the IgG1 Fc N-glycoforms were analyzed by SDS-PAGE (**Figure 3.4**). SDS-PAGE result did not show any proteolyzed bands nor contaminant bands coming from the enzyme preps after purification. Each N-glycoform showed only a single band. The production of homogenous N-glycoforms using this strategy produced one oligomannose N-glycoform (M5), four hybrid N-glycoforms (M5H, M5HF, M3H, M3HF), and two complex N-glycoforms (G0 and G0F).

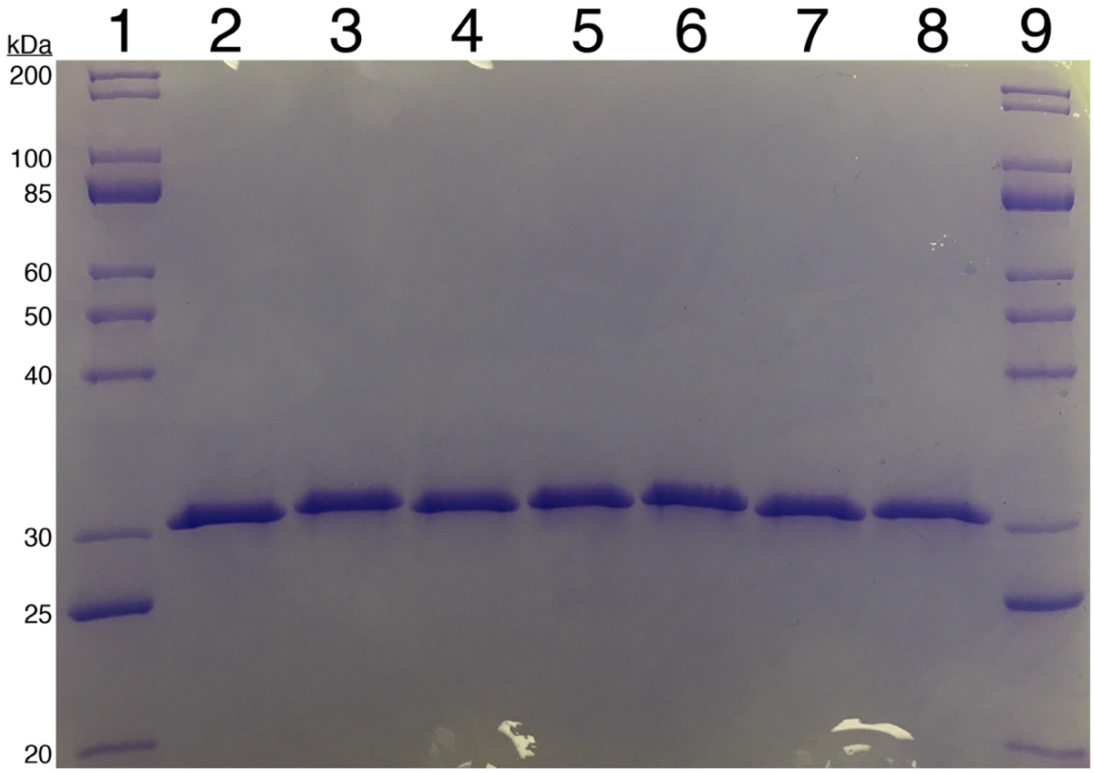

Figure 3.4: SDS-PAGE of homogenous IgG1 Fc N-glycoforms prepared by *in-vitro* enzymatic synthesis. Lanes: 1 & 9, 10-200 kDa MW protein marker; 2, M5; 3, M5H; 4, M3H; 5, G0; 6, M5HF; 7, M3HF; and 8, G0F. All samples were reduced with DTT prior to loading.

3.3.3 Comparison of IgG1 Fc N-glycoform stability

The non-fucosylated N-glycoforms were compared against one another using DSC (**Figure 3.5**). DSC has been used by other researchers to compare the thermal stability of different IgG1 Fc variants.[2, 54-56] The fucosylated N-glycoforms were not tested because previous results in the Tolbert laboratory by Dr. Al-Kinani comparing IgG2 Fc M5H vs. M5HF did not show any differences (unpublished results). Additionally, Mimura *et al.* reported DSC results from homogenous non-fucosylated N-glycoforms of IgG1 Fc in one manuscript[55] and their fucosylated counterparts in another[56]. Comparing the results didn't show any significant differences upon fucosylation. Therefore, it was suspected that fucosylation would not have affected stability. In this work, the results showed that the T_{onset} and T_{m1} for the M5, M5H, and

M3H IgG1 Fc N-glycoforms were very similar, with a T_{onset} of 54.6ºC and T_{m1} of 67.6ºC. However, G0-IgG1 Fc showed a significant difference from the other N-glycoforms. The G0 N-glycoform showed a T_{onset} of 61.3ºC and T_{m1} of 71.4ºC. Compared to the other N-glycoforms, this is an increase the T_{onset} of unfolding by almost 7ºC and the T_{m1} by almost 4ºC. The T_{m1} corresponds to unfolding of the CH2 domain, which is where the N-glycan is located. The T_{m2}, which corresponds to unfolding of the CH3 domain, didn't show any mentionable differences.

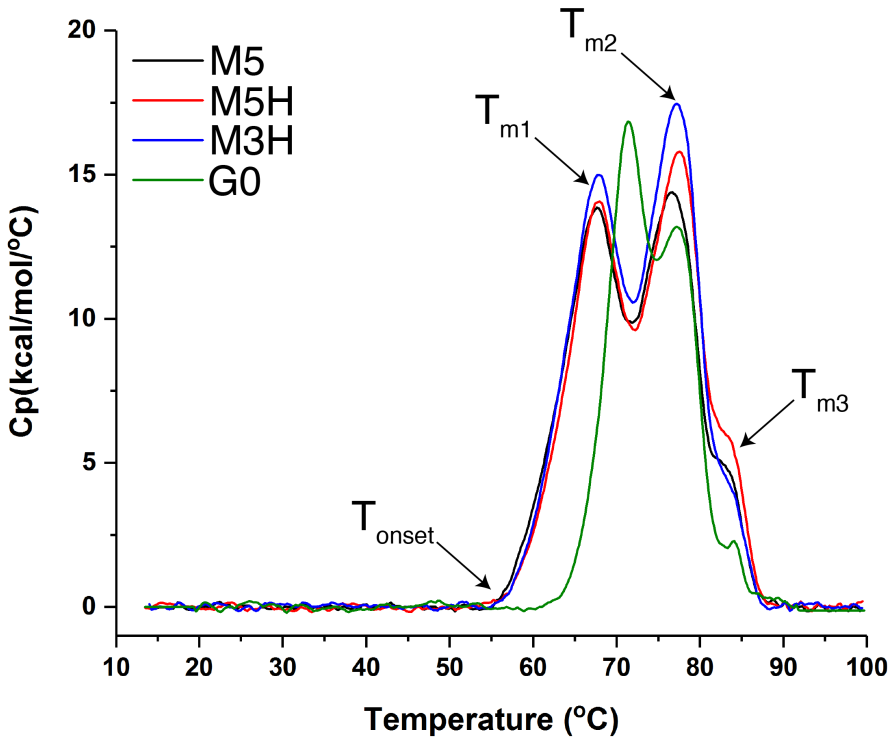

Glycoform (n = 3)	T_{onset} (ºC)	T_{m1} (ºC)	T_{m2} (ºC)	T_{m3} (ºC)
M5	54.6 ± 0.3	67.1 ± 0.1	77.0 ± 0.0	83.7± 0.1
M5H	54.6 ± 0.2	67.6 ± 0.1	77.6 ± 0.1	84.1± 0.1
M3H	54.7 ± 0.3	67.6 ± 0.1	77.3 ± 0.0	84.1± 0.1
G0	61.3 ± 0.2	71.4 ± 0.1	77.7 ± 0.1	84.3± 0.1

Figure 3.5: DSC thermograms of non-fucosylated homogenous IgG1 Fc N-glycoforms. Samples were analyzed in triplicate. Each thermogram represents the average values from triplicate measurements after correction from a buffer reference. Table shows average T_{onset}, T_{m1}, T_{m2}, and T_{m3} values ± standard deviation.

It has been reported from crystal structures as well as from NMR studies that there is an interaction with the GlcNAc on the α-1,6-arm on the N-glycan with Phe243 of the Fc (**Figure 3.6**).[57-59] It has also been reported that this interaction results in a stability benefit by researchers who compared homogenous IgG1 Fc N-glycoforms by DSC.[55, 56, 58] These reports compared M5H to G0 and M3F to G0F. However, these comparisons still left ambiguity as to which sugar residue, or absence of sugar residue, is causing the stability difference. The stability difference could have been caused by loss of either the α1,3- and/or α1,6-mannose residues on the α1,6 arm and/or the addition of the β1,2-GlcNAc on the α1,6 arm. In this work, the N-glycoforms used provided a more conclusive determination because M3H was compared to G0. The only difference between these two N-glycoforms was the addition of the β1,2-GlcNAc on the α1,6 arm. Therefore, the results in this work showed clearly that the β1,2-GlcNAc on the α1,6 arm was causing the increase in stability.

The non-fucosylated N-glycoforms were also compared to one another using analytical SEC to check for the presence of soluble aggregates (**Appendix 2: Figure A.2.5**). The results showed that all N-glycoforms showed a very high percentage (>97.7%) of monomer, with the G0 N-glycoform showing the highest percentage of monomer (99.5%). Furthermore, the non-fucosylated N-glycoforms were compared to one another using OD350 to measure aggregation propensity as a function of temperature (**Appendix 2: Figure A.2.6**). Results showed that the M5 N-glycoform showed the earliest T_{onset} of turbidity (72.3ºC). Both hybrid N-glycoforms showed very similar T_{onset} values (74.1-74.2ºC). Lastly, the G0 showed the highest T_{onset}, suggesting that the G0 N-glycoform was less prone to aggregation (76.2ºC).

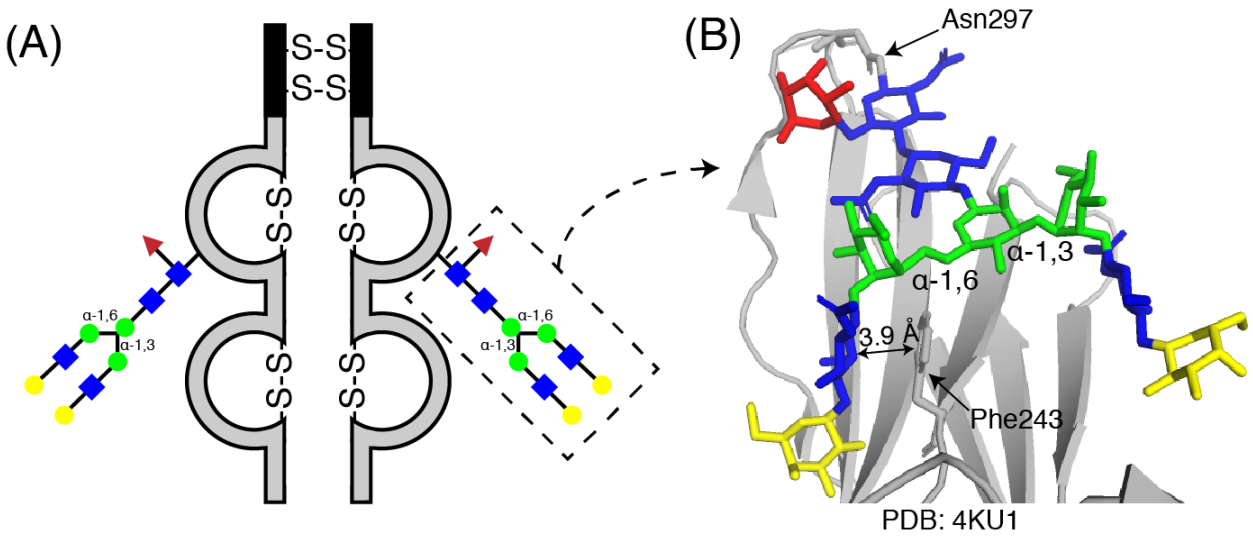

Figure 3.6: Representation of GlcNAc on the α1,6-arm interacting with the IgG1 Fc backbone. (A) Representation of G2F-IgG1 Fc. (B) Crystal structure of G2F-IgG1 Fc highlighting the interaction between GlcNAc on the α-1,6 arm of the N-glycan and Phe243 (PDB: 4KU1). Glycosylation symbols: blue, GlcNAc; green, mannose; red, fucose; yellow, galactose.

3.3.4 Comparison of IgG1 Fc N-glycoform binding to FcγRIIIa

The function of the IgG1 Fc N-glycoforms were compared in a receptor binding assay with FcγRIIIa. This receptor was chosen for the comparability assessment because it is the primary FcγR receptor found on NK cells that is involved in activating ADCC.[60] IgG1 Fc is a symmetric homodimer, but FcγRIIIa binds to the Fc asymmetrically in a 1:1 ratio.[61] More specifically, FcγRIIIa interacts with the BC, C'E, and FG loops in the CH2 domain of one Fc chain and residues S239 and L235 on both Fc chains.[62] These regions are put into proper orientation by intramolecular contacts between the Fc N-glycan and Fc polypeptide, which restrict the dynamics of the Fc protein-glycan.[13-15] The type of glycosylation determines which contacts occur and therefore affect the binding affinity to FcγRIIIa.

In this work, seven homogenous N-glycoforms were compared in a receptor binding assay with FcγRIIIa using BioLayer Interferometry (**Figure 3.7**). A comparison of the non-

fucosylated N-glycoforms showed an overall trend of increasing affinity with increasing N-glycan processing (M5 ≈ M5H < M3H < G0) (**Table 3.3**). This trend is somewhat apparent in the progressively faster association rate constants (k_a) (M5 < M5H < M3H < G0), and more significant trend differences are present in the progressively slower dissociation rate constants (k_d) (M5 ≈ M5H > M3H > G0) (**Figure 3.8**). The results did not show a significant difference in K_D between the M5 and M5H N-glycoforms. However, there was a significant difference between the M5H and M3H N-glycoforms, showing that the removal of the α-1,3/6 mannose residues improved binding affinity. Furthermore, there was a significant difference between the M3H and G0 N-glycoforms, indicating that the addition of the GlcNAc on the α1,6-arm of the Fc N-glycan increased binding affinity. This difference could be due to the additional interaction between the GlcNAc on the α1,6-arm of the Fc N-glycan interacting with Phe243 (**Figure 3.6**). These trends also hold true when comparing the N-glycoforms' affinities from equilibrium binding (**Figure 3.9**).

Furthermore, comparing the non-fucosylated N-glycoforms to their fucosylated counterparts showed about a 10-fold lower affinity upon fucosylation from analysis of the kinetic K_D results and a 25-fold difference from equilibrium K_D results (**Figure 3.8 and Figure 3.9**). Comparing the kinetic rate constants showed that fucosylation caused a decrease in k_a and increase in k_d, with the biggest difference coming from the k_a. This result is in agreement with Subedi and Barb (2016), who also reported these trends in kinetic rate constants when comparing non-fucosylated vs. fucosylated homogenous N-glycoforms.[19] In literature, there are a large range of values reported for the reduced affinity of binding to FcγRIIIa upon fucosylation. The differences range from 2 to 50-fold.[12, 17-21] The differences in K_D between fucosylated and non-fucosylated are caused not only by differences in Fc N-glycosylation but differences in FcγRIIIa

N-glycosylation as well.[18] Falconer *et al.* (2018) showed that comparing G2 vs G2F N-glycoforms of the Fc using homogenous M5 N-glycosylation of FcγRIIIa, the affinity upon Fc fucosylation decreased 17.5-fold. However, when comparing these same Fc N-glycans using FcγRIIIa with N-glycosylation containing only a single GlcNAc, the affinity upon fucosylation only decreased 2-fold. In our work, a homogenous M8-10 N-glycosylation for the FcγRIIIa was used (**Appendix 2: Figure A.2.7**). Using this receptor, comparing homogenous N-glycoforms with and without fucose showed about a 10-fold (kinetic) and 25-fold (equilibrium) weaker affinity upon fucosylation.

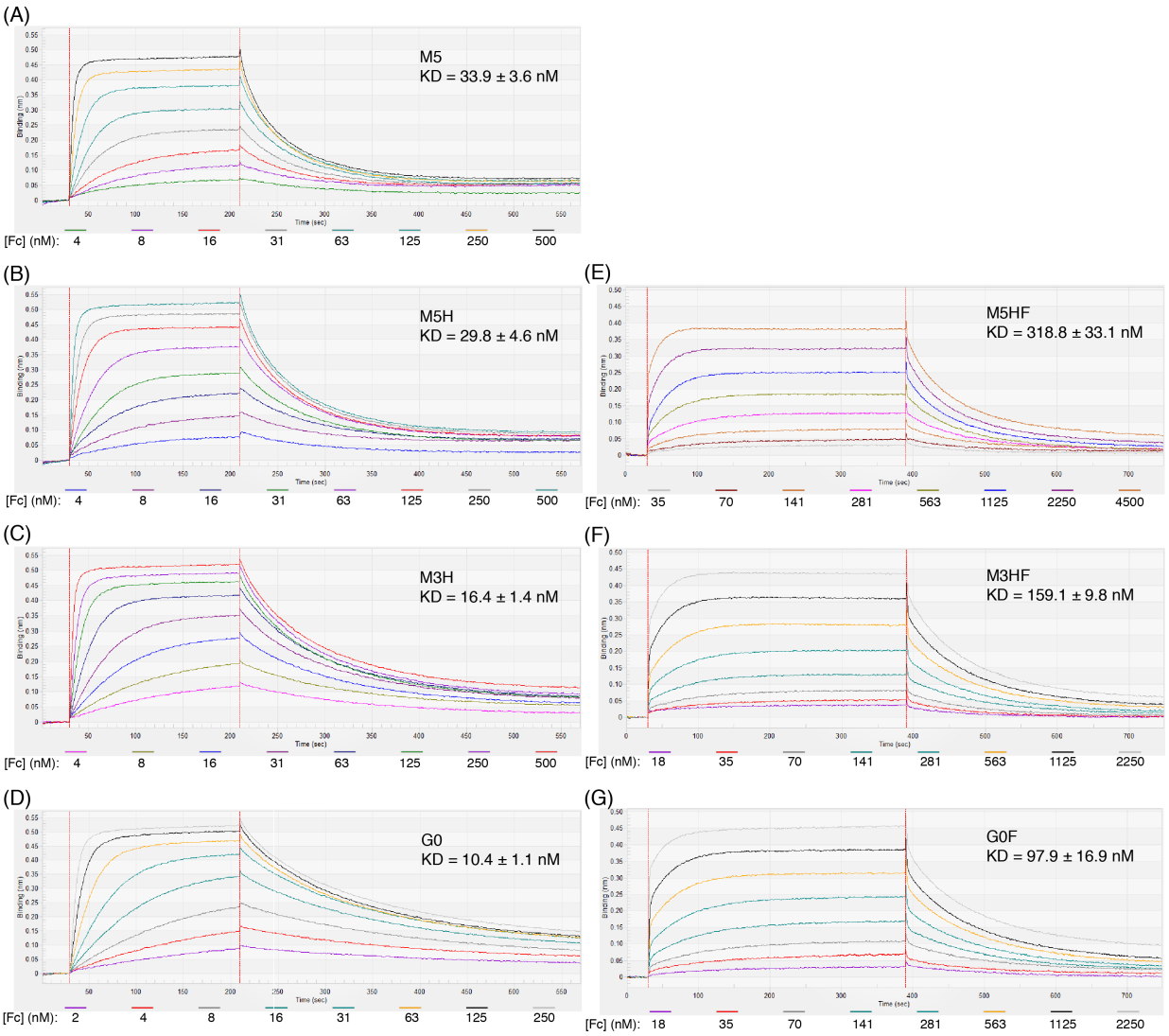

Figure 3.7: Representative sensorgrams of FcγRIIIa binding to homogenous IgG1 Fc N-glycoforms. Shown below each sensorgrams is the set of IgG1 Fc concentrations that were tested. N-glycoforms: (A) M5, (B) M5H, (C) M3H, (D) G0, (E) M5HF, (F) M3HF, and (G) G0F. Reported K_D is the average value of triplicate runs ± standard deviation.

Table 3.3: Kinetic Values For IgG1 Fc N-glycoforms Binding To FcγRIIIa*

N-glycoform	K_D (nM)#	k_a x 10^5 (1/Ms)	k_d x 10^{-2} (1/s)
M5	33.9 ± 3.6	4.20 ± 0.28	1.42 ± 0.12
M5H	29.8 ± 4.6	4.77 ± 0.49	1.42 ± 0.17
M3H	16.4 ± 1.4	5.07 ± 0.42	0.83 ± 0.02
G0	10.4 ± 1.1	5.50 ± 0.05	0.57 ± 0.06
M5HF	318.8 ± 33.1	0.39 ± 0.01	1.24 ± 0.12
M3HF	159.1 ± 9.8	0.81 ± 0.04	1.28 ± 0.05
G0F	97.9 ± 16.9	1.10 ± 0.19	1.06 ± 0.04

*Reported values are the average of triplicate runs ± standard deviation.
#Standard deviations were calculated by taking into account the error of propagation.

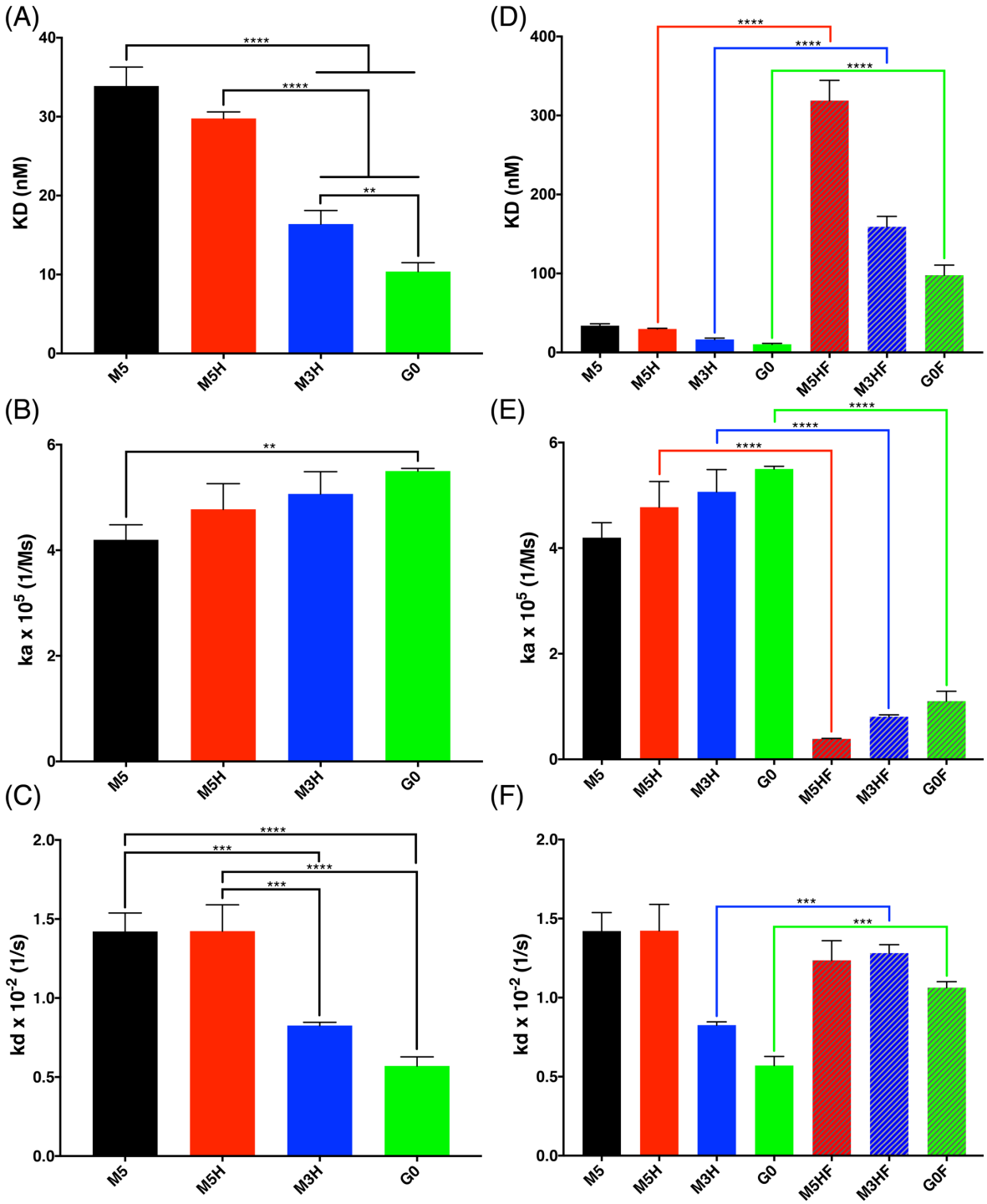

Figure 3.8: Bar graphs comparing kinetic values of IgG1 Fc N-glycoforms in binding assay with FcγRIIIa. (A-C) Comparison of non-fucosylated N-glycoforms. (A) Kinetic dissociation value (K_D), (B) kinetic association rate constant (k_a), and (C) kinetic dissociation rate constant (k_d). (D-F) Comparison of non-fucosylated (solid bars) vs. fucosylated (hatched bars) N-glycoforms. (D) K_D, (E) k_a, and (F) k_d. The top of each bar represents the average value of triplicate runs and the error bar represents standard deviation. Significance: ** = $p < 0.01$, *** = $p < 0.001$, and **** = $p < 0.0001$.

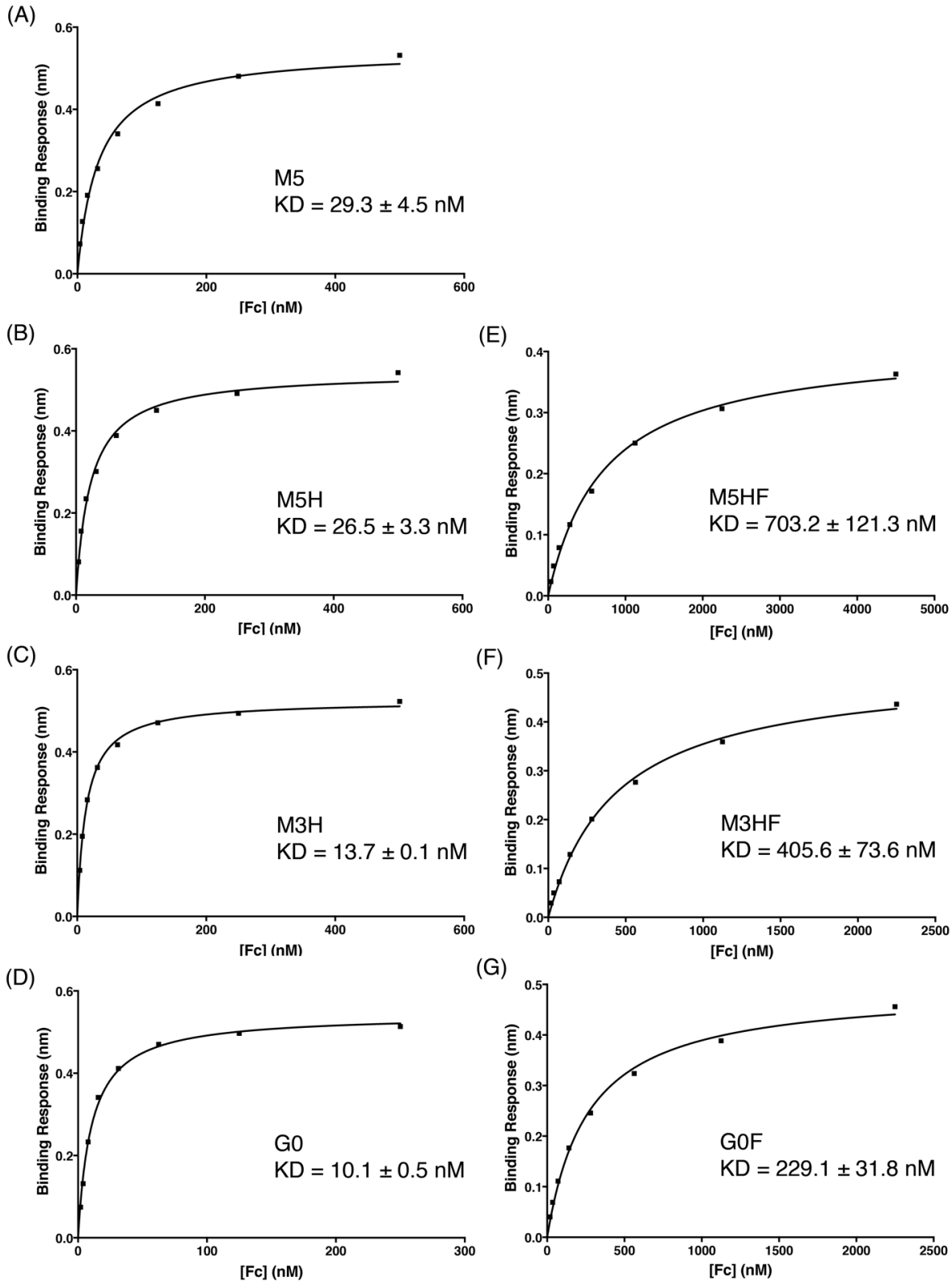

Figure 3.9: Equilibrium binding curves of homogenous IgG1 Fc N-glycoforms binding to FcγRIIIa. (A) M5, (B) M5H, (C) M3H, (D) G0, (E) M5HF, (F) M3HF, (G) G0F. K_D values shown are the average ± standard deviation from triplicate experiments.

Most FcγRIIIa binding assays were done using FcγRIIIa from recombinant expression in mammalian cell lines, which produces FcγRIIIa with mostly complex-type N-glycosylation. However, an analysis of the N-glycosylation of FcγRIIIa from donor NK cells showed that almost a quarter of N-glycosylation was hybrid and almost another quarter was oligomannose.[63] Furthermore, in a comparison between FcγRIIIa with complex vs. oligomannose N-glycosylation, IgG1 Fc with G0F N-glycosylation bound the oligomannose-containing receptor with 12-fold greater affinity than the complex. It was shown that the N-linked glycosylation affected the conformation of FcγRIIIa differently when the glycosylation was complex vs M5. The FcγRIIIa used in this study was M8-10 and showed a K_D using G0F-IgG1 Fc as 97.9 nM, which is in between the K_D results reported by Patel *et al.* (2018) using the M5 and complex FcγRIIIa, which showed 25 nM and 310 nM, respectively.

One hypothesis for the effects of IgG1 fucosylation on FcγRIIIa binding that is supported by crystal structures of complexed Fc-FcγRIIIa is that there are intermolecular glycan-glycan contacts between the Asn297 glycan of the Fc Asn162 glycan of the FcγRIIIa,[21, 64] and the addition of core-linked fucose on the Fc N-glycan inhibits these contacts, thereby weakening the binding affinity. When the Fc Asn297 glycan is afucosyated, the two N-glycans are in close proximity. However, when the Fc Asn297 glycan is fucosylated, the distance between the glycans increases. The contacts that are involved in the Fc are mainly in the core pentasaccharide, especially the innermost GlcNAc residue. However, it was observed that trimming all N-glycans of FcγRIIIa down to single GlcNAc, which should have abolished the some of the proposed glycan-glycan contacts, actually increased binding affinity.[18] Falconer *et al.* (2018) recently proposed a second hypothesis whereby the amount of volume sampled by the Asn162 glycan is limited when the Asn297 glycan of the Fc is fucosylated.[18] Our results provide

support for this second hypothesis because, when comparing non-fucosylated N-glycoforms, the biggest difference in binding was between the M3H and M5H. Removing the two mannoses may have allowed for more volume to be sampled by the Asn162 glycan of FcγRIIIa. Also, these two mannose residues were not involved in any of the intermolecular glycan-glycan or glycan-polypeptide contacts that were reported from the crystal structure data.[21, 64] Furthermore, comparison of M3H to G0 showed that the addition of GlcNAc improved binding. It allowed for the Phe243 contact, which may have help to orient the Fc interface to allow for optimal binding by restricting the mobility of the Fc Asn 297 glycan[15] and also possibly increasing the sampling volume of the FcγRIIIa Asn162 glycan.

3.3.5 Comparison of core-linked fucosylation.

The rates of the core-linked fucosylation of the different homogenous N-glycoforms by FUT8 were compared by measuring initial rate kinetics in a coupled enzyme assay (**Figure 3.10**). FUT8 adds an α1,6-fucose residue to the innermost GlcNAc of the N-glycan of IgG1 Fc. In order for the N-glycan to be a substrate for FUT8, the presence of GlcNAc on the α1,6 arm of the biantennary N-glycan is required.[65] The FUT8-catalyzed transfer of fucose to IgG1 Fc was detected using a coupled enzyme assay in which GDP produced by the FUT8 reaction was phosphorylated to GTP using pyruvate kinase and PEP. The resulting pyruvate was then reduced to lactic acid by NADH in a reaction catalyzed by lactate dehydrogenase. Loss of NADH was detected by monitoring absorbance at 340 nm. Large excesses of pyruvate kinase and lactate dehydrogenase were utilized such that the FUT8 reaction was the rate-limiting step of the coupled enzyme assay.

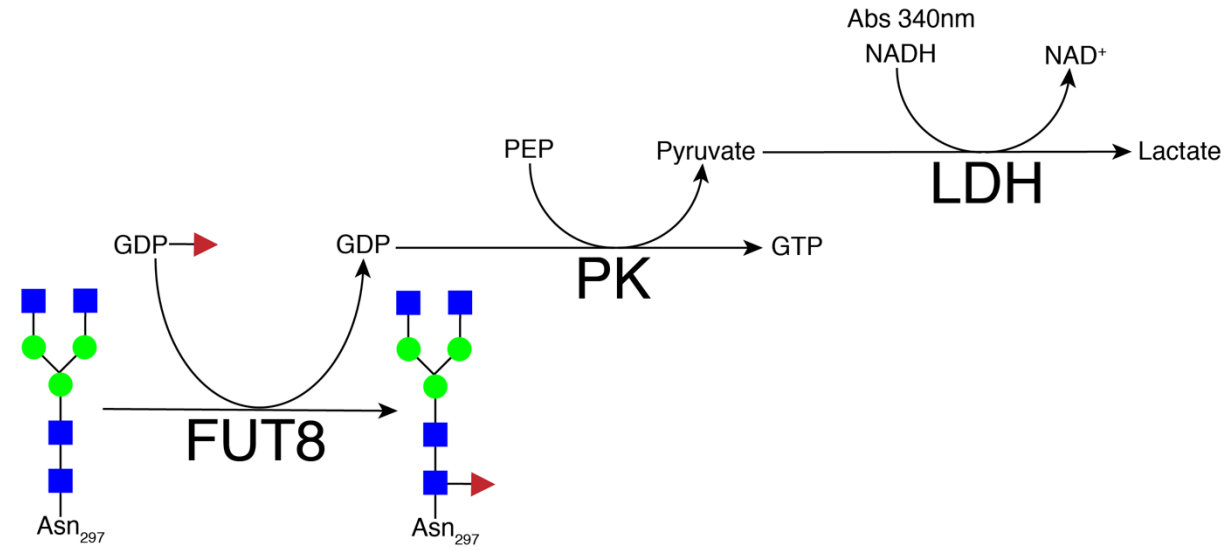

■ = N-acetylglucosamine, ● = Mannose, ▶ = Fucose
FUT8 = α-1,6-fucosyltransferase, GDP = Guanosine Diphosphate, PEP = Phosphoenolpyruvate, PK = Pyruvate Kinase, LDH = Lactate Dehydrogenase, NADH = Nicotinamide Adenine Dinucleotide Hydrogen

Figure 3.10: Representation of coupled enzyme assay. FUT8 was coupled to PK/LDH enzymes. Fucose transfer by FUT8 produces GDP as a byproduct. GDP is accepted as a substrate for PK which transfers phosphate from PEP to GDP to form GTP and pyruvate. Pyruvate is reduced by LDH and NADH to form lactate and NAD^+. NADH absorbs light at 340 nm, whereas NAD^+ does not. The loss of signal at 340 nm correlates to the loss of NADH, which correlates to core-linked fucosylation.

The K_M of FUT8 for the M5H, M3H, and G0 N-glycoforms were determined for both free glycans and glycans N297-bound to IgG1 Fc. The free glycan was obtained by treating the corresponding IgG1 Fc N-glycoform with PNGase F with completion of the de-glycosylation being confirmed using intact mass spectrometry (**Appendix 2: Figure A.2.8**). The M5 N-glycoform was not tested because it was previously reported that M5 is not a substrate for FUT8,[53] except under unique conditions.[14, 66] The results showed that the K_M for the free glycans were all in the low µM range and were within 2-fold of one another (17 µM for M5H, 13 µM for M3H, and 25 µM for G0) (**Figure 3.11A-C** and **Table 3.4**). These data are near the K_M previously reported by Ihara *et. al* (2005) for human FUT8 using a free agalactosylated

biantennary glycan, which was 12.9 ± 1.2 μM. The results showed that the affinities for the different N-glycoforms (glycan types) were relatively similar when the glycans were free in solution. However, when the glycans were Asn297-bound to IgG1 Fc, the K_M values of M5H and M3H were relatively similar at 244 μM and 189 μM, respectively, while the G0 N-glycoform had a significantly larger K_M of 3437 μM (**Figure 3.11D-F** and **Table 3.4**). Compared to the corresponding free glycans, the K_M values for the bound M5H and M3H N-glycoforms increased approximately 14-fold while the K_M for G0 increased 137-fold. For both the free glycan and glycoprotein bound states, the M3H N-glycoform showed a slightly higher affinity for FUT8 than M5H. The loss of the 2 mannose residues may be making the innermost GlcNAc and/or the GlcNAc on the α1,3-arm more accessible, although the difference in affinities between M3H and M5H substrates was not dramatic. The trends between M5H, M3H, and G0 bound to IgG1 Fc were also observed using intact mass spectrometry (**Appendix 2: Figure A.2.9**) and showed very similar trends to those observed from the coupled enzyme assay.

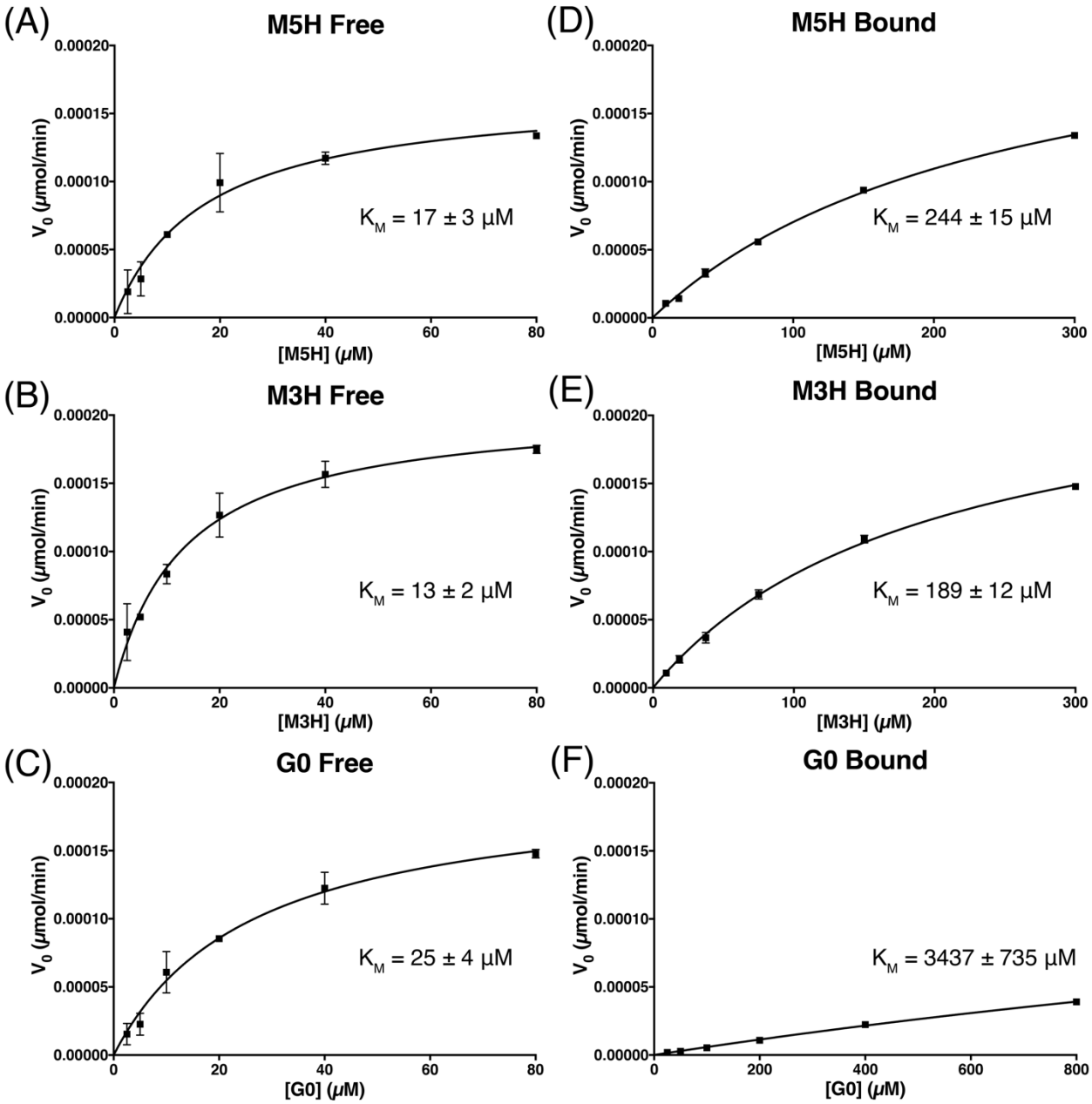

Figure 3.11: Michaelis-Menton plots for fucosylation by FUT8 of glycans either free or bound to IgG1 Fc. Free glycans were produced from IgG1 Fc N-glycoforms using PNGase F, whereas the bound N-glycoforms were Asn_{297}-linked to IgG1 Fc. Free N-glycoforms: (A) M5H, (B) M3H, and (C) G0. IgG1 Fc-bound N-glycoforms: (D) M5H, (E) M3H, (F) G0. The reported K_M values are the fitted values of triplicate runs. The error bars represent ± the standard error.

Table 3.4: Michaelis-Menton Values Of Fucosylation Kinetics

N-glycoform	Free or Bound	K_M (μM)*	K_M Ratio (Bound/Free)	V_{max} (μmol/min) x10^{-3}*
M5H	Free	17 ± 3	14	0.17 ± 0.01
	Bound	244 ± 15		0.25 ± 0.01
M3H	Free	13 ± 2	14	0.21 ± 0.01
	Bound	189 ± 12		0.25 ± 0.01
G0	Free	25 ± 4	137	0.20 ± 0.01
	Bound	3437 ± 735		0.22 ± 0.04

*The reported K_M and V_{max} values are the fitted values of triplicate runs ± standard error.

The extremely high K_M for the G0 N-glycoform when bound to IgG1 Fc could be caused by the interaction between the GlcNAc on the α1,6-arm of the N-glycan and Phe243 of the IgG1 Fc polypeptide (**Figure 3.6**). This interaction could be reducing the accessibility of FUT8 to the glycan. Mutations at the 243 position have been shown to lead to more highly-processed types of glycosylation such as increased levels of galactose, sialic acid, and bisecting GlcNAc.[14, 15, 67] This suggests that disrupting this interaction increased the glycan processing activities of galactosyltransferase, sialyltransferase, and N-acetylglucosaminyltransferase-III, respectively. Based on this work, the glycan-protein contact at position 243 may also be affecting the activity of FUT8. Interestingly, the reports that showed increased bisecting GlcNAc upon Phe243 mutation also observed that the fucosylation levels were maintained. Increasing bisecting GlcNAc usually decreases fucosylation levels.[22] Perhaps the fucosylation levels were maintained because removing the Phe243 interaction made the N-glycan more accessible to FUT8. In the literature, Calderon *et al.* (2016) showed that fucosylation of free glycans is occurring throughout the hybrid and complex-type glycans.[53] Even glycans with terminal galactose and sialyation are capable of being fucosylated. However, this work showed that when the glycans were N-linked to IgG1 Fc, only hybrid glycans were fucosylated to any practical extent. This suggests that, during N-glycan biosynthesis of IgG1 in B cells, fucosylation is occurring

primarily during the hybrid stages (**Figure 3.12**). Therefore, this work allowed us to make new insights into the fucosylation during N-glycan biosynthesis IgG1.

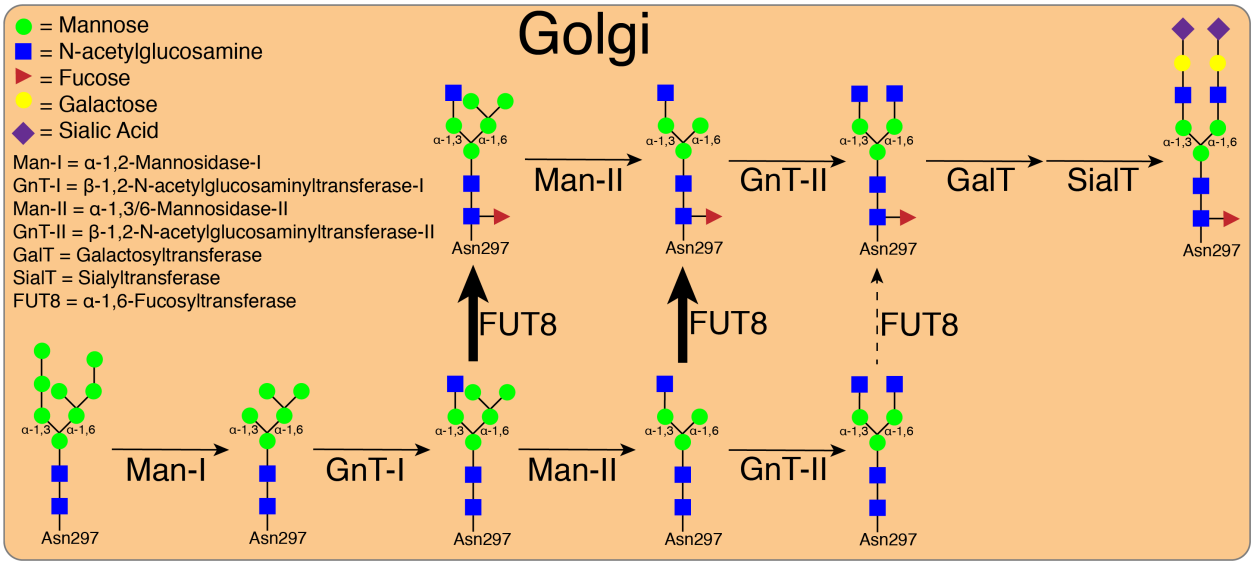

Figure 3.12: Representation of N-linked glycan processing of IgG1 in the Golgi of mammalian cells. Shown is the most prominent pathway for N-linked glycan processing after taking into account the FUT8 kinetic studies reported herein. For the fucosylation step, the thick arrows represent the more likely pathway whereas the dashed arrow represents the less likely pathway.

3.4 Conclusions

IgG1-based therapeutics are important biomolecules for the treatment of a variety of complex diseases including cancer, autoimmune disease, and organ-transplant rejection. Their bioactivity can engage immune system function through interaction with FcγRs. FcγRs can activate both pro- and anti-inflammatory pathways. The specific type of activation can be influenced by the N-glycosylation of IgG1. Subtle differences in N-glycosylation can have large influences on the immune response. However, these differences are difficult to determine because expression of IgG1 results in a mixture of N-glycoforms and different N-glycoforms can have different effects.

In this work, IgG1 Fc was used as a model system to prepare seven homogenous IgG1 N-glycoforms. IgG1 Fc was expressed in glycosylation-deficient yeast to obtain a relatively homogenous high mannose N-glycoform. This N-glycoform was then used as a starting substrate to for *in-vitro* enzymatic synthesis to produce a series of oligomannose, hybrid, and complex type N-glycoforms with and without fucose. At each step, >98% conversion was obtained as determined by intact mass spectrometry.

The influence of the different N-glycoforms on IgG1 Fc stability were compared using DSC. Compared to the other non-fucosylated N-glycoforms, the G0 N-glycoform showed a large increase in thermal stability in the CH2 domain. This stability is likely due to an intramolecular glycan-protein interaction between the GlcNAc on the α1,6-arm and the Phe243 residue of the IgG1 Fc polypeptide. This is the first report of a comparison between M3H and G0 N-glycoforms, which is the most direct comparison to demonstrate this stability effect.

Furthermore, the seven homogenous IgG1 Fc N-glycoforms were compared in a binding assay with FcγRIIIa. In literature, there is a big range in reported values for IgG1 Fc binding to FcγRIIIa. The measured affinity can depend on several factors such as N-glycosylation of the IgG1, the N-glycosylation of FcγRIIIa, and the methodology. This work attempted to clarify the variation by comparing all seven N-glycoforms in a consistent assay. The results showed an increased affinity for M3H compared to M5H. This could be due to reduced sterics of M3H compared to M5H, which may be have increased the freedom within the Fc-FcγRIIIa interface. Results also showed an increased affinity for G0 compared to M3H. This could be due to the interaction between GlcNAc on the α1,6-arm of the N-glycan and the Phe243 that is present for G0 but not M3H. Additionally, comparing the non-fucosylated N-glycoforms to their fucosylated counterparts, results showed an about 10-fold kinetic (or 25-fold equilibrium)

difference in affinity upon fucosylation. To the best of our knowledge, this is the first report of a binding affinity of FcγRIIIa to IgG1 Fc using homogenous M3H and M3HF N-glycoforms.

Lastly, the M5H, M3H, and G0 N-glycoforms were compared in a FUT8 kinetic coupled enzyme assay. The N-glycoforms were measured in both their free and Asn-297 bound states. In their free states, the N-glycoforms were relatively similar. However, when bound to IgG1 Fc, the G0 N-glycoform showed much lower affinity to FUT8. This could be due to the GlcNAc on the α1,6-arm of the N-glycan interacting with Phe243 on the Fc. Previous reports showed that both hybrid and complex N-glycoforms were acceptable substrates for FUT8 when the glycan is free. Our work supports this data. However, our work also shows that when the G0 N-glycoform is bound to the Fc, the glycan has a much weaker affinity for the FUT8 active site compared to the hybrid N-glycoforms. This suggests that, during N-glycan biosynthesis, fucosylation is likely occurring at the hybrid stages. These studies improve our fundamental understanding of IgG1 N-glycosylation and may also help in the development of improved antibody-based therapeutics.

3.5 References

(1) Grilo, A. L., and Mantalaris, A. (2019) The increasingly human and profitable monoclonal antibody market. *Trends in biotechnology 37*, 9-16.

(2) More, A. S., Toprani, V. M., Okbazghi, S. Z., Kim, J. H., Joshi, S. B., Middaugh, C. R., Tolbert, T. J., and Volkin, D. B. (2016) Correlating the impact of well-defined oligosaccharide structures on physical stability profiles of IgG1-Fc glycoforms. *Journal of pharmaceutical sciences 105*, 588-601.

(3) Higel, F., Seidl, A., Sörgel, F., and Friess, W. (2016) N-glycosylation heterogeneity and the influence on structure, function and pharmacokinetics of monoclonal antibodies and Fc fusion proteins. *European Journal of Pharmaceutics and Biopharmaceutics 100*, 94-100.

(4) Zheng, K., Bantog, C., and Bayer, R. (2011) The impact of glycosylation on monoclonal antibody conformation and stability. *MAbs 3*, 568-576.

(5) Abès, R., and Teillaud, J.-L. (2010) Impact of glycosylation on effector functions of therapeutic IgG. *Pharmaceuticals 3*, 146-157.

(6) Giorgetti, J., D'Atri, V., Canonge, J., Lechner, A., Guillarme, D., Colas, O., Wagner-Rousset, E., Beck, A., Leize-Wagner, E., and François, Y.-N. (2018) Monoclonal antibody N-glycosylation profiling using capillary electrophoresis–Mass spectrometry: Assessment and method validation. *Talanta 178*, 530-537.

(7) Baković, M. P. i., Selman, M. H., Hoffmann, M., Rudan, I., Campbell, H., Deelder, A. M., Lauc, G., and Wuhrer, M. (2013) High-throughput IgG Fc N-glycosylation profiling by mass spectrometry of glycopeptides. *Journal of proteome research 12*, 821-831.

(8) Scallon, B. J., Tam, S. H., McCarthy, S. G., Cai, A. N., and Raju, T. S. (2007) Higher levels of sialylated Fc glycans in immunoglobulin G molecules can adversely impact functionality. *Molecular immunology 44*, 1524-1534.

(9) Kurai, J., Chikumi, H., Hashimoto, K., Yamaguchi, K., Yamasaki, A., Sako, T., Touge, H., Makino, H., Takata, M., and Miyata, M. (2007) Antibody-dependent cellular cytotoxicity mediated by cetuximab against lung cancer cell lines. *Clinical Cancer Research 13*, 1552-1561.

(10) Arnould, L., Gelly, M., Penault-Llorca, F., Benoit, L., Bonnetain, F., Migeon, C., Cabaret, V., Fermeaux, V., Bertheau, P., and Garnier, J. (2006) Trastuzumab-based treatment of HER2-positive breast cancer: an antibody-dependent cellular cytotoxicity mechanism? *British journal of cancer 94*, 259-267.

(11) Thomann, M., Reckermann, K., Reusch, D., Prasser, J., and Tejada, M. L. (2016) Fc-galactosylation modulates antibody-dependent cellular cytotoxicity of therapeutic antibodies. *Molecular immunology 73*, 69-75.

(12) Wada, R., Matsui, M., and Kawasaki, N. (2019) Influence of N-glycosylation on effector functions and thermal stability of glycoengineered IgG1 monoclonal antibody with homogeneous glycoforms. *mAbs 11*, 350-372.

(13) Subedi, G. P., and Barb, A. W. (2015) The structural role of antibody N-glycosylation in receptor interactions. *Structure 23*, 1573-1583.

(14) Yu, X., Baruah, K., Harvey, D. J., Vasiljevic, S., Alonzi, D. S., Song, B.-D., Higgins, M. K., Bowden, T. A., Scanlan, C. N., and Crispin, M. (2013) Engineering hydrophobic protein–carbohydrate interactions to fine-tune monoclonal antibodies. *Journal of the American Chemical Society 135*, 9723-9732.

(15) Subedi, G. P., Hanson, Q. M., and Barb, A. W. (2014) Restricted motion of the conserved immunoglobulin G1 N-glycan is essential for efficient FcγRIIIa binding. *Structure 22*, 1478-1488.

(16) Okbazghi, S. Z., More, A. S., White, D. R., Duan, S., Shah, I. S., Joshi, S. B., Middaugh, C. R., Volkin, D. B., and Tolbert, T. J. (2016) Production, characterization, and

biological evaluation of well-defined IgG1 Fc glycoforms as a model system for biosimilarity analysis. *Journal of pharmaceutical sciences 105*, 559-574.

(17) Shields, R. L., Lai, J., Keck, R., O'Connell, L. Y., Hong, K., Meng, Y. G., Weikert, S. H., and Presta, L. G. (2002) Lack of fucose on human IgG1 N-linked oligosaccharide improves binding to human FcγRIII and antibody-dependent cellular toxicity. *Journal of Biological Chemistry 277*, 26733-26740.

(18) Falconer, D. J., Subedi, G. P., Marcella, A. M., and Barb, A. W. (2018) Antibody fucosylation lowers the FcγRIIIa/CD16a affinity by limiting the conformations sampled by the N162-glycan. *ACS chemical biology 13*, 2179-2189.

(19) Subedi, G. P., and Barb, A. W. (2016) The immunoglobulin G1 N-glycan composition affects binding to each low affinity Fc γ receptor. *MAbs 8*, 1512-1524.

(20) Kanda, Y., Yamada, T., Mori, K., Okazaki, A., Inoue, M., Kitajima-Miyama, K., Kuni-Kamochi, R., Nakano, R., Yano, K., and Kakita, S. (2006) Comparison of biological activity among nonfucosylated therapeutic IgG1 antibodies with three different N-linked Fc oligosaccharides: the high-mannose, hybrid, and complex types. *Glycobiology 17*, 104-118.

(21) Ferrara, C., Grau, S., Jäger, C., Sondermann, P., Brünker, P., Waldhauer, I., Hennig, M., Ruf, A., Rufer, A. C., and Stihle, M. (2011) Unique carbohydrate–carbohydrate interactions are required for high affinity binding between FcγRIII and antibodies lacking core fucose. *Proceedings of the National Academy of Sciences 108*, 12669.

(22) Wang, Q., Chung, C. Y., Chough, S., and Betenbaugh, M. J. (2018) Antibody glycoengineering strategies in mammalian cells. *Biotechnology and bioengineering 115*, 1378-1393.

(23) Loo, T., Patchett, M. L., Norris, G. E., and Lott, J. S. (2002) Using secretion to solve a solubility problem: high-yield expression in Escherichia coli and purification of the bacterial glycoamidase PNGase F. *Protein expression and purification 24*, 90-98.

(24) White, D. R., Khedri, Z., Kiptoo, P., Siahaan, T. J., and Tolbert, T. J. (2017) Synthesis of a Bifunctional Peptide Inhibitor–IgG1 Fc Fusion That Suppresses Experimental Autoimmune Encephalomyelitis. *Bioconjugate Chemistry 28*, 1867-1877.

(25) Xiao, J., Chen, R., Pawlicki, M. A., and Tolbert, T. J. (2009) Targeting a homogeneously glycosylated antibody Fc to bind cancer cells using a synthetic receptor ligand. *Journal of the American Chemical Society 131*, 13616-13618.

(26) Shah, I. S., Lovell, S., Mehzabeen, N., Battaile, K. P., and Tolbert, T. J. (2017) Structural characterization of the Man5 glycoform of human IgG3 Fc. *Molecular immunology 92*, 28-37.

(27) Choi, B.-K., Warburton, S., Lin, H., Patel, R., Boldogh, I., Meehl, M., d'Anjou, M., Pon, L., Stadheim, T. A., and Sethuraman, N. (2012) Improvement of N-glycan site occupancy

of therapeutic glycoproteins produced in Pichia pastoris. *Applied microbiology and biotechnology 95*, 671-682.

(28) Cuskin, F., Lowe, E. C., Temple, M. J., Zhu, Y., Cameron, E. A., Pudlo, N. A., Porter, N. T., Urs, K., Thompson, A. J., Cartmell, A., Rogowski, A., Hamilton, B. S., Chen, R., Tolbert, T. J., Piens, K., Bracke, D., Vervecken, W., Hakki, Z., Speciale, G., Munoz-Munoz, J. L., Day, A., Pena, M. J., McLean, R., Suits, M. D., Boraston, A. B., Atherly, T., Ziemer, C. J., Williams, S. J., Davies, G. J., Abbott, D. W., Martens, E. C., and Gilbert, H. J. (2015) Human gut Bacteroidetes can utilize yeast mannan through a selfish mechanism. *Nature 517*, 165-169.

(29) Chen, R., Pawlicki, M. A., Hamilton, B. S., and Tolbert, T. J. (2008) Enzyme-catalyzed synthesis of a hybrid N-linked oligosaccharide using N-acetylglucosaminyltransferase I. *Advanced Synthesis & Catalysis 350*, 1689-1695.

(30) Wang, W., Hu, T., Frantom, P. A., Zheng, T., Gerwe, B., Del Amo, D. S., Garret, S., Seidel, R. D., and Wu, P. (2009) Chemoenzymatic synthesis of GDP-L-fucose and the Lewis X glycan derivatives. *Proceedings of the National Academy of Sciences 106*, 16096-16101.

(31) Nakajima, K., Kitazume, S., Angata, T., Fujinawa, R., Ohtsubo, K., Miyoshi, E., and Taniguchi, N. (2010) Simultaneous determination of nucleotide sugars with ion-pair reversed-phase HPLC. *Glycobiology 20*, 865-871.

(32) Gersten, K. M., Natsuka, S., Trinchera, M., Petryniak, B., Kelly, R. J., Hiraiwa, N., Jenkins, N. A., Gilbert, D. J., Copeland, N. G., and Lowe, J. B. (1995) Molecular cloning, expression, chromosomal assignment, and tissue-specific expression of a murine α-(1, 3)-fucosyltransferase locus corresponding to the human ELAM-1 ligand fucosyl transferase. *Journal of Biological Chemistry 270*, 25047-25056.

(33) Gasteiger, E., Hoogland, C., Gattiker, A., Duvaud, S., Wilkins, M. R., Appel, R. D., and Bairoch, A. (2005) Protein Identification and Analysis Tools on the ExPASy Server, in *The Proteomics Protocols Handbook* (Walker, J. M., Ed.) pp 571-607, Humana Press.

(34) Miura, M., Hirose, M., Miwa, T., Kuwae, S., and Ohi, H. (2004) Cloning and characterization in Pichia pastoris of PNO1 gene required for phosphomannosylation of N-linked oligosaccharides. *Gene 324*, 129-137.

(35) Hopkins, D., Gomathinayagam, S., Rittenhour, A. M., Du, M., Hoyt, E., Karaveg, K., Mitchell, T., Nett, J. H., Sharkey, N. J., and Stadheim, T. A. (2011) Elimination of β-mannose glycan structures in Pichia pastoris. *Glycobiology 21*, 1616-1626.

(36) Mille, C., Bobrowicz, P., Trinel, P.-A., Li, H., Maes, E., Guerardel, Y., Fradin, C., Martínez-Esparza, M., Davidson, R. C., and Janbon, G. (2008) Identification of a new family of genes involved in beta-1, 2 mannosylation of glycans in Pichia pastoris and Candida albicans. *Journal of Biological Chemistry*.

(37) Gomathinayagam, S., Mitchell, T., Zartler, E. R., Heiss, C., Azadi, P., Zha, D., Houston-Cummings, N. R., Jiang, Y., Li, F., and Giaccone, E. (2011) Structural elucidation of an α-1, 2-mannosidase resistant oligosaccharide produced in Pichia pastoris. *Glycobiology 21*, 1606-1615.

(38) Vervecken, W., Kaigorodov, V., Callewaert, N., Geysens, S., De Vusser, K., and Contreras, R. (2004) In vivo synthesis of mammalian-like, hybrid-type N-glycans in Pichia pastoris. *Applied and environmental microbiology 70*, 2639-2646.

(39) Krainer, F. W., Gmeiner, C., Neutsch, L., Windwarder, M., Pletzenauer, R., Herwig, C., Altmann, F., Glieder, A., and Spadiut, O. (2013) Knockout of an endogenous mannosyltransferase increases the homogeneity of glycoproteins produced in Pichia pastoris. *Scientific reports 3*, 3279.

(40) Ha, S., Ou, Y., Vlasak, J., Li, Y., Wang, S., Vo, K., Du, Y., Mach, A., Fang, Y., and Zhang, N. (2011) Isolation and characterization of IgG1 with asymmetrical Fc glycosylation. *Glycobiology 21*, 1087-1096.

(41) Moremen, K. W., Tiemeyer, M., and Nairn, A. V. (2012) Vertebrate protein glycosylation: diversity, synthesis and function. *Nature reviews Molecular cell biology 13*, 448-462.

(42) Hamilton, S. R., Li, H., Wischnewski, H., Prasad, A., Kerley-Hamilton, J. S., Mitchell, T., Walling, A. J., Davidson, R. C., Wildt, S., and Gerngross, T. U. (2005) Intact α-1, 2-endomannosidase is a typical type II membrane protein. *Glycobiology 15*, 615-624.

(43) Laukens, B., Visscher, C. D., and Callewaert, N. (2015) Engineering yeast for producing human glycoproteins: where are we now? *Future microbiology 10*, 21-34.

(44) Duman, J. G., Miele, R. G., Liang, H., Grella, D. K., Sim, K. L., Castellino, F. J., and Bretthauer, R. K. (1998) O-Mannosylation of Pichia pastoris cellular and recombinant proteins. *Biotechnology and applied biochemistry 28*, 39-45.

(45) Harpaz, N., and Schachter, H. (1980) Control of glycoprotein synthesis. Processing of asparagine-linked oligosaccharides by one or more rat liver Golgi alpha-D-mannosidases dependent on the prior action of UDP-N-acetylglucosamine: alpha-D-mannoside beta 2-N-acetylglucosaminyltransferase I. *The Journal of biological chemistry 255*, 4894.

(46) Shah, N., Kuntz, D. A., and Rose, D. R. (2008) Golgi α-mannosidase II cleaves two sugars sequentially in the same catalytic site. *Proceedings of the National Academy of Sciences 105*, 9570-9575.

(47) Schachter, H. (2002) N-Acetylglucosaminyltransferase-II, in *Handbook of GLycosyltransferases and Related Genes* pp 70-79, Springer.

(48) Bendiak, B., and Schachter, H. (1987) Control of glycoprotein synthesis. Kinetic mechanism, substrate specificity, and inhibition characteristics of UDP-N-

acetylglucosamine: alpha-D-mannoside beta 1-2 N-acetylglucosaminyltransferase II from rat liver. *Journal of Biological Chemistry 262*, 5784-5790.

(49) Zhao, G., Guan, W., Cai, L., and Wang, P. G. (2010) Enzymatic route to preparative-scale synthesis of UDP–GlcNAc/GalNAc, their analogues and GDP–fucose. *Nature protocols 5*, 636-646.

(50) Ihara, H., Ikeda, Y., and Taniguchi, N. (2005) Reaction mechanism and substrate specificity for nucleotide sugar of mammalian α1, 6-fucosyltransferase—a large-scale preparation and characterization of recombinant human FUT8. *Glycobiology 16*, 333-342.

(51) Ihara, H., Ikeda, Y., Toma, S., Wang, X., Suzuki, T., Gu, J., Miyoshi, E., Tsukihara, T., Honke, K., Matsumoto, A., Nakagawa, A., and Taniguchi, N. (2006) Crystal structure of mammalian α1, 6-fucosyltransferase, FUT8. *Glycobiology 17*, 455-466.

(52) Calderon, A. D., Li, L., and Wang, P. G. (2017) FUT8: from biochemistry to synthesis of core-fucosylated N-glycans. *Pure and Applied Chemistry 89*, 911-920.

(53) Calderon, A. D., Liu, Y., Li, X., Wang, X., Chen, X., Li, L., and Wang, P. G. (2016) Substrate specificity of FUT8 and chemoenzymatic synthesis of core-fucosylated asymmetric N-glycans. *Organic & biomolecular chemistry 14*, 4027-4031.

(54) Wozniak-Knopp, G., Stadlmann, J., and Rüker, F. (2012) Stabilisation of the Fc fragment of human IgG1 by engineered intradomain disulfide bonds. *PloS one 7*, 1-11.

(55) Mimura, Y., Church, S., Ghirlando, R., Ashton, P., Dong, S., Goodall, M., Lund, J., and Jefferis, R. (2000) The influence of glycosylation on the thermal stability and effector function expression of human IgG1-Fc: properties of a series of truncated glycoforms. *Molecular immunology 37*, 697-706.

(56) Mimura, Y., Sondermann, P., Ghirlando, R., Lund, J., Young, S. P., Goodall, M., and Jefferis, R. (2001) Role of oligosaccharide residues of IgG1-Fc in FcγRIIb binding. *Journal of Biological Chemistry*, 45539-45547.

(57) Barb, A. W. (2014) Intramolecular N-Glycan/Polypeptide Interactions Observed at Multiple N-Glycan Remodeling Steps through [13C, 15N]-N-Acetylglucosamine Labeling of Immunoglobulin G1. *Biochemistry 54*, 313-322.

(58) Bowden, T. A., Baruah, K., Coles, C. H., Harvey, D. J., Yu, X., Song, B.-D., Stuart, D. I., Aricescu, A. R., Scanlan, C. N., Jones, E. Y., and Crispin, M. (2012) Chemical and structural analysis of an antibody folding intermediate trapped during glycan biosynthesis. *Journal of the American Chemical Society 134*, 17554-17563.

(59) Krapp, S., Mimura, Y., Jefferis, R., Huber, R., and Sondermann, P. (2003) Structural analysis of human IgG-Fc glycoforms reveals a correlation between glycosylation and structural integrity. *Journal of molecular biology 325*, 979-989.

(60) Román, V. R. G., Murray, J. C., and Weiner, L. M. (2014) Antibody-Dependent Cellular Cytotoxicity (ADCC), in *Antibody Fc* pp 1-27, Elsevier.

(61) Sondermann, P., Huber, R., Oosthuizen, V., and Jacob, U. (2000) The 3.2-[angst] crystal structure of the human IgG1 Fc fragment-Fc[gamma]RIII complex. *Nature 406*, 267-273.

(62) Hanson, Q. M., and Barb, A. W. (2015) A perspective on the structure and receptor binding properties of immunoglobulin G Fc. *Biochemistry 54*, 2931-2942.

(63) Patel, K. R., Roberts, J. T., Subedi, G. P., and Barb, A. W. (2018) Restricted processing of CD16a/Fc γ receptor IIIa N-glycans from primary human NK cells impacts structure and function. *Journal of Biological Chemistry 293*, 3477-3489.

(64) Mizushima, T., Yagi, H., Takemoto, E., Shibata-Koyama, M., Isoda, Y., Iida, S., Masuda, K., Satoh, M., and Kato, K. (2011) Structural basis for improved efficacy of therapeutic antibodies on defucosylation of their Fc glycans. *Genes to Cells*, 1071-1080.

(65) Longmore, G. D., and Schachter, H. (1982) Product-identification and substrate-specificity studies of the GDP-L-fucose: 2-acetamido-2-deoxy-β-D-glucoside (Fuc→ Asn-linked GlcNAc) 6-α-L-fucosyltransferase in a Golgi-rich fraction from porcine liver. *Carbohydrate research 100*, 365-392.

(66) Yang, Q., and Wang, L.-X. (2016) Mammalian α-1, 6-fucosyltransferase (FUT8) is the sole enzyme responsible for the N-acetylglucosaminyltransferase I-independent core fucosylation of high-mannose N-glycans. *Journal of Biological Chemistry 291*, 11064-11071.

(67) Mimura, Y., Kelly, R. M., Unwin, L., Albrecht, S., Jefferis, R., Goodall, M., Mizukami, Y., Mimura-Kimura, Y., Matsumoto, T., and Ueoka, H. (2016) Enhanced sialylation of a human chimeric IgG1 variant produced in human and rodent cell lines. *Journal of immunological methods 428*, 30-36.

Chapter 4

Controlled Assembly Of Multivalent IgG1 Fc – Polyacrylamide Conjugates Greatly Increases Binding To FcγRIIIa

4.1 Introduction

Multivalent display of active molecules serves important roles in several biological processes such as bacterial invasion into a host, cell-cell adhesion, DNA transcription, and in the removal of foreign pathogens.[1] In medicine, they have been used to neutralize anthrax toxin[2], inhibit bacterial entry[3], alter antigen-specific immune responses[4], and in the design of therapeutics[5]. One benefit to the multivalent display of active molecules is the increased avidity of binding.[6] For instance, etanercept (Enbrel®), the blockbuster therapeutic for the treatment of several diseases including rheumatoid arthritis, is an IgG1 Fc fusion protein with two tumor necrosis factor (TNF) receptors on its N-termini. Etanercept functions to compete with TNF receptor on immune cells for binding to the proinflammatory-inducing cytokine TNF-α. TNF-α is trivalent, so having two TNF receptors on etanercept binds TNF-α with 50-1,000X stronger avidity than monomeric TNF receptor.[7]

Previously, the production of multivalent active molecules sometimes utilized polymerization methods that were uncontrolled.[8] This lack of control can be problematic because it creates a heterogenous polymer. It has been shown that the biological activity of the polymer can be affected by the polymer's size, shape, and density.[9, 10] For example, polymerization of IgG has been shown to activate Complement-dependent Cytotoxicity (CDC),[9, 11, 12] an important effector function of the immune system to clear foreign pathogens, at much lower concentrations than required for monomeric IgGs.[9, 12] However, Smith *et al.* (1995) showed that the size of the IgG polymer affected the strength of the CDC response.[9] Therefore, there is a need to develop polymers with controlled properties.

While dimers and trimers have been made in a controlled fashion,[13, 14] producing larger size polymers in a controlled fashion has been a challenge. Some published methods to make

large polymers in a controlled fashion include using dendrimers with "click" handles on the termini of the arms,[15] fusing the 18 amino acid tail piece of IgM to IgG molecules as a way to make hexameric IgGs,[9, 12, 16] and expressing proteins with non-native amino acids that contain click functional goups[17]. Another method to control polymerization is to use a controlled radical polymerization method such as atom transfer radical polymerization (ATRP). ATRP allows for control the polymer length, polymer size, and density of incorporated monomers by controlling the ratios of the reaction components.[18] ATRP has been used previously by Appel *et al.* (2011) to incorporate two different acrylamide-containing monomers with controlled ratios into the production of high molecular weight, water-soluble co-polymers.[19]

In this work, a novel method to ligate multiple proteins together in a controlled manner is presented that combines both ATRP and sortase-mediated ligation. This work utilized the controlled polymerization reaction of ATRP to synthesize a water-soluble, linear poly(acrylamide-peptide) co-polymer (**Scheme 1**). The versatility of this polymerization method was demonstrated by synthesizing several different co-polymer scaffolds with controlled size, shape, and density of peptides. The co-polymer was used as a scaffold to site-specifically attach the Fc region of the human IgG1 antibody (IgG1 Fc) to the incorporated peptides using a sortase-mediated ligation (**Scheme 2**). Over the past twenty years, sortase has served as a valuable biotechnology tool for the site-specific ligation of a variety of molecules.[20] This mechanism for this ligation is as follows (**Figure 2.2**):[21-23] It requires one species contain a C-terminal sortase polypeptide sequence LPXTG, where X can be any amino acid. The sortase enzyme recognizes this sequence and cleaves between the threonine and glycine to form a thioester intermediate. Next, any species that contains an N-terminal glycine can theoretically act as a nucleophile to displace the sortase and form a new peptide bond between the two species. After sortase-mediated ligation of IgG1 Fc onto the co-polymer scaffold, the IgG1 Fc-polymer conjugate was

compared to IgG1 Fc in a receptor binding assay to FcγRIIIa, the receptor involved in activating antibody-dependent cellular cytotoxicity (ADCC). Lastly, the versatility of this controlled protein ligation method was further demonstrated by applying it to a different protein, interleukin-1 receptor antagonist (IL1ra).

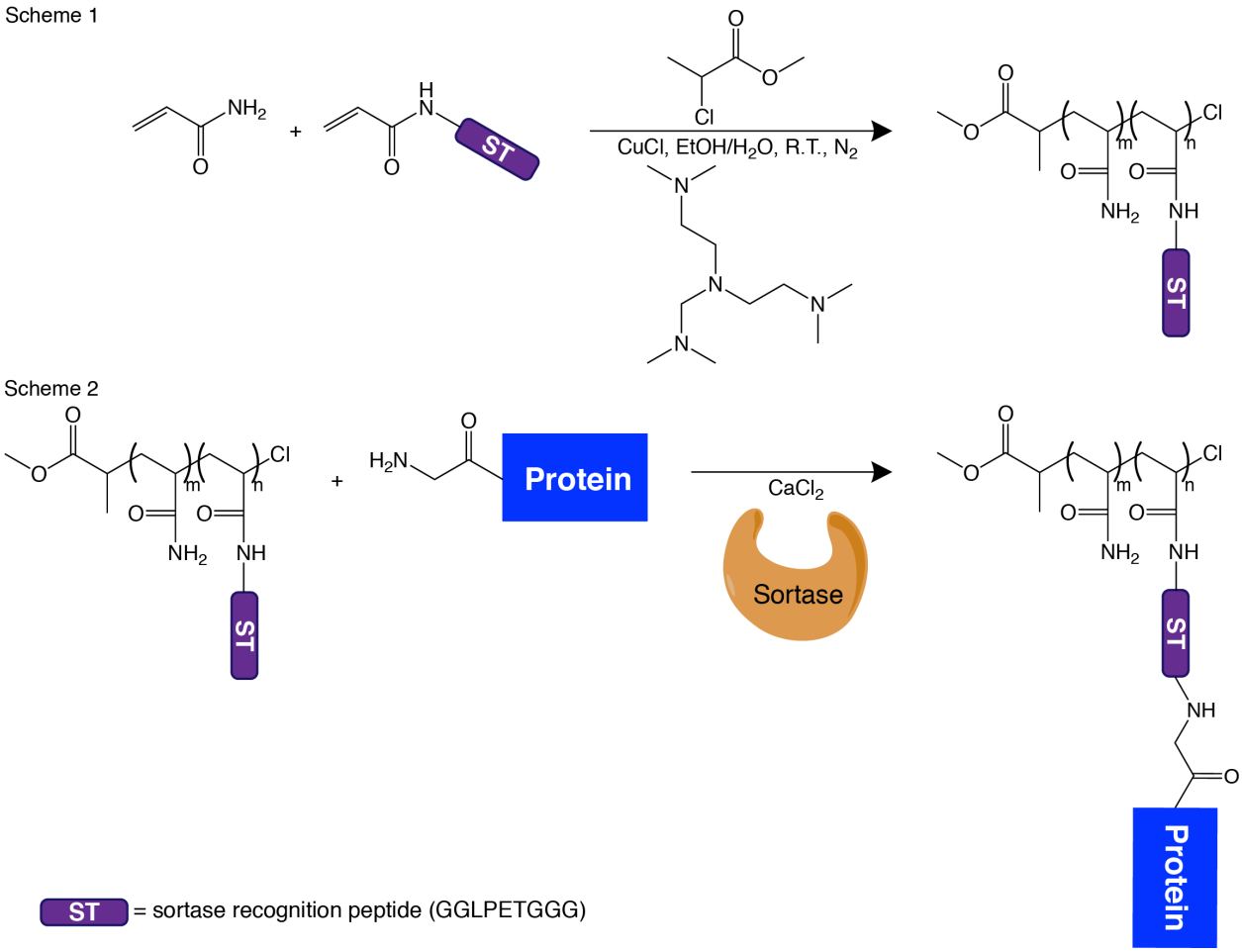

4.2 Materials and Methods

4.2.1 Materials

DNA primers were purchased from Eurofins (Huntsville, AL). pGAPzαA and pPICzαA plasmids were purchased from Invitrogen (USA). All molecular biology enzymes and protein markers were purchased from New England BioLabs (Ipswich, MA). QIAprep Spin Miniprep

and QIAquick Gel Extraction Kits were purchased from Qiagen (Germantown, MD). Zeocin was purchased from InvivoGen (San Diego, CA). Agarose was purchased from Lonza (Allendale, NJ). Agar, tryptone, and yeast extract were purchased from Becton, Dickinson and Company (Sparks, MD). Yeast Nitrogen Base was purchased from Sunrise Science Products (San Diego, CA). Antifoam 204 was purchased from Millipore-Sigma (St. Louis, MO). Protein A and phenyl-sepharose resins were purchased from GE Healthcare (Waukesha, WI). Dithiothreitol (DTT) was purchased from Bio-Rad (Hercules, CA). Bio-layer Interferometry biosensor tips were purchased from Forté Bio (Menlo Park, CA). Protease-free bovine serum albumin (BSA) was purchased from VWR (USA). Centrifugal concentrators and syringe filters were purchased from EMD-Millipore (USA). An expression plasmid for Peptide: N-glycosidase F (PNGase F) was gifted by the Lott laboratory at Massey University, from which PNGase F was prepared as previously described.[24] Additionally, an expression plasmid for sortase A was gifted by the DiMarchi laboratory at Indiana University, from which sortase A was prepared as previously described.[25] All other chemicals were obtained from commercial sources without further purifications. The methods for Gly3-IL1ra cloning, expression, purification, and ligation to the AM-ST co-polymers can be found in **Appendix 3: A.3.1**.

4.2.2 Preparation of AM-ST co-polymer

A series of co-polymers were synthesized, purified, and characterized by Dr. Zahra Khedri. The co-polymers were comprised of acrylamide (abbreviated "AM") and a sortase recognition peptide (GGLPETGGG) functionalized with an acryloyl group on the N-terminus (abbreviated "ST"), which were polymerized in varying ratios using ATRP to produce the poly(acrylamide-GGLPETGGG) co-polymers (abbreviated "AM-ST co-polymer") (**Table 4.1**). Dr. Khedri synthesized three AM-ST co-polymers, which varied in molecular weight as well as in the density of the ST peptide. The molecular weights of the polymers were determined using

gel permeation chromatography (GPC) with polyacrylamide standards. The polydispersity index (PDI) was also determined using GPC. The number of ST peptides per polymer was determined using ^{1}HNMR. A more detailed synthesis, purification, and characterization of these AM-ST co-polymers are currently being written for publication in combination with the work described in this chapter.

4.2.3 Molecular cloning of pPICzαA-Gly5-IgG1 Fc

The Fc region of the human IgG1 heavy chain (T_{225}-K_{447}) cDNA (MGC-12853) was previously cloned into the pGAPzαA plasmid to form pGAPzαA-IgG1 Fc with a silent mutation to produce a SacI site near the N-terminus of the Fc and used previously in our laboratory.[25] In order to add the five glycine residues to the N-terminus, the construct was digested with the restriction endonucleases XhoI and SacI-HF and gel purified. DNA primers consisting of 5'-tcgagaaaagaggtggtggaggtggaacatgcccaccgtgcccagcacctgagct (forward) and 5'-caggtgctgggcacggtgggcatgttccacctccaccacctcttttc (reverse) were designed to anneal together with the proper XhoI and SacI sticky ends. The primers were mixed together and phosphorylated using T4 Polynucleotide Kinase. They were then ligated into the digested pGAPzαA-IgG1 Fc plasmid using T4 DNA Ligase to create pGAPzαA-Gly5-IgG1 Fc. The plasmid was then transformed into *Escherichia coli* Top10f' using electroporation and grown on low salt LB agar (0.5% yeast extract, 1% tryptone, 0.5% NaCl, 1.5% agar) containing 25 μg/mL zeocin. To confirm the correct sequence, the plasmid DNA was extracted using a Qiagen QIAprep Spin Miniprep Kit and sequenced by the UC-Berkeley DNA Sequencing Facility (Berkeley, CA). For methanol-induced expression in *Pichia pastoris*, the Gly5-IgG1 Fc DNA was transferred from pGAPzαA into pPICzαA. This transfer was accomplished by digesting the pGAPzαA-Gly5-IgG1 Fc plasmid with the restriction endonucleases XhoI and NotI-HF to release the Gly5-IgG1

Fc DNA, which was gel purified. pPICzαA was digested with the same restriction enzymes and also gel purified. The digested Gly5-IgG1 Fc DNA and pPICzαA were ligated together using T4 DNA Ligase to create pPICzαA-Gly5-IgG1 Fc. The plasmid was transformed into *E. coli* Top10f' using electroporation, and the cells were plated on low salt LB agar containing 25 μg/mL zeocin and grown at 37°C overnight. To confirm the correct sequence, the plasmid DNA was extracted using a Qiagen Miniprep Kit and sequenced by the UC-Berkeley DNA Sequencing Facility (Berkeley, CA). The pPICzαA-Gly5-IgG1 Fc plasmid was linearized in the AOX1 promoter region using the restriction endonuclease PmeI and transformed using electroporation into a glycosylation-deficient strain of the yeast *Pichia pastoris* that was prepared previously in our laboratory (deleted och1, pno1, and bmt 1&2 genes and inserted STT3D gene from *Leishmania major* in order to improve N-glycosylation site occupancy).[26-28] The cells were plated on YPD agar (1% yeast extract, 2% tryptone, 2% glucose, 1.5% agar) containing 100 μg/mL zeocin and grown at 30°C for 6 days.

4.2.4 Expression of Gly5-IgG1 Fc

A colony was selected and grown in a shake tube containing 2 mL YPD media (1% yeast extract, 2% tryptone, 2% glucose) and 100 μg/mL zeocin at 30°C and 250 rpm. After 3 days, the culture was transferred to a 250 mL baffled Erlenmeyer flask containing 50 mL YPD media and 100 μg/mL zeocin and grown at 30°C and 250 rpm. After 2 days, the culture was transferred to a 1 L spinner flask containing 2% tryptone, 1% yeast extract, 2% glycerol, 1.34% yeast nitrogen base, 0.00004% biotin, 100 mM potassium phosphate buffer pH 6.2, and 1 drop of Antifoam 204. The spinner flask was stirred at room temperature with an air flow of 3 L/min. After 3 days of growth, the pH of the culture was adjusted back to 6.2 using concentrated NH_4OH. Expression of Gly5-IgG1 Fc was induced by adding 0.5% methanol, which was added approximately every

12 hours. After 3 days of induction, the culture was centrifuged at 6,693 x g for 20 min using a Beckman Avanti J-series centrifuge (USA). The supernatant was collected, and the pH was adjusted to 6.5 using KOH. This expression procedure was repeated three times to produce a total of four liters.

4.2.5 Purification of Gly5-IgG1 Fc

The supernatant was then filtered using vacuum filtration through Whatman #1 filter disks. The IgG1 Fc protein was then purified from the supernatant using protein A affinity chromatography. A 2.5 cm x 20 cm column was packed with 20 mL of protein A-sepharose resin. A flow rate of 15 mL/min was used throughout the purification using a peristaltic pump. The column was equilibrated with 15 CV of 20 mM sodium phosphate buffer pH 6.5. 2 L of the filtered supernatant was passed through the column followed by 25 CV of 20 mM sodium phosphate buffer pH 6.5 containing 500 mM NaCl. The IgG1 Fc protein was eluted from the column using 3 CV of 100 mM glycine-Cl buffer pH 3.0. The eluted protein was immediately dialyzed in 2 L of 20 mM sodium phosphate buffer pH 7.5 at 4°C with 1 buffer change. This protein A affinity chromatography procedure was repeated for the remaining 2 L of supernatant. After purification by protein A affinity chromatography, the yield was 19 mg/L (76 mg total for the 4 L).

After dialysis, the Gly5-IgG1 Fc protein was further purified by hydrophobic interaction chromatography (HIC). The protein was mixed with solid $(NH_4)_2SO_4$ crystals at a final concentration of 1 M $(NH_4)_2SO_4$. An ÄKTA micro (GE Healthcare, Waukesha, WI) was used throughout this purification at a flow rate of 2 mL/min. A column containing 125 mL of phenyl-sepharose resin was first washed with 5 CV of Milli-Q H_2O and then equilibrated with 5 CV of buffer A (20 mM sodium phosphate buffer pH 7.5 containing 1 M $(NH_4)_2SO_4$). Half of the collected Gly5-Fc protein was loaded on the column. To obtain fully di-glycosylated Gly5-IgG1

Fc, the following stepwise purification method was employed: 0% buffer B (20 mM sodium phosphate pH 7.5) for 1 CV, a linear gradient of 0%-27% buffer B for 1 CV, a linear gradient of 27%-31% buffer B for 9.5 CV, a linear gradient of 31%-100% buffer B for 1 CV, and finally 100% buffer B for 1 CV. During the linear gradient of 27-31% buffer B, 10 mL fractions were collected. The fractions were analyzed for N-glycan site occupancy using intact protein mass spectrometry. The fractions containing ≥99% di-glycosylated Gly5-IgG1 Fc were pooled, concentrated to about 20 mL using a 10 kDa MWCO centrifugal concentrator, and dialyzed in 2 L of 20 mM MES buffer pH 6.5 containing 150 mM NaCl at 4°C with 1 buffer change. This purification method was repeated for the remaining half of Gly5-Fc protein. At this stage, the N-linked glycosylation was high mannose (abbreviated "HM"). After secondary purification by HIC, the yield was 22 mg.

4.2.6 Sodium Dodecyl Sulfate–Polyacrylamide Gel Electrophoresis (SDS-PAGE)

Polyacrylamide gels that were prepared with a uniform acrylamide concentration were done so in house.[29] The gel that was prepared with a gradient concentration of 4-20% acrylamide was purchased from Bio-Rad (Hercules, CA). For the small-scale, sortase-mediated ligation reactions, 80 µg of protein was loaded. For the large-scale ligation, 10 µg of protein was loaded. For screening fractions after size exclusion chromatography, 10 µL of each fraction was loaded. For all other samples, 2 µg of protein was loaded. Samples that were analyzed under reducing conditions contained 50 mM DTT. The preparation of the samples, electrophoresis, and visualization of protein by Coomassie staining were all performed as previously described.[25]

4.2.7 Intact protein mass spectrometry

The proteins were analyzed by intact protein mass spectrometry as previously described (**3.2.4**).

4.2.8 *In-vitro* enzymatic conversion of the Gly5-IgG1 Fc N-glycoform from HM to M5

α-1,2-mannosidase from *Bacteroides thetaiotaomicron* and an endomannosidase from rat were prepared previously.[27, 30] The concentrations of these enzyme preparations were determined using a Pierce BCA Protein Assay Kit (Thermo Scientific, Waltham, MA) according to manufacturer's instructions. 22 mg of Gly5-IgG1 Fc with the HM N-glycoform at approximately 0.5 mg/mL was mixed with 1.6 mg of α-1,2-mannosidase and 0.09 mg of rat endomannosidase. The reaction mixture was transferred to 3.5 kDa MWCO dialysis tubing and dialyzed at r.t. in 2 L of 20 mM MES buffer pH 6.5 containing 150 mM NaCl and 5 mM $CaCl_2$. Conversion of HM into the M5 N-glycoform was monitored using intact protein mass spectrometry. After 4 days, the reaction was stopped by purifying the Gly5-IgG1 Fc protein from the enzymes using protein A affinity chromatography according to the purification procedure described in section **4.2.5**. After elution, the protein was immediately dialyzed in 2 L of tris-buffered saline (TBS, 50 mM Tris, 150 mM NaCl) pH 7.5 at 4°C with 1 buffer change. At this stage, Gly5-IgG1 Fc protein contains the homogenous M5 N-glycoform, and this protein is abbreviated as "Fc".

4.2.9 Sortase-mediated ligation of Fc to AM-ST co-polymer

The Fc was concentrated using a 30 kDa MWCO centrifugal concentrator and filtered through a 0.22 μm syringe filter. After concentration and filtration, the final concentration was 265 μM. The AM-ST co-polymer concentration was based on the number of ST sites. A series of 30 μL, small-scale, sortase-mediated ligation reactions were prepared using the following: 242 μM Fc, 2 μM $CaCl_2$, 10 μM sortase A, and a series of 0, 0.02, 0.04, 1, and 5 μM AM-ST co-polymer in TBS pH 7.5. The reactions were allowed to proceed at 37ºC for 24 hours. After which, they were analyzed using SDS-PAGE. Based on the SDS-PAGE data, the reaction using 5 μM of co-polymer showed the best balance between obtaining the largest size Fc-polymer conjugates and having the largest yield of ligated Fc. Therefore, this reaction was scaled-up to

860 µL. The reaction was again analyzed using SDS-PAGE. Fc ligated to the AM-ST co-polymer was abbreviated as "Fc-polymer conjugate".

The Fc-polymer conjugate was purified from the free protein (sortase and un-ligated Fc) using size exclusion chromatography. A 2.5 cm x 30 cm column containing 100 mL of Bio-Gel P100 resin (Bio-Rad, Hercules, CA) was equilibrated using 5 CV of TBS pH 7.5 at 0.3 mL/min. 850 µL of the reaction were pipetted on the top of the resin bed. Then TBS pH 7.5 was pumped through the column at a rate of 0.3 mL/min. 1 mL fractions were collected. Every 3rd fraction was manually checked for protein using UV/VIS spectrophotometry at 280 nm. The fractions that indicated protein were analyzed using SDS-PAGE. 5 fractions showed Fc-polymer conjugate with very little un-ligated Fc. These fractions were pooled, concentrated to 2 mL using a 30 kDa MWCO centrifugal concentrator, and dialyzed in PBS pH 7.4.

4.2.10 Analytical size exclusion chromatography

A Phenomenex Yarra (3µm, 7.8 mm ID x 300 mm) SEC-3000 column (Torrance, CA) was attached to a Shimadzu UFLC (Kyoto, Japan). The column was equilibrated with 200 mM sodium phosphate buffer pH 6.8. 50 µL of 0.3 mg/mL of each sample was injected. The method consisted of an isocratic gradient of 200 mM sodium phosphate buffer pH 6.8 for 40 minutes at a flow rate of 0.4 mL/min and column temperature of 30ºC. A blank was injected between each sample.

4.2.11 BioLayer interferometry of Fc and Fc-polymer conjugate binding to FcγRIIIa

The concentration for both the Fc and Fc-polymer conjugate were determined by measuring the absorbance at 280 nm using UV/VIS spectrophotometry in quintuplicate and then using the average value to solve for concentration using Beer's law using an extinction coefficient of $\varepsilon_{280\ nm} = 71570\ M^{-1}cm^{-1}$.[31] The AM-ST co-polymer did not show any absorbance

signal at 280 nm. After determining the concentration, BSA was added to both the Fc and Fc-polymer conjugate to a final concentration of 1 mg/mL. The samples were prepared using two-fold serial dilutions for the Fc and four-fold serial dilutions for the Fc-polymer conjugate. The extracellular region of human FcγRIIIa was cloned, expressed, purified, and biotinylated as described in the previous chapter (**3.2.8**). All binding samples and reagents were incubated at 25ºC prior to analysis, and all analyses were performed at 25ºC.

For analysis of the Fc, a biosensor tip coated with streptavidin was first hydrated at r.t. in PBS pH 7.4 for 10 min and then further hydrated at r.t. in kinetic buffer (PBS pH 7.4 containing 1 mg/mL BSA) overnight to ensure adequate hydration. Then, the biosensor tip was fixed in the Forté Bio BLItz instrument (Menlo Park, CA). Next, FcγRIIIa was immobilized on to the biosensor tip according to the following steps: 1.) a baseline was established for 30 sec using kinetic buffer, 2.) the biosensor tip was loaded with biotinylated FcγRIIIa to a response level of 0.3 nm, and 3.) a baseline was re-established using kinetic buffer for 360 sec. After the FcγRIIIa was immobilized, a reference (with no Fc present) was performed using kinetic buffer for the duration of an experiment (30 sec baseline, 180 sec association, and 360 sec dissociation). Then, the following series of Fc concentrations were tested from low to high: 4, 8, 16, 31, 63, 125, 250, and 500 nM on the same biosensor tip according to the following steps: 1.) a baseline was established for 30 sec using kinetic buffer, 2.) association was performed by placing the tip in the Fc solution for 180 sec, and 3.) dissociation was performed by placing the tip in kinetic buffer for 360 sec. Between each Fc concentration, the tip was regenerated according to the following steps: 1.) the tip was placed in 1 mM NaOH for 30 sec, 2.) the tip was placed in kinetic buffer for 60 sec, and 3.) both steps were repeated. The entire procedure was performed in triplicate. Each series of concentrations was fitted to a 1:1 binding model in the BLItz Pro software to obtain

kinetic rate constants (k_a and k_d) and the kinetic dissociation constant (K_D). Additionally, the response values from 206.0-208.8 sec were averaged and plotted against their respective Fc concentrations. These data were fitted using a non-linear regression, and an equilibrium K_D was determined using a "one site--specific binding" model in the Prism 7 software.

For analysis of the Fc-polymer conjugate, a biosensor tip coated with streptavidin was hydrated and immobilized with biotinylated FcγRIIIa using the same procedure described for the Fc. After the FcγRIIIa was immobilized, a reference (with no Fc-polymer conjugate present) was performed using kinetic buffer for the duration of an experiment (30 sec baseline, 1800 sec association, and 3600 sec dissociation). Then, the following series of Fc-polymer conjugate concentrations were tested from low to high: 0.1, 0.5, 2, and 8 nM according to the following steps: 1.) a baseline was established for 30 sec using kinetic buffer, 2.) association was performed by placing the tip in the Fc-polymer conjugate solution for 1800 sec, and 3.) dissociation was performed by placing the tip in kinetic buffer for 3600 sec. Multiple regeneration strategies were attempted, but no regeneration procedure was found that completely dissociated the polymer from the tip without inactivating FcγRIIIa. Therefore, a new tip was used for each Fc polymer-conjugate concentration. Only 4 concentrations of Fc-polymer conjugate were tested because each concentration required a 10x increase in time for each analysis (compared to the Fc), a new reference, and a fresh tip. The entire procedure was performed in triplicate. Each series of concentrations was fitted to a 1:1 binding model in the BLItz Pro software to obtain kinetic rate constants (k_a and k_d) and the kinetic K_D dissociation constant.

4.3 Results and Discussion

4.3.1 Expression and purification of Gly5-IgG1 Fc

Gly5-IgG1 Fc was expressed in a glycosylation-deficient strain of the yeast *P. pastoris*. The yield after protein A affinity chromatography was 19 mg/L (76 mg total). The 5 glycine residues on the N-terminus were initially chosen in order to allow enough space between the Fc and the AM-ST co-polymer. However, based on the peak heights from the intact mass spectrum (**Figure 4.1A**), about 2% of the Gly5-IgG1 Fc was proteolyzed to Gly3. This was not seen as a problem for two reasons: 1.) 2% does not constitute a large amount of the total Fc and 2.) ligands with 3 glycine residues on the N-terminus are still accepted as nucleophilic substrates by sortase A and so can be utilized in sortase ligations.[25]

Based on the peak heights of the intact mass spectrum after protein A affinity chromatography, 8% of the total Fc chains were non-glycosylated at the conserved N-linked glycosylation site (**Figure 4.1A**). This translated to the site occupancy being 85% di-glycosylated, 15% mono-glycosylated, and <1% non-glycosylated. Additionally, SDS-PAGE showed two bands near the 30 kDa MW marker, wherein the more intense band corresponded to glycosylated Gly5-Fc and the less intense band corresponded to non-glycosylated Gly5-Fc (**Figure 4.1B**). To simplify the analysis of the Fc-polymer conjugate, the mono-glycosylated and non-glycosylated Fc forms were removed using HIC (**Figure 4.1C**). After secondary purification by HIC, the Mass Hunter software could not quantify a peak height for the non-glycosylated Fc single chain, so it was concluded that all Fc was di-glycosylated. However, after HIC, only 22 mg of fully di-glycosylated Gly5-Fc was obtained (29% yield). A higher yield could have been obtained if the criteria for di-glycosylated were less stringent. However, in order to make the Gly5-IgG1 Fc as homogenous as possible, a high purity was favored over yield.

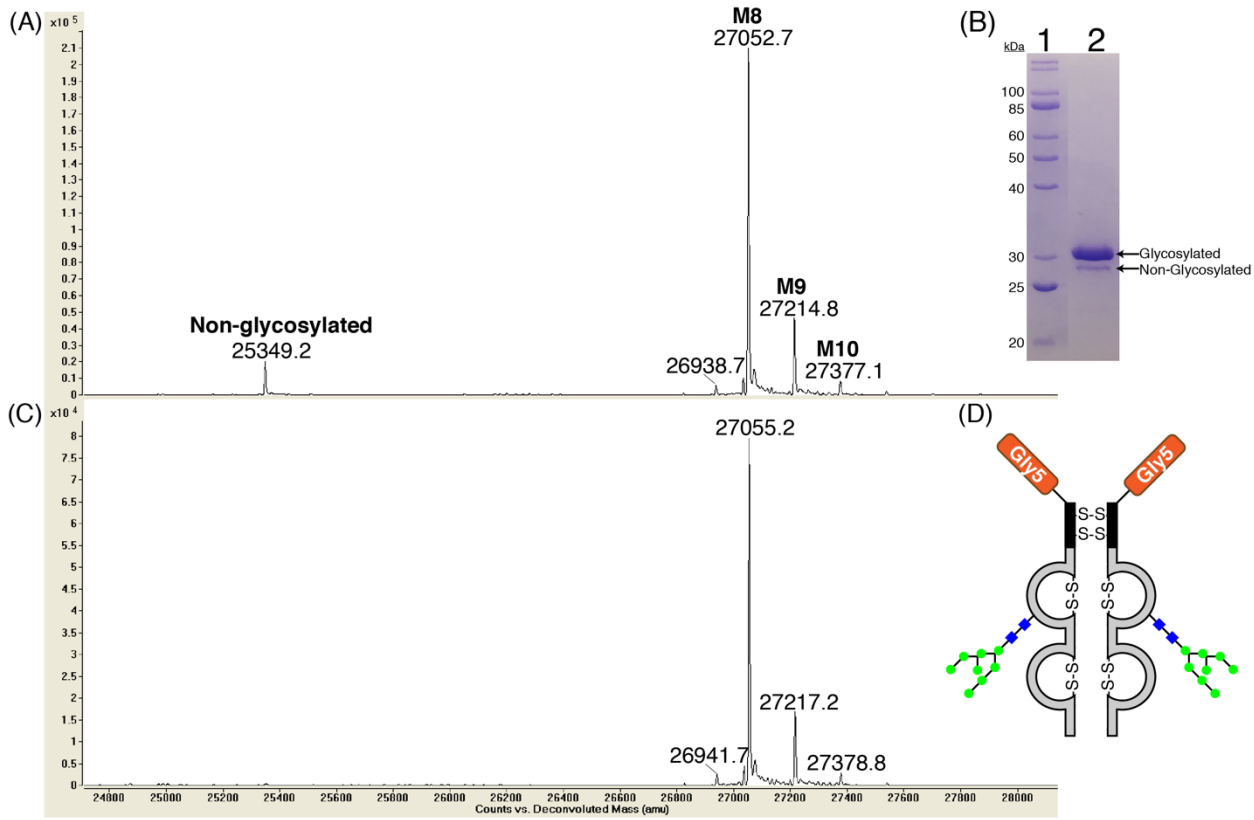

(E)

Gly5-IgG1 Fc Expression Products		
Species	**Observed MW (Da)**	**Expected MW (Da)**
Non-glycosylated	25349.2	25351.7
M8 (w/o 2 Gly)	26938.7	26941.1
M8	27052.7	27055.2
M9	27214.8	27217.3
M10	27377.1	27379.5
M11	27538.9	27541.6

Figure 4.1: Characterization of Gly5-IgG1 Fc. (A) Intact mass spectrum and (B) SDS-PAGE of Gly5-IgG1 Fc after purification by protein A affinity chromatography, Lanes: 1, 10-200 kDa MW Marker; 2, Gly5-IgG1 Fc after purification. (C) Mass spectrum of Gly5-IgG1 Fc after secondary purification by HIC. (D) Representation of di-glycosylated Gly5-IgG1 Fc. Glycosylation symbols: Blue squares, N-acetylglucosamine; Green circles, mannose. (E) Table showing observed and expected molecular weights of Gly5-IgG1 Fc species in mass spectrum after protein A affinity chromatography. All samples were reduced with DTT before analysis.

4.3.2 Conversion of Gly5-IgG1 Fc from the HM to the M5 N-glycoform

To further improve the homogeneity of the Gly5-Fc, the N-glycoform was converted from HM to M5. HM was a mixture of N-glycoforms ranging from M8-M11. The heterogenous HM N-glycoform was converted to a homogenous M5 N-glycoform to remove the heterogeneity coming from the glycosylation in order to simplify analysis of the Fc-polymer conjugate (**Figure**

4.2A). Gly5-IgG1 Fc with HM N-glycoform was treated with a bacterial α-1,2-mannosidase[30] and well as a rat endomannosidase[27]. The endomannosidase was added to help improve conversion to M5 by removing any terminal glucose residues that may be present on the N-glycan due to incomplete processing during N-glycan biosynthesis.[32] After treatment for 4 days at r.t., the conversion was 98% based on the peak heights from intact protein mass spectrometry (**Figure 4.2B** and **Appendix 3: Figure A.3.1**). The calculation of 98% was performed by dividing the peak height for the M5 N-glycoform by the sum of the peak heights for the M5, M6, M7 N-glycoforms after subtracting the contribution of O-linked glycosylation. O-linked glycosylation was determined by observing the glycosylation peaks that remained after treatment with PNGase F, which removed the N-linked glycosylation (**Appendix 3: Figure A.3.2**). Based on the literature, the remaining glycosylation peaks were likely O-linked mannose,[32, 33] which accounted for about 5% of the total N-glycoform peak heights. Additionally, SDS-PAGE showed just one band (**Figure 4.2 D**), which provided further evidence that the HIC purification step was successful in obtaining the completely di-glycosylated N-glycoform. The gel also suggested that the α-1,2-mannosidase and endomannosidase enzymes were not present after Protein A affinity purification. Having only one band for the Fc during SDS-PAGE analysis simplifies analysis of the Fc-polymer conjugate.

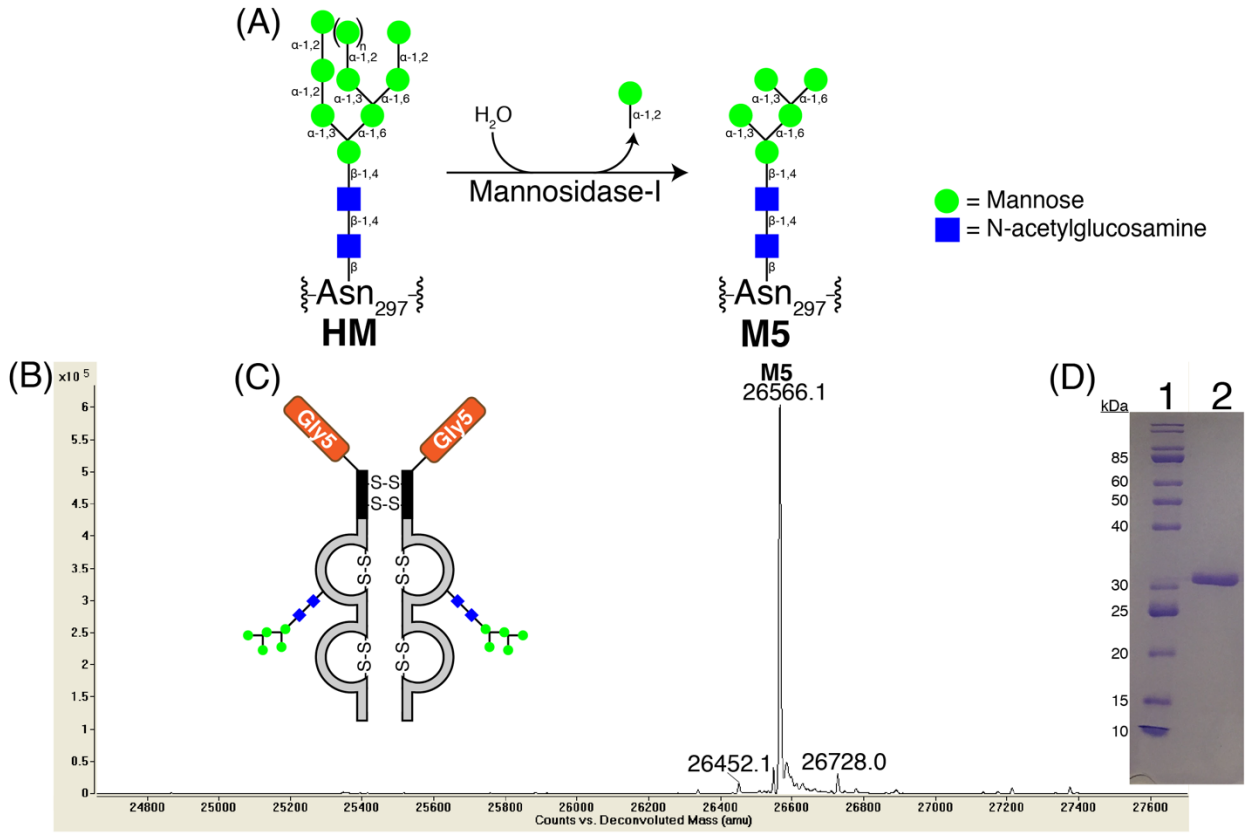

Figure 4.2: Characterization of the conversion of Gly5-IgG1 Fc from the HM to M5 N-glycoform. (A) Representation of the *in-vitro* enzymatic conversion. (B) Intact mass spectrum, (C) Representation, and (D) SDS-PAGE of Gly5-IgG1 Fc after conversion to the M5 N-glycoform. Samples for (B) and (D) were reduced with DTT before analysis. Expected MW: Gly5-IgG1 Fc with the M5 N-glycoform = 26568.8 Da. Lanes: 1, 10-200 kDa MW protein marker; 2, Gly5-IgG1 Fc with the M5 N-glycoform after purification by protein A affinity chromatography.

4.3.3 Sortase-mediated ligation of Fc to AM-ST co-polymers

Dr. Khedri synthesized a series of AM-ST co-polymers using ATRP that were used as scaffolds for attaching multiple Fc proteins (**Table 4.1**). The polymers varied in size as well as in the number of ST peptides incorporated. These parameters were controlled by adjusting the relative ratios of reaction components, such as the ratio of acrylamide to acrylamide-ST monomers. The largest polymer was 25 kDa in size as determined by GPC and contained an

average of 20.5 ST peptides/polymer (co-polymer #3) as determined by ^{1}H NMR (unpublished data). This co-polymer was chosen for use in the Fc ligation because it would allow for the most Fcs to be attached, which would potentially allow for the largest avidity effect when compared to free Fc in a receptor-binding assay. The Fc was ligated to the AM-ST co-polymer #3 (**Table 4.1**) using a sortase-mediated ligation. This ligation was utilized to ligate multiple Fc's to interior sites in the co-polymer (**Figure 4.3**).

Table 4.1: Properties of synthesized AM-ST co-polymers

Polymer	M:MCP:L:CuCl , pH, time (hr), (AM:ST), %EtOH in H_2O[a]	# ST/Polymer	AM/ST Ratio	MW (Da)	PDI
1	15:1:1:1, 7, 12 (10:1), 30	2.8	13.1	4798	1.13
2	16.8:1:1:1, 9, 17 (4.7:1), 30	6.6	9.5	9778	1.12
3	17:1:1:1, 9, 24, (3:1), 16	20.5	6.0	25000	1.13

[a]M = monomer, MCP = Methyl 2-chloropropionate, L = Tris[2-(dimethylamino)ethyl]amine

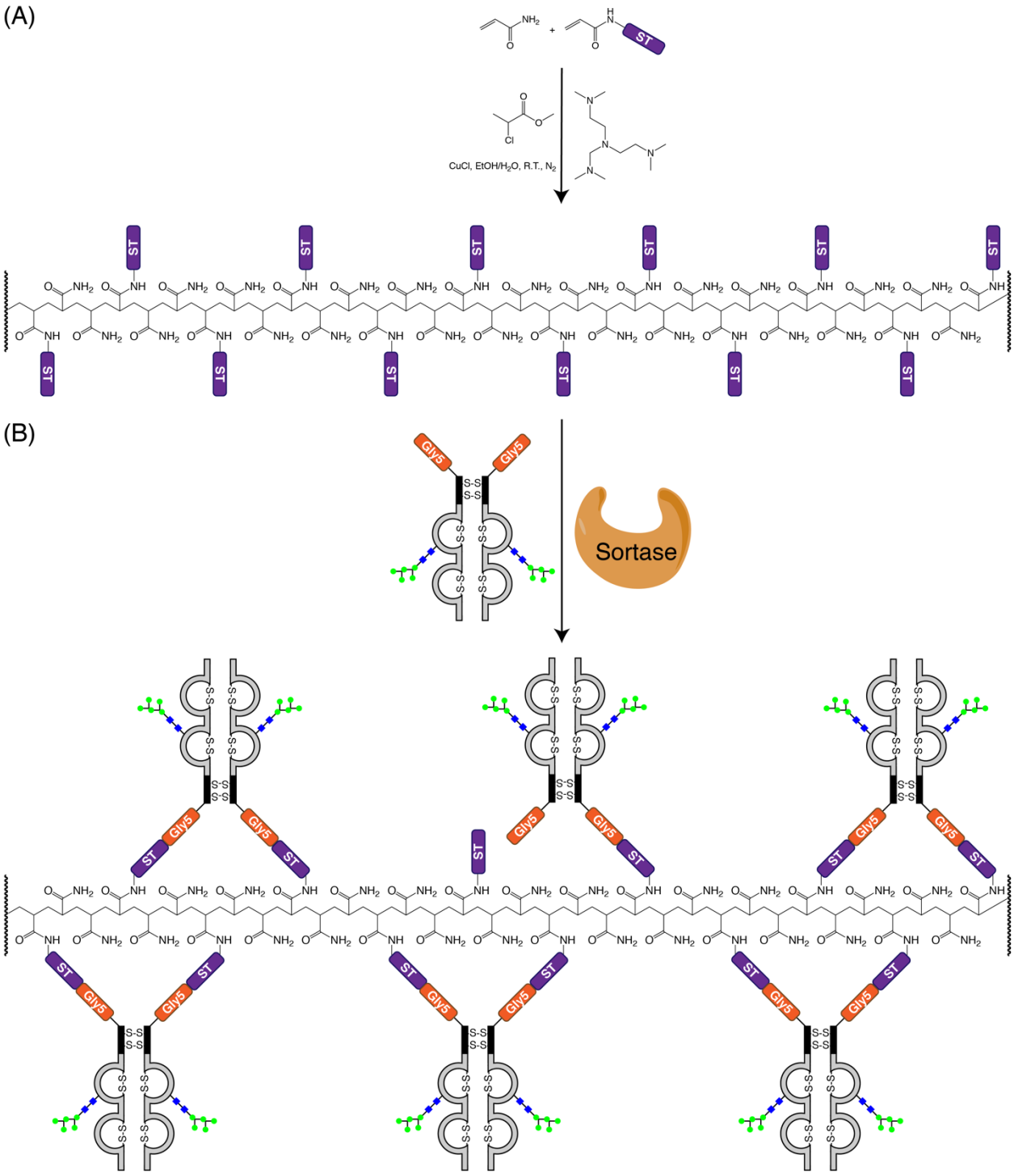

Figure 4.3: Representation of the controlled assembly of an Fc-polymer conjugate. (A) ATRP reaction using acrylamide (AM) and an acrylamide-containing sortase recognition tag (ST) as monomers to form the AM-ST co-polymer. (B) Sortase-mediated ligation of Fcs to the ST peptides within the AM-ST co-polymer to create an Fc-polymer conjugate with multiple internal Fcs attached.

A series of small-scale sortase-mediated ligation reactions were performed to find the optimal AM-ST co-polymer concentration that balanced obtaining the most Fcs attached per co-polymer with highest yield of Fc-polymer conjugate (**Figure 4.4**). Based on the SDS-PAGE data, the optimal AM-ST co-polymer concentration for this ligation was 5 μM (co-polymer:Fc ratio of 1:42, 210 μM Fc). At this concentration, large Fc polymers were observed as shown by Coomassie staining in the stacking layer. Additionally, there may have been even larger polymers because a Coomassie stained band was observed in the bottom of the loading well when the samples were analyzed under non-reducing conditions, suggesting that there were polymers so large that they did enter the stacking layer (**Appendix 3: Figure A.3.3**). This may have been because the Fc is a dimer, which may have caused cross-linking of multiple polymers. Adding a reducing agent broke-up the cross linking in the presence of SDS and resulted in the observed ladder-type addition (**Figure 4.4**).

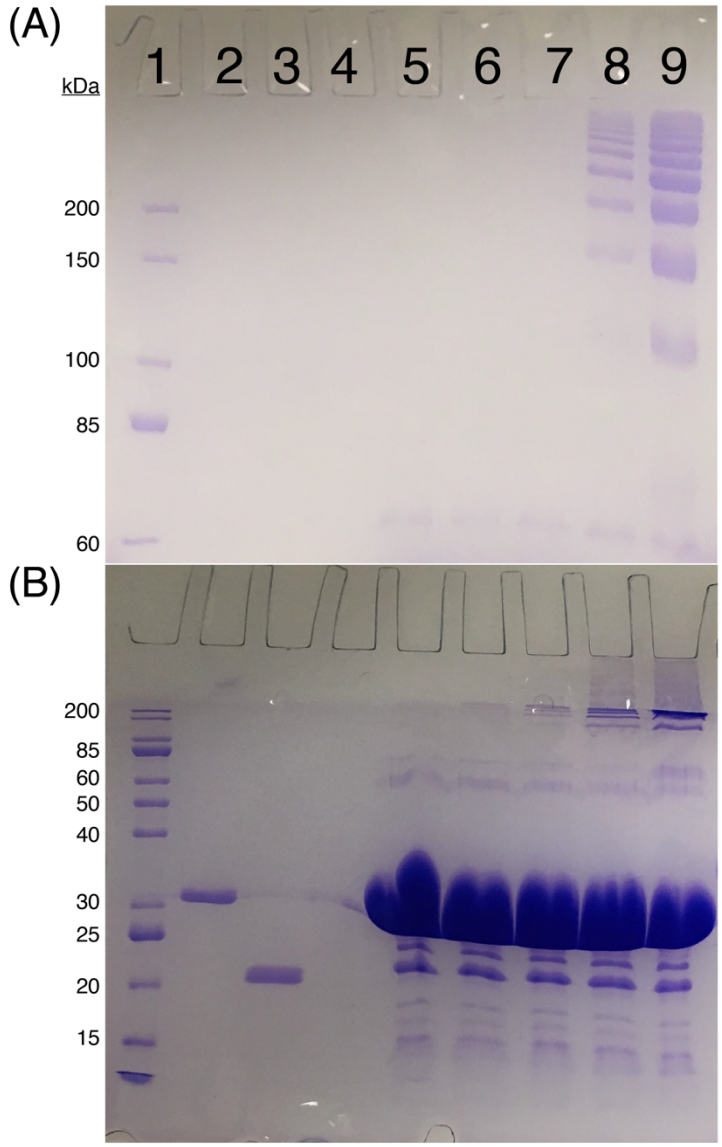

Figure 4.4: SDS-PAGE of small-scale, sortase-mediated ligations of Fc to the AM-ST co-polymer. Lanes: 1, 10-200 kDa MW protein marker; 2, Fc, 3, sortase A, 4, AM-ST co-polymer; 5-9, sortase-mediated ligations of Fc to AM-ST co-polymer: [AM-ST co-polymer] (μM): Lane 5 = 0, Lane 6 = 0.02, Lane 7 = 0.04, Lane 8 = 1, Lane 9 = 5. In order to obtain resolution in different size ranges, the samples were analyzed on gels prepared with both (A) 6% and (B) 12% acrylamide. All samples were reduced with DTT prior to loading.

The Fc-ligation using 5 μM AM-ST co-polymer was chosen for scale-up, which was performed with the remaining Fc protein (29 times larger scale) (**Figure 4.5**). Scaling up the reaction did not hurt the formation of large Fc-polymer conjugates. Based on the SDS-PAGE the average is size is 5 Fcs/co-polymer, with Fc-polymer conjugates ranging from approximately 2-

10 Fc/co-polymer. Although, it is difficult to determine the largest size Fc-polymer conjugates formed because band intensity becomes poor after >10 Fc/co-polymer are attached. There are two sites of attachment because the Fc is a homodimer, and the majority of the Fcs attached to the polymer twice. This result is shown by analysis of the protein-polymer conjugate after SEC purification with SDS PAGE under reducing conditions, which showed ~20% corresponding to Fc (This band is of similar intensity to lane 3 in which 2 µg of Fc was loaded. In lane 4, the amount of Fc polymer conjugate loaded was 10 µg). This implies that the majority of ligated Fcs are attached to the polymer at both N-termini.

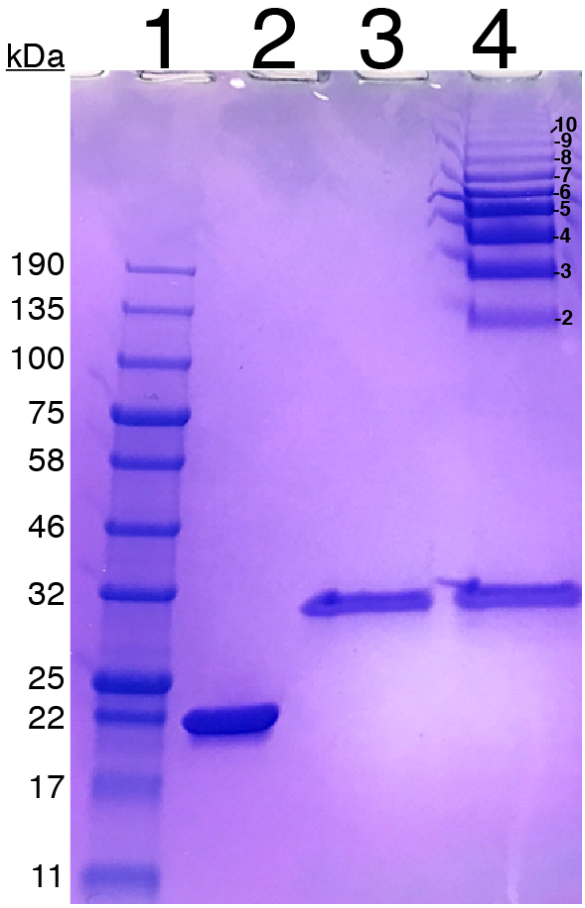

Figure 4.5: SDS-PAGE showing large-scale ligation of Fc to AM-ST co-polymer. Samples were analyzed using a 4-20% acrylamide gradient gel. Lanes: 1, 10-190 kDa MW protein marker; 2, sortase A; 3, Fc; and 4, Fc-polymer conjugate after purification by SEC. All samples were reduced with DTT prior to loading.

4.3.4 Purification of the Fc-polymer conjugate

In order to perform a comparison between the free Fc and Fc-polymer conjugate, the excess free Fc was removed from the ligation reaction using size exclusion chromatography (SEC). Bio-Gel P100 resin, with a typical fractionation range of 5-100 kDa, was used for this separation. This range allowed for separation of the free Fc (~50 kDa) from the Fc-polymer conjugates. However, fractionation of different Fc-polymer conjugates was not achieved with this resin. Based on the SEC results, almost all of the un-ligated Fc was removed (**Appendix 3: Figure A.3.4**).

After the sortase ligation and purification of the Fc-polymer conjugate, the amount of Fc-polymer conjugate obtained was 0.6 mg (5% yield of Fc). The low yield was caused by the sortase product also being a sortase substrate, which hindered formation of the Fc-polymer conjugate. In order to drive the reaction toward polymer formation, an excess of nucleophile is needed. In this ligation method, the nucleophile is the Fc. The Fc was concentrated to 260 μM, (~15 mg/mL), as practical limitations of protein precipitation at high concentrations limited concentrating the Fc further. For sortase-mediated ligations, the glycine-containing nucleophile is typically used in mM concentrations to obtain a high ligation yield.[34] The ligation yield could theoretically be improved by formulating the Fc to make it more stable at higher concentrations or by using a more soluble protein.

After purification, the Fc and Fc-polymer conjugates were analyzed by analytical SEC (**Figure 4.6**). The Fc showed a single peak, whereas the Fc-polymer conjugate showed multiple peaks that all eluted earlier than the Fc. The earlier elution suggested that the Fc-polymer conjugate was larger in size than the Fc. The multiple peaks were caused by the heterogeneity in polymer size. Additionally, the Fc-polymer conjugate did not show any peaks corresponding to the Fc, which suggested that any un-ligated Fc was removed during purification. Lastly, the AM-

ST co-polymer showed an elution peak using UV/VIS spectrophotometry at 220 nm (**Figure 4.6A**) but not at 280 nm (**Figure 4.6B**). The observed signal at 220 nm was due to the amide bonds in the polyacrylamide backbone of the AM-ST co-polymer. The absence of a signal at 280 nm for the polymer allowed us to use absorbance at 280 nm to calculate the Fc concentration of the Fc-polymer conjugate during binding studies. The Fc and Fc-polymer conjugate showed signal at both wavelengths because they contain both amide bonds and aromatic residues.

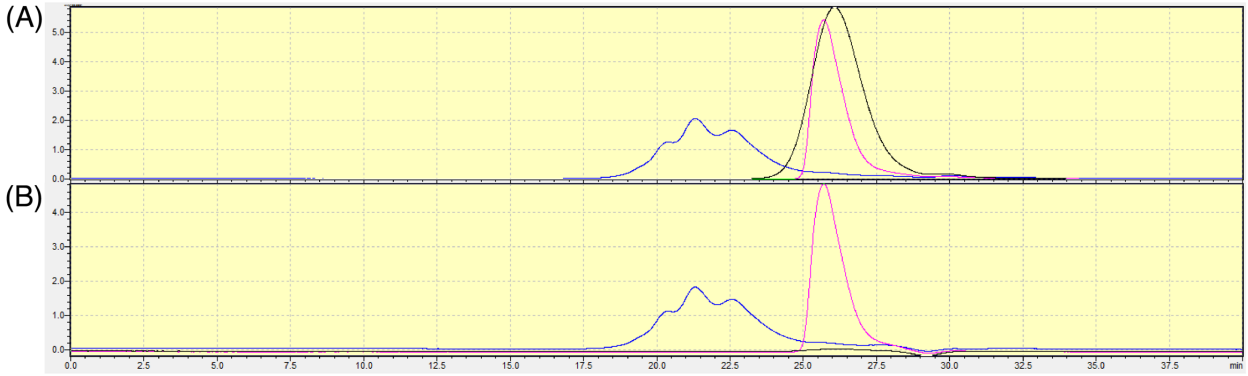

Figure 4.6: Characterization of Fc polymer components by analytical size exclusion chromatography. Elution from the SEC column was observed at both (A) 220 nm and (B) 280 nm. Black = AM-ST co-polymer #3 (**Table 4.1**), Pink = Fc, and Blue = Fc-polymer conjugate. The three components were analyzed separately, and their chromatograms were overlaid.

4.3.5 Comparison of the Fc and Fc-polymer conjugate binding to FcγRIIIa

For a comparison of the binding affinity, FcγRIIIa was used. This receptor was chosen because FcγRIIIa is the primary Fcγ receptor found on NK cells that is necessary for IgG to activate ADCC.[35] It has been shown that ADCC activity can be increased by increasing the affinity of the antibody to the foreign antigen.[36, 37] For example, aglycosylated IgG1, which is believed to not bind most FcγRs even at low μM concentrations when tested in monomeric binding assays, was shown to bind FcγRs at nM concentrations when tested in an *in-vitro* assay

that allowed for avidity of binding.[38] In another example, formation of IgG1 Fc hexamers has been shown to increase the binding to FcγRI 2.5-fold compared to a dimer using surface plasmon resonance.[16]

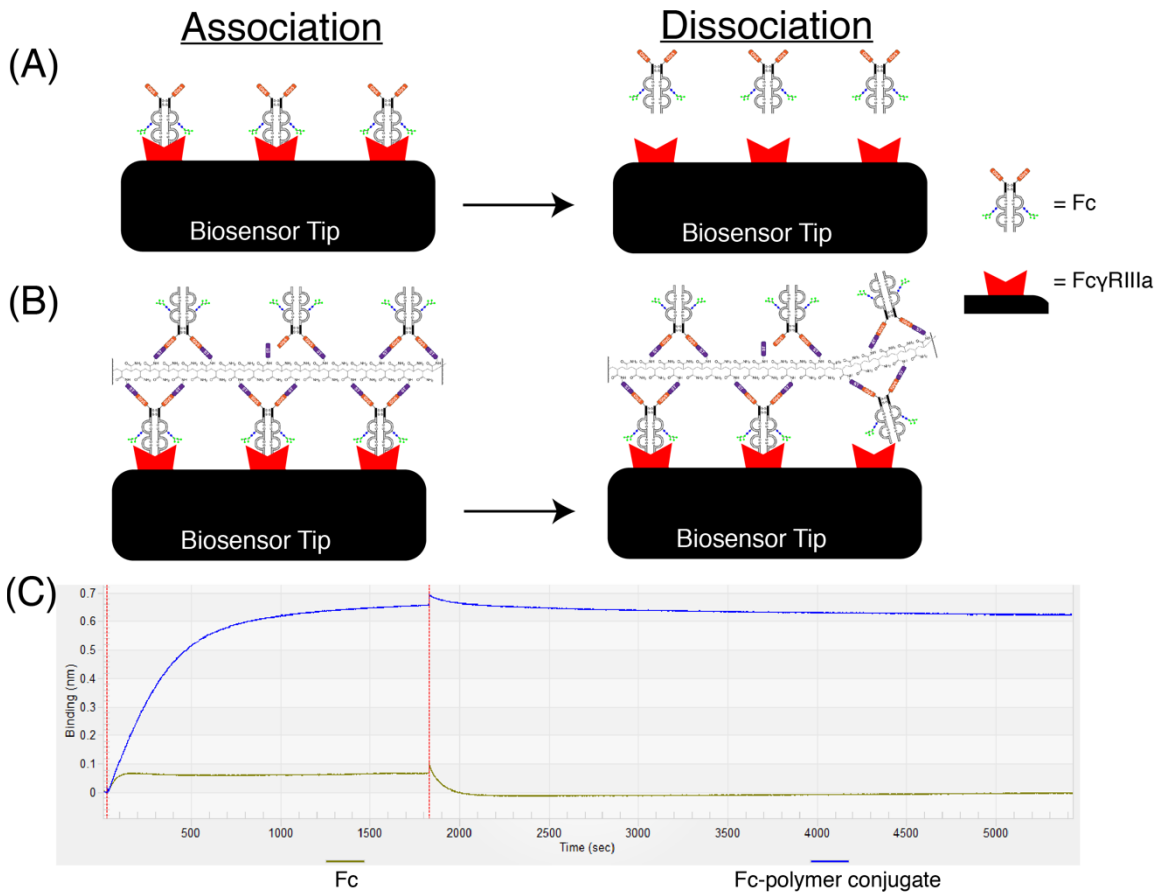

Figure 4.7: Comparison of binding response to FcγRIIIa of Fc and Fc-polymer conjugate. Representations of binding of (A) Fc and (B) Fc-polymer conjugate. (C) BioLayer interferometry sensorgram comparing the binding response of the Fc and Fc-polymer conjugate. The Fc (green) and Fc-polymer conjugate (blue) were both tested at the same protein concentration (8 nM) on the same biosensor.

FcγRIIIa was site-specifically biotinylated on the C-terminus using a sortase-mediated ligation with a triglycine-biotin compound that was synthesized in house as previously described.[39] The Fc and Fc-polymer conjugate binding to FcγRIIIa were tested on the same

biosensor tip at the same concentration (**Figure 4.7**). Performing the comparison on the same biosensor ensured that the same amount of receptor was present. This result showed that Fc-polymer conjugate provided about 10 times more signal at the end of the association phase compared to the Fc. This observation suggested that the FcγRIIIa bound to the Fc-polymer conjugate with greater strength than to the Fc. Additionally, the Fc had reached equilibrium at the end of the association phase of 180 sec, whereas the polymeric Fc had not even after 1800 sec. If the Fc-polymer conjugate had been allowed to reach equilibrium (assuming equilibrium could be obtained using this technique), then the difference in signal would have been even greater.

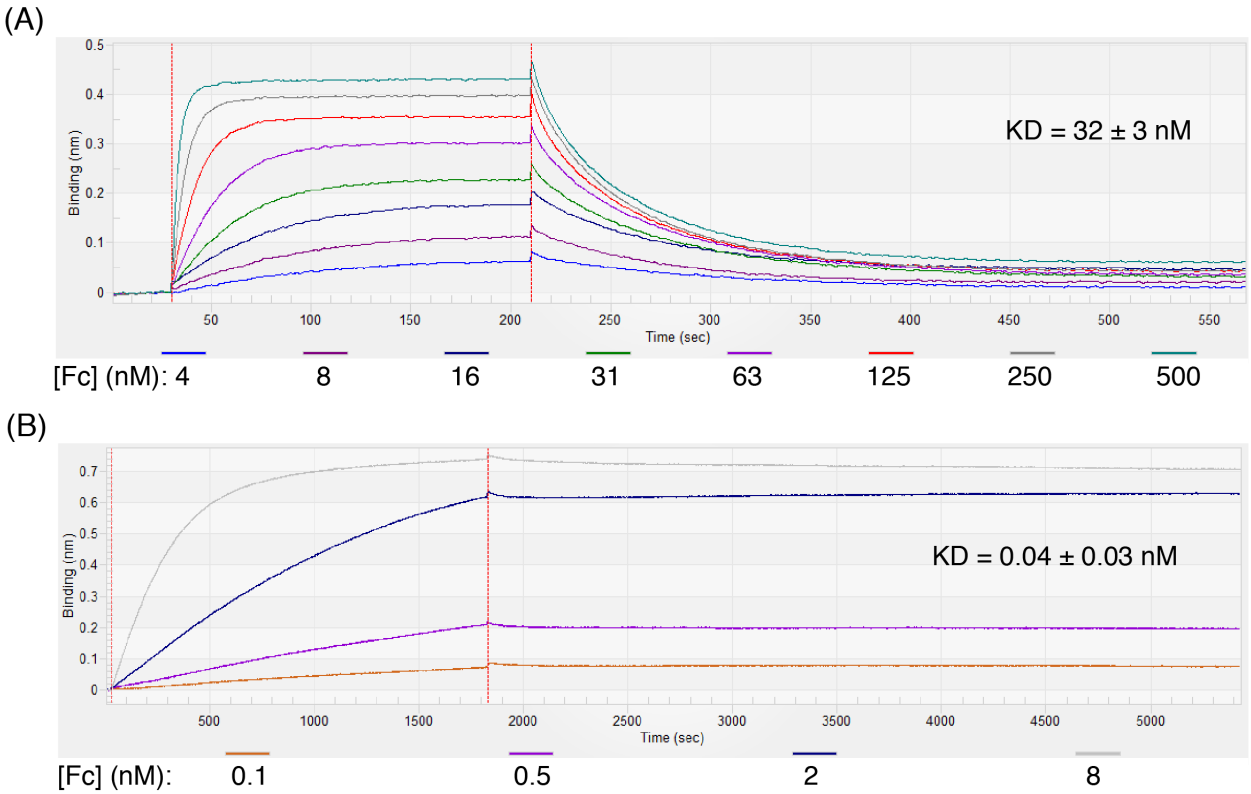

Figure 4.8: Representative biolayer interferometry sensorgrams of the (A) Fc and (B) Fc-polymer conjugate binding to FcγRIIIa. Reported K_D values are the average of triplicate runs ± standard deviation.

Table 4.2: Kinetic Binding Results Of Fc vs. Fc-polymer Conjugate Binding To FcγRIIIa[a]

Species	**k_a ± SD x 10^5 (1/Ms)**	**k_d ± SD x 10^{-2} (1/s)**	**K_D ± SD (nM)[b]**
Fc	5.0 ± 0.4	1.6 ± 0.1	32 ± 3
Fc-polymer conjugate	4.2 ± 0.2	0.002 ± 0.001	0.04 ± 0.03

[a]Shown are the average values of triplicate runs ± the standard deviation (SD).
[b]The SD for the K_D was calculated taking into account the error of propagation.

For a quantitative analysis, several concentrations of Fc and Fc-polymer conjugate were tested in triplicate. The binding results from the Fc showed a K_D value of 32 ± 3 nM (**Figure 4.8A**). This result was similar to what was observed for the M5-IgG1 Fc measured in the previous chapter (**Table 3.3**) and in literature.[39] This observation suggested that the addition of 5 glycine residues to the N-terminus did not affect the binding between IgG1 Fc and FcγRIIIa significantly. Additionally, the kinetic binding and equilibrium binding results did not show any statistically significant differences (**Figure 4.8A** vs. **Appendix 3: Figure A.3.5**). Compared to the Fc, the Fc-polymer conjugate showed a K_D of 0.04 ± 0.03 nM (**Figure 4.8B**). The K_D of the Fc-polymer conjugate was 800 times lower than the Fc. Interestingly, the k_a rate constants were quite similar, with the Fc-polymer conjugate showing only a 1.2-fold slower association rate than the Fc (**Table 4.2**). On the other hand, the k_d rate constants were very different, with the Fc-polymer conjugate showing a 800 times slower dissociation rate. This was likely due to the increase in avidity of the Fc-polymer conjugate having multiple Fc-FcγRIIIa interactions. In the free Fc, when the Fc and receptor dissociated, the Fc diffused away. However, in the Fc-polymer conjugate, if one Fc-receptor interaction dissociated, then there were still other binding events that kept the polymer associated with the receptor. The binding for the Fc was complete in 180 sec association and 360 sec association. However, the Fc-polymer analysis association and dissociation times had to be increased 10-fold due to the slower kinetics, such that the

association was 1800 sec and the dissociation was 3600 sec. However, even after an association time of 1800 sec, the Fc-polymer conjugate samples had not reached binding equilibrium.

4.3.6 Sortase-mediated ligation of IL1ra to AM-ST co-polymers

To demonstrate the versatility of this controlled ligation method, another protein was attached to the same co-polymers (**Table 4.1**). Interluekin-1 receptor antagonist (IL1ra) plays an important role in the immune system by working to downregulate the proinflammatory response invoked by interleukin-1.[40] Its biological role makes it a useful therapeutic, as it is FDA approved under the name Anakinra (Kineret®) for the treatment of several diseases including rheumatoid arthritis. IL1ra was chosen for ligation to AM-ST co-polymers because it is a single chain protein, so it has only one ligation site per protein. Therefore, the IL1ra-polymer conjugate didn't show the heterogeneity that was observed with the Fc-polymer conjugate, which had 2 ligation sites per protein, when analyzed by SDS-PAGE under non-reducing conditions (**Appendix 3: Figure A.3.3**). IL1ra was expressed as a fusion protein with an N-terminal hexa-histidine tag, followed by a Tobacco Etch Virus (TEV) cleavage tag, followed by two N-terminal glycine residues on its N-terminus. The TEV cleavage site is (Glu-Asn-Leu-Tyr-Phe-Gln-Xxx), where Xxx can be many different amino acids.[41] TEV protease is a cysteine protease that cleaves between the Gln and Xxx. In this work, a glycine residue was used for the Xxx, so that cleavage by TEV protease produced an IL1ra with an N-terminal glycine (**Appendix 3: Figure A.3.6A**). TEV cleavage was complete as shown by SDS-PAGE wherein the band corresponding to the IL1ra fusion migrated a greater distance after cleavage compared to before (**Appendix 3: Figure A.3.6B**). Also, there was just a single band after cleavage, which corresponded to a single peak on the intact mass spectrum (**Appendix 3: Figure A.3.6C**).

Sortase-mediated ligation of IL1ra to AM-ST co-polymers was performed using several different AM-ST co-polymers (**Appendix 3: Figure A.3.7**) concentrations. The results looked

similar to what was observed for sortase-mediated ligation of IgG1 Fc to the co-polymer when analyzed under reducing conditions. This result provided further evidence that the less defined bands of the Fc-polymer conjugate under non-reducing conditions was due to the fact that there were two ligation sites per IgG1 Fc (**Appendix 3: Figure A.3.3**). Increasing the AM-ST co-polymer concentration led to smaller sized protein-polymer conjugates because the Gly3-IL1ra nucleophile became less in excess. Additionally, Gly3-IL1ra was ligated to the AM-ST co-polymers #1 and #2. It was observed by SDS-PAGE that AM-ST co-polymer #1 produced the smallest size IL1ra-polymer conjugates, followed by #2, and lastly #3 produced the largest IL1ra-polymer conjugates. This trend was consistent with the relative sizes of the polymer scaffolds (**Table 4.1**). The Gly3-IL1ra-polymer conjugate was purified from the free Gly3-IL1ra using SEC, just like the Fc-polymer conjugate. SDS-PAGE results showed separation of most of the Gly3-IL1ra from the Gly3-IL1ra-polymer conjugate (**Appendix 3: Figure A.3.8**). These results showed that this method for the controlled assembly of multivalent protein-polymer conjugates was not limited to just IgG1 Fc.

4.4 Conclusions

The multivalent display of protein ligands is important in a variety of biological processes. The ability to produce multivalent protein-polymer conjugates is potentially very useful in studying such biological processes as well as in designing improved therapeutics. However, the activity of the synthesized protein-polymer conjugates is dependent on being able to control the physical characteristics of the initial polymer. Therefore, a combination of controlled polymerization with selective protein ligation holds promise for producing well defined protein-polymer conjugates. In this work, a novel method for the controlled assembly of multivalent protein-polymer conjugates was presented. First, ATRP was used to prepare water

soluble poly(acrylamide-peptide) co-polymers. Three co-polymers were prepared with controlled length and peptide density. The largest and most peptide-dense co-polymer was used as a scaffold for the site-specific attachment of protein to the peptide using a sortase-mediated ligation. This was demonstrated using IgG1 Fc by preparing IgG1 Fc with 5 N-terminal glycine residues. The N-linked glycosylation was modified to a di-glycosylated, homogenous M5 N-glycoform in order to make the Fc as homogenous has possible. This Fc was ligated to the co-polymer and then compared against the Fc alone in a kinetic receptor-binding assay with FcγRIIIa. The results showed that the Fc-polymer conjugate bound FcγRIIIa 800 times stronger than the Fc. This large increase in binding strength was caused by the large difference in dissociation rates, wherein the Fc-polymer conjugate dissociated 800-fold more slowly than the Fc.

This method of producing protein-polymer conjugates allows the researcher to control many of the polymer's characteristics. First, this method allows for control of the size of the polymer. In this work, the three poly(acrylamide-ST peptide) scaffolds ranged in size from ≈ 5,000-25,000 Da. Second, it allows the researcher to control the density of the protein by adjusting the ratio of acrylamide to the ST peptide. In this work, the three poly(acrylamide-ST peptide) scaffolds contained an antigen density ranging from ≈ 3-20 ST peptides/polymer. Third, the protein is attached site-specifically, which allows for a more uniform protein-polymer and also prevents the heterogeneity in protein activity that may result with other polymerization and ligation methods where the site of attachment is less specific. In this work, the proteins were covalently attached to the co-polymer scaffold on their N-termini. And fourth, this method could be used to ligate a variety of proteins to water soluble co-polymer scaffolds. In this work, both IgG1 Fc and IL1ra were ligated to AM-ST co-polymers. Also, the proteins don't theoretically

have to be the same as this technique could be used to ligate a mixture of proteins as long as they contain an N-terminal glycine.

Many different molecules can be ligated to the co-polymer scaffold using a sortase-mediated ligation. Sortase-mediated ligations have been used to ligate a variety of molecules onto the ST recognition peptide including proteins, peptides, sugars, nucleic acids, molecular probes, and small molecule cytotoxic drugs.[20] These types of molecules could be ligated to the co-polymer scaffold to increase their valency. Therefore, this method of producing co-polymers containing internal sortase ligation sites may be used in combination with other, peptide-, protein- and glyco-engineering strategies for a variety of applications.

4.5 References

(1) Mammen, M., Choi, S. K., and Whitesides, G. M. (1998) Polyvalent interactions in biological systems: implications for design and use of multivalent ligands and inhibitors. *Angewandte Chemie International Edition 37*, 2754-2794.

(2) Vance, D., Shah, M., Joshi, A., and Kane, R. S. (2008) Polyvalency: a promising strategy for drug design. *Biotechnology and bioengineering 101*, 429-434.

(3) Sigal, G. B., Mammen, M., Dahmann, G., and Whitesides, G. M. (1996) Polyacrylamides bearing pendant α-sialoside groups strongly inhibit agglutination of erythrocytes by influenza virus: the strong inhibition reflects enhanced binding through cooperative polyvalent interactions. *Journal of the American Chemical Society 118*, 3789-3800.

(4) Hartwell, B. L., Antunez, L., Sullivan, B. P., Thati, S., Sestak, J. O., and Berkland, C. (2015) Multivalent nanomaterials: learning from vaccines and progressing to antigen-specific immunotherapies. *Journal of pharmaceutical sciences 104*, 346-361.

(5) Joshi, A., Vance, D., Rai, P., Thiyagarajan, A., and Kane, R. S. (2008) The design of polyvalent therapeutics. *Chemistry–A European Journal 14*, 7738-7747.

(6) Kitov, P. I., and Bundle, D. R. (2003) On the nature of the multivalency effect: a thermodynamic model. *Journal of the American Chemical Society 125*, 16271-16284.

(7) Goffe, B., and Cather, J. C. (2003) Etanercept: an overview. *Journal of the American Academy of Dermatology 49*, 105-111.

(8) Walker, L., Hay, F., and Roitt, I. (1979) Characteristics of complexes for arming and inhibiting effector cells for antibody-dependent cell-mediated cytotoxicity. *Clinical and experimental immunology 36*, 397-407.

(9) Smith, R. I., Coloma, M. J., and Morrison, S. L. (1995) Addition of a mu-tailpiece to IgG results in polymeric antibodies with enhanced effector functions including complement-mediated cytolysis by IgG4. *The Journal of Immunology 154*, 2226-2236.

(10) Gestwicki, J. E., Cairo, C. W., Strong, L. E., Oetjen, K. A., and Kiessling, L. L. (2002) Influencing receptor− ligand binding mechanisms with multivalent ligand architecture. *Journal of the American Chemical Society 124*, 14922-14933.

(11) Uchida, T., and Murao, Y. (1984) Complement activation by polymer binding IgG. *Biomaterials 5*, 281-283.

(12) Smith, R. I., and Morrison, S. L. (1994) Recombinant polymeric IgG: an approach to engineering more potent antibodies. *Nature Biotechnology 12*, 683-688.

(13) Xiao, J., Hamilton, B. S., and Tolbert, T. J. (2010) Synthesis of N-terminally linked protein and peptide dimers by native chemical ligation. *Bioconjugate chemistry 21*, 1943-1947.

(14) Xiao, J., and Tolbert, T. J. (2009) Synthesis of N-terminally linked protein dimers and trimers by a combined native chemical ligation-CuAAC click chemistry strategy. *Organic Letters 11*, 4144-4147.

(15) Gupta, K., Singh, S., Gupta, K., Khan, N., Sehgal, D., Haridas, V., and Roy, R. P. (2012) A bioorthogonal chemoenzymatic strategy for defined protein dendrimer assembly. *ChemBioChem 13*, 2489-2494.

(16) Mekhaiel, D. N., Czajkowsky, D. M., Andersen, J. T., Shi, J., El-Faham, M., Doenhoff, M., McIntosh, R. S., Sandlie, I., He, J., and Hu, J. (2011) Polymeric human Fc-fusion proteins with modified effector functions. *Scientific reports 1*, 1-11.

(17) Albayrak, C., and Swartz, J. R. (2013) Direct polymerization of proteins. *ACS synthetic biology 3*, 353-362.

(18) Matyjaszewski, K., and Xia, J. (2001) Atom transfer radical polymerization. *Chemical Reviews 101*, 2921-2990.

(19) Appel, E. A., Del Barrio, J., Loh, X. J., Dyson, J., and Scherman, O. A. (2012) High molecular weight polyacrylamides by atom transfer radical polymerization: Enabling advancements in water-based applications. *Journal of Polymer Science Part A: Polymer Chemistry 50*, 181-186.

(20) Proft, T. (2010) Sortase-mediated protein ligation: an emerging biotechnology tool for protein modification and immobilisation. *Biotechnology letters 32*, 1-10.

(21) Clancy, K. W., Melvin, J. A., and McCafferty, D. G. (2010) Sortase transpeptidases: insights into mechanism, substrate specificity, and inhibition. *Peptide Science 94*, 385-396.

(22) Popp, M. W. L., Antos, J. M., and Ploegh, H. L. (2009) Site-Specific Protein Labeling via Sortase-Mediated Transpeptidation. *Current Protocols in Protein Science*, 15.3.1-15.3.9.

(23) Parthasarathy, R., Subramanian, S., and Boder, E. T. (2007) Sortase A as a novel molecular "stapler" for sequence-specific protein conjugation. *Bioconjugate chemistry 18*, 469-476.

(24) Loo, T., Patchett, M. L., Norris, G. E., and Lott, J. S. (2002) Using secretion to solve a solubility problem: high-yield expression in Escherichia coli and purification of the bacterial glycoamidase PNGase F. *Protein expression and purification 24*, 90-98.

(25) White, D. R., Khedri, Z., Kiptoo, P., Siahaan, T. J., and Tolbert, T. J. (2017) Synthesis of a Bifunctional Peptide Inhibitor–IgG1 Fc Fusion That Suppresses Experimental Autoimmune Encephalomyelitis. *Bioconjugate Chemistry 28*, 1867-1877.

(26) Xiao, J., Chen, R., Pawlicki, M. A., and Tolbert, T. J. (2009) Targeting a homogeneously glycosylated antibody Fc to bind cancer cells using a synthetic receptor ligand. *Journal of the American Chemical Society 131*, 13616-13618.

(27) Shah, I. S., Lovell, S., Mehzabeen, N., Battaile, K. P., and Tolbert, T. J. (2017) Structural characterization of the Man5 glycoform of human IgG3 Fc. *Molecular immunology 92*, 28-37.

(28) Choi, B.-K., Warburton, S., Lin, H., Patel, R., Boldogh, I., Meehl, M., d'Anjou, M., Pon, L., Stadheim, T. A., and Sethuraman, N. (2012) Improvement of N-glycan site occupancy of therapeutic glycoproteins produced in Pichia pastoris. *Applied microbiology and biotechnology 95*, 671-682.

(29) Simpson, R. J. (2006) SDS-PAGE of proteins. *Cold Spring Harbor Protocols*.

(30) Cuskin, F., Lowe, E. C., Temple, M. J., Zhu, Y., Cameron, E. A., Pudlo, N. A., Porter, N. T., Urs, K., Thompson, A. J., Cartmell, A., Rogowski, A., Hamilton, B. S., Chen, R., Tolbert, T. J., Piens, K., Bracke, D., Vervecken, W., Hakki, Z., Speciale, G., Munoz-Munoz, J. L., Day, A., Pena, M. J., McLean, R., Suits, M. D., Boraston, A. B., Atherly, T., Ziemer, C. J., Williams, S. J., Davies, G. J., Abbott, D. W., Martens, E. C., and Gilbert, H. J. (2015) Human gut Bacteroidetes can utilize yeast mannan through a selfish mechanism. *Nature 517*, 165-169.

(31) Gasteiger, E., Hoogland, C., Gattiker, A., Duvaud, S., Wilkins, M. R., Appel, R. D., and Bairoch, A. (2005) Protein Identification and Analysis Tools on the ExPASy Server, in *The Proteomics Protocols Handbook* (Walker, J. M., Ed.) pp 571-607, Humana Press.

(32) Laukens, B., Visscher, C. D., and Callewaert, N. (2015) Engineering yeast for producing human glycoproteins: where are we now? *Future microbiology 10*, 21-34.

(33) Duman, J. G., Miele, R. G., Liang, H., Grella, D. K., Sim, K. L., Castellino, F. J., and Bretthauer, R. K. (1998) O-Mannosylation of Pichia pastoris cellular and recombinant proteins. *Biotechnology and applied biochemistry 28*, 39-45.

(34) Guimaraes, C. P., Witte, M. D., Theile, C. S., Bozkurt, G., Kundrat, L., Blom, A. E., and Ploegh, H. L. (2013) Site-specific C-terminal and internal loop labeling of proteins using sortase-mediated reactions. *Nature protocols 8*, 1787-1799.

(35) Nimmerjahn, F., Gordan, S., and Lux, A. (2015) FcγR dependent mechanisms of cytotoxic, agonistic, and neutralizing antibody activities. *Trends in immunology 36*, 325-336.

(36) Tang, Y., Lou, J., Alpaugh, R. K., Robinson, M. K., Marks, J. D., and Weiner, L. M. (2007) Regulation of antibody-dependent cellular cytotoxicity by IgG intrinsic and apparent affinity for target antigen. *The Journal of Immunology 179*, 2815-2823.

(37) Velders, M., Van Rhijn, C., Oskam, E., Fleuren, G., Warnaar, S., and Litvinov, S. (1998) The impact of antigen density and antibody affinity on antibody-dependent cellular cytotoxicity: relevance for immunotherapy of carcinomas. *British journal of cancer 78*, 478-483.

(38) Nesspor, T. C., Raju, T. S., Chin, C. N., Vafa, O., and Brezski, R. J. (2012) Avidity confers FcγR binding and immune effector function to aglycosylated immunoglobulin G1. *Journal of Molecular Recognition 25*, 147-154.

(39) Okbazghi, S. Z., More, A. S., White, D. R., Duan, S., Shah, I. S., Joshi, S. B., Middaugh, C. R., Volkin, D. B., and Tolbert, T. J. (2016) Production, characterization, and biological evaluation of well-defined IgG1 Fc glycoforms as a model system for biosimilarity analysis. *Journal of pharmaceutical sciences 105*, 559-574.

(40) Furst, D. E. (2004) Anakinra: review of recombinant human interleukin-I receptor antagonist in the treatment of rheumatoid arthritis. *Clinical therapeutics 26*, 1960-1975.

(41) Kapust, R. B., Tozser, J., Copeland, T. D., and Waugh, D. S. (2002) The P1' specificity of tobacco etch virus protease. *Biochemical and biophysical research communications 294*, 949-55.

Chapter 5

Conclusions And Future Directions

5.1 Conclusions

Antibody-based therapeutics have the ability to treat a variety of different diseases including cancer, autoimmune disease, and organ transplant rejection. Some work by modulating the immune system. This work further explored the use of antibody-mediated immunomodulation by utilizing the Fc region of the human IgG1 antibody. In Chapter 2, an IgG1 Fc fusion was prepared with the Bifunctional Peptide Inhibitor (BPI) as a potential treatment for multiple sclerosis (MS). In a mouse-model of MS, BPIs have been shown to selectively prevent the activation of T-cells that are involved in causing the symptoms of MS.[1] In this proof-of-concept study, a BPI-Fc fusion was successfully prepared, and, when tested in a mouse model of MS, the BPI-Fc fusion was highly active. BPI-Fc fusions are a promising research avenue in the development of antigen-specific immunotherapy for the potential treatment of multiple sclerosis. In Chapter 3, the effect of IgG1 N-glycosylation was explored. Different N-glycoforms can have different IgG1-mediated immunomodulatory effects. However, these differences are difficult to determine because expression of IgG1 results in a mixture of N-glycoforms, so the production of homogenous N-glycoforms was needed. Using IgG1 Fc as a model system, seven homogenous N-glycoforms were prepared to near complete yield. Comparing the thermal stability of the IgG1 Fc N-glycoforms showed that IgG1 Fc stability can be altered based on the particular N-glycoform. Furthermore, comparing the binding affinity of the IgG1 Fc N-glycoforms to FcγRIIIa showed that binding affinity can also be altered based on the particular N-glycoform. Lastly, comparing the substrate specificity of α1,6-fucosyltranferase, the enzyme responsible for adding core-linked fucose, for different IgG1 Fc N-glycoforms showed that fucosylation kinetics can be altered based on the particular N-glycoform. These results may be used to design more stable therapeutics with tailored immunomodulatory activity.

Additionally, these results improve our fundamental understanding of N-glycan biosynthesis by providing us with additional information about the occurrence of fucosylation during the process. In Chapter 4, IgG1 Fc was ligated to multiple sites on a polymer scaffold to simulate the multivalent binding event that is needed to activate ADCC. An IgG1 Fc-polymer conjugate was prepared using a novel method by combining atom transfer radical polymerization (ATRP) with sortase-mediated ligation. The polymerized IgG1 Fc was then compared to the monomer in a binding assay with FcγRIIIa. Compared to IgG1 Fc, the Fc-polymer conjugate showed an 800-fold increase in binding affinity. This increased binding affinity was caused by an 800-fold decrease in the dissociation rate. These results suggest that the multivalent binding mechanism needed to activate ADCC may involve slowing the dissociation rate of Fc-FcγR interactions. The research presented in this dissertation improves our fundamental understanding of IgG1-mediated immunomodulation and may also help in the development of improved antibody-based therapeutics.

5.2 Future Directions

Building off the results presented in Chapter 2, there are many research avenues that could be explored. For instance, other antigenic peptides could be tested. It was already shown in Chapter 2 that the BPI-Fc fusion can be successfully synthesized using the MOG antigenic peptide. Testing this peptide in a BPI-Fc fusion *in-vivo* would demonstrate the applicability of the synthesis because the LABL-Fc-ST scaffold can be used again instead of having to perform the cloning, expression, and purification for each BPI-Fc fusion. Additionally, BPI-Fc fusions can be tested in a different disease model, such as diabetes. The Siahaan laboratory has shown efficacy using the BPI peptide in a mouse model of diabetes.[2, 3] In this model, the signal-2

blocking peptide is LABL, just like in the MS model. Therefore, the LABL-Fc-ST protein scaffold would work well during the synthesis. A peptide derived from glutamic acid decarboxylase could be used as the diabetes-specific antigenic peptide. Furthermore, a BPI-Fc fusion could be prepared using multiple antigenic peptides to combat the threat of antigen spreading.[4-6] This synthesis could be performed in a variety of ways: 1.) by performing a sortase-mediated ligation on the LABL-Fc-ST scaffold with a mixture of antigenic peptides, or 2.) by synthesizing a long peptide that contains multiple antigenic sequences within one peptide, or 3.) by using the controlled assembly of multivalent active molecules strategy that was presented in Chapter 4 (To attach the AM-ST co-polymer to LABL-Fc-ST, a triglycine-containing functional group that would allow linking of LABL-Fc-ST to the terminus of a AM-ST co-polymer could be used.). Furthermore, measuring the *in-vivo* half-life of the BPI-Fc would be useful. Theoretically, the BPI-Fc has a longer half-life then the BPI peptides because it has a slower renal clearance and can be rescued from lysosomal degradation by FcRn.[7] This half-life study could be analyzed using a western blot by quantifying the band intensity over time. The western blot could be useful because it would also show an approximate size of the BPI-Fc fusion, which would allow us to see if proteolysis is occurring. Additionally, the western blot could be detected using different detection antibodies that recognize different regions of the molecule: the Fc, the signal 2-blocking peptide, and the antigenic peptide. Similarly, a dose-response study could be performed. If the Fc is promoting an increased half-life, then perhaps a lower dose could be given to achieve similar results. Lastly, the N-linked glycosylation of IgG1 Fc could be modified in order to better suppress the disease. For instance, adding sialic acid to the termini of the glycan branches has been suggested to promote anti-inflammatory activity.[8] Combining this anti-inflammatory activity with the immunosuppressive activity of the BPI peptides could produce a better molecule.

Building off the results presented in Chapter 3, additional homogenous IgG1 Fc N-glycoforms could be tested. For instance, terminal galactose or sialic acid could be prepared, with and without fucose. Also, the substrate specificities of the N-glycoforms could be tested using other glyco-processing enzymes, such as N-acetylglucosaminyltransferase-III which adds bisecting N-acetylglucosamine (GlcNAc). Bisecting GlcNAc is important because its presence reduces fucosylation levels.[9] Reduced fucosylation has been shown to increase ADCC activity, and ADCC activity is important for the cell-killing ability of some cancer immunotherapies.[10] Additionally, Hydrogen-Deuterium exchange could be performed on the IgG1 Fc N-glycoforms produced in this chapter. Hydrogen-Deuterium exchange was previously performed using a different series of homogenous IgG1 Fc N-glycoforms produced in the Tolbert laboratory.[11] The results presented in Chapter 3 and findings in the literature would lead us to hypothesize that the G0 N-glycoform would show less flexibility compared to the M5, M5H, and M3H N-glycoforms because the G0 N-glycoform contains an additional intramolecular glycan-polypeptide interaction that the other N-glycoforms do not contain.[12-14] Furthermore, the IgG1 N-glycoforms produced in this chapter could be tested in a binding assay FcγRIIIa using different N-glycoforms of FcγRIIIa. Falconer *et. al* (2018) showed an increase in binding affinity for IgG1 Fc by changing the N-glycosylation of FcγRIIIa from complex to oligomannose.[15]

Building off the results presented in Chapter 4, the IgG1 Fc-polymer conjugate could be tested in an ADCC assay to see if it can stimulate ADCC without needing to bind a target cell. Promega sells an ADCC reporter bioassay assay that induces luciferase expression upon effector cell activation.[16] If successful, then IgG1 Fc-polymer conjugates of different N-glycoforms could be prepared and compared for their relative abilities to induce ADCC. This work would build off of the FcγRIIIa binding assay that was performed in Chapter 3. In another potential project, the

N-glycosylation of Gly5-IgG1 Fc could be modified with terminal sialic acid using *in-vitro* enzymatic synthesis, and the sialylated IgG1 Fc could be prepared as an Fc-polymer conjugate. This sialylated IgG1 Fc-polymer conjugate could be tested to see if it increased binding for DC-SIGN, a receptor involved in promoting anti-inflammatory activity.[8] If successful, this concept may have use as a potential immunosuppressant.

5.3 References

(1) Kiptoo, P., Büyüktimkin, B., Badawi, A., Stewart, J., Ridwan, R., and Siahaan, T. (2013) Controlling immune response and demyelination using highly potent bifunctional peptide inhibitors in the suppression of experimental autoimmune encephalomyelitis. *Clinical & Experimental Immunology 172*, 23-36.

(2) Murray, J. S., Oney, S., Page, J. E., Kratochvil-Stava, A., Hu, Y., Makagiansar, I. T., Brown, J. C., Kobayashi, N., and Siahaan, T. J. (2007) Suppression of type 1 diabetes in NOD mice by bifunctional peptide inhibitor: modulation of the immunological synapse formation. *Chemical biology & drug design 70*, 227-236.

(3) Badawi, A. H., Büyüktimkin, B., Kiptoo, P., and Siahaan, T. J. (2011) Peptides and Proteins for Treatment and Suppression of Type 1 Diabetes, in *Type 1 Diabetes-Pathogenesis, Genetics and Immunotherapy* pp 339-354, IntechOpen.

(4) McMahon, E. J., Bailey, S. L., Castenada, C. V., Waldner, H., and Miller, S. D. (2005) Epitope spreading initiates in the CNS in two mouse models of multiple sclerosis. *Nature medicine 11*, 335-339.

(5) Vanderlugt, C. L., and Miller, S. D. (2002) Epitope spreading in immune-mediated diseases: implications for immunotherapy. *Nature Reviews Immunology 2*, 85-95.

(6) Badawi, A. H., and Siahaan, T. J. (2013) Suppression of MOG-and PLP-induced experimental autoimmune encephalomyelitis using a novel multivalent bifunctional peptide inhibitor. *Journal of neuroimmunology 263*, 20-27.

(7) Roopenian, D. C., and Akilesh, S. (2007) FcRn: the neonatal Fc receptor comes of age. *Nature reviews immunology 7*, 715-725.

(8) Anthony, R. M., and Ravetch, J. V. (2010) A novel role for the IgG Fc glycan: the anti-inflammatory activity of sialylated IgG Fcs. *Journal of clinical immunology 30*, 9-14.

(9) Wang, Q., Chung, C. Y., Chough, S., and Betenbaugh, M. J. (2018) Antibody glycoengineering strategies in mammalian cells. *Biotechnology and bioengineering 115*, 1378-1393.

(10) Arnould, L., Gelly, M., Penault-Llorca, F., Benoit, L., Bonnetain, F., Migeon, C., Cabaret, V., Fermeaux, V., Bertheau, P., and Garnier, J. (2006) Trastuzumab-based treatment of HER2-positive breast cancer: an antibody-dependent cellular cytotoxicity mechanism? *British journal of cancer 94*, 259-267.

(11) More, A. S., Toth IV, R. T., Okbazghi, S. Z., Middaugh, C. R., Joshi, S. B., Tolbert, T. J., Volkin, D. B., and Weis, D. D. (2018) Impact of Glycosylation on the Local Backbone Flexibility of Well-Defined IgG1-Fc Glycoforms Using Hydrogen Exchange-Mass Spectrometry. *Journal of pharmaceutical sciences 107*, 2315-2324.

(12) Barb, A. W. (2014) Intramolecular N-Glycan/Polypeptide Interactions Observed at Multiple N-Glycan Remodeling Steps through [13C, 15N]-N-Acetylglucosamine Labeling of Immunoglobulin G1. *Biochemistry 54*, 313-322.

(13) Subedi, G. P., Hanson, Q. M., and Barb, A. W. (2014) Restricted motion of the conserved immunoglobulin G1 N-glycan is essential for efficient FcγRIIIa binding. *Structure 22*, 1478-1488.

(14) Yu, X., Baruah, K., Harvey, D. J., Vasiljevic, S., Alonzi, D. S., Song, B.-D., Higgins, M. K., Bowden, T. A., Scanlan, C. N., and Crispin, M. (2013) Engineering hydrophobic protein–carbohydrate interactions to fine-tune monoclonal antibodies. *Journal of the American Chemical Society 135*, 9723-9732.

(15) Patel, K. R., Roberts, J. T., Subedi, G. P., and Barb, A. W. (2018) Restricted processing of CD16a/Fc γ receptor IIIa N-glycans from primary human NK cells impacts structure and function. *Journal of Biological Chemistry 293*, 3477-3489.

(16) Parekh, B. S., Berger, E., Sibley, S., Cahya, S., Xiao, L., LaCerte, M. A., Vaillancourt, P., Wooden, S., and Gately, D. (2012) Development and validation of an antibody-dependent cell-mediated cytotoxicity-reporter gene assay. *mAbs 4*, 19-18.

Appendix 1

Synthesis of a Bifunctional Peptide Inhibitor–IgG1 Fc Fusion that Suppresses Experimental Autoimmune Encephalomyelitis

A.1.1 Methods

A.1.1.1 DNA cloning

A.1.1.1.1 Cloning of pPICzαA-PLP-Fc-LABL

DNA primers were designed that allowed for the C-terminal addition of the LABL peptide to IgG1 Fc with a three alanine residue spacer (5'-ggccgccggaggtggaattactgatggagaagctactgattctggataat-3’ and 5'-ctagattatccagaatcagtagcttctccatcagtaattccacctccggc-3’) and for the proper NotI and XbaI sticky ends when mixed together. The primers were phosphorylated on the 5’-termini using PNK. pGAPzαA-Fc with no stop codon after the Fc, as described in the “Cloning of pPICzαA-LABL-Fc-ST” experimental section, was digested using NotI-HF and XbaI and gel purified. The LABL DNA primers and digested pGAPzαA-Fc with complimentary NotI and XbaI sticky ends were ligated together using T4 DNA Ligase to create pGAPzαA-Fc-LABL.

DNA primers were designed that allowed for the N-terminal addition of the PLP peptide to IgG1 Fc with a three glycine residue spacer (5'-ggcgccctcgagaaaagacattctttgggaaaatggttgggacatccagataaatttggaggtg-3’ and 5'-cgccgcgagctcaggtgctgggcacggtgggcatgttccacctccaaatttatctggatgtccc-3’). The primers were extended using PCR. The PCR product was purified using the Qiagen QIAquick Gel Extraction Kit (USA). The PLP PCR product and pGAPzαA-Fc-LABL were digested using XhoI and SacI-HF and gel purified. The digested pGAPzαA-Fc-LABL and PLP DNA were ligated together using T4 DNA Ligase to create pGAPzαA-PLP-Fc-LABL. In a separate reaction, pGAPzαA-Fc-LABL was digested using XhoI and XbaI and gel purified. pPICzαA was also digested using XhoI and XbaI and gel purified. The digested Fc-LABL and pPICzαA DNA were ligated together using T4 DNA Ligase to produce pPICzαA-Fc-LABL. pGAPzαA-PLP-Fc-LABL and pPICzαA-Fc-LABL were both digested using XhoI and NotI-HF and gel purified. The digested

PLP-Fc and pPICzαA-Fc-LABL DNA were gel purified and then ligated together using T4 DNA Ligase to create pPICzαA-PLP-Fc-LABL.

A.1.1.1.2 Cloning of pPICzαA-MOG-Fc

DNA primers were designed that allowed for the N-terminal addition of the MOG peptide to IgG1 Fc with a three glycine spacer (5'-ggcgccctcgagaaaagaggatggtatagatctccattttctagagttgttcatttgggagg-3' and 5'-cgccgcgagctcaggtgctgggcacggtgggcatgttccacctcccaaatgaacaactctagaaaatgg-3'). The primers were annealed and extended using PCR. The PCR product was purified using the Qiagen QIAquick Gel Extraction Kit and digested with XhoI and SacI-HF. pGAPzαA-Fc with a stop codon after the Fc (prepared similarly to pGAPzαA-Fc with no stop codon as described in the "Cloning of pPICzαA-LABL-Fc-ST" experimental section) was also digested with XhoI and SacI-HF. Both digests were gel purified, and the digested MOG and pGAPzαA-Fc DNA were ligated together using T4 DNA Ligase to produce pGAPzαA-MOG-Fc. pGAPzαA-MOG-Fc and pPICzαA were digested with XhoI and NotI-HF. The digested MOG-Fc and pPICzαA DNA were gel purified and ligated together using T4 DNA Ligase to produce pPICzαA-MOG-Fc.

A.1.1.2 Protein expression

A.1.1.2.1 Expression of PLP-Fc-LABL (Spinner Flask)

P. pastoris OCH1 KO cells transformed with pPICzαA-PLP-Fc-LABL were inoculated in a shake tube containing 2 mL of YPD media and 100 µg/mL Zeocin. The culture was shaken at 250 rpm and 25°C. After 3 days, the 2 mL culture was transferred to a 250 mL baffled shake flask containing 50 mL YPD media and 100 µg/mL Zeocin. The culture was shaken at 250 rpm at 25°C. After 2 days, the 50 mL culture was transferred to a 1 L spinner flask containing Buffered Glycerol-complex (BMGY) media, 0.004% histidine, and 1 drop of Antifoam 204 (Sigma-Aldrich). The culture was stirred at room temperature with an air flow rate of 3 L/min.

After 70 hours of growth, 25 mL of 20%(v/v) methanol was added every 12 hours. After 60 hours of induction, the culture was centrifuged at 6000 rpm for 20 min. The supernatant was collected and the pH was adjusted to 7.0 and placed in the 4°C refrigerator for 4 hours. The supernatant was vacuum filtered using Whatman #1 filter. PLP-Fc-LABL protein was purified from the supernatant using Protein G affinity chromatography. The Protein G column was equilibrated using 200 mL of 20 mM Sodium Phosphate buffer, pH 7.0. The 1 L of supernatant was loaded and then the column was washed using 200 mL of 20 mM Sodium Phosphate buffer, pH 7.0. The Fc-containing protein was eluted from the column using 200 mL of 100 mM glycine pH 2.7. The protein was immediately dialyzed against 2 L of 20 mM Sodium Phosphate buffer, pH 7.0 at 4 °C with 1 buffer change. The yield of purified protein obtained was measured to be 3.0 mg as determined by measuring the optical density of the solution at 280 nm (MW = 56133.2 Da, ε_{280} = 82570 $M^{-1}cm^{-1}$).

A.1.1.2.2 Expression of PLP-Fc-LABL (Fermentor)

In order to avoid adding histidine to the fermentor media, *P. pastoris* OCH1 KO cells containing pPICzαA-PLP-Fc-LABL was transformed with pPIC9K. First, pPIC9K was linearized using SalI. The transformation of SalI-linearized pPIC9K into *P. pastoris* OCH1 KO cells containing pPICzαA-PLP-Fc-LABL was performed using electroporation. The electroporated cells were plated on Minimal Dextrose plates and incubated for 5 days at 25°C. After which, a colony was inoculated into 2 mL YPD media and 100 µg/mL Zeocin. The culture was shaken at 250 rpm and 25°C. After 3 days, the culture was transferred to a baffled shake flask containing 250 mL YPD media, 100 µg/mL Zeocin, and 1 drop of Antifoam 204. After 4 days, the 250 mL culture was transferred to a New Brunswick BioFlo 415 fermentor using a fermentation basal salts medium and PTM_1 trace salts. 50% glycerol was added as a carbon source for 2 days. Then 100% methanol was added for 2 days. pH was maintained by the

addition of NH_4OH. The culture was centrifuged at 6000 rpm for 15 minutes. Approximately 6 L of supernatant was collected and stored at 4°C overnight. The supernatant was filtered, concentrated, and then subjected to Protein G affinity chromatography using a similar purification procedure as described in Chapter 2, 2.2.3 "Expression and purification of LABL-Fc-ST (Fermentor)". The yield of purified protein obtained was 150 mg as determined by measuring the optical density of the solution at 280 nm (MW = 56133.2 Da, ε_{280} = 82570 $M^{-1}cm^{-1}$).

A.1.1.2.3 Expression of PLP-Fc-LABL (spinner flask, media change)

P. pastoris OCH1 KO cells transformed with pPICzαA-PLP-Fc-LABL was inoculated in a shake tube containing 2 mL of YPD media and 100 µg/mL Zeocin. The culture was shaken at 250 rpm and 25°C. After 3 days the 2 mL culture was transferred to a baffled shake flask containing 50 mL YPD media and 100 µg/mL Zeocin. The culture was shaken at 250 rpm and 25°C. After 3 days, the 50 mL culture was transferred to a 1 L spinner flask containing BMGY media, 0.004% histidine, and 1 drop of Antifoam 204 (Sigma). The culture was stirred at room temperature with an air flow rate of 3 L/min. After 3 days of growth, the culture was centrifuged at 4500 rpm for 15 minutes. The supernatant was discarded, and the cell pellet was re-suspended in approximately 60 mL of YPD media. The re-suspended cells were transferred to a spinner flask containing 1 L of fresh Buffered Methanol-complex (BMMY) media, 0.004% histidine, and 1 drop of Antifoam 204. The culture was stirred at room temperature with an air flow rate of 3 L/min. Every 12 hours, 25 mL of 20%(v/v) methanol was added. After 47 hours of induction, the culture was centrifuged at 6000 rpm for 20 min. The supernatant was collected and the pH was adjusted to 7.0 and placed in the 4°C refrigerator for 1.5 hours. The supernatant was vacuum filtered using a Whatman #1 filter. PLP-Fc-LABL protein was purified from the supernatant using Protein G affinity chromatography using the purification procedure described in the

"Expression of PLP-Fc-LABL (spinner flask)" experimental section. The yield of purified protein obtained was measured to be 2.1 mg as determined by measuring the optical density of the solution at 280 nm (MW = 56133.2 Da, ε_{280} = 82570 $M^{-1}cm^{-1}$).

A.1.1.2.4 Expression of MOG-Fc

MOG-Fc was expressed in a 1 L spinner flask and purified using a similar procedure described in the "Expression of PLP-Fc-LABL (spinner flask)" experimental section. The yield of purified protein obtained was measured to be 2.7 mg as determined by measuring the optical density of the solution at 280 nm (MW = 53634.8 Da, ε_{280} = 85550 $M^{-1}cm^{-1}$).

A.1.1.2.5 Expression of LABL-Fc-ST (Spinner Flask)

LABL-Fc-ST was expressed in a 1 L spinner flask and purified using a similar procedure described in the "Expression of PLP-Fc-LABL (spinner flask)" experimental section. The yield of purified protein obtained was measured to be 15 mg as determined by measuring the optical density of the solution at 280 nm (MW = 54006.8 Da, ε_{280} = 71570 $M^{-1}cm^{-1}$).

A.1.1.3 Characterization

A.1.1.3.1 Sodium Dodecyl Sulfate–Polyacrylamide Gel Electrophoresis (SDS-PAGE)

Polyacrylamide gels for SDS-PAGE were prepared in house using a Bio-Rad Mini-PROTEAN Tetra casting stand and clamps. First, the resolving layer was prepared by mixing 12% acrylamide/Bis solution (29:1), 375 mM Tris pH 8.8, 0.1% (w/v) SDS, 0.1% (w/v) Ammonium Persulfate (APS), and 0.04% (v/v) N,N,N',N'-Tetramethylethylenediamine (TEMED). The mixture was poured between a Mini-PROTEAN short plate and 0.75 mm spacer plate, topped with a layer of n-butanol, and allowed to sit for 30 minutes at room temperature. After which, the butanol was rinsed off. The stacking layer was prepared by mixing 5% acrylamide/Bis solution (29:1), 125 mM Tris pH 6.8, 0.1% (w/v) SDS, 0.1% (w/v) APS, and 0.1% (v/v) TEMED. The mixture was poured on top of the resolving gel, a 10 well comb was

inserted, and the gel was allowed to sit for 30 minutes at room temperature. The protein samples for SDS-PAGE were prepared by mixing each sample with a 1:1 ratio of 2X sample loading buffer (100 mM Tris pH 6.8, 4% (w/v) SDS, 20% (v/v) Glycerol, 100 mM DTT, 0.02% (w/v) Bromophenol Blue). The samples were placed in a heat block at 94°C for 5 minutes, then 2 µg of protein was loaded into each well. The gel was placed in a Mini-PROTEAN Tetra electrophoresis chamber containing electrophoresis running buffer (0.25 M Glycine, 0.025 M Tris Base, 0.1% (w/v) SDS, pH 8.3). The samples were electrophoresed at 200 V for 50 minutes. After which, the gel was stained in a staining solution (0.25% (w/v) Coomassie Blue R-250, 50% (v/v) Methanol, 40% Water, 10% (v/v) Acetic Acid) for 1 hour at room temperature on a rotary shaker. The staining solution was poured off, and the gel was destained in a destaining solution (50% (v/v) Methanol, 40% Water, and 10% (v/v) Acetic Acid) for 30 minutes at room temperature on a rotary shaker. The destaining solution was poured off, and the gel was further destained in a weaker destaining solution (10% (v/v) Methanol, 88% Water, and 2% (v/v) Acetic Acid) for 3 hours.

A.1.2 Figures

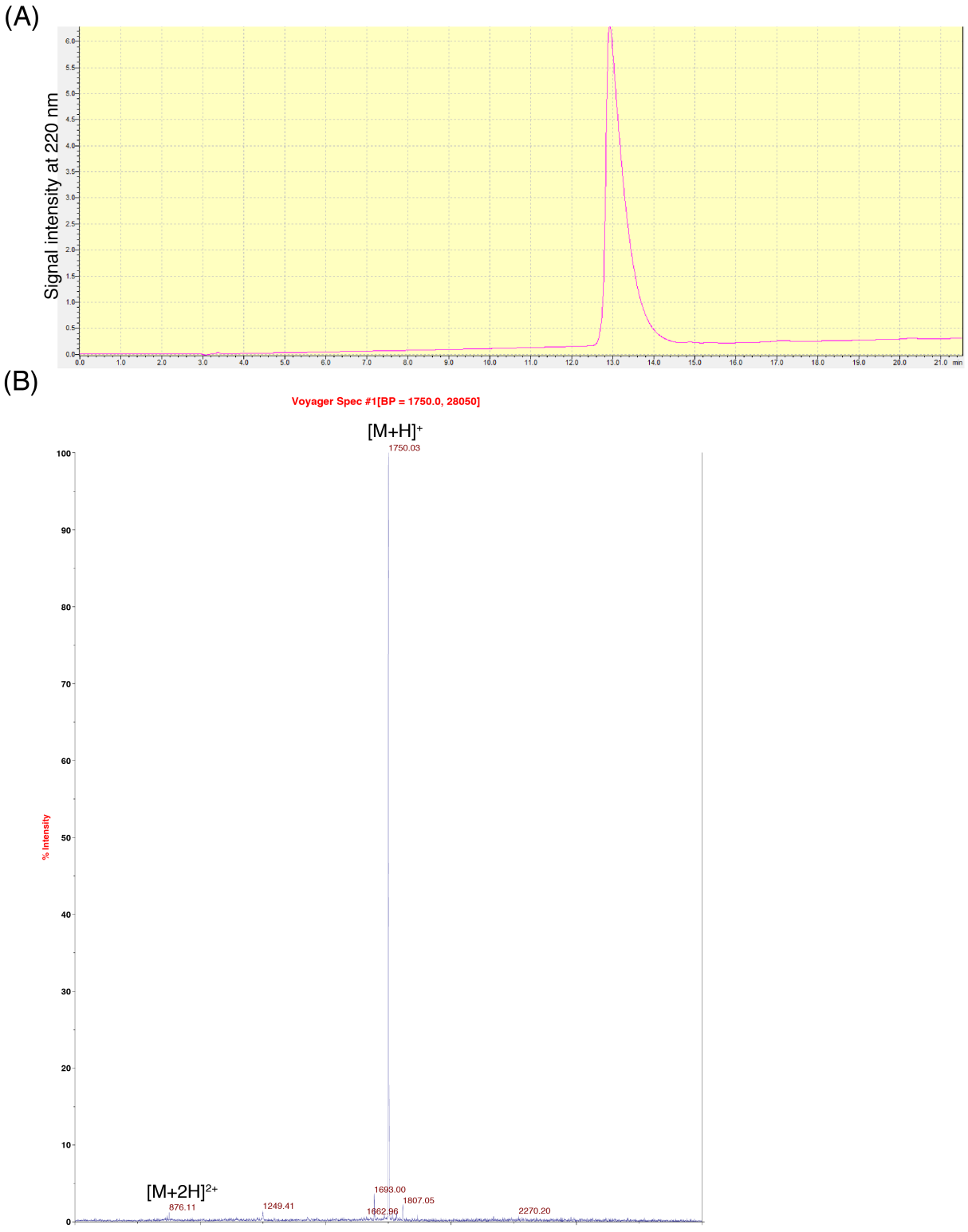

Figure A.1.1: Characterization of PLP peptide. (A) Analytical HPLC chromatogram of the PLP peptide monitored by UV absorbance at 220 nm. (B) MALDI mass spectrum. $[M+H]^+$ mass (Da): Expected = 1749.9 and Observed = 1750.0.

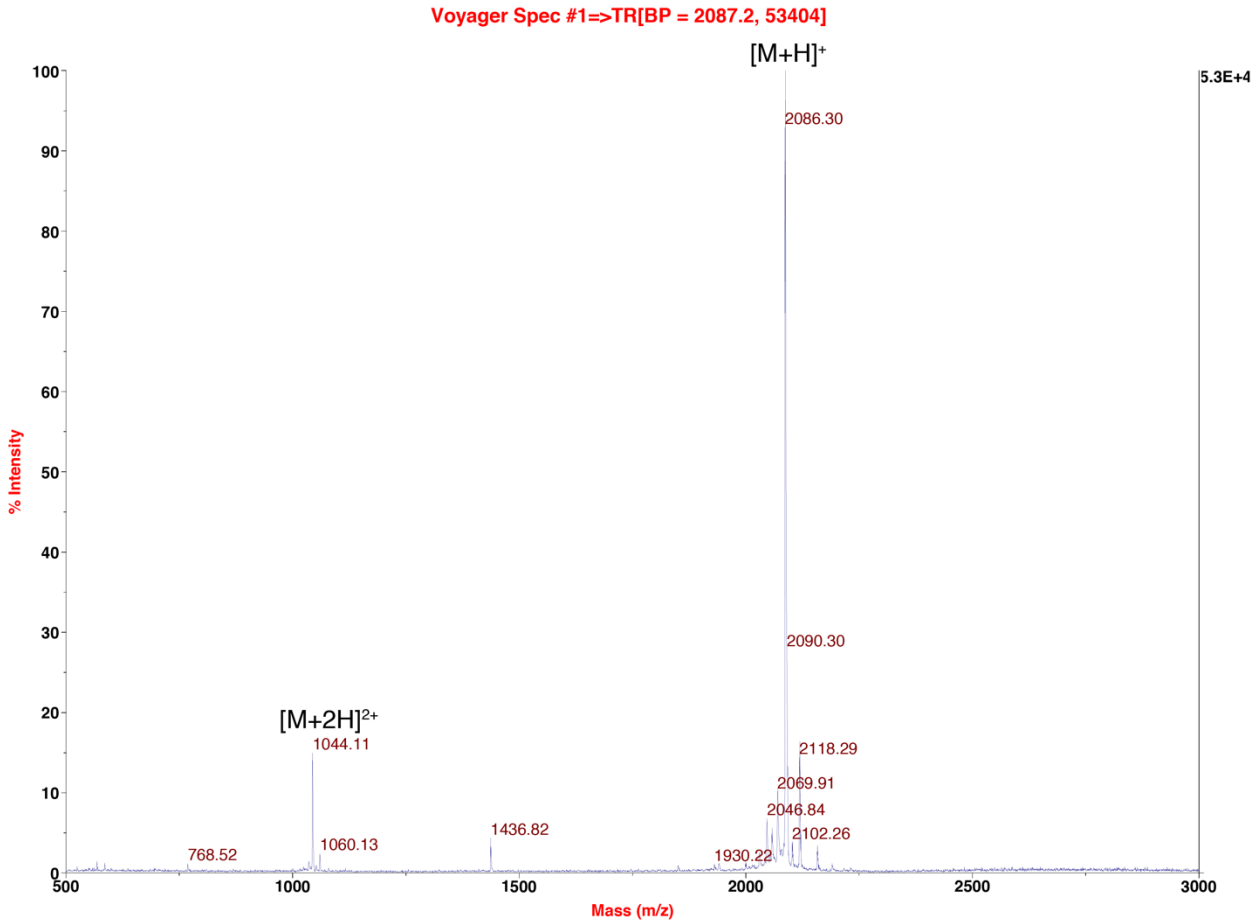

Figure A.1.2: Characterization of MOG peptide synthesized for a sortase-mediated ligation. MALDI mass spectrum. $[M+H]^+$ mass (Da): Expected = 2087.1 and Observed = 2087.2.

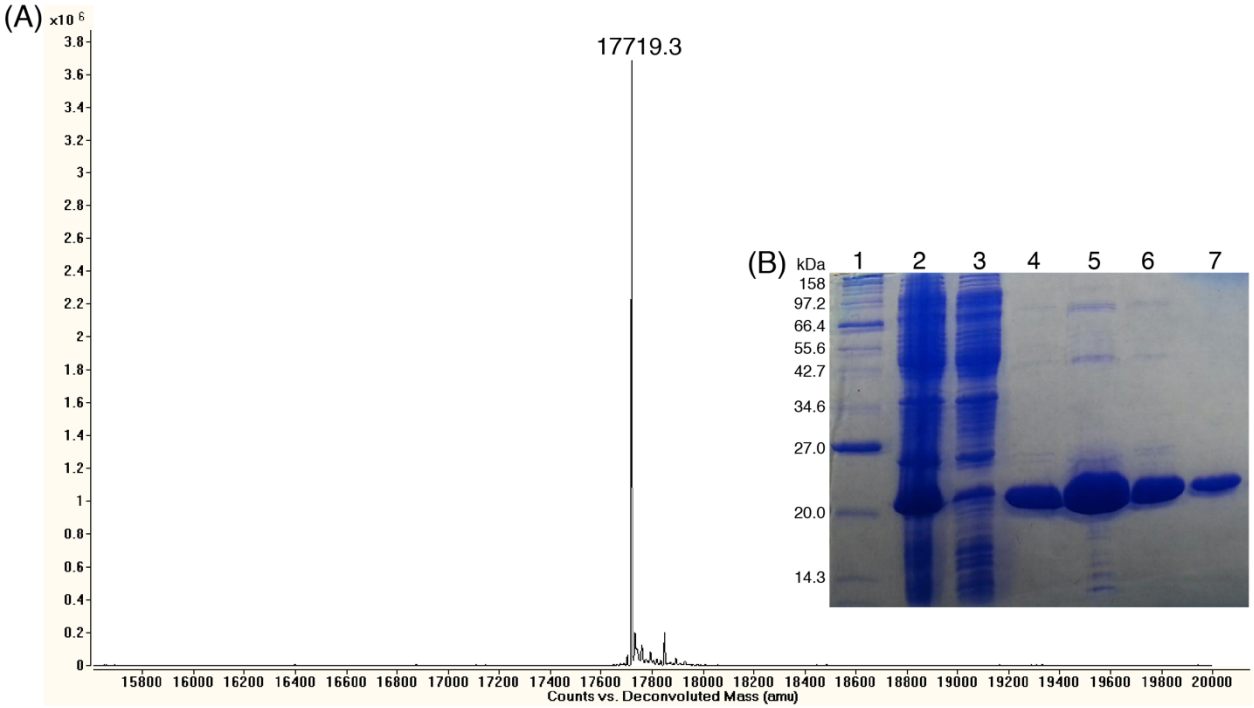

Figure A.1.3: Characterization of sortase A. (A) Mass spectrum of Sortase A after Ni^{2+}-NTA purification. Sortase A MW (Da): Expected = 17719.0, Observed = 17719.3. (B) SDS-PAGE of Sortase A Ni^{2+}-NTA purification fractions. Lanes: 1, 2-212 kDa MW marker; 2, cell lysate of *E. coli* Rosetta 2 that overexpressed sortase A; 3, Ni^{2+}-NTA flow through of cell lysate; and 4-7, Ni^{2+}-NTA elution fractions. Elution fractions shown in lanes 4-6 were pooled and used for the sortase-mediated ligation experiments described herein.

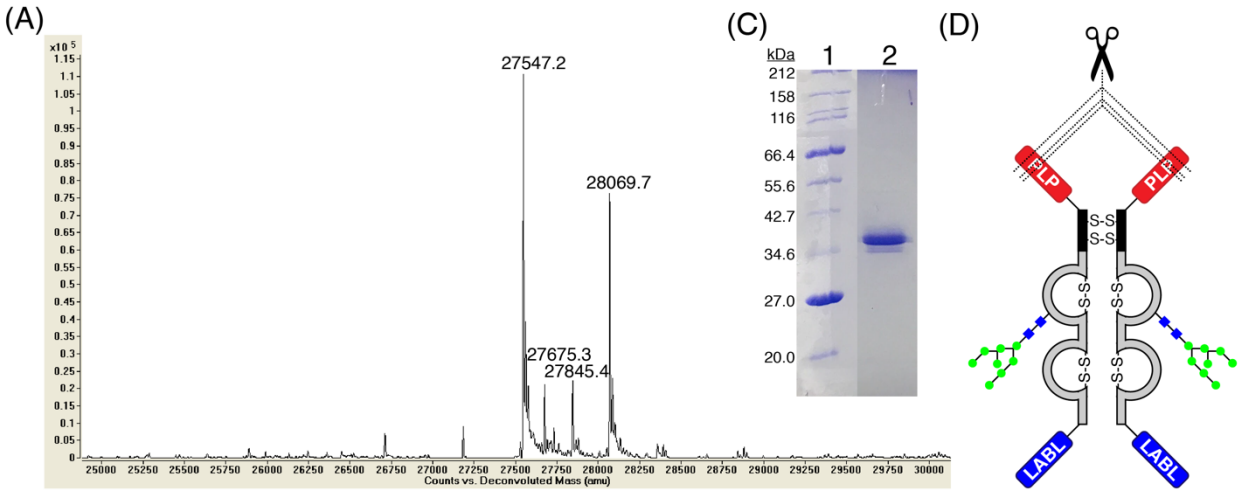

(B)

PLP-Fc-LABL Expression Products	Observed MW (Da)	Expected MW (Da)
HSLGKWLGHPDKF-Fc-ITDGEATDSG	28069.7	28073.6
LGKWLGHPDKF-Fc-ITDGEATDSG	27845.4	27849.4
KWLGHPDKF-Fc-ITDGEATDSG	27675.3	27679.2
WLGHPDKF-Fc-ITDGEATDSG	27547.2	27551.0

Figure A.1.4: Characterization of recombinant expression of PLP-Fc-LABL dual fusion protein in a spinner flask. (A) Mass spectrum of PLP-Fc-LABL expression products. Prior to characterization, the protein was de-glycosylated with PNGase F and reduced to its monomeric state using DTT. (B) Table showing peptide sequences and observed vs. expected molecular weights of expression products. PLP sequence = H_3N^+-HSLGKWLGHPDKF, LABL sequence = H_3N^+-ITDGEATDSG. (C) SDS-PAGE of PLP-Fc-LABL reduced with DTT. Lanes: 1, 2-212 kDa MW marker and 2, PLP-Fc-LABL after purification by protein G affinity chromatography. (D) Representation of PLP-Fc-LABL dual fusion protein showing sites of proteolysis that were observed in the mass spectrum.

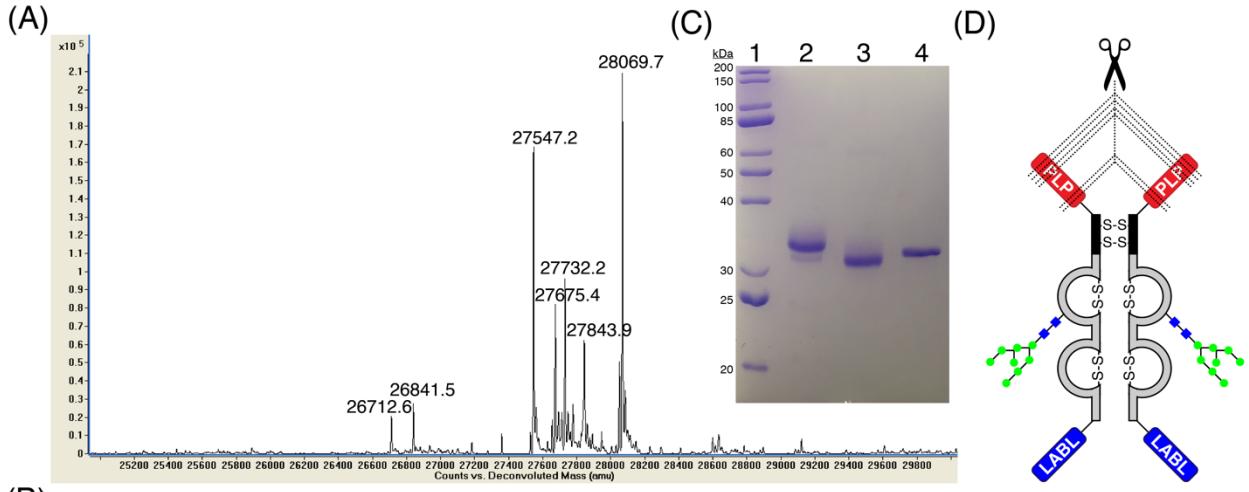

(B)

PLP-Fc-LABL Expression Products	Observed MW (Da)	Expected MW (Da)
HSLGKWLGHPDKF-Fc-ITDGEATDSG	28069.7	28073.6
LGKWLGHPDKF-Fc-ITDGEATDSG	27843.9	27849.4
GKWLGHPDKF-Fc-ITDGEATDSG	27732.2	27736.2
KWLGHPDKF-Fc-ITDGEATDSG	27675.4	27679.2
WLGHPDKF-Fc-ITDGEATDSG	27547.2	27551.0
KF-Fc-ITDGEATDSG	26841.5	26845.3
F-Fc-ITDGEATDSG	26712.6	26717.1

Figure A.1.5: Characterization of recombinant expression of PLP-Fc-LABL dual fusion protein in a fermentor. (A) Mass spectrum of PLP-Fc-LABL expression products. Prior to characterization, the protein was de-glycosylated with PNGase F and reduced to its monomeric state using DTT. (B) Table showing peptide sequences and observed vs. expected molecular weights of expression products. PLP sequence = H_3N^+-HSLGKWLGHPDKF, LABL sequence = H_3N^+-ITDGEATDSG. (C) SDS-PAGE of PLP-Fc-LABL reduced with DTT. Lanes: 1, 10-200 kDa MW marker; 2, PLP-Fc-LABL after purification by protein G affinity chromatography; 3, PLP-Fc-LABL de-glycosylated with PNGase F; and 4, PNGase F. (D) Representation of PLP-Fc-LABL dual fusion protein showing sites of proteolysis that were observed in the mass spectrum.

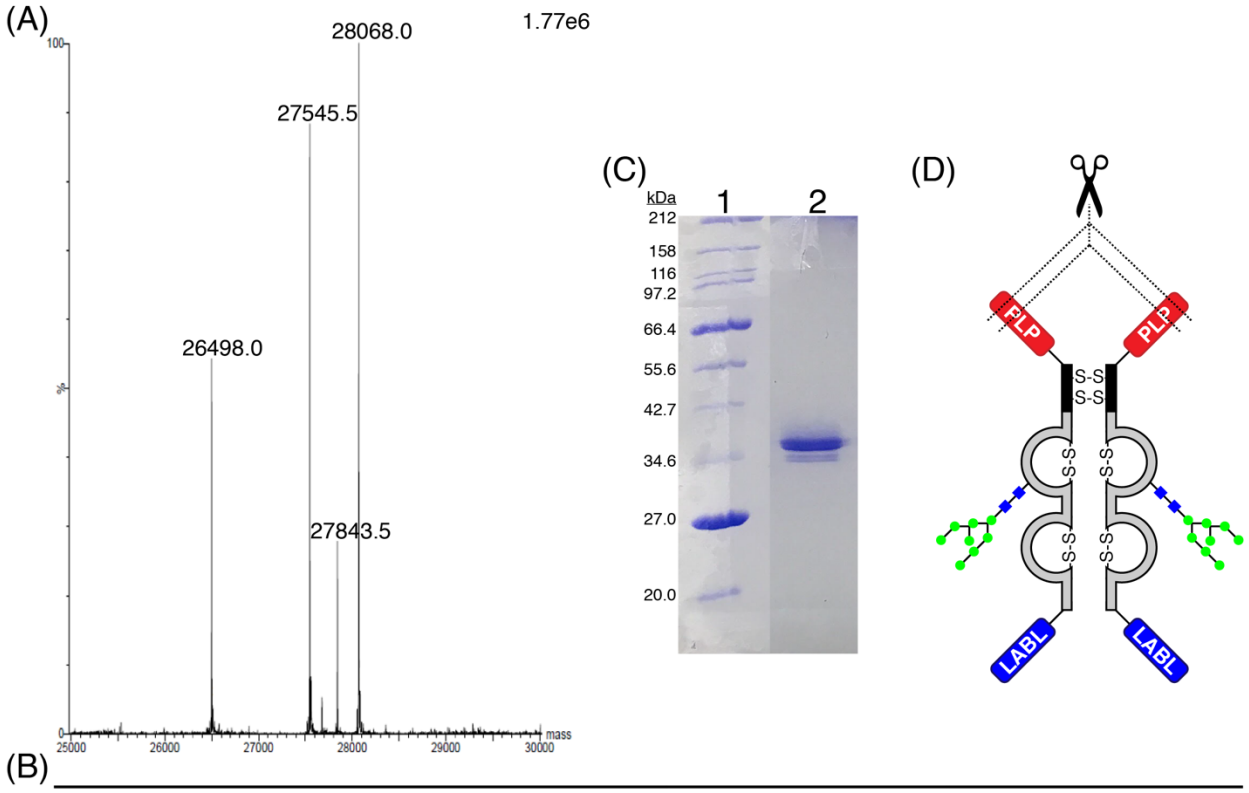

(B)

PLP-Fc-LABL Expression Products	Observed MW (Da)	Expected MW (Da)
HSLGKWLGHPDKF-Fc-ITDGEATDSG	28068.0	28073.6
LGKWLGHPDKF-Fc-ITDGEATDSG	27843.5	27849.4
WLGHPDKF-Fc-ITDGEATDSG	27545.5	27551.0

Figure A.1.6: Characterization of recombinant expression of PLP-Fc-LABL dual fusion protein in a spinner flask with a media change prior to induction. (A) Mass spectrum of PLP-Fc-LABL expression products. Prior to characterization, the protein was de-glycosylated with PNGase F and reduced to its monomeric state using DTT. The peak with the observed MW of 26498.0 Da was determined to be carryover from an unrelated protein sample and was excluded from the yield calculation. (B) Table showing peptide sequences and observed vs. expected molecular weights of expression products. PLP sequence = H_3N^+-HSLGKWLGHPDKF, LABL sequence = H_3N^+-ITDGEATDSG. (C) SDS-PAGE of PLP-Fc-LABL reduced with DTT. Lanes: 1, 2-212 kDa MW marker; and 2, PLP-Fc-LABL after purification by protein G affinity chromatography. (D) Representation of PLP-Fc-LABL dual fusion protein showing sites of proteolysis that were observed in the mass spectrum.

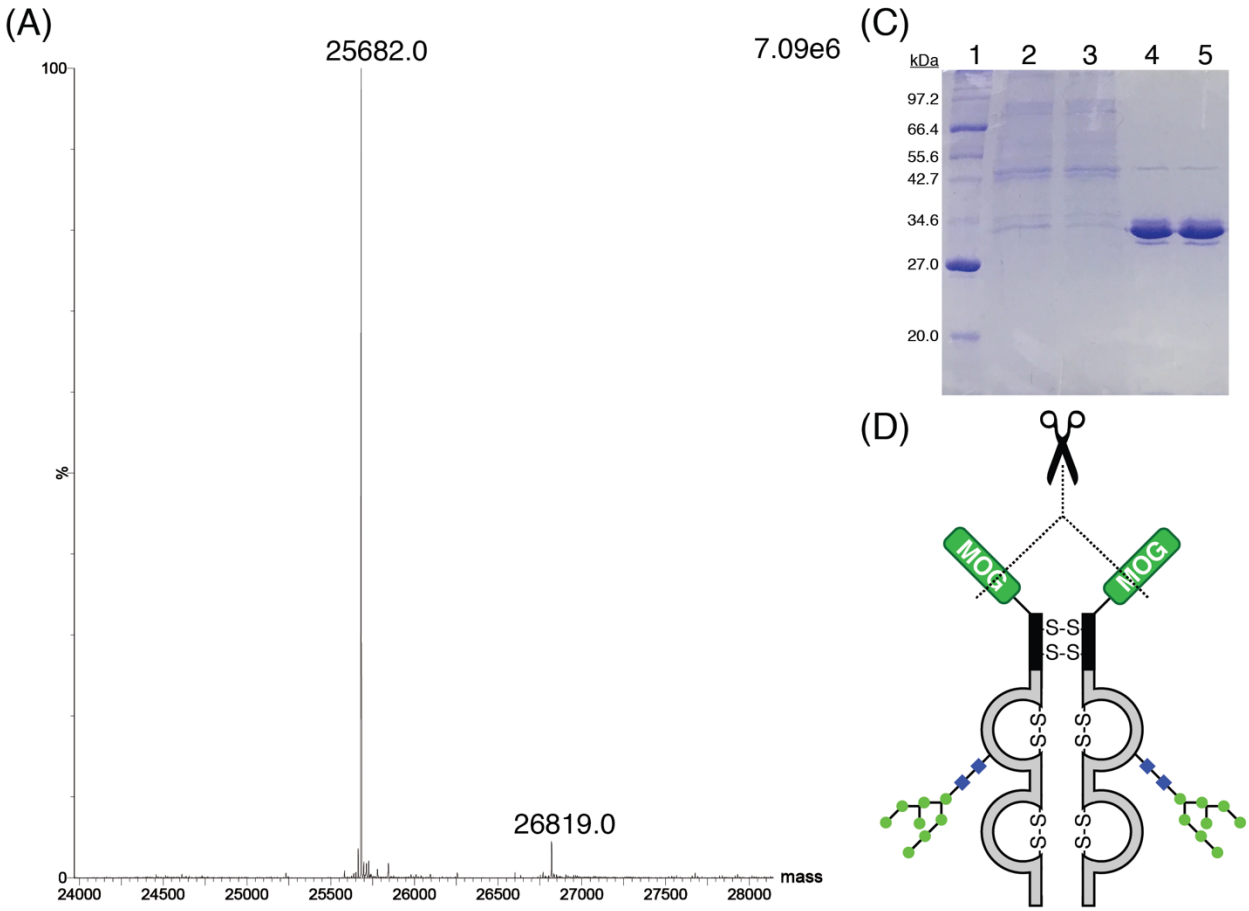

(B)

MOG-Fc Expression Products	Observed MW (Da)	Expected MW (Da)
GWYRSPFSRVVHL-Fc	26819.0	26824.4
VVHL-Fc	25682.0	25687.2

Figure A.1.7: Characterization of recombinant expression of MOG-Fc single fusion protein in a spinner flask. (A) Mass spectrum of MOG-Fc expression products. Prior to characterization, the protein was de-glycosylated with PNGase F and reduced to its monomeric state using DTT. (B) Table showing peptide sequences and observed vs. expected molecular weights of expression products. MOG sequence = H_3N^+-GWYRSPFSRVVHL. (C) SDS-PAGE of MOG-Fc after purification from Protein G affinity chromatography. All samples were treated with DTT. Lanes: 1, 2-212 kDa MW marker; 2, supernatant from culture media; 3, flow through from protein G affinity chromatography of supernatant from culture media; and 4-5 = elution fractions of MOG-Fc from protein G affinity chromatography. (D) Representation of MOG-Fc single fusion protein showing sites of proteolysis that were observed from mass spectrometry.

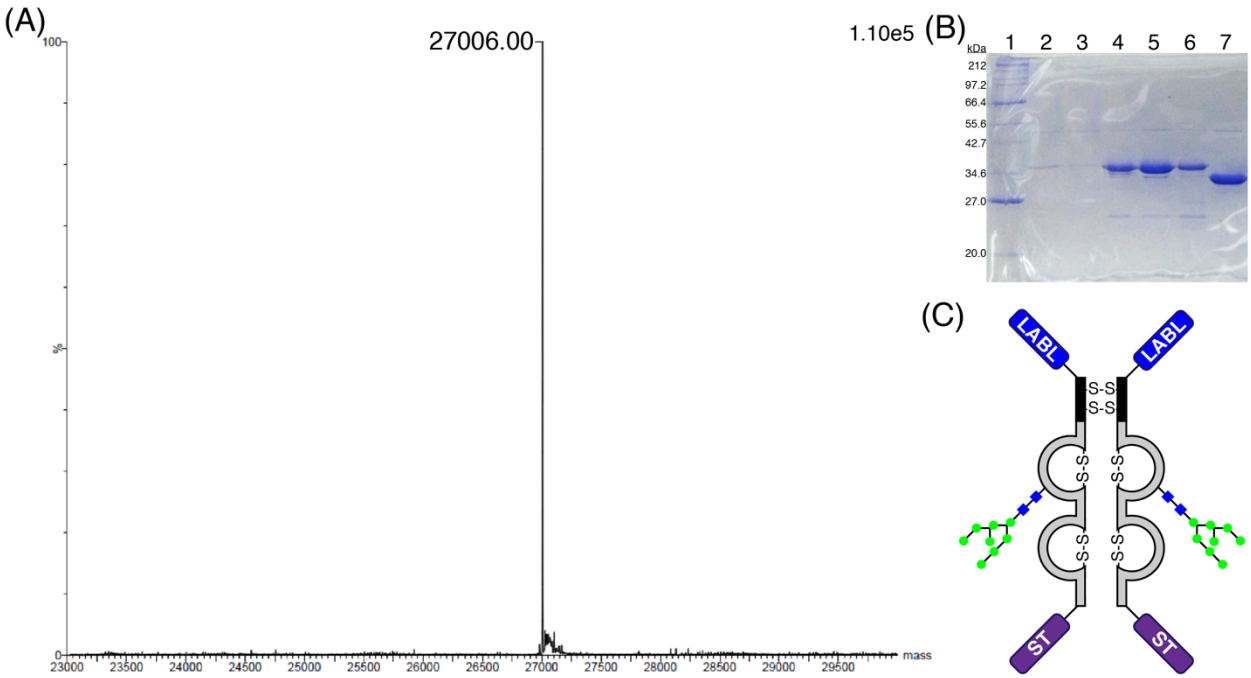

Figure A.1.8: Characterization of recombinant expression of LABL-Fc-ST fusion protein in spinner flask. (A) Mass spectrum of LABL-Fc-ST from recombinant expression. Prior to characterization, the protein was de-glycosylated with PNGase F and reduced to its monomeric state using DTT. LABL-Fc-ST MW (Da): Expected = 27010.41, Observed = 27006.00. LABL sequence = H_3N^+-ITDGEATDSG and ST sequence = AAALPETGGG. (B) SDS-PAGE of LABL-Fc-ST after purification from protein G affinity chromatography. All samples were treated with DTT. Lanes: 1, 2-212 kDa MW marker; 2, supernatant from culture media; 3, flow through from protein G affinity chromatography of supernatant from culture media; 4-6, elution fractions of LABL-Fc-ST from protein G affinity chromatography; 7, LABL-Fc-ST treated with PNGase F. (C) Representation of LABL-Fc-ST fusion protein.

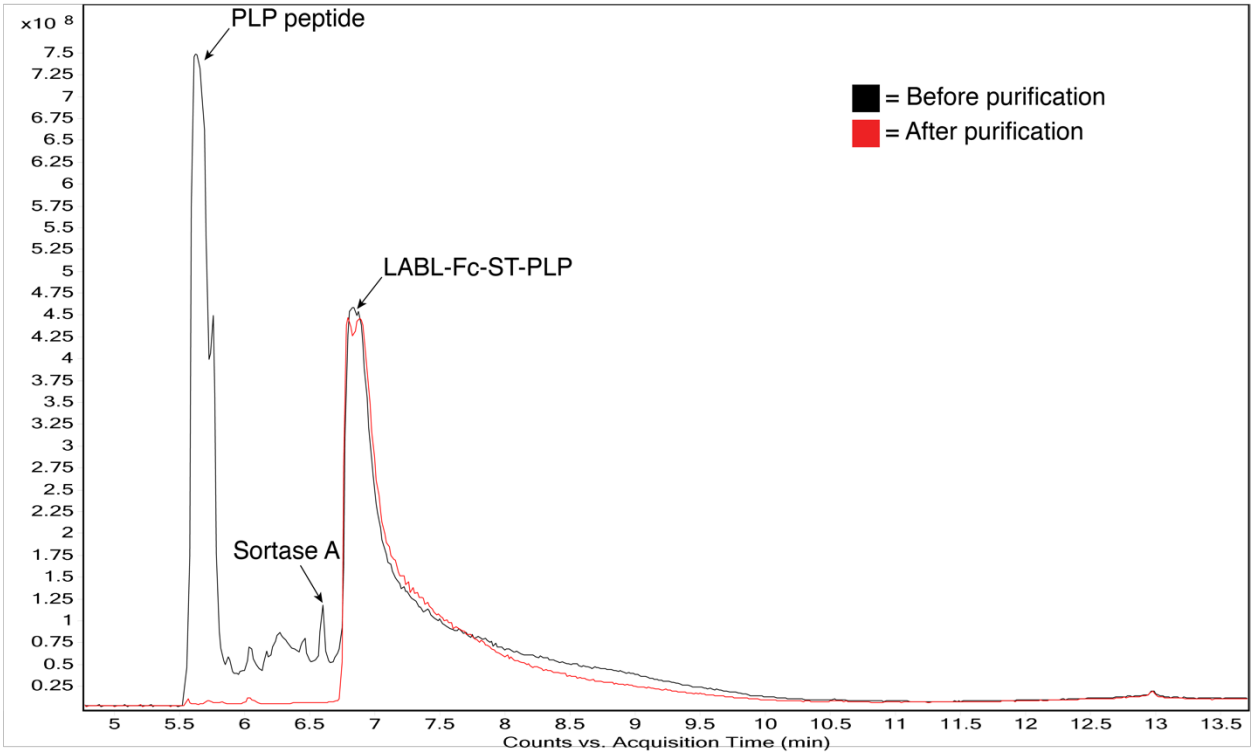

Figure A.1.9: LC-MS TIC overlay of LABL-Fc-ST-PLP before (black) and after (red) purification by protein G affinity chromatography and dialysis. Peaks corresponding to the unreacted PLP peptide and sortase A were no longer present after purification.

Appendix 2

β-1,2-N-acetylglucosamine On The α-1,6-Arm Of The N-linked Glycan Of IgG1 Fc Increases Stability And FcγRIIIa Binding Affinity But Decreases Core-linked Fucosylation Kinetics

A.2.1 Methods

A.2.1.1 Cloning, expression, and purification of glycotransferases and glycosidases

The concentrations of the enzyme preps were determined using a Pierce BCA Protein Assay Kit (Thermo Scientific, Waltham, MA) according to manufacturer's instructions.

A.2.1.1.1 Mannosidase-I and endomannosidase

An expression plasmid for mannosidase-I from *Bacteroides thetaiotaomicron* was provided by the Gilbert laboratory at New Castle University and expressed in *E. coli* Rosetta 2 cells and purified in the Tolbert laboratory by Dr. Ishan Shah.[1, 2] An endomannosidase (accession #: NM_080785) from rat was also cloned, expressed in *E. coli* Rosetta 2 (Novagen), and purified in the Tolbert laboratory by Dr. Shah.[1]

A.2.1.1.2 GnT-I

A GnT-I enzyme from human (MGC-2304) was cloned in the Tolbert laboratory by Dr. Mark Pawlicki, and it was expressed in *E. coli* Rosetta gami2(DE3) (Novagen) and purified by Dr. Khalid Al-Kinani as previously described.[3]

A.2.1.1.3 Mannosidase-II

A mannosidase-II from mouse was cloned and transformed into *P. pastoris* KM71H strain (Invitrogen) in the Tolbert laboratory by Dr. Hamilton (unpublished procedure, can be found in Hamilton dissertation). The cells were grown in a shake tube containing 2 mL YPD media and 100 µg/mL zeocin at 25ºC and shaken at 250 rpm. After 3 days, the culture was transferred to a 250 baffled Erlenmeyer flask containing 50 mL YPD media and 100 µg/mL zeocin and grown at 25ºC and shaken at 250 rpm. After 2 days, the culture was transformed to a 1 L spinner flask containing 1% yeast extract, 2% tryptone, 2% glycerol, 100 mM potassium phosphate buffer pH 6.2, 1.34% yeast nitrogen base, 0.00004% biotin, 0.004% histidine, and 1

drop Antifoam 204. The culture was stirred on a stir plate at r.t. with an air flow of 3 L/min. After 2 days, the pH of the culture was adjusted to 6.2 using NH_4OH. Also, an additional 0.004% histidine was added, and induction was started by adding 0.5% methanol. Induction was maintained by adding 0.5% methanol every 12 hours for 2.5 days. After induction, the cultures were harvested by centrifugation at 6693 x g for 20 min using a Beckman JLA 10.5 rotor and Beckman Avanti J-series centrifuge (USA).

The pellet was resuspended in approximately 100 mL of 100 mM potassium phosphate buffer pH 7.5. The resuspension was then mixed with 50% (v/v) glass beads and subjected to 7 cycles of the following: 1 min bead beating (Biospec Products, Bartlesville, OK) and 20 min cool down on ice. The lysate was filtered through a cheese cloth and centrifuged at 27,216 x g for 30 min at 4°C using a Beckman JA-20 rotor and Avanti J-series centrifuge. The supernatant was saturated to 50% with $(NH_4)_2SO_4$ and slowly stirred overnight at 4ºC. The precipitate was centrifuged at 48,384 x g for 30 min at 4°C using a Beckman JA-20 rotor and Avanti J-series centrifuge. The pellet was resuspended in approximately 50 mL of 10 mM potassium phosphate buffer pH 7.5 and dialyzed in 4 L of 10 mM potassium phosphate buffer pH 7.5 at 4°C with 1 buffer change. An anion exchange column containing 50 mL of Toyopearl DEAE-650M resin (King of Prussia, PA) was equilibrated with 10 CV of 10 mM potassium phosphate buffer pH 7.5. The dialyzed protein was loaded, and then the proteins were separated using a linear gradient of 0-500 mM NaCl in 10 mM potassium phosphate buffer pH 7.5 over 10 CV at a flow rate of 0.5 mL/min. The fractions were screened for mannosidase-II activity mixing each fraction with 100 mM p-nitrophenol-mannose in 100 mM MES buffer pH 5.6 in a fraction:substrate volume ratio of 1:10. The fractions were incubated at 37°C for 1 hr. The fraction that showed the most intense yellow color was confirmed for mannosidase-II activity by mixing the fractions with 0.3

mg/mL M5H-IgG1 Fc in 20 mM MES buffer pH 6.0 at a fraction:M5H-Fc volume ratio of 1:10 and checking for the presence of M3H-IgG1 Fc after 2 hrs using intact mass spectrometry.

A.2.1.1.4 GnT-II

The gene sequence for a mammalian GnT-II was codon optimized for expression in yeast by Dr. Tolbert, synthesized by GenScript (Piscataway, NJ), cloned into pPICzαA by Dr. Tolbert, and then expressed in glycosylation-deficient strain of *P. pastoris* (OCH1 deleted)[4] and purified by Dr. Al-Kinani (unpublished procedure, can be found in Hamilton dissertation).

A.2.1.1.5 FUT8

An α1,6-fucosyltransferase (FUT8) from mouse was cloned into a pET30a expression plasmid and transformed into *E. coli* SHuffle strain (New England BioLabs, Ipswich, MA) in the Tolbert laboratory by Dr. Al-Kinani (unpublished procedure, can be found in Al-Kinani dissertation). FUT8 used in **3.2.3.6** and **3.2.10.5** was prepared as previously described (unpublished procedure, can be found in Al-Kinani dissertation). FUT8 used in **3.2.10.1**-**3.2.10.4** was prepared as follows: The *E. coli* SHuffle strain containing pET30a-FUT8 and pRARE (Novagen) was inoculated in a shake tube containing 5 mL LB media, 35 µg/mL chloramphenicol, and 37 µg/mL kanamycin and grown at 30ºC overnight. The 5 mL culture was transferred to a shake flask containing 1 L of LB media, 25 µg/mL chloramphenicol, and 37 µg/mL kanamycin and grown at 30ºC. After 6 hrs, 0.2 mM isopropyl β-d-1-thiogalacopyranoside was added, and the culture was grown at 16ºC overnight. The culture was centrifuged at 11,899 x g for 20 min at 4°C using a Beckman JLA 10.5 rotor and Avanti J-series centrifuge (USA). The supernatant was discarded, and the pellet was resuspended in 50 mM sodium phosphate buffer pH 7.5 and sonicated using a Fisher Scientific sonicator at 60% amplitude. Sonication was performed on ice, with 10 sec sonication followed by 50 sec of no sonication for a total of 30

min (5 min total sonication). The lysate was immediately centrifuged at 27,216 x g for 30 min at 4°C using a Beckman Avanti J-series centrifuge. The supernatant was filtered through a cotton plug and then FUT8 was purified from the lysate using Ni-NTA affinity chromatography. First, 2 mL of Ni-NTA-agarose resin was washed with 25 CV of sodium phosphate buffer pH 7.5. Next, the lysate was passed through. Then the column was washed with wash buffer (50 mM sodium phosphate buffer pH 7.5, 500 mM NaCl, 5% glycerol, 10 mM imidazole). The FUT8 was eluted using 50 mM sodium phosphate buffer pH 7.5 containing 250 mM imidazole. 1.5 mL fractions were collected and screened for fucosylation activity using intact mass spectrometry with the M3H-IgG1 Fc glycoform substrate (0.5 mg/mL M3H-Fc, 0.5 mM GDP-fucose, 1% (v/v) FUT8, 20 mM MES buffer pH 7.0, r.t.). Additionally, the fractions were screened for background activity in the PK/LDH coupled enzyme assay as described in **3.2.10.1** (no glycan, 1%(v/v) FUT8). The fraction that showed the most M3HF-IgG1 Fc after 21 hrs with the least amount of background activity was pipetted into 6-8 kDa MWCO dialysis tubing and dialyzed in 2 L of TBS pH 7.5 at 4°C with 1 buffer change. The enzyme was then mixed with 50% glycerol and stored at -20°C.

A.2.2 Results

A.2.2.1 Production of FcγRIIIa

FcγRIIIa was expressed in a glycosylation-deficient yeast strain of *P. pastoris* (deleted och1, pno1, and bmt 1&2 genes and inserted STT3D gene from *L. major* in order to improve N-glycosylation site occupancy).[1, 4, 5] The extracellular region contains 5 N-glycosylation sites (**Figure A.2.7**). Expression and purification by Ni-NTA affinity chromatography showed both tetra- and penta-N-glycosylation by SDS-PAGE analysis (**Figure A.2.7A**). In order to make the

receptor more homogenous, it was further purified using HIC. After polishing by HIC, fully penta-glycosylated FcγRIIIa was obtained as determined by the presence of a single band on SDS-PAGE. For use in receptor binding studies, the receptor was biotinylated on its C-terminus using a sortase-mediated ligation (**Figure A.2.7B**). A biotin compound containing an N-terminal triglycine was synthesized previously in the Tolbert laboratory by Dr. Shaofeng Duan.[6] It was reacted with FcγRIIIa in the presence of sortase, which was also produced previously in the Tolbert laboratory.[7] Sortase is a transpeptidase that has been used extensively in literature for the C-terminal ligation of a variety of molecules including proteins, peptides, molecular probes, nucleic acids, sugars, solid supports, and others.[8-10] The ligation required that FcγRIIIa contain the C-terminal sortase recognition sequence (GGLPETGGG), and the biotin contain a glycine with the N-terminus exposed. After the ligation, FcγRIIIa-biotin was purified from the sortase as well as from any unbiotinylated FcγRIIIa using Ni-NTA affinity chromatography by collecting the flow through because both the sortase and unbiotinylated FcγRIIIa contained His6 tags.

A.2.3 Figures

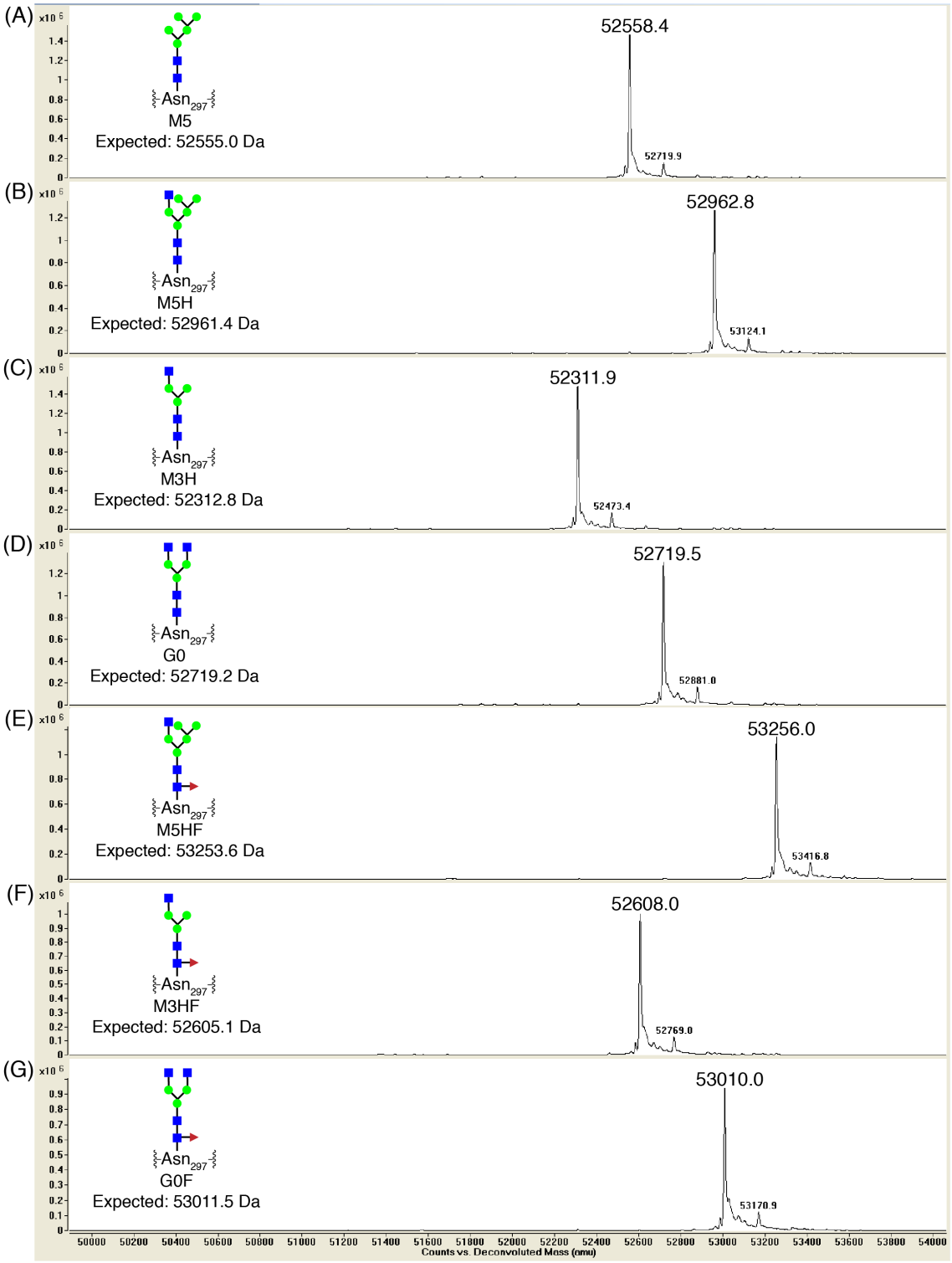

Figure A.2.1: Characterization of homogenous IgG1 Fc N-glycoforms under non-reducing conditions. Shown for each N-glycoform is an intact mass spectrum, representation of the N-glycoform, and the expected MW of the N-glycoform. (A) M5, (B) M5H, (C) M3H, (D) G0, (E) M5HF, (F) M3HF, and (G) G0F.

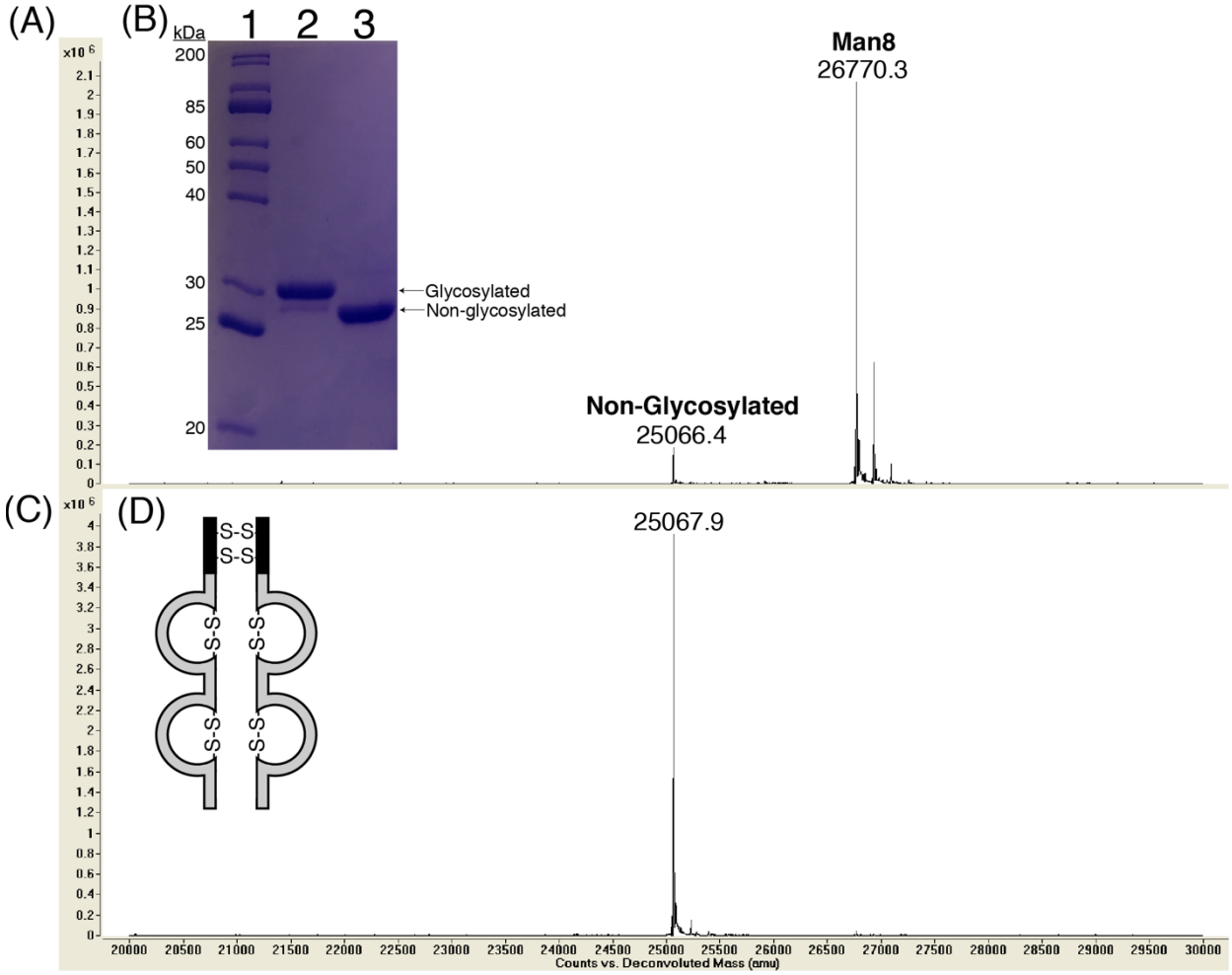

Figure A.2.2: Characterization of IgG1 Fc after de-glycosylation using PNGase F. (A) Intact mass spectrum of IgG1 Fc after purification by Protein A affinity chromatography. (B) SDS-PAGE of IgG1 Fc. Lanes: 1, 10-200 kDa MW protein marker; 2, IgG1 Fc after purification by protein A affinity chromatography; and 3, de-glycosylated IgG1 Fc. (C) Intact mass spectrum of de-glycosylated IgG1 Fc. (D) Representation of de-glycosylated IgG1 Fc. All samples were reduced with DTT prior to analysis. Expected MW of IgG1 Fc species (Da): non-glycosylated = 25066.5, Man8 = 26770.0, de-glycosylated = 25067.5.

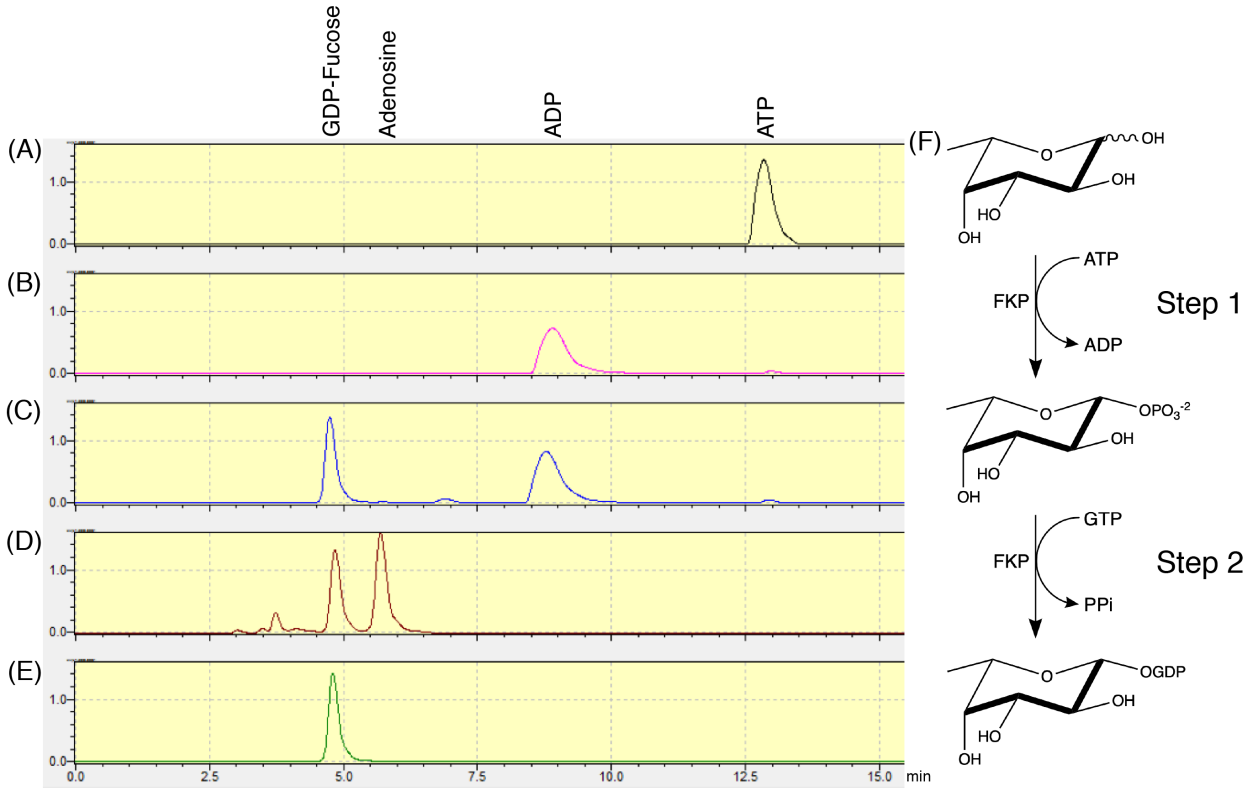

FKP = L-fucokinase/guanosine 5'-diphosphate-L-fucose pyrophosphorylase, ATP = Adenosine Triphosphate, ADP = Adenosine Diphosphate, GTP = Guanosine Triphosphate, GDP = Guanosine Diphosphate

Figure A.2.3: Analysis of the synthesis of GDP-fucose using IPC. Signal was observed using UV/VIS Spectrophotometry at 254 nm. (A) Before reaction: contains ATP and fucose but no FKP, (B) After completion of step 1, (C) After completion of step 2, (D) After treatment alkaline phosphatase, (E) After purification using SEC. (F) Reaction scheme showing FKP-mediated conversion of fucose, ATP, and GTP into GDP-fucose.

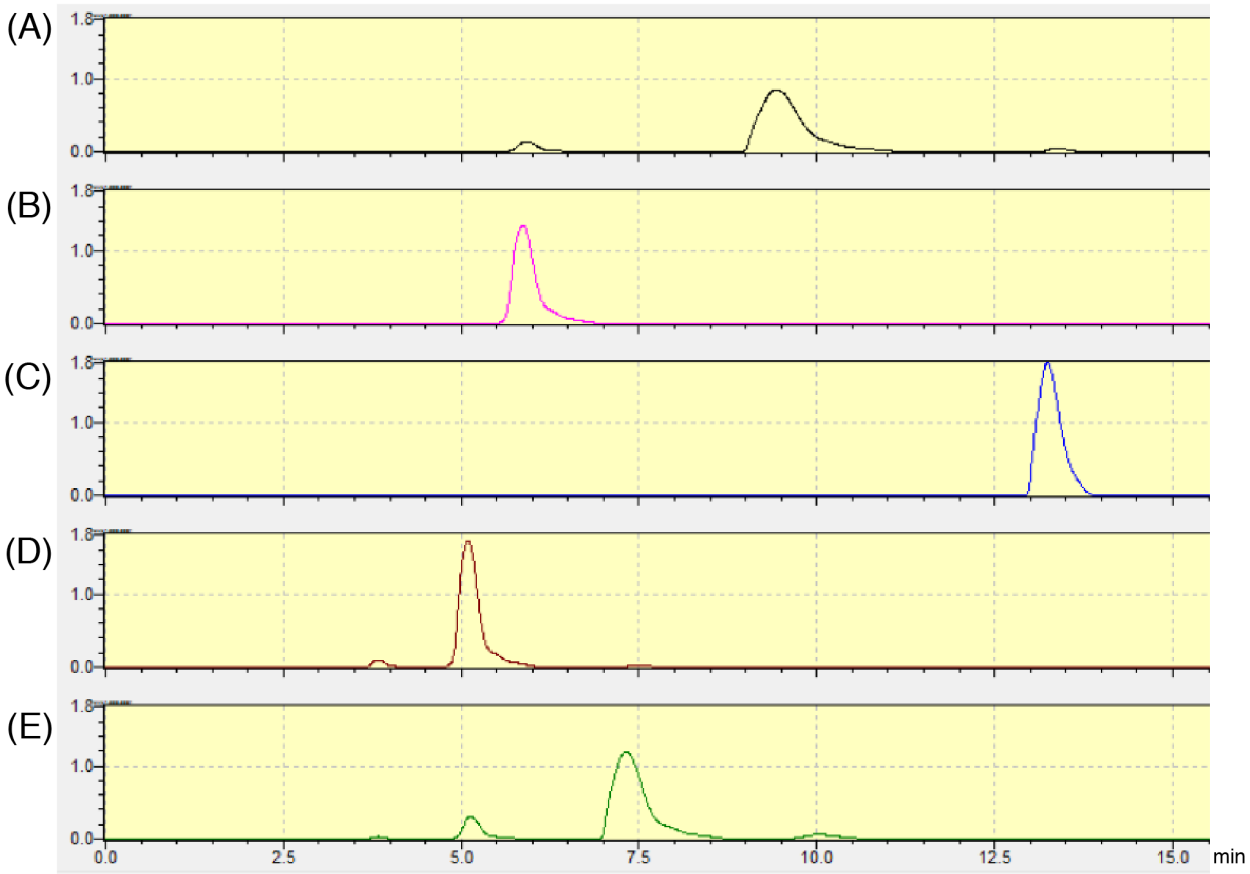

Figure A.2.4: IPC chromatograms of standards that were used to identify peaks during synthesis of GDP-fucose. Signal was observed using UV spectrophotometry at 254 nm. (A) ADP, (B) Adenosine, (C) ATP, (D) GDP, (E) GTP.

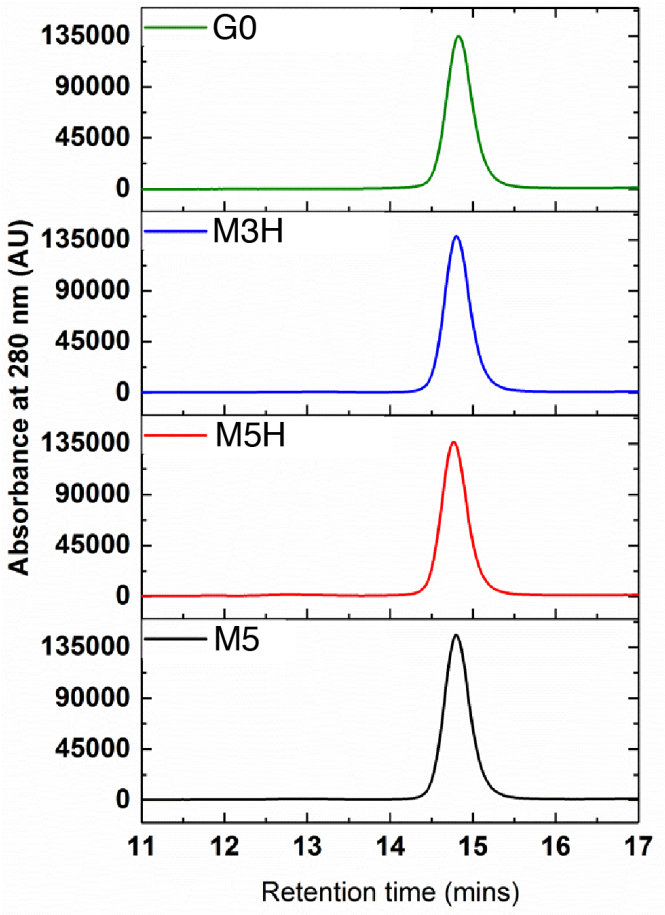

Glycoform (n = 3 replicates)	% Monomer	% Soluble Aggregates
M5	98.1 ± 0.3	1.9 ± 0.3
M5H	97.7 ± 0.3	2.3 ± 0.3
M3H	98.4 ± 0.4	1.6 ± 0.4
G0	99.5 ± 0.2	0.5 ± 0.2

Figure A.2.5: Comparison of IgG1 Fc N-glycoforms using analytical SEC. The reported % Monomer and % Soluble Aggregate values are the average of triplicate runs ± standard error.

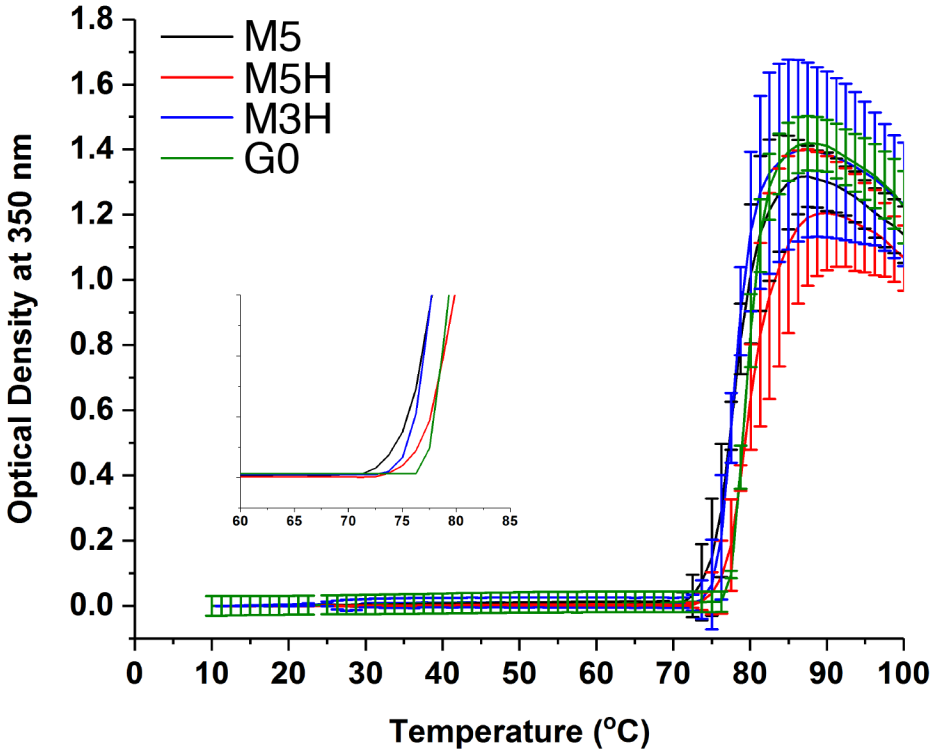

Glycoform (n = 3 replicates)	T_{onset} (°C)
M5	72.3 ± 0.3
M5H	74.2 ± 0.2
M3H	74.1 ± 0.1
G0	76.2 ± 0.1

Figure A.2.6: Comparison of IgG1 Fc N-glycoforms using OD_{350}. The reported T_{onset} values are the average of triplicate runs ± standard error.

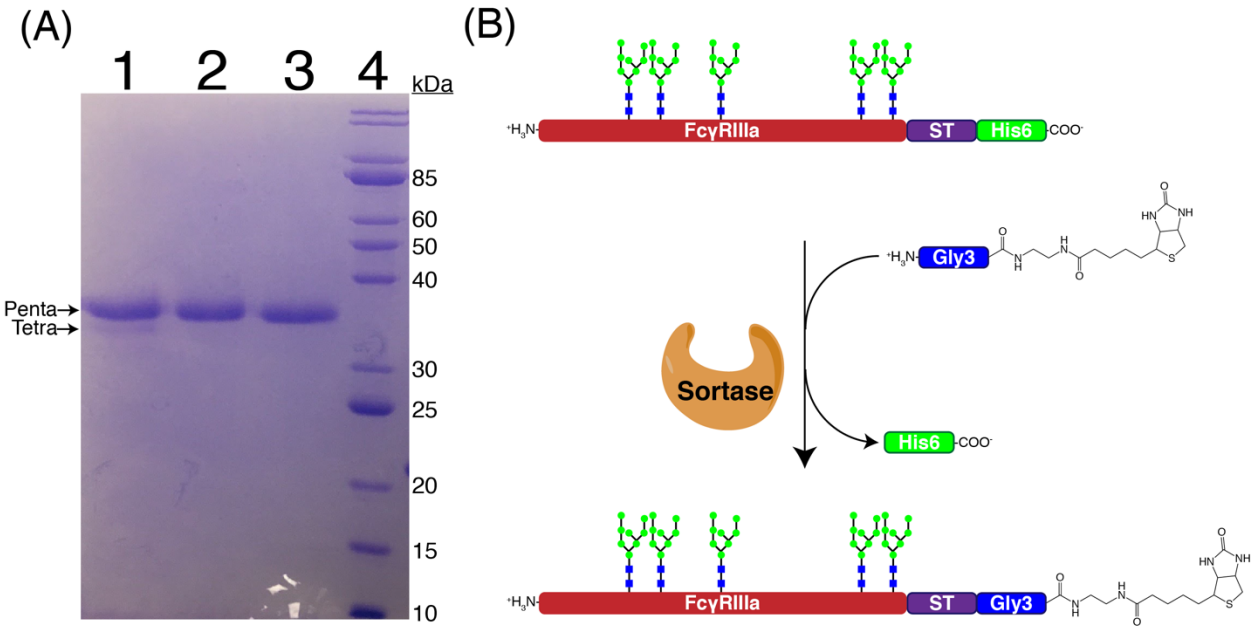

Figure A.2.7: Characterization of the purification and biotinylation of FcγRIIIa. (A) SDS-PAGE of FcγRIIIa. Lanes: 1, FcγRIIIa after Ni-NTA affinity chromatography; 2, FcγRIIIa after HIC; 3, FcγRIIIa after C-terminal biotinylation using a sortase-mediated ligation and subsequent purification by Ni-NTA affinity chromatography; and 4, 10-200 kDa MW protein marker. (B) Representation of C-terminal biotinylation of FcγRIIIa using a sortase-mediated ligation.

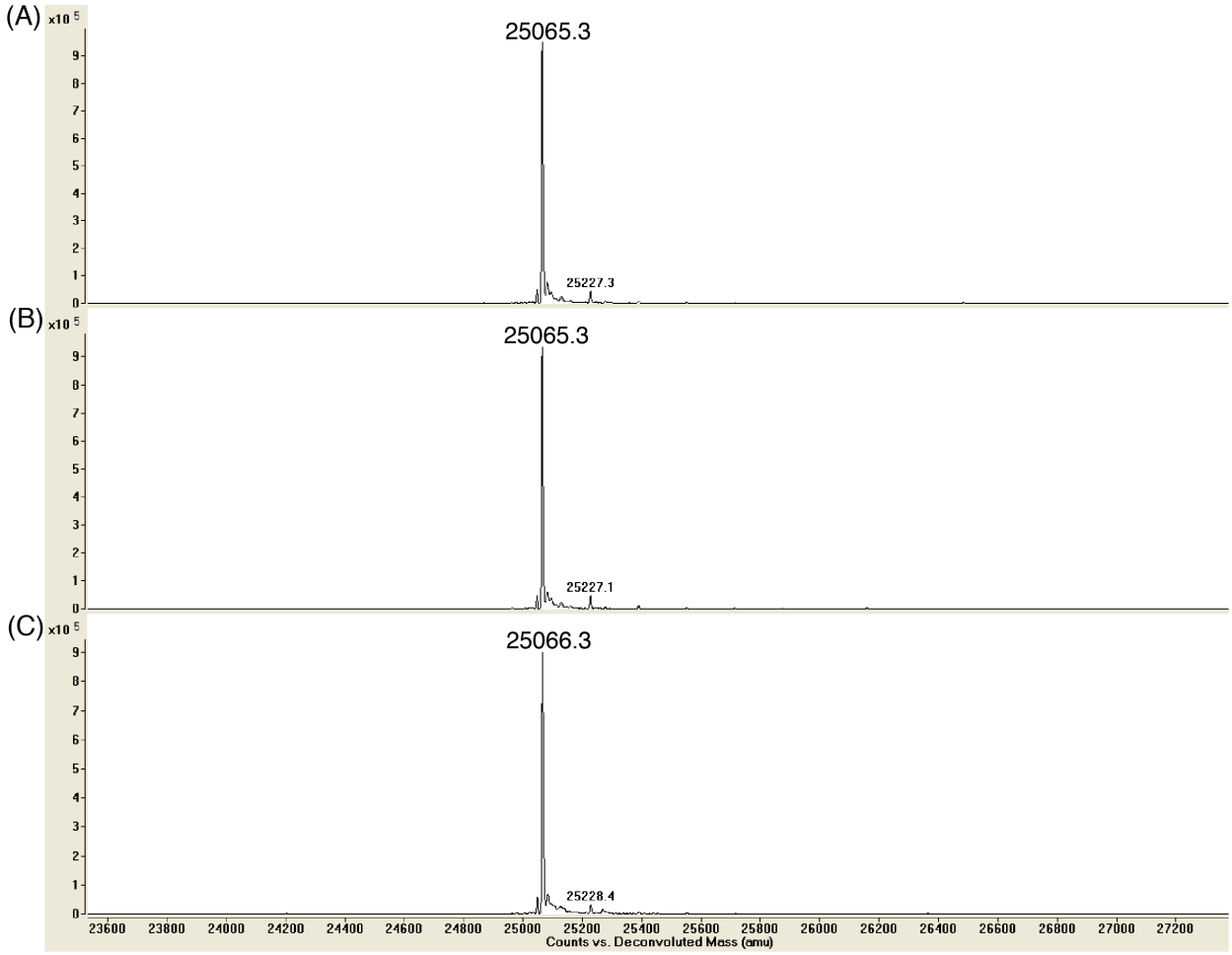

Figure A.2.8: Intact mass spectra of de-glycosylated IgG1 Fc N-glycoforms using PNGase F. Shown are de-glycosylated IgG1 Fc samples from starting substrates of (A) M5H, (B) M3H, and (C) G0. Expected MW of de-glycosylated IgG1 Fc = 25067.5 Da. All samples were reduced with DTT prior to analysis.

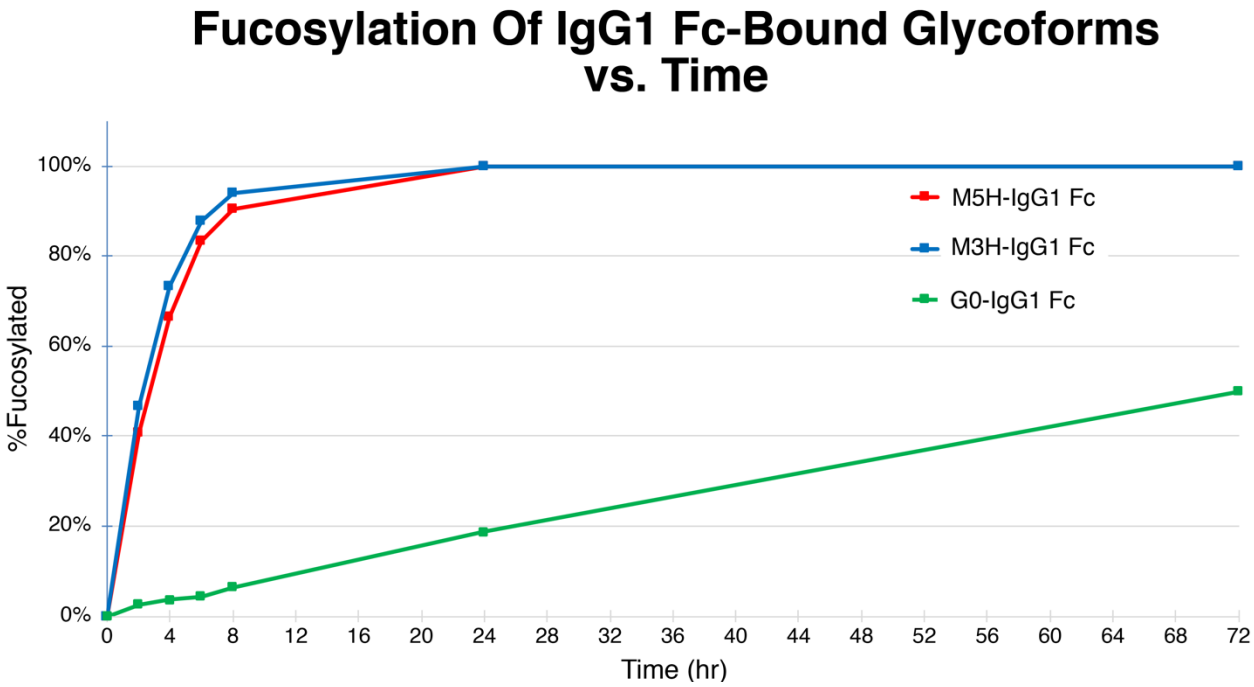

Figure A.2.9: Fucosylation of IgG1 Fc-bound N-glycoforms vs. time. The fucosylation reactions were monitored by intact mass spectrometry, and the % fucosylated was determined by observing the ratio in peaks heights.

A.2.4 References

(1) Shah, I. S., Lovell, S., Mehzabeen, N., Battaile, K. P., and Tolbert, T. J. (2017) Structural characterization of the Man5 glycoform of human IgG3 Fc. *Molecular immunology 92*, 28-37.

(2) Cuskin, F., Lowe, E. C., Temple, M. J., Zhu, Y., Cameron, E. A., Pudlo, N. A., Porter, N. T., Urs, K., Thompson, A. J., Cartmell, A., Rogowski, A., Hamilton, B. S., Chen, R., Tolbert, T. J., Piens, K., Bracke, D., Vervecken, W., Hakki, Z., Speciale, G., Munoz-Munoz, J. L., Day, A., Pena, M. J., McLean, R., Suits, M. D., Boraston, A. B., Atherly, T., Ziemer, C. J., Williams, S. J., Davies, G. J., Abbott, D. W., Martens, E. C., and Gilbert, H. J. (2015) Human gut Bacteroidetes can utilize yeast mannan through a selfish mechanism. *Nature 517*, 165-169.

(3) Chen, R., Pawlicki, M. A., Hamilton, B. S., and Tolbert, T. J. (2008) Enzyme-catalyzed synthesis of a hybrid N-linked oligosaccharide using N-acetylglucosaminyltransferase I. *Advanced Synthesis & Catalysis 350*, 1689-1695.

(4) Xiao, J., Chen, R., Pawlicki, M. A., and Tolbert, T. J. (2009) Targeting a homogeneously glycosylated antibody Fc to bind cancer cells using a synthetic receptor ligand. *Journal of the American Chemical Society 131*, 13616-13618.

(5) Choi, B.-K., Warburton, S., Lin, H., Patel, R., Boldogh, I., Meehl, M., d'Anjou, M., Pon, L., Stadheim, T. A., and Sethuraman, N. (2012) Improvement of N-glycan site occupancy of therapeutic glycoproteins produced in Pichia pastoris. *Applied microbiology and biotechnology 95*, 671-682.

(6) Okbazghi, S. Z., More, A. S., White, D. R., Duan, S., Shah, I. S., Joshi, S. B., Middaugh, C. R., Volkin, D. B., and Tolbert, T. J. (2016) Production, characterization, and biological evaluation of well-defined IgG1 Fc glycoforms as a model system for biosimilarity analysis. *Journal of pharmaceutical sciences 105*, 559-574.

(7) White, D. R., Khedri, Z., Kiptoo, P., Siahaan, T. J., and Tolbert, T. J. (2017) Synthesis of a Bifunctional Peptide Inhibitor–IgG1 Fc Fusion That Suppresses Experimental Autoimmune Encephalomyelitis. *Bioconjugate Chemistry 28*, 1867-1877.

(8) Proft, T. (2010) Sortase-mediated protein ligation: an emerging biotechnology tool for protein modification and immobilisation. *Biotechnology letters 32*, 1-10.

(9) Popp, M. W. L., Antos, J. M., and Ploegh, H. L. (2009) Site-Specific Protein Labeling via Sortase-Mediated Transpeptidation. *Current Protocols in Protein Science 15*, 15.3.1-15.3.9.

(10) Mao, H., Hart, S. A., Schink, A., and Pollok, B. A. (2004) Sortase-mediated protein ligation: a new method for protein engineering. *Journal of the American Chemical Society 126*, 2670-2671.

Appendix 3

Controlled Assembly Of Multivalent IgG1 Fc – Polyacrylamide Conjugates Greatly Increases Binding To FcγRIIIa

A.3.1 Methods

A.3.1.1 Cloning of His6-TEV-Gly3-IL1ra

IL1ra (MGC: 10430) was PCR-amplified using primers (forward: 5'-ggcccgggatccgaaaacctgtatttccagggcggtggcatgcgaccctctgggagaaaatcc and reverse: 5'-gcgccgctcgagttactcgtcctcctggaagtagaatttg) that added a hexahistidine tag followed by a TEV recognition sequence followed by two additional glycine residues to the N-terminus. The PCR product was digested with the restriction endonucleases BamHI-HF and XhoI. A pET28a expression vector (Novagen) was digested with the same restriction endonucleases. The digested IL1ra construct and expression vector were ligated together using T4 DNA Ligase and transformed into electrocompetent *E. coli* Top10f' cells using electroporation. The transformed cells were plated on LB agar containing 37 μg/mL of kanamycin and incubated at 37°C overnight. The DNA was extracted from the cells using the QIAprep Spin Miniprep Kit, and the sequence was confirmed by the UC-Berkeley DNA Sequencing Facility. The plasmid was then transformed into electrocompetent *E. coli* Rosetta 2 cells (Novagen) using electroporation and plated on LB agar containing 37 μg/mL of kanamycin and incubated at 37°C overnight.

A.3.1.2 Expression and purification of His6-TEV-Gly3-IL1ra

The His6-TEV-Gly3-IL1ra was expressed in *E. coli* Rosetta 2 cells and purified by Ni-NTA affinity chromatography using a similar procedure as previously described.[1] Also, an expression construct for TEV protease was prepared previously in the Tolbert laboratory, and it was expressed and purified as previously described.[1] 130 mg/L of His-TEV-Gly3-IL1ra was obtained. Lastly, His6-TEV-Gly3-IL1ra was reacted with TEV protease to produce Gly3-IL1ra using a similar procedure as previously described.[1]

A.3.1.3 Sortase ligation of Gly3-IL1ra to AM-ST co-polymers

Several reactions were prepared on 50 µL scale which all contained following reaction conditions: 500 µM Gly3-IL1ra, 2 mM $CaCl_2$, and 10 µM Sortase A in TBS pH 7.5. Additionally, they contained AM-ST co-polymers (**Table 4.1**) as follows: no co-polymer, 125 µM #1, 125 µM #2, 5 µM #3, 25 µM #3, 125 µM #3, and 600 µM #3. The reactions were incubated at 37°C for 24 hrs and analyzed using SDS-PAGE.

The two reactions containing 125 µM and 600 µM AM-ST co-polymer #3 were combined, and the Gly3-IL1ra-polymer conjugate was separated from the free Gly3-IL1ra using SEC. 20 mL of Bio-Rad Bio-Gel P100 was equilibrated with 5 CV H_2O. Then the polymerized mixtures were pipetted onto the volume. Next, H_2O was passed through the column at a flow rate of approximately 0.3 mL/min. 1.5 mL fractions were collected. Fractions that showed signal at 280 nm using UV spectrophotometry were analyzed using SDS-PAGE.

A.3.2 Figures

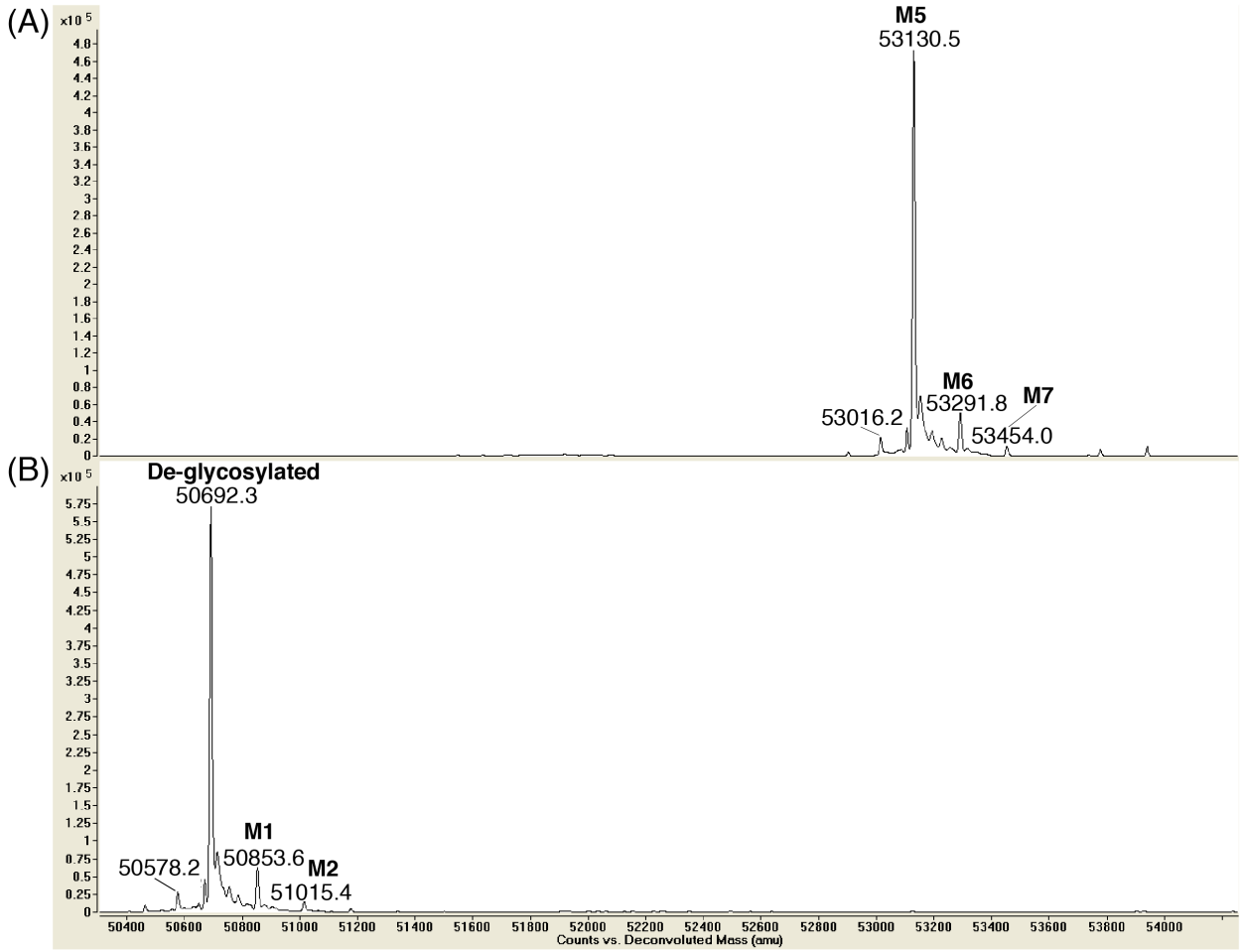

(C)

Gly5-IgG1 Fc Expression Products Under Non-Reducing Conditions		
Species	**Observed MW (Da)**	**Expected MW (Da)**
De-glycosylated	50692.3	50693.3
Man1	50853.6	50855.4
Man2	51015.4	51016.6
Man5	53130.5	53125.5
Man6	53291.8	53287.6
Man7	53454.0	53449.8

Figure A.3.1: Characterization of Gly5-IgG1 Fc with the M5 N-glycoform under non-reducing conditions. (A) Intact mass spectrum of the Gly5-IgG1 Fc with the M5 N-glycoform. (B) Intact mass spectrum of Gly5-IgG1 Fc after digestion with PNGase F. (C) Table showing observed vs. expected MWs of the observed N-glycoforms. All samples were analyzed under non-reducing conditions.

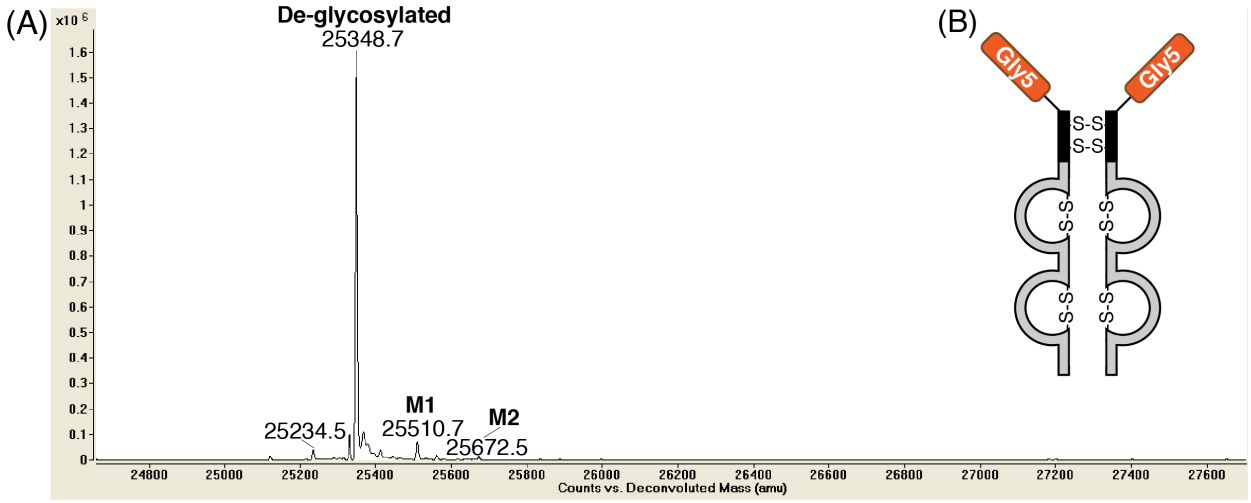

Figure A.3.2: Characterization of de-glycosylated Gly5-IgG1 Fc. (A) Intact mass spectrum of Gly5-IgG1 Fc (originally containing M5 N-glycoform) after de-glycosylation using PNGase F. The sample was reduced with DTT before analysis. De-glycosylated Gly5-IgG1 Fc: Expected MW (Da) = 25352.7, Observed MW (Da) = 25348.7; M1-Gly5-IgG1 Fc: Expected MW (Da) = 25514.8, Observed MW (Da) = 25510.7; M2-Gly5-IgG1 Fc: Expected MW (Da) = 25677.0, Observed MW (Da) = 25672.5. (B) Representation of de-glycosylated Gly5-IgG1 Fc.

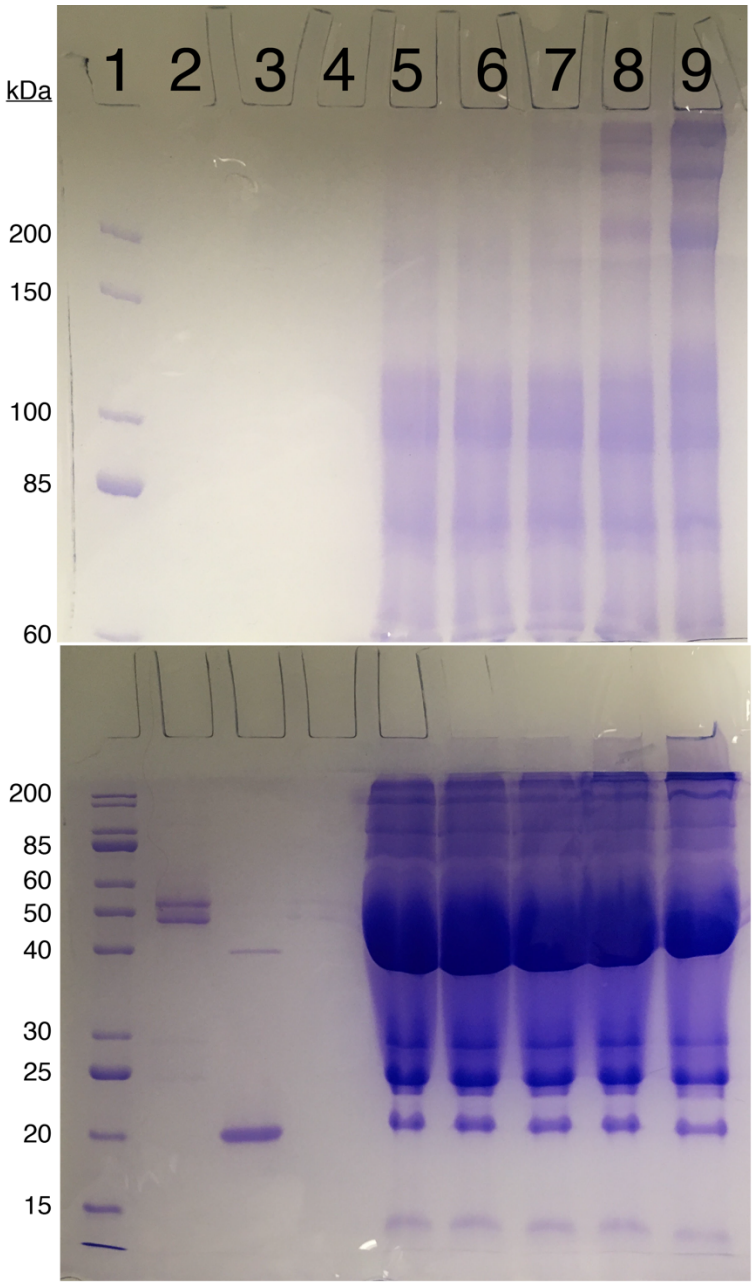

Figure A.3.3: SDS-PAGE of small-scale, sortase-mediated ligations of Fc to the AM-ST co-polymer under non-reducing conditions. Lanes: 1, 10-200 kDa MW protein marker; 2, Fc; 3, sortase A; 4, AM-ST co-polymer; 5-9, sortase-mediated ligations of Fc to AM-ST co-polymer: [AM-ST co-polymer] (μM): Lane 5 = 0, Lane 6 = 0.02, Lane 7 = 0.04, Lane 8 = 1, Lane 9 = 5. In order to obtain resolution in different size ranges, the samples were analyzed on gels prepared with both (A) 6% and (B) 12% acrylamide. All samples were reduced with DTT prior to loading.

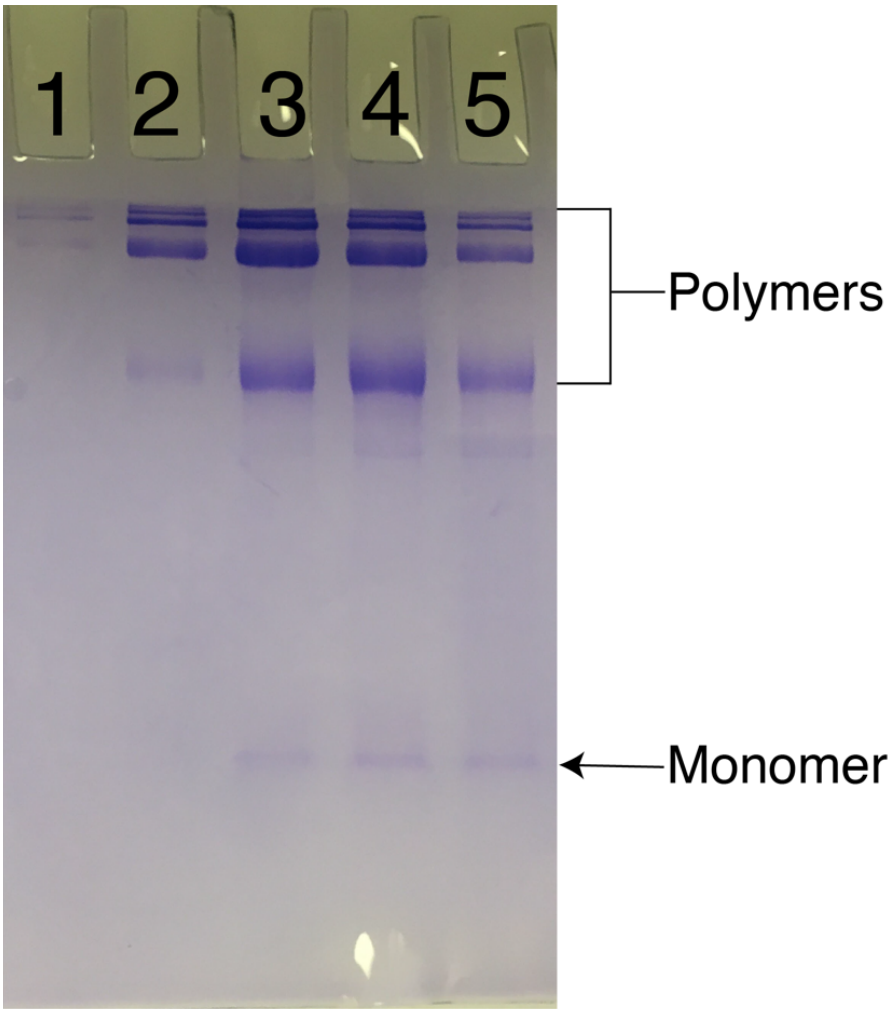

Figure A.3.4: SDS-PAGE of fractions during purification of Fc-polymer conjugate by SEC. Lanes: 1-5 are SEC fractions from earliest to latest elution that contained polymer and very little monomer. These fractions were pooled and constituted the Fc-polymer conjugate sample. All samples were analyzed under non-reducing conditions.

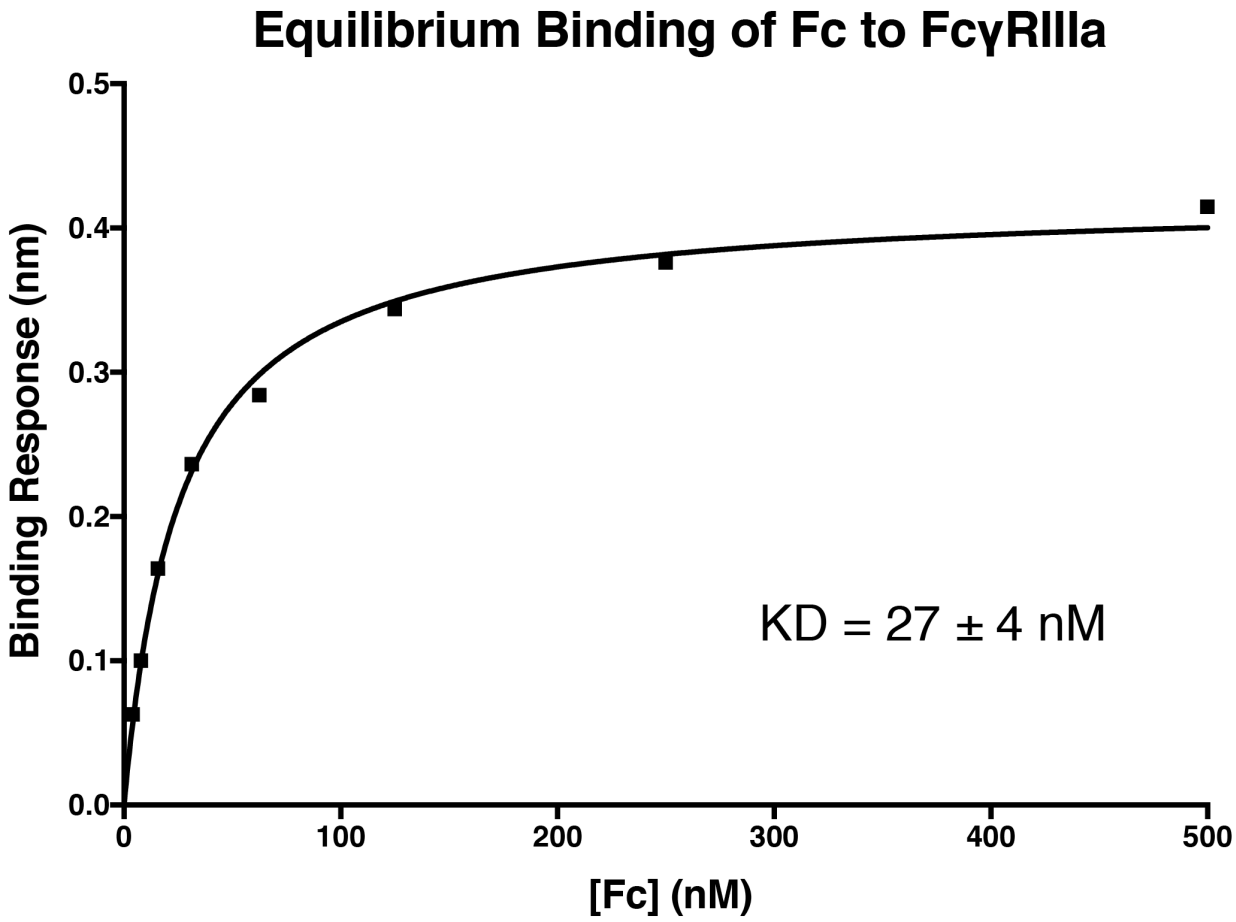

Figure A.3.5: Representative equilibrium binding curve Fc to FcγRIIIa. Reported K_D is the average value from triplicate runs ± standard deviation.

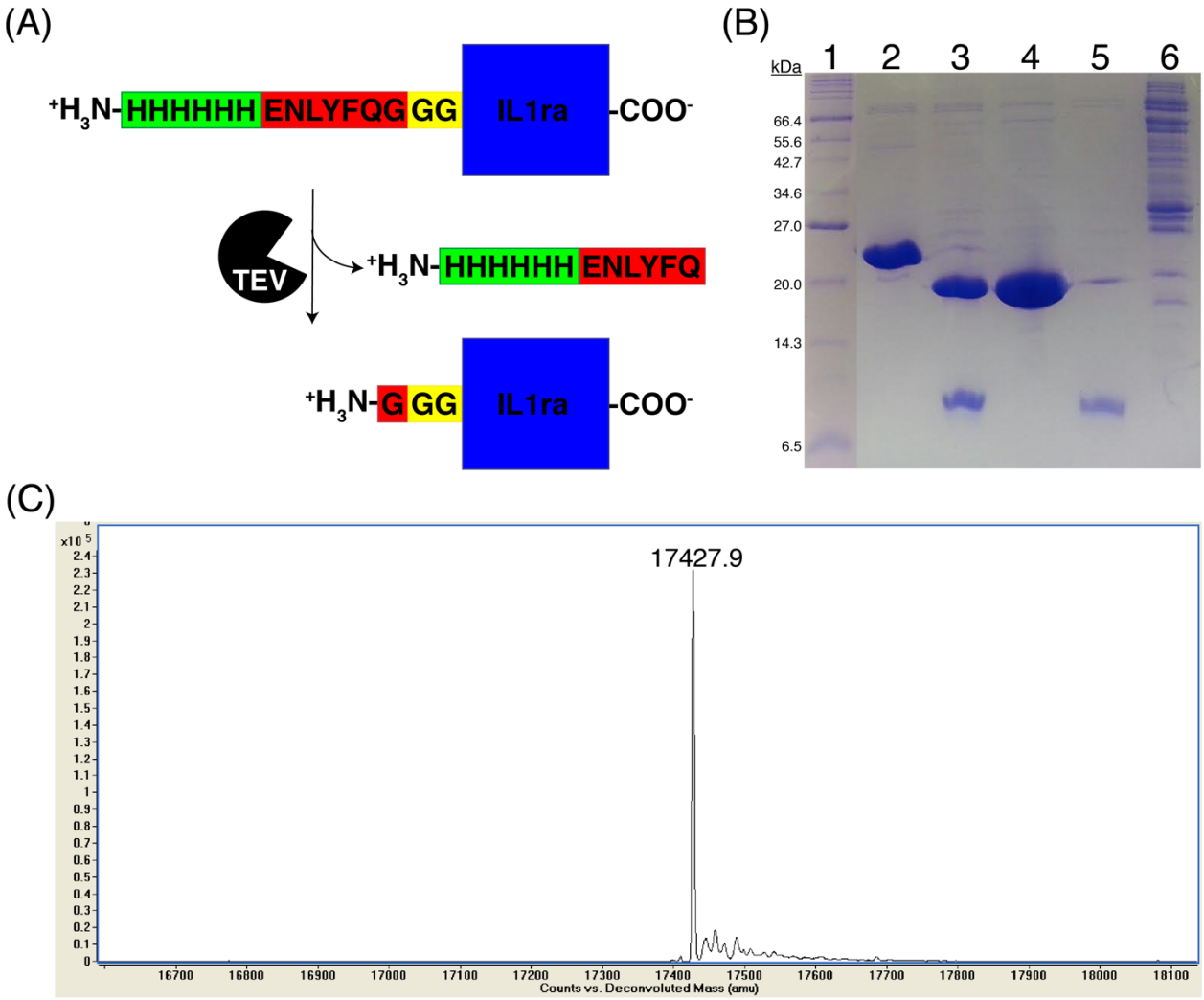

Figure A.3.6: Characterization of Gly3-IL1ra. (A) Representation of cleavage to expose N-terminal tri-glycine by TEV protease. IL1ra was expressed with an N-terminal hexa-histidine tag (green), followed by a TEV protease (red) tag with a glycine residue at the P1' position, followed by two additional glycine residues (yellow). Cleavage by TEV protease cleaves between the glutamine and glycine within the protease recognition sequence to expose a glycine on the N-terminus of IL1ra. (B) SDS-PAGE of Gly3-IL1ra before and after cleavage by TEV protease. Lanes: 1, 2-212 kDa MW protein marker; 2, His6-TEV-Gly3-IL1ra; 3, His6-TEV-Gly3-IL1ra + TEV protease reaction mixture; 4, Gly3-IL1ra after purification by Ni-NTA affinity chromatography; 5, Elution fraction of the purification by Ni-NTA affinity chromatography of Gly3-IL1ra from TEV protease reaction; and 6, TEV protease. The SDS-PAGE gel was prepared using 12% Acrylamide. (C) Intact mass spectrometry of Gly3-IL1ra. Expected MW = 17428.8 Da

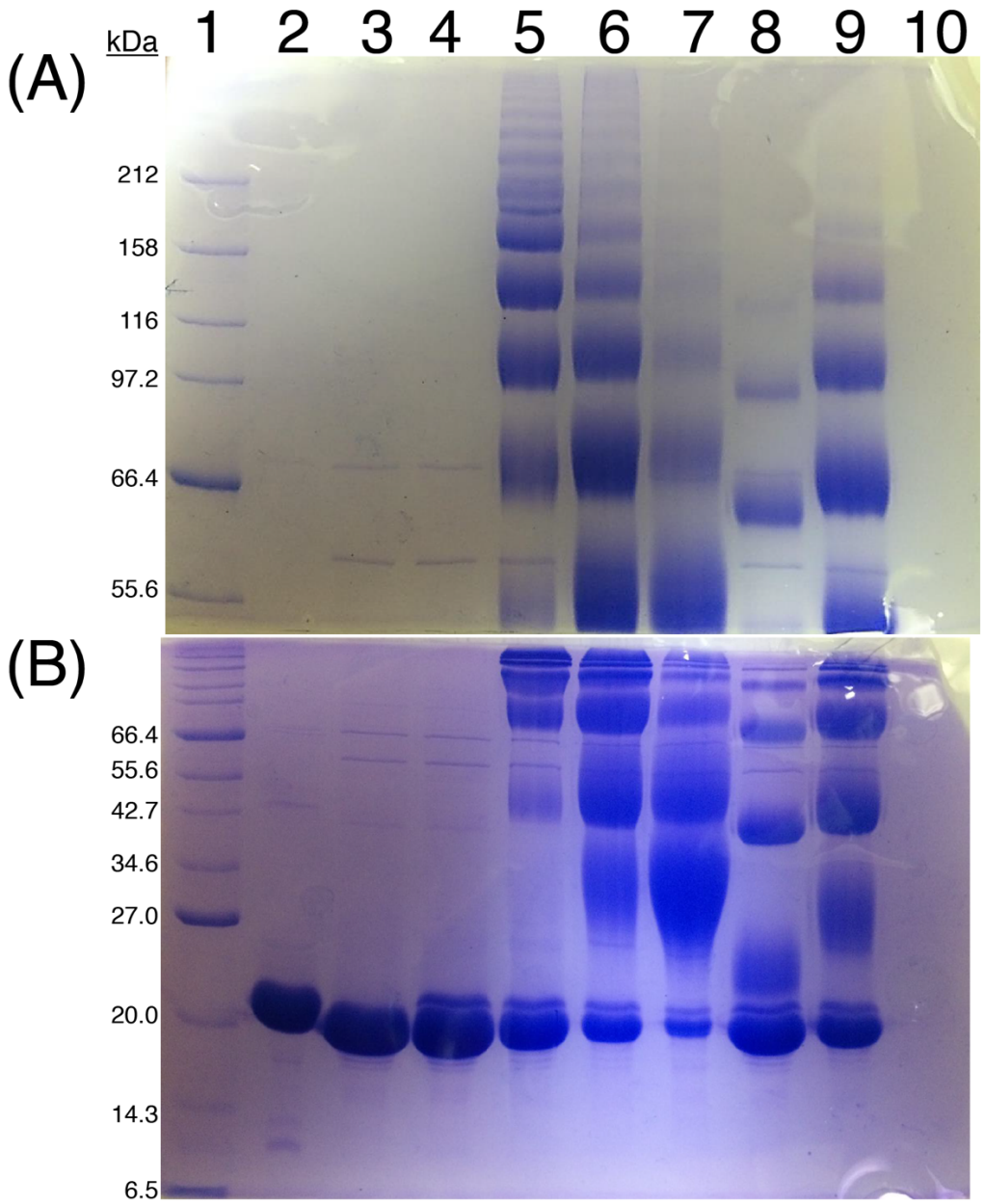

Figure A.3.7: SDS-PAGE of small-scale, sortase-mediated ligation of Gly3-IL1ra to AM-ST co-polymers. In order to obtain resolution in different size ranges, the samples were analyzed on gels prepared with both (A) 6% and (B) 12% acrylamide. Lanes: 1, 2-212 kDa MW protein marker; 2, sortase A; 3, Gly3-IL1ra; 4-9, Sortase-mediated ligation of Gly3-IL1ra to AM-ST co-polymer using: 4, no co-polymer; 5, 25 μM #3; 6, 125 μM #3; 7, 600 μM #3; 8, 125 μM #1; 9, 125 μM #2; and 10, AM-ST co-polymer #3 only.

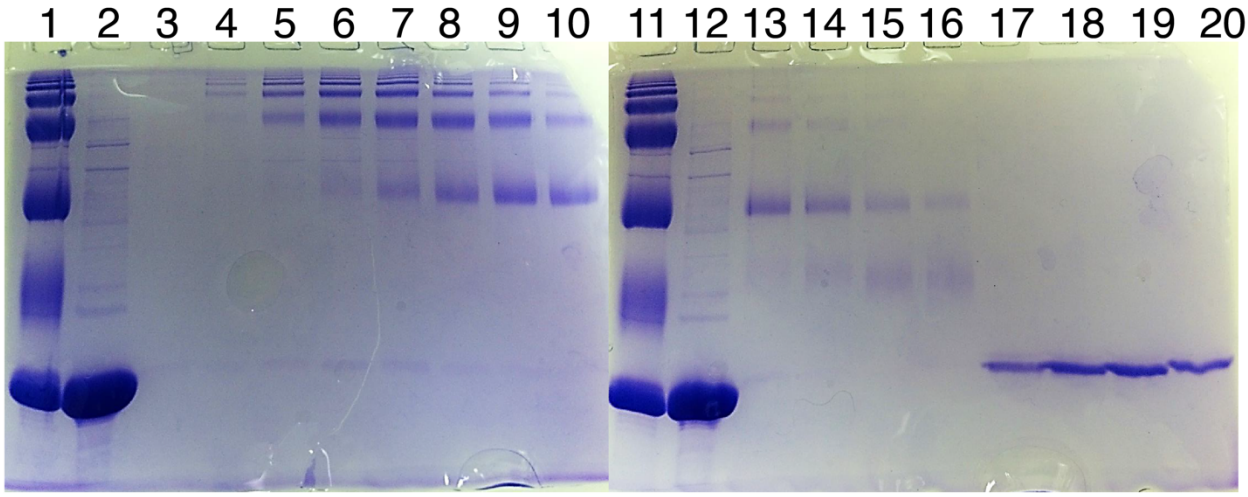

Figure A.3.8: SDS-PAGE of fractions of Gly3-IL1ra-polymer conjugate purification by SEC. Lanes: 1 & 11, Sortase-mediated polymerization reaction of Gly3-IL1ra using 125 μM AM-ST co-polymer #3; 2 & 12, Gly3-IL1ra monomer; 3-10 & 13-20, SEC fractions of Gly3-IL1ra-polymer conjugate purification. Both SDS-PAGE gels were prepared using 12% Acrylamide.

A.3.3 References

(1) Tolbert, T. J., and Wong, C. H. (2002) New methods for proteomic research: preparation of proteins with N-terminal cysteines for labeling and conjugation. *Angewandte Chemie 114*, 2275-2278.